Cellular Antagonization of the Type 1 Interferon Response for the Potentiation of Oncolytic Virotherapy

by
Boaz Wong

A Thesis Submitted in Partial Fulfillment of the Requirements for the Degree of

Doctor of Philosophy in Microbiology and Immunology

in the

University of Ottawa

Department of Biochemistry, Microbiology, and Immunology

Faculty of Medicine

Supervisor: Dr. Jean-Simon Diallo, PhD

Approval

Name:	**Boaz Wong**
Degree:	**Doctor of Philosophy in Microbiology and Immunology**
Title:	**Cellular Antagonization of the Type 1 Interferon Response for the Potentiation of Oncolytic Virotherapy**
Examining Committee:	**Dr. Jean-Simon Diallo** Thesis Supervisor
	Dr. Harry Atkins Internal Examiner Thesis Advisory Committee Member
	Dr. Ian Lorimer Internal Examiner
	Dr. Robin Parks Internal Examiner
	Dr. Don Gammon External Examiner
Date of Thesis Submission:	Tuesday, October 31, 2023
Date of Thesis Defense:	Tuesday, December 19, 2023

Abstract

Oncolytic viruses (OVs) have made tremendous strides as a viable cancer therapeutic in recent years; however, variable infectivity rates have since limited clinical efficacy. Residual type 1 interferon (IFN-1) responses are integral to the tumour's innate antiviral defense and confer resistance to OVs. To combat this, small molecules with viral sensitizing ability can be used in combination to transiently knockdown IFN-1 responses, allowing OVs to gain a foothold for increased infectivity and therapeutic efficacy. Accordingly, we hypothesize that some chemical or genetic manipulations of cellular processes can indirectly antagonize antiviral IFN-1 responses and modulate pro-inflammatory pathways to potentiate oncolytic virotherapy. In this thesis, we identify several avenues to modify cell signalling events to increase OV therapeutic efficacy through IFN-1 inhibition. Firstly, with respect to the demonstrated OV-enhancing effects of vanadium, a pan-phosphatase (PP) inhibitor, we elucidate that its IFN-1 suppressing activity involves activation of the epidermal growth factor receptor (EGFR) pathway via STAT1/2 and NF-κB. Pharmacological inhibition of EGFR abrogated vanadium's viral sensitizing ability *in vivo*. Secondly, using high-throughput screening methodology, we identify protein phosphatases that inherently regulate the IFN-1 response as targets for oncolytic vesicular stomatitis virus (VSVΔ51) potentiation. Indeed, cloning interfering RNA against one of these PP targets, acid phosphatase 2 (ACP2), into the VSVΔ51 platform demonstrated superior infectivity and cancer cell cytotoxicity compared to the non-targeting VSVΔ51 control. Thirdly, we characterize pevonedistat, a first in-class neddylation activating enzyme inhibitor, to potentiate OV therapeutic efficacy across several *in vitro* and *in vivo* contexts. We demonstrate pevonedistat's ability to inhibit IFN-1 signalling and pro-inflammatory cytokine production using both neddylation independent and dependent mechanisms. Taken altogether,

we dissect multiple signaling mechanisms by which the IFN-1 response can be modulated for the purposes of improving OV therapeutic efficacy. This knowledge can subsequently be directly translated into designing optimized OV strategies for clinical testing.

Keywords: Cancer; Oncolytic virus; Innate immunity; Interferon response; Viral sensitization; Cell signaling; Protein phosphatases; Neddylation

Acknowledgements

Completing a graduate degree on an accelerated timeframe throughout a global pandemic was no easy feat, one that would certainly have not been possible without the support of many individuals. First and foremost, I would like to thank my supervisor, Dr. Jean-Simon Diallo, for his unrelenting support across all facets of this milestone. Not only did he craft the perfect research environment, but often went out of his way to give me the opportunities the shape my career aspirations into what they are today. Knowing that my supervisor had full confidence in my research abilities motivated me to give it my all each and every day.

I would like to sincerely thank Dr. Rozanne Arulanandam, who provided significant amounts of guidance and mentorship throughout my thesis, taking me under her wing to answer questions, suggest experiments, and just about everything to ensure that I was always making swift progress. My thesis also would not have been as successful without the foundational work laid down by Anabel Bergeron. Thank you for being first to show me the ropes in the lab and allowing me to progress your project. I would like to thank to my thesis advisory committee: Dr. Tommy Alain, Dr. Harry Atkins, and Dr. Marceline Côté for their kind input and guidance throughout, I distinctly remember coming out of each milestone highly motivated and beaming with confidence. As well, thank you to my collaborators, Rayanna Birtch and Dr. Carolina Ikow (OHRI), Dr. David Olagnier (Aarhus University, Denmark) for their added expertise.

To each of the members of the Diallo lab, who have all contributed to this thesis in one way or another, I would like to thank you for your patience and willingness to help. I was shown nothing but kindness throughout my studies. I would like to especially recognize Andrew Chen for his support with every *in vivo* experiment. I would also like to acknowledge the help from Marcus Spinelli, who is a perseverant fighter both in and out of the lab. The many close

friendships that I've gained over my 4 years with the lab truly made the difference in keeping my studies as enjoyable as possible. A special thank you to Keara Sutherland, Michael Phan, Samriti Birdi, Anna Jirovec, Glib Maznyi, and Ben Yeung for all the memories whether they were over lunch at Tim Hortons or our activities around Ottawa. Last, but not least, I have to give thanks to my friends and family who all believed in me throughout. A special thank you to my loving parents, and to my sisters, Phoebe and Eunice; every life achievement will always be credited to all the support you have provided me.

Table of Contents

List of Abbreviations

ACP-2	Acid phosphatase 2, lysosomal
Ad5	Adenovirus type 5
CD	Cluster of differentiation
DNA	Deoxyribonucleic acid
EGFR	Epidermal growth factor receptor
FLuc	Firefly luciferase
GAS	Gamma interferon activating site
GFP	Green fluorescent protein
GM-CSF	Granulocyte-macrophage colony stimulating factor
HSV-1	Herpes simplex virus 1
HTS	High-throughput screen
ICD	Immunogenic cell death
IFN	Interferon
IFN-β	Interferon beta
IFNAR	IFN-α receptor
IFNGR	IFN-ɣ receptor
IKK	Inhibitor of inhibitor of NF-κB kinase
IL	Interleukin
IRF	Interferon response factor
ISGF3	IFN-stimulated gene factor 3
ISRE	Interferon-stimulated response element
IVIS	In vivo imaging system
IκB-α	Inhibitor of NF-κB alpha
JAK	Janus-associated kinase
LDL-R	Low density lipoprotein receptor
MeV	Measles virus
MOI	Multiplicity of infection
mRNA	Messenger RNA
NAE	Neddylation activating enzyme
NDV	Newcastle disease virus
NEDD8	Neuronal precursor cell-expressed developmentally down-regulated protein 8

NF-κB	Nuclear factor kappa-beta
NTC	Non-targeting control
OV	Oncolytic virus
PD-1	Programmed cell death protein 1
PP	Phosphatase
PTP	Protein tyrosine phosphatase
qPCR	Quantitative real-time polymerase chain reaction
RIG-I	Retinoic acid-inducible gene I
RNA	Ribonucleic acid
RNAi	RNA interference
shRNA	Short hairpin RNA
SinV	Sindbis virus
siRNA	Silencing RNA
STAT	Signal transducer and activator of transcription
T-VEC	Talimogene laherparepvec
TLR	Toll-like receptor
TNF-α	Tissue necrosis factor alpha
TRIF	TIR-domain-containing adapter-inducing interferon-beta
TYK	Tyrosine kinase
UBA3	Ubiquitin-like modifier activating enzyme 3
VACV	Vaccinia virus
VSe	Viral sensitizer
VSV	Vesicular stomatitis virus
VVdd	Double deleted vaccinia virus

List of Tables

List of Figures

Chapter 1. Introduction

1.1 Cancer

Even in the modern age, cancer continues to prove itself as the “emperor of all maladies”. Cancer is currently one of the leading causes of death in Canada and worldwide, accounting for approximately 233 deaths per day in Canada (1, 2). Computational models project the annual number of new cancer cases to increase by 84% to 148,000 in males and by 74% to 129,000 in females by 2032 (3). Respective to economic impact, cancer care cost to our health-care system was $26.2 billion in 2021 and is this amount is expected to steadily rise (4). Despite all these consequences, the medical community remains without an effective cure, allowing cancer to continue devastating Canadian patients and the health-care system with little resistance.

At the very root, cancer is a disease of uncontrolled cell growth and impedance of surrounding tissue. However, decades of extensive investigation have further revealed the intricacies of tumour biology which are categorized into eight succinct characteristics: sustained proliferative signaling, growth suppressor evasion, activation of invasion and metastasis, enabling of replicative immortality, induction of angiogenesis, resistance to cell death, reprogramming of energy metabolism and evading immune destruction (5, 6). Different cancer types accumulate different genetic mutations and epigenetic changes that confer advantages to thrive in their respective physiological environments (7, 8). Continued bidirectional communication between the tumour and its microenvironment eventually nurtures a niche optimized for malignant cancer cell growth (9, 10). In order to lead to clinical

symptoms in a patient, tumours must finally overcome the last obstacle, that is the elimination phase of cancer immunoediting, and overwhelm the immune system's ability to limit tumour progression (11).

1.2 Current cancer therapeutics

The current mainstay of cancer treatment comprises one or more of three different modalities: surgery, radiation therapy and systemic therapy (consisting of chemotherapy, targeted therapy and immunotherapy), each with their own set of limitations. Early-stage patients with localized tumours are often successfully cured with surgical resection, radiation therapy or a combination of both. Over the last few decades, numerous advancements have drastically increased the safety and success of these regimens with documented decreases in mortality and time to recurrence across a multitude of cancer types (12–14). However, surgery and radiation are both limited options for the many patients who present with more advanced disease, especially in many cancer types such as lung where 40% present initially in stage IV (15). Since its introduction in 1946, chemotherapy has become the bread and butter of both curative and palliative cancer treatments (16). Targeting cell cycle characteristics, standard chemotherapy agents are largely unable to differentiate between tumour cells and normal rapidly-dividing cells. The result is a broad and sometimes severe side effect profile, including immunosuppression, which predisposes patients to infection (17).

The last two decades of cancer research have seen the development of novel targeted therapies with drastically increased efficacy. By taking advantage of slight aberrations in the tumour genome, monoclonal antibodies and small molecules inhibit cellular components essential for tumour proliferation that may be mutated or overexpressed (18). Targeted

therapies can also facilitate the selective delivery of chemotherapeutic agents to tumour sites to reduce systemic toxicity (19, 20). Operating under a similar principle is immunotherapy, consisting of biotherapeutics that are designed to empower the patient's own immune system or supply immune cells to contain and eradicate the tumour (21, 22). Immunotherapy also increases adaptive antitumour immunological memory to decrease the risk of future recurrence. However, despite their potential, both targeted therapies and immunotherapies remain dependent on tumours being inherently responsive to the therapeutic regimen (*i.e.,* through expression of an antigen or overexpressed biomarker). With current immunotherapies, there is also the chance for severe immune-related adverse effects (23, 24).

1.3 Oncolytic virotherapy

Oncolytic virotherapy represents a novel therapy option that offers opportunity for development and holds tremendous promise, with a relatively favourable risk-benefit ratio. Reports of viral infection influencing cancer progression has been reported as early as the 1800s; however, it was the advent of genetic engineering that enabled oncolytic viruses (OV) to gain traction as a viable anti-cancer therapeutic (25). Describing a class of biotherapeutics using engineered viruses to selectively infect, replicate within and lyse tumours cells, oncolytic virotherapies have made tremendous progress over the last decade including the approval of talimogene laherparepvec (T-VEC), a genetically engineered herpes simplex virus (HSV-1) expressing granulocyte-macrophage colony-stimulating factor (GM-CSF), in the treatment of melanoma (26, 27). This is just one example of many different strains of viruses that have been demonstrated to have anti-cancer properties, each with their own unique advantages and target niche (28). To increase their versatility even further, modern advances in genetic engineering

techniques allow for OVs to act as payloads for genetic products such as transgenes or silencing RNAs (siRNA). In the aforementioned example, GM-CSF increases maturation of immune cells to enhance anti-tumour immunity (27). The result is the selective delivery of these payloads to cancer cells via the viral genome that further improves the efficacy or safety of the oncolytic virotherapy (29). To date, hundreds of different clinical trials evaluating OV products using different viral platforms and genetic payloads are currently underway (30).

The selectivity mechanism of OVs take advantage of many cancer hallmarks. One such hallmark is the frequent inherent deficiencies in antiviral defences found in tumours. To orchestrate rapid growth and invasion into surrounding tissue, tumours commonly harbour cellular modifications that confer survival advantages, including resistance to cell death and immune destruction (6, 31). This creates an opportunity to engineer OVs that selectively replicate in cancer cells that have forsaken their ability to mount an antiviral immune response, while being unable to propagate in normal cells. Upon entry, OVs then induce mechanisms of cancer cell killing through direct viral lysis and the release of immunogenic particles to induce stronger innate and adaptive antitumour immunity to further clear any residual tumour (32, 33). Different viruses each have their own benefits and drawbacks as an oncolytic platform, making certain viruses more optimal than others for different malignancies. Further genetic tailoring can then be pursued to engineer oncolytic virus candidates for improved clinical translation.

1.3.1 Oncolytic vesicular stomatitis virus (VSV)

One viral platform of particular interest is vesicular stomatitis virus (VSV), a negative-sense, single-stranded RNA rhabdovirus that is enzootic in North America and causes nasal

and oral vesicular lesions in cattle, horses, and swine. While rare cases of human infection have been reported, many were either asymptomatic or only produced mild flu-like symptoms (34). The entire 11-kilobase viral genome is enveloped within a bullet-shaped virion, which codes for 5 distinct viral proteins in order from the 3' end: nucleoprotein (N), phosphoprotein (P), matrix protein (M), glycoprotein (G), and large RNA polymerase protein (L). These components each come together to orchestrate its rapid lifecycle, starting with recognition of the G protein by the ubiquitously expressed receptors such as LDL-R on host cells for viral entry by clathrin-mediated endocytosis. Upon release of the genome into the cytoplasm, the L and P proteins transcribe viral mRNA from the viral genome coated by N. The M protein blocks host mRNA nuclear export to shutoff host antiviral gene products and allows for preferential translation of viral proteins, which combine at the cell membrane for assembly and budding of viral progeny (35). The M protein is also capable of other viral-propagating functions through the NF-κB pathway (36).

The small genome of VSV is also favourable for genetic manipulation, allowing for opportunities to increase safety and therapeutic potency. While wild-type VSV (VSV-WT) shows unacceptable toxicity, introducing a deletion of sequence encoding methionine 51 in the M protein attenuates the resulting VSVΔ51 to only infect cells defective in antiviral responses, thereby increasing oncoselectivity and safety profile (37, 38). Another strategy is to encode VSV to express human interferon beta (IFN-β), which can powerfully stimulate cells with intact antiviral defenses to resist infection while simultaneously increasing immune cell infiltration, promoting stronger antitumor immunological memory (39). For improving therapeutic efficacy, many strategies have been devised. For example, VSV can be modified

to encode tumour suppressor genes (*e.g.,* p53) to enhance direct oncotoxicity (40), or to encode immunostimulatory effectors (*e.g.,* IL-12) (41).

Altogether, VSV offers several benefits as an oncolytic virus given its rapid viral life cycle, broad tissue tropism, amenability to systemic administration, genetic malleability, strong ability to induce humoral immune responses, and lack of pre-established immunity in humans (42). Several phase I and II clinical trials are underway investigating the use of VSV as an anticancer agent in both solid and hematological tumour types. Many of these trials combine strategies to achieve maximal therapeutic efficacy including VSV expressing transgenes such as IFN-β to enhance safety and immunogenicity (NCT03865212, NCT01628640), or co-administration of VSV with other immunotherapy regimens such as the PD-1 inhibitor pembrolizumab (NCT03647163) or chemotherapies (NCT03017820, NCT02923466). With countless other therapeutic regimens involving VSV in pre-clinical development, this list is expected to grow exponentially in the coming decade (43).

1.3.2 Other relevant oncolytic viruses

In addition to oncolytic rhabdoviruses, several other viral platforms have successfully been used as oncolytic agents. As mentioned above, the only currently approved oncolytic virotherapy in North America, T-VEC, utilizes HSV-1. Herpesviruses are enveloped, double-stranded DNA viruses with a large genome (>125 kb), leaving large capacity for transgene insertion. HSV-1 also has high infectivity potential, broad tissue tropism, and potent oncolytic activity. Further, there are numerous established anti-herpetic drugs to counter HSV-1 infection, as an added safety feature. Altogether these characteristics, make HSV-1 an attractive platform for cancer therapy (44). To further improve its safety, numerous genetic

modifications to HSV-1 (*e.g.,* deletion of *γ34.5/RL-1*) have been considered to reduce neuroinvasiveness and control viral growth, and are being tested in clinical trials. Furthermore, trials aiming to combine HSV-1 with checkpoint inhibitor immunotherapies (*e.g.,* pembrolizumab) have also recently shown promising results, although they have not yet translated to therapeutic benefit in later stage trials (45).

Oncolytic poxviruses, which include the vaccinia virus (VACV), are another class of double-stranded, DNA viruses that are advantageous as an oncolytic agent given their tumour selectivity, inability to integrate with host genome, and genetic malleability. Given its large genomic capacity, VACV can be likened to a "battleship" that is equipped with many tools to modify both its safety profile and immunogenicity (46). The goal is to find the optimal combination of strategic deletions of virulence factors and addition of therapeutic and/or immunomodulatory transgenes to ultimately maximize therapeutic efficacy (46). Among other poxviruses that have been tested in clinical trials, JX-594 is a VACV that exemplifies this strategy by inactivating its thymidine kinase gene, confining replication competency to rapidly dividing cancer cells, and inserting human GM-CSF to further augment the antitumour immune response (47).

Many other viral platforms with various genetic modifications are currently being tested clinically including adenovirus (Ad5), measles virus (MeV), Newcastle disease virus (NDV), and reovirus. While most phase 1 and 2 clinical trials report generally acceptable safety profiles at high viral doses, observed tumour responses have been more variable. Completed clinical trials overwhelmingly support that a lack of representative pre-clinical models has set-up majority of these trials for failure. Firstly, viral tropism is species-specific, which can complicate interpretation of animal models. Also, *in vivo* pre-clinical studies often use human

xenografts in immunocompromised mice, which lack a representative immune response (28). This aspect, governing immune resistance to infection and induction of immunological memory towards the tumor, is according to some even more important in determining therapeutic efficacy than direct cancer cell killing by viral lysis (48).

1.4 Innate antiviral defense and the interferon (IFN) response

The vertebrate immune system, responsible for antiviral defenses, can be divided into the innate immune response, which reacts first indiscriminately to suppress infection, and the adaptive response, which is responsible for generating immunological memory to rapidly control future infections. The cellular innate immune system is the first line of defense and is triggered by detection of infection-related pathogen-associated molecular patterns (PAMP) using pattern recognition receptors (PRR) (Fig. 1). This subsequently initiates signalling cascades to produce key polypeptide cytokines known as interferons (IFN) to suppress viral infection, block cellular proliferation, and modulate local innate and adaptive immune responses. Indeed, the IFN system represents a core antiviral mechanism which is employed by the innate immune response (49). IFNs also work to bridge and modulate the adaptive immune response for complete pathogen clearance, tissue regeneration, and immunological memory development. Several viruses, including the attenuated VSVΔ51, are engineered to be highly IFN sensitive, pinpointing this system as a crucial determinant of resistance to these oncolytic virotherapies.

Physiological antiviral responses act through two main classes of the IFN family, the type 1 (IFN-1) and type 2 (IFN-2) systems, each with different primary functions but with

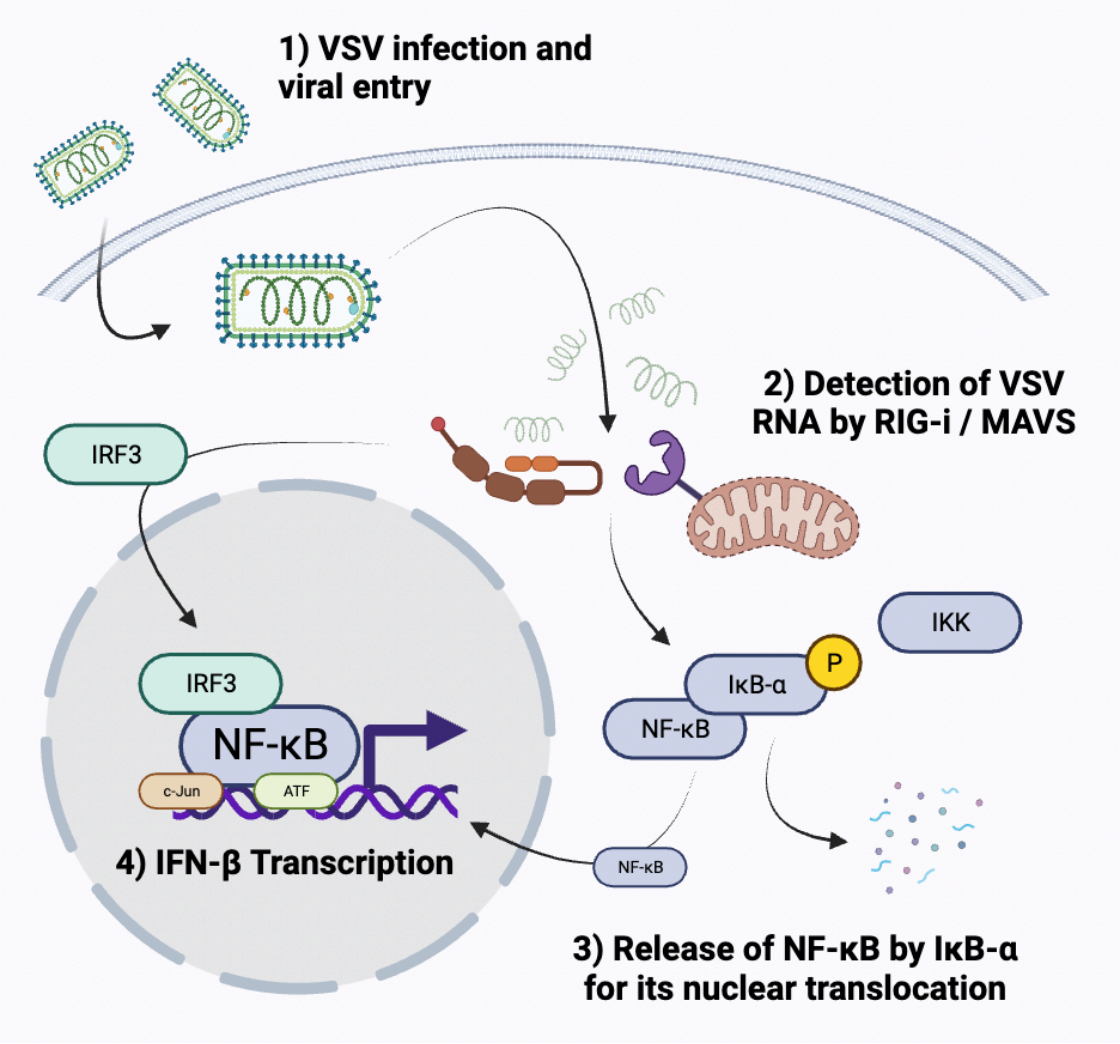

Figure 1. Early phase detection of viral VSV RNA to IFN-β production. As vesicular stomatitis virus (VSV) infects the cell, the viral RNA is released into cytoplasm where it is detected by RIG-I receptors. This triggers a pathway through MAVS to degrade IκB-α via its phosphorylation by IKK. This unmasks the nuclear localization sequence of NF-κB, allowing for its translocation into the nucleus to join the IFN-β enhnaceosome, along with other factors such as IRF3, to begin transcription of IFN-β, kickstarting the anti-viral interferon response.

overlapping effects. IFN-1 consists of several cytokines (IFN-α, IFN-β, IFN-ε, IFN-κ and IFN-ω) encoded by human chromosome 9 and are produced by a large variety of cell types in early phases of infection. This rapid, first-line system operates to directly upregulate antiviral programs in local cells to suppress viral replication, trigger inflammation, and alert nearby immune cells to respond. In contrast, IFN-2 consists of IFN-ɣ encoded by human chromosome 12 and are mostly produced by natural killer (NK) cells and lymphocytes. While they also have inherent antiviral boosting effects, IFN-2 generally operates to enhance inflammatory processes to bridge towards adaptive immunity (31). There also exist type III IFNs (IFN-3), comprised of isoforms of IFN-λ, which have antiviral roles akin to type I IFNs in specific locations within the body (50).

Successful activation of the IFN system results in the production of gene products known as IFN-stimulated genes (ISG), which work via various mechanisms to suppress viral infection (51). In the case of ISGs known to affect the anti-VSV response, myxovirus resistance (MX) genes are dynamin-like GTPases that block viral primary transcription by inhibiting the viral polymerase complex and destabilizing VSV mRNA (52). Another example includes interferon inducible transmembrane (IFITM) proteins, which act to block VSV entry by inhibiting lipid membrane fusion events (53). Expectedly, the overexpression of *MxA* and *IFITM1* genes confer increased resistance against VSV infection in human cells (54). TRIM69 is another example of an ISG that selectively inhibits VSV (55).

1.4.1 NF-κB signaling and the IFN response

In the early phase of tissue or tumour infection, the production of IFN-β by infected fibroblasts serves as the central regulator to amplify the antiviral response at the infection site.

PAMPs such as viral glycoproteins and nucleic acid are recognized by various PRR pathways. Some viruses may activate membrane-bound toll-like receptors (TLR) to signal to downstream adaptor molecules TIR domain-containing adaptor gene inducing IFN-beta (TRIF) and myeloid differentiation primary response gene 88 (MyD88) (56). On the other hand, other viruses including VSV act upon intracellular PRRs like RIG-I like receptors (RLR), which bridge to downstream adaptor molecules using their caspase recruitment domain (CARD) (57). Both pathways cumulate in the activation of multiple transcription factors (*e.g.,* IRF3, IRF7, NF-κB) that come together to form the IFN-β enhanceosome to significantly increase IFN-β transcription, production, and secretion into the microenvironment. A central player to the effective upregulation of IFN-β and other pro-inflammatory cytokines (*e.g.,* TNF-α, IL-6, CCL5) in early phases of viral infection is nuclear factor κB (NF-κB). In the absence of NF-κB, IFN-β production is significantly delayed before IRF3 can compensate, resulting in difficulty controlling initial RNA virus infection (58). Accordingly, several viruses such as VACV have evolved to encode several proteins that inhibit NF-κB nuclear translocation as a strategy to blunt antiviral defences (59).

In general, NF-κB signaling is central to many of the hallmarks of cancer, regulating processes such as proliferation, angiogenesis, tissue invasion, therapy resistance, and immunosuppression (60). The NF-κB family is composed of 5 different subunits (p50, p52, RelA/p65, RelB, c-Rel), each containing a DNA-binding Rel domain, that come together as homo- or heterodimers to induce different signaling programs. Given its potent role in promoting tumorigenesis, it comes with no surprise that many cancer types harbour mutations in NF-κB regulatory pathways resulting in its constitutive activation (61). NF-κB can be activated through canonical (classical) and non-canonical (alternative) pathways. While the

latter is generally more related to maintenance of adaptive immune function, the canonical signaling pathway dominates virus-induced activation of NF-κB. In the absence of infection, inhibitor of NF-κB alpha (IκB-α) masks the nuclear localisation sequence of NF-κB to sequester it in the cytoplasm (62). Upon sensing of tissue necrosis factor alpha (TNF-α) or TLR activation, autophosphorylation of the IKK complex allows for downstream phosphorylation and targeted degradation of IκB-α. Subsequent release of the p50: p65 NF-κB heterodimer allows for its nuclear translocation for signaling (63). Finally, several ISGs, such as protein kinase R (PKR), have been shown to directly potentiate NF-κB activation leading to positive feedback (64, 65). PKR has also been shown to be important for promoting tumour cell death during oncolytic VSVΔ51 infection (66).

1.4.2 JAK/STAT signaling and the IFN response

The next phase of the antiviral response is initiated by sensing of IFN-α/β by their corresponding heterodimeric IFN-α receptor (IFNAR) composed of IFNAR1 and IFNAR2 subunits. Activation of IFNAR recruits Janus-associated kinase 1 (JAK1) and tyrosine kinase 2 (TYK2), which are protein tyrosine kinases required to phosphorylate the downstream signal transducer and activator of transcription 1 and 2 (STAT1, STAT2) factors on their respective tyrosine residues. In the case of IFN-1, phosphorylated STAT1 and STAT2 form a heterodimer, which translocates into the nucleus and then combines with IRF9 to form the IFN-stimulated gene factor 3 (ISGF3) complex. This complex then recognizes IFN-stimulated response element (ISRE) sequences to promote transcription of the aforementioned ISGs to control the viral infection and establish the cellular antiviral state (31, 67). Indeed, this signaling pathway is paramount to a functional antiviral response. In knockout models of

IFNAR or STAT1, mice quickly succumbed to viral infection, even at low viral loads (68, 69). IFN-1 signalling can be controlled after it has peaked, for example, IFN-1s also induce expression of suppressor of cytokine signaling (SOCS) proteins that compete with STATs for IFNAR binding and inhibit the kinase activity of JAK (70).

JAK/STAT signaling also plays a key role in coordinating adaptive immunity. Sensing of IFN-ɣ produced by immune cells through IFN-ɣ receptors (IFNGR) cumulates in the phosphorylation by JAK1/2 and formation of STAT1-STAT1 homodimers, programming cells towards a pro-inflammatory IFN-2 profile. This STAT-1 homodimer instead binds to gamma-activating sequences (GAS) that promote the transcription of pro-inflammatory IFN-2 cytokines such as C-X-C motif chemokine ligand 9 (CXCL9). Instead of having direct antiviral properties, IFN-2 cytokines focus on promoting innate and immunological memory through functions of increasing NK cell activity, inflammation, antigen presentation, and recruitment of leukocytes to the infected tumour site (71). In the case of oncolytic virotherapy, secretion of these immunostimulatory IFN-2 cytokines can also promote a more robust anti-tumour immune response. Indeed, our research group has shown that VSVΔ51 encoding IFN-ɣ is effective in slowing tumour growth, prolonging survival and driving anti-tumour immunity in *in vivo* models of mammary adenocarcinoma (72).

Both IFN-1 and IFN-2 pathways are subject to fine-tuning by other co-activators and signaling pathways. For example, cAMP response element binding (CREB)-binding protein (CBP) is a co-activator with histone acetyltransferase activity. Through recruitment by STAT transactivation domains, CBP remodels chromatin to increase genomic availability to cooperatively promote transcription downstream to STAT (73). Epidermal growth factor

receptor (EGFR) signaling, typically responsible for cell growth and differentiation events, has also been shown to independently increase STAT1 phosphorylation (74, 75).

1.5 Resistance to oncolytic virotherapy

When oncolytic virotherapy was still in its infancy, researchers hypothesized that tumour cells would be particularly susceptible to infection where IFN mechanisms are typically defunct. Malignant transformation favours downregulation of IFN-1 pathways given the inherent antitumour activity of ISGs (76, 77); it has been estimated that 65-70% of cancer cells harbour some defects in their IFN response (78). For example, macrophage-derived RAW cancer cells have lower expression of IFN-1 effectors (*e.g.,* RIG-I, IRF3, IFN-β) compared to their primary macrophage counterparts. Subsequently, RAW cells were found to be especially susceptible to oncolytic Newcastle disease virus (NDV) infection (79). In another study, when the transcriptomes of patient bladder cancer tumour cores were assessed by microarray, it was found that IFNAR expression was decreased relative to normal bladder tissue and this correlated with increased susceptibility to oncolytic VSV (80).

However, early pre-clinical studies and clinical trials with oncolytic virotherapy quickly revealed that not all tumours are equally susceptible to infection owing to intact or only partially defective anti-viral responses (47, 81). One study found that across a panel of sarcoma cell lines, 3 of the 8 cell lines had high baseline upregulation of RIG-I and IFIT1 expression, which correlated with resistance against oncolytic MeV (82). Similarly, another study found high heterogeneity in a panel of pancreatic ductal adenocarcinoma in their ability to respond to IFN-α/β. The subset of cell lines with constitutive activation of ISGs (*e.g.,* MxA, OAS) were found to be resistant to oncolytic VSVΔ51 (83). To further complicate the matter, tumour

microenvironments can also be contributory to oncolytic virotherapy resistance. External IFN stimulation from surrounding CD68+ tumour-associated macrophages can activate JAK/STAT in tumour cells resulting in functional expression of ISGs (84). Accordingly, another study demonstrated that the depletion of peripheral macrophages was able to increase viral titers of oncolytic HSV-1 by in murine models of glioma (85). Altogether, it is apparent that oncolytic virotherapy resistance can be at least in part attributed to residual tumour IFN-1 activity.

1.5.1 Viral sensitizing compounds

Given the resistance to OVs as a monotherapy, several strategies have been explored in attempt to circumvent this heterogeneity in resistance amongst patients. To overcome these challenges in recent years, the field has explored combining OVs with selected pharmacological compounds in attempt to boost anti-tumour efficacy. Indeed, several classes of compounds with viral sensitizing properties have been explored: classic chemotherapy agents, epigenetic modulators, PI3K/mTOR pathway inhibitors, and compounds with other modes of action (86). Given their immunosuppressive nature, traditional chemotherapeutics have been shown to boost OVs by suppressing immune-mediated virus neutralization and immune cell activation events. However, for the purposes of this thesis, we will focus on compounds that specifically impinge upon the IFN-1 pathway to increase OV infectivity.

Direct pharmacological inhibition of the JAK/STAT pathway compromises the cellular IFN-1 response. Accordingly, ruxolitinib, a JAK/STAT inhibitor, has been shown to abrogate resistance to VSV and HSV-mediated OV (39, 87, 88). By inhibiting STAT1 phosphorylation, ISG expression was reduced to render resistant tumour cells susceptible to infection and ultimately, improved survival rates in *in vivo* murine models. Heterogeneity in residual IFN-1

activity in tumour types can also be attributed to differences in epigenetic silencing via DNA promoter hypermethylation and suppressive histone modifications (78). By decreasing ISG transcriptional availability using histone-deacetylase (HDAC) inhibitors, studies have demonstrated this combinational strategy improves OV therapeutic efficacy, even in the presence of exogenously added IFN-β (89, 90). At the protein translation level, PI3K/mTOR are relevant targets given their control of global protein translation. Inhibition of this pathway has been proposed to preferentially suppress IFN-1 owing to the translational regulation of IRF-7, a key modulator of IFN-1 and IFN-1 effectors (91). Rapamycin, a well-established mTOR inhibitor, has been shown to improve VSV efficacy in an aggressive rat glioma model via IFN-1 production blockade (92).

Diallo *et al.* applied a high-throughput screening approach using diverse chemical libraries to identify novel compounds that could potentiate VSVΔ51 infectivity in a murine mammary carcinoma cell line. One identified compound (3,4-dichloro-5-phenyl-2,5-dihydrofuran-2-one), named viral sensitizer 1 (VSe1), was found to increase VSVΔ51 viral replication and spread by 1,000-fold, improved survival rates in murine *in vivo* models and increased VSVΔ51 viral infectivity in primary human clinical patient samples (93). The results of this hallmark paper cultivated the focus of our research group, which is to discover novel IFN-antagonizing compounds with viral sensitizing abilities, and to characterize their combinational impact on OV therapeutic efficacy.

Our research group has since identified and characterized several other compounds with viral sensitizing ability. Structural derivatives of VSe1 were developed to maintain selectivity of VSe1 to tumour cells, while simultaneously increasing the potency of VSVΔ51 viral titer enhancement (94). Microtubule destabilizers (MDA) such as colchicine were identified in to

increase VSVΔ51 viral spread through suppression of IFN-1 mRNA translation, protein expression and secretion. MDAs were also found to synergize with cytokines secreted in response to viral infection to increase tumour cell killing (95). Dimethyl fumarate, an FDA-approved drug for psoriasis and multiple sclerosis, was also found to have a previously appreciated role in IFN-1 suppression and potentiation of OV. Through blockade of NF-κB nuclear translocation, the production of IFN-β and downstream ISGs are inhibited by DMF. Combinational treatment with DMF and VSVΔ51 in resistant syngeneic and xenograft *in vivo* tumour models demonstrated increased intratumoural infection and overall survival compared to either monotherapy (96). Further exploration of combinational regimens using these compounds with viral sensitizing properties appears to be a promising avenue for establishing the use of OV in the clinic.

1.6 Vanadium-based compounds

Vanadium is a naturally-occurring transitional metal that is physiologically found in trace amounts in the human body and has various functions in both health and disease (97). This element exists in a variety of oxidation states from -III to +V, but mainly as a vanadate anion (VO_3^-) in extracellular compartments, or as a vanadyl cation (VO_2^+) in intracellular compartments. While vanadium toxicity is an uncommon event, its role in human health has not yet been fully established. However, given its trigonal pyramid geometry and natural negative charge, vanadium has a unique, natural property to operate as a pan-phosphatase (PP) inhibitor. By imitating a phosphate group, vanadium can slot into the active site of many PPs, both serine/threonine and tyrosine types, for reversible and competitive inhibition (98, 99).

Currently, the most commonly used indication for vanadium is as vanadyl sulfate, which has been touted as a bodybuilding supplement to increase muscle gain, reduce risk of fat accumulation, and improve bone integrity. These claims however remain controversial and have even been disproved by several studies (100). In medical applications, a wide range of properties of vanadium have been reported including anti-viral, anti-bacterial, anti-fungal, anti-cancer, anti-hypercholesterolemic, anti-obesity, cardioprotective and neuroprotective effects (101). At the time of writing, its more advanced indication is for the treatment for diabetes (102). With respect to cancer, the first instance of the anti-neoplastic properties of vanadium was described in 1984, where the study demonstrated that dietary vanadyl sulfate was able to prolong median cancer-free survival in an *in vivo* rat model of mammary carcinogenesis (103). Follow-up studies suggested that this mechanism could be attributed to vanadium's properties of anti-proliferation, apoptosis induction and cell cycle arrest through upregulation of tumour suppressor p53 (104). Since then, vanadium's anti-tumour properties have also been observed in other breast, colon, liver, blood and connective tissue cancers (105). Despite all this evidence, none of these studies have been able to translate into an approved therapy given its unfavourable toxicity at the required therapeutic doses. Taken together, any advancement of vanadium into the clinic remains unclear at this time (101).

1.6.1 Viral sensitizing properties of vanadium-based compounds

Recently, our group has identified a secondary use for vanadium compounds to have viral sensitizing properties for oncolytic virotherapy. In this original study, Selman *et al.* demonstrated that the addition of vanadium subverts the antiviral IFN-1 response towards a pro-inflammatory, death-inducing IFN-2 response in tumour cells (106). This immune profile

is subsequently favourable for OV infectivity and the vanadium + VSVΔ51 combinational therapy showed superior therapeutic outcomes compared to either monotherapy across multiple refractory murine tumour models *in vivo*. Additionally, supported by prior evidence that vanadium is immunomodulatory (107), the addition of vanadium increased immune cell infiltration into the tumour site and improved the induction of anti-tumour immunological memory by VSVΔ51. A similar phenomenon has been described between vanadium and Newcastle disease virus (NDV) although here innate immune cells were more predominantly involved (108). Together, this ultimately contributes to greater tumour control and provides a more durable cure against future recurrence. The study also identified differential activation of STAT1 and STAT2, where vanadium blunted the IFN-1 response by inhibiting STAT2 phosphorylation but maintained STAT1 nuclear accumulation to favour IFN-2 signaling. However, the exact mechanism of action by which these properties are conferred remained unknown.

1.6.2 Targeting the cellular phosphatome

Phosphorylation is a common post-translational modification used to regulate the activity of intracellular protein effectors. Through the covalent addition of a phosphate group to a protein by a regulatory kinase, the phosphate negative charge induces conformational change to regulate activity. This process can then be reversed in most cases by PPs to restore the original conformation. It is estimated that between 1/3 – 2/3 of the eukaryotic proteome is regulated by phosphorylation (109), making pharmacological modulation of phosphorylation an attractive therapeutic opportunity. Indeed, as of 2021, 71 small-molecular kinase inhibitors have been given FDA-approval across a large span of diseases with another estimated 110

kinase targets under investigation by clinical trial (110). On the other hand, only 6 PP inhibitors are currently in clinical trial with none clinically approved. This difference can be attributed to several reasons: 1) a highly conserved active site or phosphatase binding pocket makes engineering specificity difficult, and 2) the positively charged active site challenges cell membrane permeability (111, 112).

1.6.3 RNA interference and OVs

RNA interference (RNAi) describes the mechanism of gene expression knockdown by disrupting cellular mRNA levels using short sequences of non-coding RNA such as small interfering RNA (siRNA). Depending on the siRNA sequence, delivery of these 21-23 nucleotide RNA strands can knockdown expression of any gene target, conferring incredible versatility. While RNAi therapeutics are faced with obstacles regarding delivery and processing efficiency, the use of RNAi allows for creative therapies for targets that cannot be typically inhibited by pharmacological compounds (113).

In the case of cancer therapy, siRNA has been successfully used across a multitude of targets. A good example of this would be the *KRAS* oncogene, whose mutation in several cancer subtypes results in hyperactivation of cell proliferation and transformation pathways. Exogenous introduction of siRNA targeting KRAS has shown efficacy in knocking down KRAS expression resulting in tumour control and improved survival in *in vivo* murine tumour models (114, 115). A phase 1 clinical trial using siRNA targeting KRAS in KRAS-mutated pancreatic ductal adenocarcinoma is currently underway (NCT03608631). Likewise, other siRNA targets can be applied to induce tumour cell death, restimulate the immune system by

silencing immune checkpoints, or modulate the tumour microenvironment to discourage malignant growth (116).

OVs make for an intriguing avenue of exploration for the delivery of RNAi in a cancer context. Firstly, viruses are stable platforms for delivery of genetic material and are naturally resistant to degradation in the extracellular matrix. Non-replicating viral platforms are already well-established to successful delivery genetic material into cancer cells (117). Secondly, the natural tropism and oncolysis potential of different viruses respectively allows for tumour selectivity and therapeutic synergy with the siRNA therapeutic. Furthermore, this tissue tropism can be artificially modified using a variety of strategies (118). Finally, the production process for genetically engineered viruses has become increasingly simple and cost-effective. A full review on the cassette design, target selection, and efficiency of siRNA delivery by OVs for cancer therapy can be found in Appendix A (116).

1.7 Neddylation

The above, as well as other examples such as HDAC inhibitors (119), illustrate the potential to exploit post-translational modifications to alter cell-signalling to promote OV efficacy. As will be explored further in Chapter 4, neddylation is another potential opportunity to this end. Neddylation is a post-translational regulatory mechanism by which neddylation-activating enzyme (NAE) complex conjugates neuronal precursor cell-expressed developmentally down-regulated protein 9 (NEDD8) onto target proteins to regulate their activity. This neddylation process, which has crucial roles in multiple pathophysiological processes, is as follows. Firstly, deneddylase 1 (DEN1) processes NEDD8 by removing 5 amino acids from the C-terminus. The processed NEDD8 is then activated using adenosine

triphosphate (ATP) by the E1 enzyme, which is the NAE complex comprised of a ubiquitin-like modifier activating enzyme 3 (UBA3) and NAE E1 subunit 1 (APPBP1). Secondly, a transthiolation reaction transfers the activated NEDD8 to an E2 enzyme (UBE2M, UBE2F). Thirdly, with the activity of a NEDD8-E3 ligase (DCN1), the NEDD8 is transferred to the target protein substrate on a lysine residue (120).

The primary purpose of neddylation works alongside ubiquitination and assists in tagging proteins with ubiquitin for targeted, proteasome-mediated degradation to encourage protein turnover (121). At the intersection of these post-translational modification processes are cullin-ring ligases (CRL), which are the most common and best-characterized substrates for neddylation. Covalent attachment of NEDD8 onto CRL are required for its ubiquitin-transferring ability onto its respective substrates. Disruption of neddylation results in a variety of physiological consequences including cell cycle dysregulation, induction of DNA damage responses, apoptosis, tumorigenesis, and immunosuppression (122, 123). Indeed, dysregulation of neddylation has been implicated as a driver of malignancy in several tumour subtypes (124, 125).

1.7.1 Pevonedistat (MLN4924)

Pevonedistat, also known as MLN4924, is a first in-class NAE inhibitor developed by Takeda pharmaceuticals. As an adenosine monophosphate (AMP) mimetic, pevonedistat can be incorporated into the catalytic pocket of the NAE complex with NEDD8 instead of ATP. The resulting NEDD8-drug adduct cannot be used for subsequent reactions and halts the neddylation process (126). Despite having potent and specific neddylation inhibitory activity, pevonedistat is currently not approved for any clinical indication. In its most clinically

advanced indication in hematological cancer subtypes, the recent phase III PANTHER clinical trial found that a combination of pevonedistat and azacytidine chemotherapy was unable to improve event-free survival (EFS) compared to azacytidine alone despite showing promise in phase II trials (127, 128). Several clinical trials investigating the anti-tumour effect of pevonedistat in solid tumours and other hematological cancers are underway.

Through decreased CRL activation, pevonedistat stabilizes a plethora of protein targets, sparing them from degradation by the ubiquitin-proteasome system. In a cancer setting, aberrant proteome turnover promotes tumour progression, hence inhibition of protein degradation by pevonedistat has been proposed as a therapeutic opportunity (129). Indeed, a study by Soucy *et al.* was first to report that administration of pevonedistat induced cell-death through the DNA damage response, leading to tumour regression in xenograft models (122). In models of hematological cancers, other mechanisms have been proposed including stabilization of IκB-α to inhibit NF-κB signaling in tumours with constitutive NF-κB signaling or intracellular oxidative stress generation to induce apoptosis (130, 131).

Given its ability to impact such a large battery of cellular substrates, pevonedistat is also a potent immunomodulatory compound. From an immune cell standpoint, neddylation inhibition has demonstrated decreased activation and increased apoptosis in reacting lymphocytes through decreased local secretion of pro-inflammatory cytokines (*e.g.,* IL-6, TNF-α). At the cellular level, pevonedistat achieves this by inhibiting NF-κB nuclear translocation, which controls expression of these pro-inflammatory cytokines (123, 132). Reports have also demonstrated a neddylation-independent suppression of IFN-β secretion through blockade of IRF3 signaling (133).

1.7.2 Other NEDD8-activating enzyme (NAE) inhibitors

As the first compound in its class, pevonedistat expectedly has several drawbacks. Firstly, pevonedistat inhibits all neddylation activity in the cell, which ultimately results in high cytotoxicity and probability for side-effects through clinical use. Secondly, general stabilization of multiple substrate proteins could in principle promote the accumulation of oncogenic effectors during chronic regimentation. Thirdly, while pevonedistat is relatively specific, off-target cellular effects have been reported unrelated to neddylation inhibition (134). Finally, several phase I clinical trials have revealed that the use of pevonedistat as a monotherapy has limited applications, likely owing to intra-tissue heterogeneity in neddylation activation (135).

Alternatively, several other compounds have been identified to block neddylation either through covalent modification of NAE similar to pevonedistat, or via another non-covalent mechanism. Structure-activity relationship (SAR) analyses were able to identify structural determinants of pevonedistat, which were subsequently modified to increase both selectivity and potency (136). TAS4464 is another front-runner NAE inhibitor developed by Taiho Pharmaceuticals that is reportedly ten times more potent compared to pevonedistat, inhibiting CRL activation and showing anti-tumour activity at nanomolar concentrations in a covalent matter (137). Moreover, to improve substrate selectivity and reduce off-target effects, inhibitors have also been developed for specific CRLs to only stabilize certain substrates as opposed to the entire neddylation system; however, none have been found to be as effective as pevonedistat thus far (138).

1.8 Rationale and hypothesis

Despite recent advancements in oncolytic virotherapy, tumour heterogeneity in antiviral defences, namely in the IFN-1 response, continues to represent a significant hurdle for its clinical translation. Thus, the discovery of novel strategies to transiently modulate the antiviral response to sensitize resistant tumours to OVs is warranted. Given the previous successes by our research group and others in increasing OV efficacy through genetic and pharmacological antagonism of the IFN-1 response, the aim of this thesis is to identify and characterize novel mechanisms that govern the IFN-1 response and exploit these mechanisms to improve the therapeutic efficacy of oncolytic virotherapy. The overarching hypothesis of this thesis is that some chemical or genetic manipulations of cellular processes can indirectly antagonize antiviral IFN-1 responses and modulate pro-inflammatory pathways to potentiate oncolytic virotherapy.

In Chapter 2 of this thesis, we build upon previous work establishing the OV sensitizing ability of vanadium-based compounds via subverting the IFN-1 response to the IFN-2 response through PP inhibition (106). In this first sub-hypothesis, *we hypothesize that the vanadium viral sensitizing mechanism of action involves the EGFR pathway*, as suggested by an initial high-throughput kinase inhibitor screen.

In Chapter 3, we perform a high-throughput screen in an effort to identify the key PPs that are responsible for vanadium's viral enhancing activity. While effective in potentiating RNA-viruses such as VSV, measles and NDV, vanadium treatment is actually detrimental for the growth of DNA-viruses, namely HSV-1 and VACV, both of which are further along the clinical approval process (106). Indeed, it has been shown that these larger viruses require PP activity as part of their lifecycle (139). For this reason, it is in our interest to identify the specific

PPs inhibited by vanadium that contribute to its viral sensitizing ability. Moreover, by only inhibiting relevant PPs, we could potentially reduce the likelihood for adverse side effects by sparing all other uninvolved PPs. We found that ACP2, our top candidate PP, is involved in the anti-viral IFN-1 response. Therefore, as a second sub-hypothesis, *we hypothesize that viral sensitizing effects can be reproduced through the knockdown of key PPs such as ACP2 using siRNA and viral engineering strategies.*

Finally, in Chapter 4, we follow from discoveries made during the kinase inhibitor screen that was designed both to elucidate the mechanism of action of Vanadium (Chapter 2) as well as uncover novel enhancers of VSVΔ51. We introduce a candidate compound from this screen that has viral sensitizing properties: pevonedistat, a first in-class NAE inhibitor. In my third sub-hypothesis, *we consider that inhibition of neddylation regulatory mechanisms lead to the downregulation of IFN-1 and can sensitize cancer cells to oncolytic virotherapy*.

Chapter 2. Dependency of EGFR activation in Vanadium-based Sensitization to Oncolytic Virotherapy

Boaz Wong[1,2], Anabel Bergeron[1,2], Nouf Alluqmani[1,2], Glib Maznyi[1], Andrew Chen[1], Rozanne Arulanandam[1], Jean-Simon Diallo[1,2]*

[1] Centre for Innovative Cancer Research, Ottawa Hospital Research Institute, Ottawa, Ontario, Canada, K1H 8L6. [2] Department of Biochemistry, Microbiology and Immunology, Faculty of Medicine, University of Ottawa, Ottawa, Ontario, Canada, K1H 8M5. * denotes corresponding author.

Published on June 16, 2022 in *Molecular Therapy – Oncolytics*

2.1 Abstract

Oncolytic virotherapy is a clinically validated approach to treat cancers such as melanoma; however, tumor resistance to virus makes its efficacy variable. Compounds such as sodium orthovanadate (vanadate) can overcome viral resistance and synergize with RNA-based oncolytic viruses. In this study, we explored the basis of vanadate mode of action and identified key cellular components in vanadate's oncolytic virus-enhancing mechanism using a high-throughput kinase inhibitor screen. We found that several kinase inhibitors affecting signaling downstream of the epidermal growth factor receptor (EGFR) pathway abrogated the oncolytic virus-enhancing effects of vanadate. EGFR pathway inhibitors such as gefitinib negated vanadate-associated changes in the phosphorylation and localization of STAT1/2 as well as NF-κB signaling. Moreover, gefitinib treatment could abrogate the viral sensitizing response of vanadium compounds in vivo. Together, we demonstrate that EGFR signaling plays an integral role in vanadium viral sensitization and that pharmacological EGFR blockade can counteract vanadium / oncolytic virus combination therapy.

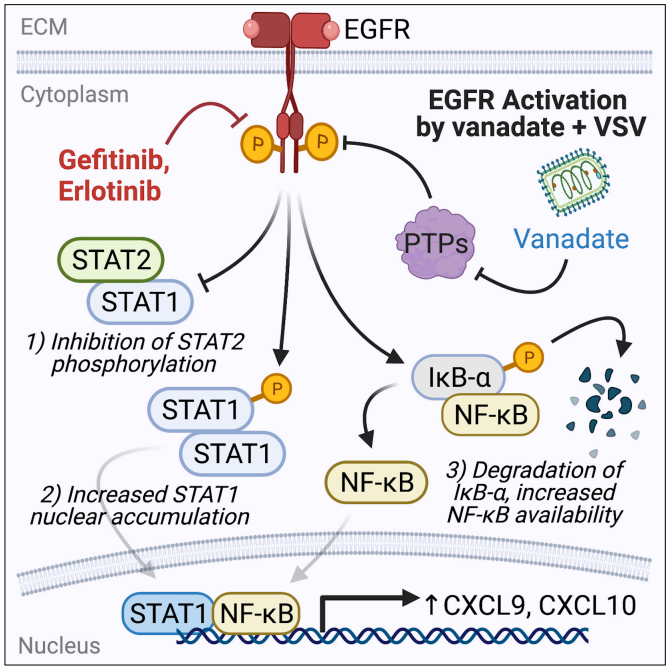

2.2 Introduction

Oncolytic virotherapy (OV) is a class of biotherapeutics that utilizes viruses to selectively infect, replicate within, and lyse tumor cells while triggering a lasting anti-tumor immune response (140–142). OV therapy can result in lasting cures with an improved long-term side effect profile when compared to conventional chemotherapy modalities (143). Over the last several years, oncolytic virotherapy has made tremendous progress towards clinical use. Hundreds of different OV products using different viral platforms and genetic payloads are currently in clinical trial (30). Notably, the clinical regulatory approval of talimogene laherparepvec (T-VEC), a genetically engineered herpes simplex virus (HSV-1) for the treatment of melanoma, has unveiled the potential of OVs as a staple cancer therapeutic in years to come (26, 27).

Unfortunately, clinical developments of OV monotherapies have stalled in part due to frequent tumor resistance to infection (28). A key mediator of the resistance to OV therapy is the type 1 interferon (IFN-1) response which induces antiviral gene expression and inhibits viral spread (83, 84). To combat this, small molecules that transiently modify the interferon response have been investigated in order to recover oncolytic efficacy (86, 93, 94, 144). Our group has identified sodium orthovanadate (vanadate) and other vanadium-based compounds as being capable not only of attenuating the antiviral IFN-1 response, but also simultaneously increasing pro-inflammatory activity through type II interferon (IFN-2) signals when co-administrated with the oncolytic vesicular stomatitis virus (VSVΔ51) (106, 145). In addition to reducing IFN-1 responses, vanadate treatment increases virus-induced pro-inflammatory cytokines including interferon-beta (IFN-β), tissue necrosis factor alpha (TNF-α) and interleukin 6 (IL-6). We have previously shown that the effect of vanadate on the IFN-1 and

IFN-2 response correlates with the accumulation of phosphorylated STAT1 (signal transducer and activation of transcription) transcription factor in the nucleus and reduced STAT2 expression/activation (106). However, the exact cell signaling cascade that gives rise to this effect currently remains unknown.

Vanadium-based compounds confer their biological effects through pan-inhibition of protein tyrosine phosphatases (PTP) in part through competition with phosphate (98, 99). PTPs normally elicit their effects through the de-phosphorylation of substrates, counteracting the action of kinases that phosphorylate these same substrates. Given this homeostasis, vanadium maintains the phosphorylated state of multiple cellular substrates, typically resulting in the persistent activation of their downstream signal transduction pathways. By shifting homeostasis towards the activity of kinases, inhibiting PTPs using vanadium therefore leads to multiple effects, including drug resistance reversal, inhibition of cellular proliferation and of particular interest, immunomodulation (146). The objective of the current study was to further elucidate the mechanism of action by which vanadium-based compounds confer viral sensitizing properties with intentions to further understand OV resistance patterns and to inform the design of improved viral sensitization strategies. As a strategy to achieve greater mechanistic insight, we rationalized that systematically testing the impact of kinase inhibition on vanadate's OV-enhancing effect might allow us to identify key shared PTP/kinase target substrates implicated in mediating the enhancing effects of vanadate.

2.3 Results

High throughput kinase inhibitor screen identifies importance of EGFR in viral sensitization

We hypothesized that, as a pan-PTP inhibitor, vanadate might potentiate virotherapy by promoting the phosphorylation state of one or more proteins relevant in modulating the response to IFN-1. Inhibition of related kinases would thus reverse the required phosphorylation states for IFN-1 inhibition (Fig. 2.1A). To pinpoint these relevant kinases, 800 small molecules (kinase inhibitors and various tool compounds) were tested using a reverse screen strategy. Briefly, 786-0 cells, a human renal adenocarcinoma cell line naturally resistant to VSVΔ51 infection (93), were treated with an optimized vanadate concentration previously shown to enhance the activity of VSVΔ51 in these cells. Kinase inhibitor library compounds (or vehicle control) were added prior to infection with VSVΔ51 encoding firefly luciferase (VSVΔ51-FLuc). The use of VSVΔ51-FLuc allowed us to simultaneously measure the impact of treatments on virus output via a secondary assay measuring viral expression unit output from supernatants (viral expression units or VEU, akin to viral titer (147)) as well as cellular metabolic activity by resazurin assay (Alamar blue), a surrogate for detection of cell viability and cytopathic effect. Hits from this screen were defined as kinase inhibitors that counteracted vanadate's viral sensitization capacity either through a reduction in virus output or through a reduction in the cytopathic effect, or both. Kinase inhibitors that simultaneously prevented vanadate-mediated oncolysis to a threshold of 60% and decreased viral output below a log fold-change threshold of 1.5 are shown in the upper left quadrant of Fig. 2.1B. Addition of selected kinase inhibitor hits within the upper left quadrant restored cell viability and/or fold-change viral output to levels not significantly different from mock treated, infected controls

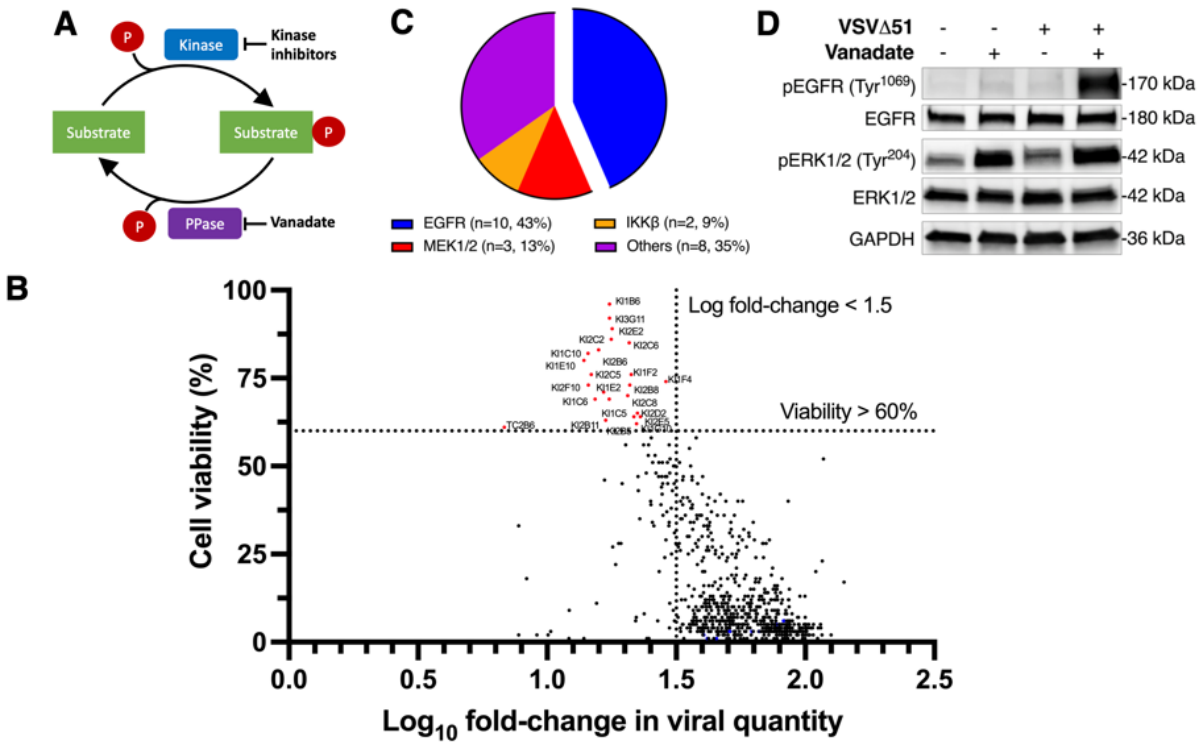

Fig. 2.1. Identification of EGFR signaling to vanadate viral sensitization (A) Schematic depicting kinase-phosphatase homeostasis as a mechanistic principle for understanding vanadate-mediated viral sensitization, PPase = phosphatase. (B) Human renal carcinoma 786-0 cells were pre-treated for 4 hours with vanadate (125μM) and kinase inhibitors (1μM), then subsequently infected with VSVΔ51-FLuc (MOI 0.1). Viability was assessed 48 hours by resazurin (Alamar blue) assay after infection and measures were normalized against VSVΔ51 plate controls. Viral titers were quantified 48 hours post infection (hpi) by high-throughput titration. Plot shows cell viability against log fold-change in viral titers of all compounds. Compiled viability and viral titer data highlights a subset of 23 kinase inhibitors that simultaneously prevent vanadate's oncolysis and viral replication, depicted in red (Table 1). Vanadate + VSVΔ51 plate controls are depicted in blue (n=2-3). Dotted lines represent viability and titer thresholds (60% and 1.5 fold-change respectively). (C) Pie chart representing relative proportions of molecular targets of shortlisted kinase inhibitors identified in (B)**.** (D) 786-0 cells were pre-treated ± vanadate (150μM), then infected with VSVΔ51 (MOI 0.1). Cell lysates were collected 24hpi and probed for phosphorylated EGFR, total EGFR, phosphorylated ERK1/2, total ERK1/2 and GAPDH by western blot.

(Fig. S2.1, S2.2). A total of 23 small molecule kinase inhibitors were found to antagonize vanadate's viral sensitizing effect (listed in Table 2.1). Nearly half of the selected inhibitors (43%) target EGFR, while several others (13%) target the downstream mitogen-activated protein kinase kinase (MAP2K or MEK1/2) (Fig. 2.1C).

Inhibition of the EGFR pathway abrogates vanadate-mediated viral infectivity

EGFR is a receptor tyrosine kinase found on the cellular membrane, responsible for regulation of cell proliferation and survival events (148). Given that over half of the identified hits targeted the EGFR-MEK1/2 signaling axis, we sought to first examine the activation status of these two kinases upon combined treatment with vanadate and VSVΔ51 in 786-0 cells. Densitometry following western blotting uncovered that the phosphorylation ratios of EGFR and the downstream extracellular signal-regulated kinase 1/2 (ERK1/2) were increased with vanadate and VSVΔ51 combinational treatment compared to all other conditions (Fig. 2.1D, S2.3).

By western blot, we found that a concentration as low as 1μM of the EGFR inhibitor gefitinib in human 786-0 cells was sufficient to abrogate EGFR phosphorylation induced by vanadate alone and in combination with VSVΔ51 (Fig. 2.2A). Similar results were obtained using the ERK1/2 inhibitor UO126 albeit at higher concentrations (Fig. S2.4). EGFR inhibition using gefitinib and erlotinib, or of MEK1/2 (using UO126), dose-dependently decreased the vanadate-enhanced growth of VSVΔ51 tagged with a green fluorescent protein (GFP) marker in 786-0 cells as determined by phase and fluorescent microscopy images captured 24-hour post infection (hpi) (Fig. 2.2B, S2.5, S2.6). As expected, control cells treated with vanadate

Table 2.1: Full list of hits of the kinase inhibitor high-throughput screen

ID	Drug	Target(s)	Developmental stage
KI1C5	Gefitinib, Iressa, ZD1839	EGFR (ERBB1, HER1), ErbB2 (TKR1, HER2, NEU)	Approved: metastatic non-small cell lung cancer
KI1C6	Lapatinib ditosylate, Tykerb, GW572016	EGFR (ERBB1, HER1), ErbB2 (TKR1, HER2, NEU)	Approved: advanced or metastatic breast cancer
KI1C10	Vandetanib, Zactima, ZD6474, AZD-6474	EGFR (ERBB1, HER1), KDR (VEGFR2, VEGFR, FLK1), RET, ABL1 (ABL), KIT (c-KIT), FLT1 (VEGFR1), FLT4 (VEGFR3), TRKA (TRK)	Approved: local or metastatic medullary thyroid cancer
KI1E2	Erlotinib HCl, CP-358774, OSI-774, Tarceva, NSC-718781, RG-1415, Ro-50-8231	EGFR (ERBB1, HER1), ErbB2 (TKR1, HER2, NEU)	Approved: metastatic non-small cell lung cancer, metastatic pancreatic cancer.
KI1E10	GW2974	EGFR (ERBB1, HER1), ErbB2 (TKR1, HER2, NEU)	Pre-clinical
KI1F2	GW583340 dihydrochloride	EGFR (ERBB1, HER1), ErbB2 (TKR1, HER2, NEU)	Pre-clinical
KI1G10	BIBX 1382 dihydrochloride, Falnidamol	EGFR (ERBB1, HER1)	Clinical trial: adult solid tumors.
KI2B6	PD-153035, AG-1517, Compound 32, SU-5271, ZM-252868, WHI-P79	EGFR (ERBB1, HER1)	Pre-clinical
KI2C2	BIBW-2992, Tovok, Afatinib	EGFR (ERBB1, HER1)	Approved: NSCLC
KI2C5	CI-1033, Canertinib, PD-183805, SN-26606	EGFR (ERBB1, HER1), ErbB2 (TKR1, HER2, NEU) - Irreversible	Clinical trials: breast cancer
KI1B6	PD-184352, CI-1040	MAP2K1 (MEK1), MAP2K2 (MEK2), Erk2 (ERK, p38), RAF1 (c-Raf)	Clinical trials: lung, breast, pancreatic and colorectal cancers
KI2B11	AZD6244, ARRY-142886, AZD-6244, Selumetinib, ARRY-886	MAP2K1 (MEK1), MAP2K2 (MEK2), Erk2 (ERK, p38)	Clinical trials: carcinoma, NSCLC, melanoma
KI2E2	SL327	MAP2K1 (MEK1), MAP2K2 (MEK2)	Pre-clinical
KI3G11	IMD 0354, IMD-0354	IKKb (IKK2)	Pre-clinical
KI2C6	SC-514	IKKb (IKK2)	Pre-clinical
KI1F4	IRAK-1/4 Inhibitor I	IRAK1 (IRAK)	Pre-clinical
TC2B6	NVP-AUY922, AUY922, VER-52296	Hsp90 inhibitor	Clinical trials: lymphoma, breast cancer, hematologic neoplasms
KI2B5	NU-7026, LY-293646	DNAPK (DNA-PKcs)	Pre-clinical
KI2B8	Sal003	eIF2a	Pre-clinical
KI2C8	Bosutinib, SKI-606, Bosulif	BCR, ABL1 (ABL), SRC (c-SRC), FGR (SRC2), LYN	Approved: leukemia
KI2D2	Ro-31-8220 mesylate, Bisindolylmaleimide IX	PKC	Pre-clinical
KI2E5	SU 4312, DMBI	KDR (VEGFR2, VEGFR, FLK1)	Pre-clinical
KI2F10	API-2, Triciribine, NSC154020, TCN, Tricibine, VQD-002	AKT1 (PKBa)	Clinical trials: leukemia, ovarian and breast cancer

alone showed significant GFP signal indicating high viral infection. To confirm that this effect was not due to increased cell toxicity elicited by the kinase inhibitors in combination with vanadate, Alamar blue assays were performed, and we observed that cell viability did not fall below 75% viability even at the highest concentrations of kinase inhibitors during vanadate co-treatment (Fig. 2.2C), doses much higher that what was found to inhibit viral growth.

The above experiment was then repeated using vanadate-inhibitory concentration ranges of gefitinib and UO126, and infected cell supernatants were titered for viral output assessment by standard plaque assay (Fig. 2.2D, S2.7). As previously reported, vanadate-treated 786-0 cells produced high viral titers compared to the mock control and addition of increasing concentrations of EGFR inhibitor in the presence of vanadate steadily decreased the viral titer, down by ~100-fold at 50μM of gefitinib – a non-toxic dose (Fig. 2.2C). Furthermore, expression of the VSV matrix (M) and nuclear (N) genes were significantly decreased upon addition of gefitinib compared to vanadate-only treated cells 24h post infection as measured by quantitative polymerase chain reaction (qPCR) (Fig. 2.2E). In line with previous observations that vanadate potentiates other RNA-based viruses, we found that EGFR inhibition also abrogated the vanadate-mediated sensitization of 786-0 cells to measles virus (Fig. S2.8, S2.9).

To test whether therapeutic antibodies against EGFR (cetuximab) could achieve the same effect as chemical inhibitors, 786-0 cells were pre-treated with vanadate and varying concentrations of cetuximab (50 ng/mL – 5 μg/mL) for 4 hours, then infected with VSVΔ51 (MOI 0.05). While cetuximab had inhibitory effects on its own at higher concentrations, the ability for vanadate to increase VSVΔ51 viral titer was greatly abrogated across all doses of

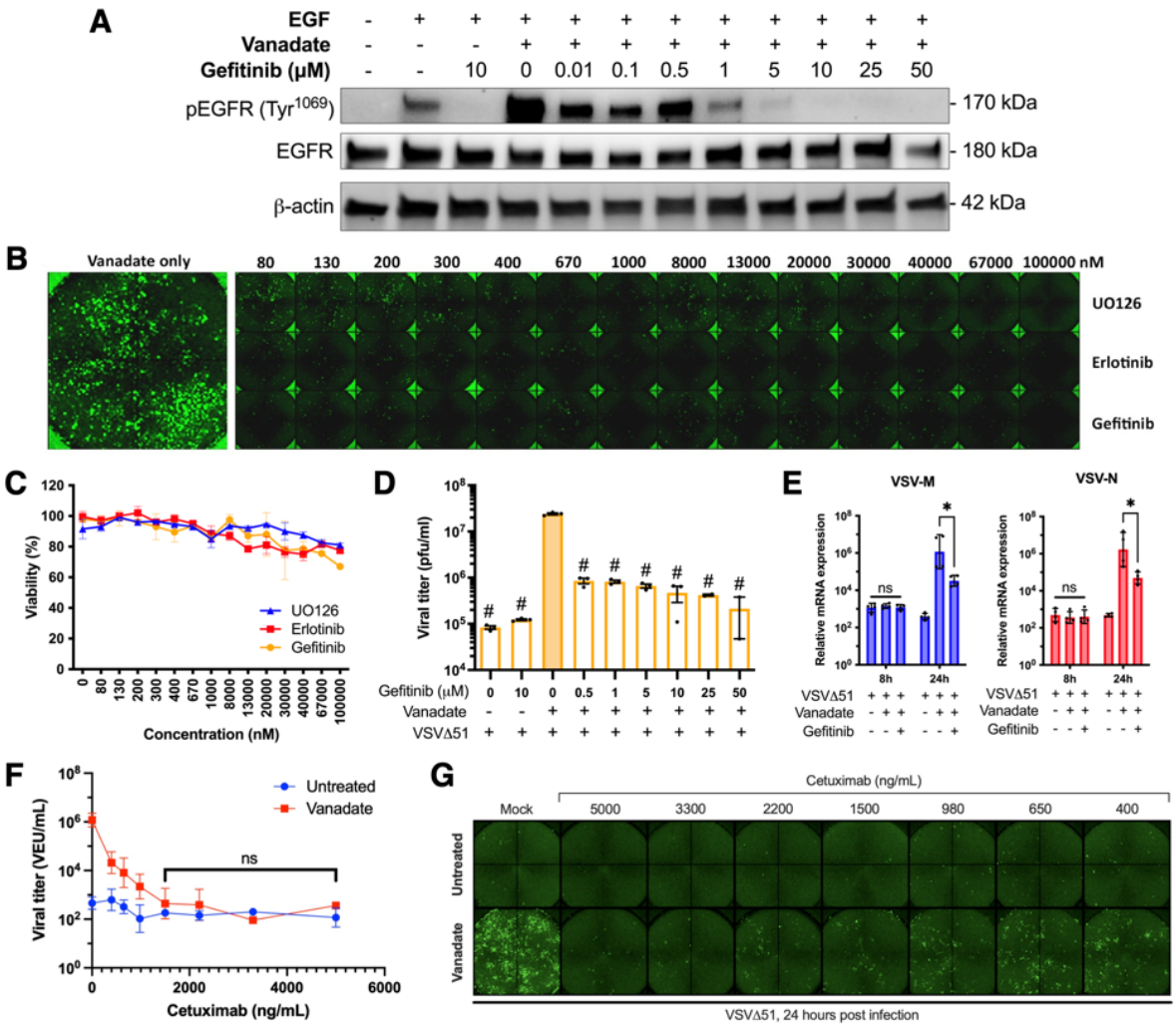

Fig. 2.2. Inhibition of the EGFR pathway abrogates vanadate-mediated viral infectivity. (A) Human 786-0 renal carcinoma cells were pre-treated with or without vanadate (150 μM) and varying concentrations of gefitinib (0 – 50μM) as indicated for four hours. Cells were then treated with 10ng/mL EGF for 10 minutes and lysates were probed by western blot for phosphorylated EGFR, total EGFR and β-actin. (B-C) 786-0 cells were simultaneously treated with varying concentrations of gefitinib, erlotinib or UO126 (0 – 100 μM) and vanadate (150 μM). Four hours later, cells were infected with VSVΔ51-GFP (MOI 0.1). (B) Fluorescence images were captured 24 hours post infection (hpi). (C) Cell viability was measured by resaruzin (Alamar blue) assay and expressed relative to untreated, uninfected cells. (D) Supernatants were collected and titered by viral plaque assay (n=3, mean ± SD; *P<0.05, #P<0.0001; one-way ANOVA compared to the infected VSVΔ51 + vanadate only condition as

indicated by the filled bar). (E) 786-0 cells were treated ± vanadate (150 μM) ± gefitinib (10 μM), then infected with VSVΔ51-GFP (MOI 0.1) 4 hours later. RNA was extracted from cell lysates at 8 and 24hpi and probed for VSV-M and VSV-N gene expression by qPCR (n=4, mean ± SD; *P<0.05, **P<0.01 by one-way ANOVA, n.s. denotes no significance). (F,G) 786-0 cells were pre-treated with or without vanadate (150 μM) and varying concentrations of anti-EGFR antibody cetuximab (500 – 5000 ng/mL) for 4 hours, then infected with VSVΔ51 (MOI 0.05). (F) Viral titer was determined 40hpi by high-throughput titration (mean ± SD; ns = no significance by two-way ANOVA). (G) Representative fluorescence images were captured 24hpi.

---

cetuximab, even at a minimal concentration of 400 ng/mL (Fig. 2.2F, 2.2G). Altogether, this data strongly supports a key role of EGFR signaling in eliciting vanadate's viral sensitizing effects.

Vanadate regulates STAT1 and STAT2 through EGFR to modulate the interferon response

The IFN-1 response is dependent on the phosphorylation and subsequent formation of STAT1-STA2 heterodimers. When combined with interferon response factor 9 (IRF9), the formed interferon-stimulated growth factor 3 (ISGF3) complex then translocates to the nucleus where it regulates the transcription of interferon-stimulated genes (ISGs) including the interferon-induced GTP-binding protein MX2. Conversely, the IFN-2 response, responsible for induction of pro-inflammatory genes such as CXCL9 and CXCL10 chemokines, is propagated through phosphorylated STAT1 homodimers binding to the respective IFN gamma-activated sequences (GAS) (31). In a previous study, we found that vanadate leads to increases in STAT1 phosphorylation with concomitant decreases in STAT2 phosphorylation

levels. This correlated with a shift from IFN-1 type toward IFN-2 type virus-induced gene expression profiles in a variety of cell types (106). This is supported by evidence that activation of the EGFR pathway and its downstream players including ERK1/2 compromise the antiviral IFN-1 defense through regulation of STAT signaling (149, 150). Therefore, we next sought to assess STAT dynamics in response to EGFR inhibition.

Human 786-0 cells pre-treated with or without vanadate and/or gefitinib were infected with VSVΔ51 and protein extraction was performed 24 hours post infection. As found in previous studies (106), probing whole cell lysates by western blot showed that following VSVΔ51 infection, vanadate increases phosphorylation of STAT1 and decreases phosphorylation of STAT2. While EGFR inhibition by gefitinib did not impact STAT1, it was interestingly able to rescue the otherwise decreased levels of STAT2 phosphorylation caused by vanadate / virus infection (Fig. 2.3A, 2.3B, S2.10). We were then interested to see whether EGFR inhibition could reduce vanadate/virus induced STAT1 nuclear translocation (106). Nuclear/cytoplasmic fractionation in samples treated with the same regimen indeed revealed increased phosphorylated and total STAT1 nuclear localization upon vanadate/virus treatment, which was abrogated by EGFR blockade by gefitinib (Fig. 2.3C). In parallel, normalization of STAT2 nuclear translocation in accordance with rescued STAT2 phosphorylation by gefitinib treatment was also observed. This was further confirmed using immunofluorescence. We found that upon stimulation using IFNβ, vanadate treatment led to concentrated nuclear localization of phosphorylated STAT1 compared to cells only treated with IFNβ, where nuclear phospho-STAT1 signal was more diffuse (Fig. 2.3D, S2.11). However, upon addition of

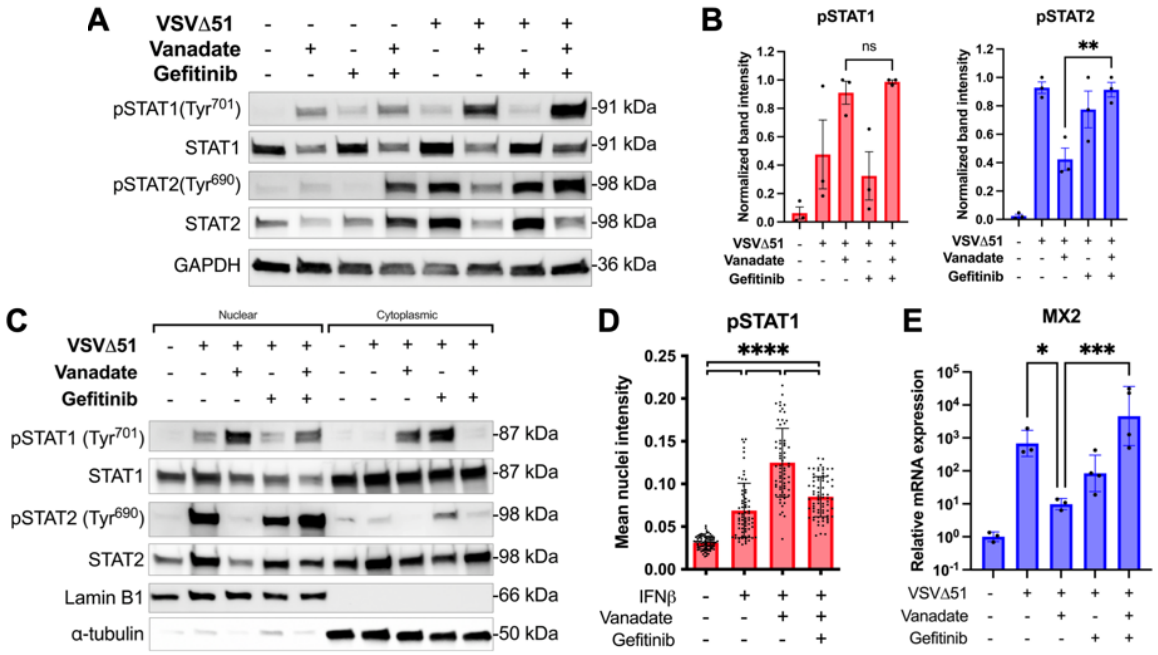

Fig. 2.3. Vanadate regulates STAT1 and STAT2 through EGFR to modulate the interferon response. (A-C,E) Human renal carcinoma 786-0 cells were treated ± vanadate (150μM) ± gefitinib (10μM), then subsequently infected with or without VSVΔ51-GFP (MOI 0.01). (A) Total cell lysates were collected 24 hours post infection (hpi) and probed for phosphorylated STAT1, total STAT1, phosphorylated STAT2, total STAT2 and GAPDH by western blot. Representative blots are shown. (B) Bands were quantified by densitometry relative to the actin loading control and expressed as a phosphorylated: total STAT1/2 ratio (n=3, mean ± SD; ns = no significance, **P<0.01 by one-way ANOVA). (C) Lysates were fractionated for nuclear and cytoplasmic fractions and probed for phosphorylated STAT1, total STAT1, phosphorylated STAT2, total STAT2, lamin B1 and alpha-tubulin by western blot. (D) 786-0 cells were treated ± vanadate (300μM) ± gefitinib (20μM) for 4 hours, then with IFNβ (100U/mL) for 1 hour. Cells were fixed and stained for phosphorylated STAT1 and nuclei with DAPI by immunofluorescence. Phospho-STAT1 nuclear intensity was quantified, and mean nucleus intensity graphed (n=3, mean ± SD; ****P<0.0001 by one-way ANOVA). Representative images can be found in Fig. S11. (E) RNA was extracted from cell lysates 24hpi and probed for *MX2* mRNA expression by qPCR (n=3, mean ± SD; ***P<0.001 by one-way ANOVA).

gefitinib, the concentration of nuclear phosphorylated STAT1 decreased markedly. Finally, coinciding with these observations, the addition of gefitinib restored the virus-induced upregulation of the downstream IFN-1 gene *MX2,* which is otherwise suppressed by vanadate in response to VSVΔ51 infection, as determined by qPCR (Fig. 2.3E). Altogether, these data support the possibility that EGFR signaling induced by vanadate/virus treatment leads to immunomodulation and improved viral growth by altering the phosphorylation status of STAT1/STAT2.

Vanadate promotes pro-inflammatory cytokine production through EGFR-NFκB activation

To gain additional insight into the vanadate viral-sensitizing mechanism, we performed in silico analysis on a previously published microarray dataset looking at the impact of combined vanadate and VSVΔ51 treatment in 786-0 cells (106). We selected genes that increased or decreased at least 3-fold in abundance in cells receiving combined vanadate and VSVΔ51 treatment. Then using the published TFactS tool(151), we found that the top predicted transcription factor to correlate with this differential gene expression profile was STAT1, confirming our previous and current findings. However, our in silico analysis also identified NF-κB as the second most likely involved transcription factor (Fig. 2.4A, S2.12-14). This was interesting given that two kinase inhibitor hits from our reverse screen (Table 2.1) target IκB kinase beta (IKKβ). Like gefitinib and UO126, the two IKKβ inhibitors, IMD-0354 and SC-514, reduced VSVΔ51-GFP infectivity as measured by GFP expression, even in the presence of vanadate (Fig. 2.4B, S2.15). This effect occurred within a broad drug treatment range leading to no more than a 25% decrease in cell viability (Fig. 2.4C).

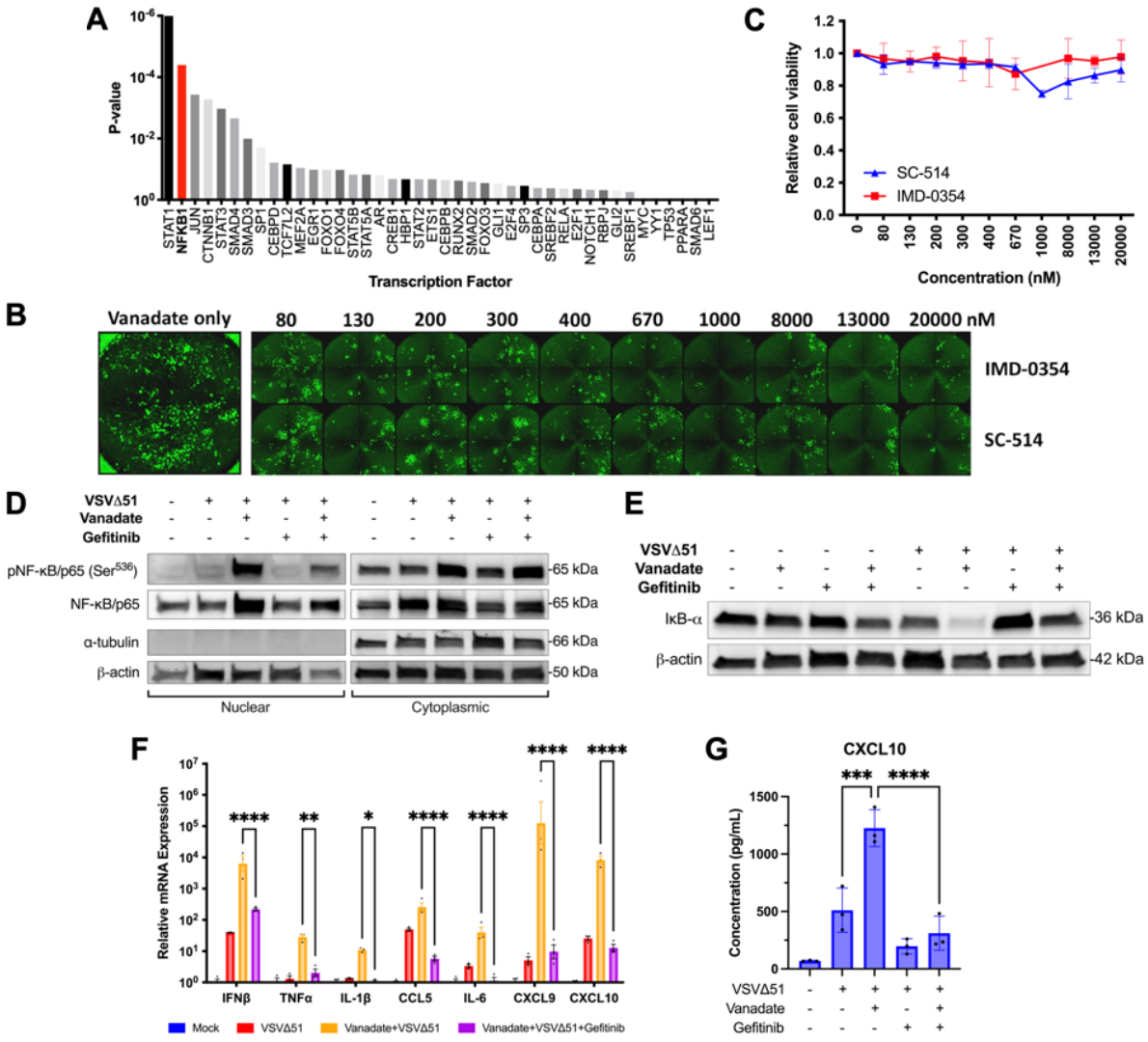

Fig. 2.4. Vanadate promotes pro-inflammatory cytokine production through EGFR-NFκB activation. (A) Previously acquired microarray data published by Selman et al. was analyzed using a computational script that selected genes that were of increased or decreased abundance 3-fold upon vanadate treatment from the infected only control. Gene lists were input into TFactS (151). The P-value for each analyzed transcription factor was plotted. (B,C) 786-0 cells were simultaneously treated with varying concentrations of IMD-0354 or SC-514 (0 – 2000 nM) and vanadate (150 μM) (n=2, mean ± SEM). Four hours later, cells were infected with VSVΔ51-GFP (MOI 0.1). (B) Fluorescence images were captured 24 hours post infection (hpi). (C) Cell viability was measured by resaruzin (Alamar blue) assay and expressed relative to untreated, uninfected cells. (D-F) 786-0 cells were treated ± vanadate (150μM) ± gefitinib

(10μM). Four hours later, cells were infected with VSVΔ51-GFP (MOI 0.1). (E) Cells were lysed 24hpi, fractionated for cytoplasmic and nuclear fractions, then probed for phosphorylated NF-κB/p65, NF-κB/p65, lamin B1 and α-tubulin. (D) Whole cell lysates extracted 24hpi and probed for IκB-α and β-actin. (F) Cells were lysed at 24hpi and analyzed for mRNA expression of NF-κB related and pro-inflammatory genes by quantitative polymerase chain reaction (n=3, mean ± SD; **P<0.01, ***P<0.001, ****P<0.0001 by one-way ANOVA). (G) Supernatant was collected 24hpi and CXCL10 concentration was assessed by ELISA (n=3, mean ± SD; ****P<0.0001 by one-way ANOVA).

We consequently sought to look at the impact of vanadate and treatments antagonizing EGFR on NF-κB nuclear translocation. Indeed, probing for NF-κB in nuclear and cytoplasmic fractions by western blot demonstrated that vanadate increases the quantity of NF-κB available in the nucleus, an effect that was abrogated with gefitinib treatment (Fig. 2.4D). The inhibitor of NF-κB alpha (IκB-α) is a cytosolic inhibitor protein that regulates NF-κB signaling by masking its nuclear localization signal and its subsequent nuclear translocation (62, 152). Interestingly, EGFR phosphorylation has also been established to increase NF-κB signaling through the degradation of IκB-α (153, 154). To explore this linkage in the context of vanadate's viral-sensitizing mechanism, we probed whole cell lysates for IκB-α by western blot. Combinatorial treatment of vanadate and VSVΔ51 led to a significant decrease in IκB-α protein levels, yet when EGFR was inhibited using gefitinib, cellular levels of IκB-α were restored (Fig. 2.4E, S2.16).

Our previous study established that the combined treatment of vanadate with VSVΔ51 upregulates pro-inflammatory cytokines such as IFNβ several hours after the infection event (106). These pro-inflammatory cytokines are in part stimulated through the NF-κB axis, which

is itself downstream of EGFR. We therefore tested to see whether EGFR inhibition was able to abrogate the expression of NF-κB target genes. Quantification by qPCR revealed that the addition of gefitinib negated increases in pro-inflammatory IFNβ, IL-1b, IL-6, TNF-α and CCL5 mRNA levels induced by vanadate (Fig. 2.4F), all of which are classically in part stimulated by NF-κB (155). Moreover, one of the most striking phenotypes of tumor cells treated with vanadate in combination with VSVΔ51 is an increase in the transcription of T-cell chemoattractant chemokines, namely the IFN-2 induced chemokines CXCL9 and CXCL10 (106). Guided by evidence that STAT1 and NF-κB can synergize to upregulate both genes (156, 157), we explored whether vanadate also utilized this mechanism to increase these chemokines through EGFR. Transcriptional expression of genes encoding immune cell-attracting cytokines CXCL9 and CXCL10 were also assessed by qPCR. Indeed, gefitinib negated the increased transcription of CXCL9 and CXCL10 induced by vanadate (Fig. 2.4F). When secreted CXCL10 was measured by enzyme-linked immunosorbent assay (ELISA) in the supernatant, the same trend was reflected (Fig. 2.4G). Together, these results provide evidence to support that vanadate facilitates increased NF-κB signaling favoring a pro-inflammatory profile in treated tumor cells by regulating IκB-α through EGFR activation.

Gefitinib reduces vanadate's effects on VSVΔ51 spread in vivo

Given the ability for gefitinib to abrogate the vanadate viral sensitization of VSVΔ51 oncolytic virotherapy, we sought to investigate whether gefitinib could block the effects of vanadate-enhanced VSVΔ51 oncolytic virotherapy in more physiologically relevant contexts. Upon confirming that the addition of gefitinib was able to reduce vanadate viral sensitization in colon CT26WT carcinoma cells when administered pre and post-infection in vitro (Fig.

S2.17, S2.18), we found that CT26WT colon mouse tumors cores pre-treated with vanadate and treated with gefitinib 4 hours prior to infection were also capable of curbing vanadate mediated VSVΔ51 viral spread ex vivo (Fig. 2.5A, 2.5B). This effect was also achieved with UO126 treatment in CT26WT tumors (Fig. S2.19).

To investigate whether gefitinib could also abrogate the enhancing effect of vanadium on VSVΔ51 spread in vivo, 8-week-old BALB/c mice were implanted subcutaneously with CT26WT tumors and underwent a similar treatment regimen consisting of vanadyl sulfate and VSVΔ51 expressing firefly luciferase (VSVΔ51-FLuc) administered intratumorally, along with gefitinib (100mg/kg) 4 hours prior to infection. At 24hpi, infection was assessed using a live in vivo imaging system (IVIS). We did not investigate tumor progression to avoid potential confounding anti-tumor effects of gefitinib treatment. Consistent with our previous findings, mice receiving combinational treatment and gefitinib after infection significantly lowered viral-associated luciferase signal compared to mice not receiving any gefitinib (Fig. 2.5C, 2.5D). Together, both our ex vivo and in vivo data support that gefitinib can reverse the effects of vanadate in combination with VSV in animal models.

2.4 Discussion

Identification of EGFR signaling to vanadate viral sensitization

Despite the exciting multimodal therapeutic effects of OVs for cancer therapy, their success has yet to be fully realized due to variable response rates. To potentiate their anti-tumor effects, our group and others have previously explored the use of approved or novel compounds

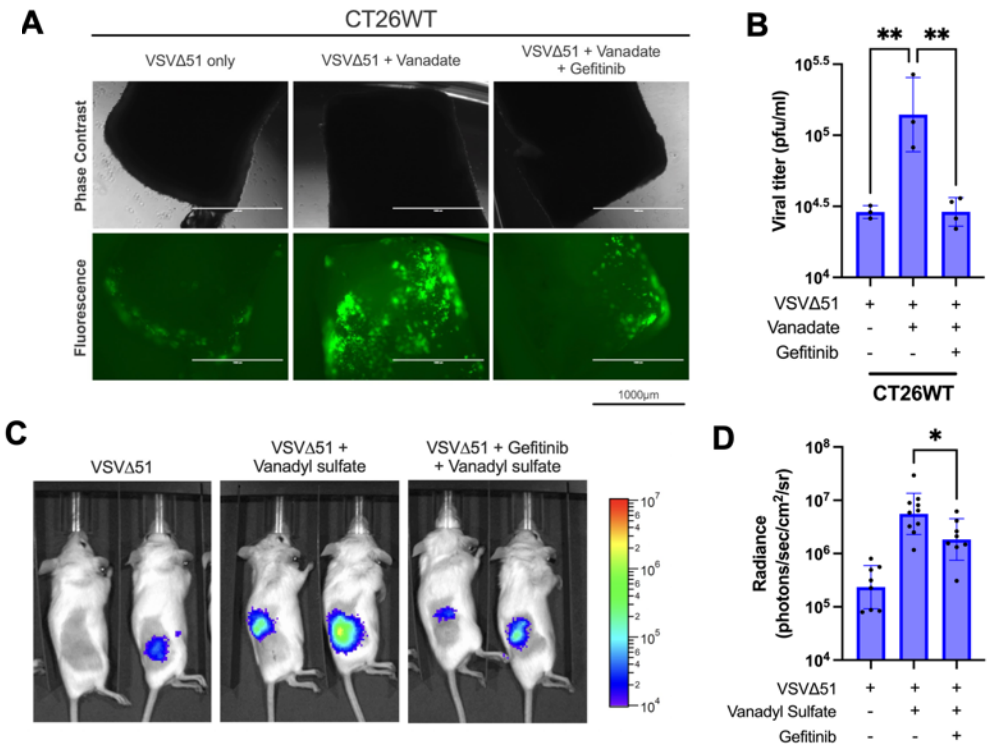

Fig. 2.5. Gefitinib reduces vanadate's effects on VSVΔ51 combinational therapy in vivo. (A,B) CT26WT tumour cores were obtained from implanted Balb/c mice and treated ex vivo with vanadate (300 μM) ± gefitinib (50 μM). Cores were infected 4 hours later with 3e4 plaque forming units (pfu) of VSVΔ51-GFP per core. (A) Fluorescence images were taken 24hpi; scale bar = 1000μm. (B) Supernatant was collected 48hpi and viral titer was assessed by plaque assay (n=3, mean ± SEM; **P<0.01 by one-way ANOVA). (C,D) Balb/c were implanted subcutaneously with CT26WT and allowed to progress to 100mm^3. Mice were then injected intratumorally with vanadyl sulfate (50mg/kg) ± gefitinib (100mg/kg) for four hours. Mice were then injected intratumorally with VSVΔ51-FLuc (1e8 pfu/tumor). At 24hpi, mice were imaged using a live imaging system (IVIS) for luminescence activity. (C) Absolute luminescence was log-transformed and graphed (n=8-10, mean ± SEM; *P<0.05 by one-way ANOVA). (D) Representative luminescence images are shown.

that can lead to the selective and transient knockdown of antiviral defenses to allow OVs to gain a foothold within the tumor (86). Vanadium-based compounds such as vanadate or vanadyl sulfate have shown promise for combinational therapy with RNA-based OVs in particular such as VSV and Newcastle disease virus (NDV) (106, 108). While we have previously shown that vanadium compounds elicit their OV-enhancing effects via a shift in IFN-1 towards IFN-2 transcriptional profiles by altering STAT1/2 expression and phosphorylation status, the specific mechanistic cascade leading to this effect remained unclear. In this study, we used a systems biology approach to successfully identify the EGFR pathway and its downstream signaling cascade as a crucial player in the viral sensitizing effect of vanadium compounds. This new mechanistic insight adds to our understanding of key signaling pathways that contribute to successful OV therapy regimens and will facilitate pre-clinical and clinical development of vanadium compounds as novel enhancers of OV-therapy. Our screen also identified 8 additional targets outside of EGFR that abrogated vanadium viral sensitizing activity (Table 2.1), some of which can play a role in viral lifecycle and antiviral pathway regulation (*e.g.,* eIF2a, AKT1) and provide avenues for further investigation (158).

In addition to the insulin-mimetic effects of vanadium that have been well explored in clinical trials (159), investigations have also suggested direct anti-cancer effects of vanadium compounds through in vitro and in vivo experimentation (105, 146, 160–162). However, their potential use in immuno-virotherapy has only recently been uncovered (106, 108). Vanadium-based compounds are potent competitive PTP inhibitors which naturally impact classes of receptor tyrosine kinases including the ErBB family. Vanadate has been previously established to sustain EGFR activation and its downstream signaling (Fig. 2.1D) (163, 164).

Guided by the mounting evidence supporting the role of the EGFR axis in oncogenesis and metastasis, several small molecules EGFR modulators have been developed and clinically approved in the last few decades (165). Gefitinib, lapatinib, vandetanib, erlotinib and afatinib are among the lead compounds identified in our screen and are clinically approved for the treatment of a variety of malignancies, particularly in tumors found to have EGFR overexpression. While several groups have explored the targeting of oncolytic viruses to take advantage of EGFR upregulation in cancer for increased therapeutic specificity (166–168), EGFR inhibitors have not typically been explored to modulate oncolytic virotherapy efficacy. Our study draws a link between virus-induced EGFR activation, increased oncolytic virus activity, and the ability to "tune" oncolytic virus activity by pharmacologically controlling the EGFR pathway.

In support of our proposed mechanism of vanadate-mediated OV enhancement via the EGFR pathway, there is ample evidence demonstrating that activation of the EGFR pathway and its downstream effectors sidetracks the antiviral system and promotes viral propagation. For instance, several viruses activate EGFR as part of their viral lifecycle to allow for their propagation (169–172). Poxviruses, which are currently used in oncolytic virotherapy, in particular encode vaccinia growth factor (VGF) which has been shown to activate EGFR (173). In a study by Wang *et al.*, tyrosine phosphorylation of the key IFN effector STING (STimulator of INterferon Genes) by EGFR was required for its proper cellular trafficking and downstream signaling (174). Without this phosphorylation by activated EGFR, STING was alternatively trafficked to autophagosomes, and cells were unable to mount a proper antiviral response against HSV infection. By the same token, inhibition of EGFR by genetic or pharmacological means has also been reported to activate the interferon pathway in several contexts (149, 175,

176). While sustained virus-induced EGFR signaling is likely in part required for its OV-enhancing effect, it is likely that vanadate requires the modulation of other signaling components. Investigation into the other specific phosphatases that vanadate may inhibit to confer viral sensitization effects is currently underway for the development and refinement of this therapeutic strategy.

Analyzing the immunomodulatory mechanism of vanadate via EGFR activation

From our findings, we elucidate three molecular events through which vanadate sensitizes cells to oncolytic virotherapy via EGFR activation: 1) dephosphorylation of STAT2, 2) induction of STAT1 nuclear accumulation, and 3) degradation of IκB-α to increase nuclear NF-κB signaling (see graphical abstract). During viral infection, IFN-1 cytokine binding to its respective IFN receptor (IFNAR1/2) triggers STAT1 and STAT2 phosphorylation and heterodimerization. We demonstrate that through EGFR activation, vanadate inhibits STAT2 phosphorylation to impair IFN-1 signal transduction. Without the phosphorylation of STAT2, the activity of the ISGF3 complex and subsequent antiviral defenses are abolished (177–179). Accordingly, EGFR blockade restores STAT2 phosphorylation and subsequent transcription of IFN-1 genes (Fig. 2.3A, 2.3B, 2.3E). As there is little known about the direct EGFR-STAT2 relationship, it is likely that an intermediate effector exists. For example, hyperactivation of the Ras/MEK pathway downstream to EGFR has been suggested to inhibit STAT2 transcriptional availability (180), and contributory to VSVΔ51 oncolysis (181). Further investigation into this relationship would broaden our understanding of STAT2 regulation of the IFN-1 responses.

Our computational analysis on microarray data identified STAT1 as the most likely involved transcriptional factor in the vanadate viral sensitizing mechanism, in accordance with this and previous studies (Fig. 2.4A, S2.13). Several groups have already shown that activation of the EGFR cascade culminates in increased STAT1 activation and expression (182–184). This is particularly relevant in the context of vanadate-based oncolytic virotherapy since we have previously shown that vanadate's mechanism of action involves the increased phosphorylation and nuclear localization of STAT1 upon VSVΔ51 infection, both of which were also observed in this study (Fig. 2.3) (106). In accordance with these findings, identified phosphatases targeting STAT1, such as Src homolog 2 domain-containing phosphatase 2 (SHP-2) (185), have been linked with impaired antiviral defenses through EGFR activation (186, 187).

At first glance, increased NF-κB signaling by vanadate appears to be counterintuitive for oncolytic potentiation as other established viral sensitizing compounds such as dimethyl fumarate (DMF) operate by inhibiting NF-κB nuclear translocation (96, 188). However, our results are in agreement with other studies that the JAK/STAT pathway is the key, dominant mechanism in controlling the IFN-1 response (67, 189). In fact, retaining NF-κB nuclear availability allows vanadate to directly upregulate the secretion of pro-inflammatory cytokines to ultimately increase immune cell infiltration to the tumor site, a unique feature of vanadium compounds (106). Through the cooperative signaling of increased STAT1 (Fig. 2.3D) and NF-κB (Fig. 2.4D) nuclear availability, vanadate achieves synergistic induction of pro-inflammatory genes controlled by GAS or NF-κB promoters (190). In the case of two IFN-2 cytokines, CXCL9 and CXCL10, the interaction between STAT1 and NF-κB has shown to increase recruitment of a third protein, CREB-binding protein (CBP) to subsequently increase

RNA polymerase II transcription activity at their respective promoters (156, 157). Indeed, we were able to demonstrate that EGFR blockade, presumably through inhibiting vanadate's STAT1 and NF-κB nuclear accumulation, significantly reduced IFN-2 cytokine transcription and secretion (Fig. 2.4F, 2.4G).

Implications for the advancement of vanadium based oncolytic virotherapy

Our findings introduce new considerations and opportunities for the advancement oncolytic virotherapy regimens. By establishing EGFR as an integral regulator of oncolytic VSV growth, it is possible that EGFR status could influence patient response to treatment regimens employing VSV and potentially other RNA-based OVs like measles and NDV. EGFR is frequently mutated in cancer, its hyperactivation confers a survival benefit to cancer cells and has been established as a resistance marker to standard cancer therapy (191–195). Interestingly, activation of EGFR has been shown to be necessary for the replication of several OVs and exploited to improve OV selectivity towards cancer cells. Alternate activation of the downstream effector ERK1/2 has also been shown to sensitize endothelial cells to OV therapy (196). Taken together with our findings, this further suggests the possibility that patients harboring mutations with hyperactivated EGFR may naturally be more susceptible to VSVΔ51 oncolytic virotherapy, a hypothesis that warrants further clinical investigation. Conversely, our results would then also naturally suggest that patients who are undergoing treatment with an EGFR inhibitor (*e.g.,* gefitinib, erlotinib, cetuximab) are less likely to respond to vanadium/ VSVΔ51 combination therapy. Furthermore, we consider that this aspect could potentially be exploited to control immune adverse events during oncolytic VSV clinical trials. EGFR inhibitors are advantageous candidates in that they are already clinically approved and

additionally offer inherent anti-cancer properties; however, whether they offer better counter-therapy than other antivirals, remains to be determined.

2.5 Material and Methods

Drugs and Chemical Reagents: The vanadium-based compound used in this study was sodium orthovanadate (Na_3VO_4, Sigma-Aldrich, cat. 450243) dissolved in water and pH adjusted to 10 at 150μM. For in vivo studies, vanadium sulfate at 50 mg/kg ($VOSO_4$, Sigma-Aldrich, cat. 204862) was used. The remainder of drugs, chemicals and cytokines used are listed in Key Resources Table (Table S2.1).

Cell Lines: 786-0 (human male renal cell adenocarcinoma, cat. CRL-1932), CT26WT (murine colon carcinoma, cat. CRL-2638) and Vero (African green monkey kidney cells, cat. CCL-81) were acquired from the American Type Culture Collection (ATCC). These cells utilized Dulbecco's modified Eagle's medium (DMEM; HyClone cat.10-013) supplemented with 1% (v/v) penicillin-streptomycin (Gibco), 30mM HEPES buffer and 10% (v/v) serum composed of 3-parts HyClone newborn calf serum (Thermo Fisher, cat. SH3011803) and 1-part Fetal Bovine Serum (Gibco, cat. 12483020). Cell lines were maintained in 37°C and 5% CO_2 conditions in a humidified incubator.

Oncolytic Virus: The Indiana serotype of VSV harboring a deletion of methionine 51 in the M protein (VSVΔ51) and insertion of green fluorescence protein (GFP) or firefly luciferase (FLuc) were used throughout this study(38). All viruses were propagated on Vero cells and purified on 5-%-50% Optiprep (Sigma-Aldrich, St. Louis, MO) gradients. All viral titers were determined by standard plaque assay according to published protocol (197). Measles virus of

the Schwartz strain expressing GFP was obtained as a generous gift from Dr. Guy Ungerechts of the Ottawa Hospital Research Institute (Ottawa, Canada).

Reverse Screen Strategy using Kinase Inhibitor Library: The Ontario Institute for Cancer Research (OICR) small molecule library was generously supplied by Rima Alawar via Dr. William Stanford of the Ottawa Hospital Research Institute. The library composed of 480 kinase inhibitors and 320 tool compounds from various developmental stages (*e.g.,* approved, pre-clinical, clinical). 3 x 10^4 786-0 cells were plated per well of a 96-well microplate and allowed to adhere overnight. Cells were pre-treated with screen compounds (1μM) and vanadate (125μM). Four hours later, cells were infected with VSVΔ51-FLuc at a MOI of 0.1. Infectivity was quantified by high-throughput titration (see below) and cell viability using resazurin (Millipore Sigma, cat. SI03200) were measured 48 hours post infection (hpi) (147). The experiment was conducted in triplicate. Every microplate included a series of positive (vanadate + VSVΔ51) and negative (untreated) controls, with a total of 80 library compounds.

High Throughput Titration: Using opaque white bottom 96-well microplates (Thermo Fisher, cat. 07-200-628), Vero cells were seeded at a density of 2.5 x 10^4 cells/well. 20 μL of the supernatant from the sample of interest was transferred onto the Vero cells and incubated for 5 hours at 37°C and 5% CO_2. 25 μL of luciferin solution (2mg/mL constituted in sterile PBS, Cederlane Lab, cat. 122799(PE)) was subsequently added and mean luminescence was analyzed 30 seconds later. Results were normalized against a standard curve of samples with known titers and normalized to an uninfected, untreated well. Refer to published protocol for further details (147).

In Silico Analysis: Microarray data from a previous study was processed (106). A list of genes of increased or decreased abundance more than 3-fold between the VSVΔ51 infected

condition and the vanadate and VSVΔ51 combinational condition was generated, then input into the TFactS computational database script to generate statistical values for each transcription factor. Related gene lists for each respective transcription factor were obtained from the published TFactS catalogue. Heatmaps of relative gene expression were generated using the R-studio pheatmap package. Refer to original published study for further details (151).

Cell Viability Assay: Metabolic activity of cells was measured 48hpi by adding 1:10 dilution resazurin metabolic dye (Millipore Sigma, cat. SI03200) to treated cells and incubated for 2 hours. Fluorescence was measured at 590nm upon excitation at 530nm using a BioTek Microplate Reader and Gen5 2.07 software (Norgen BioTek Corp, ON, Canada). Background signal was adjusted for by subtracting readings from wells only containing media.

Quantitative Real-time Polymerase Chain Reaction: RNA was extracted from samples using the QIAGEN RNeasy kit (Qiagen, cat. 74106) according to manufacturer's protocol and quantified using a Nanodrop ND-1000 spectrophotometer (Thermo Fisher Scientific, Rockford, IL). Corresponding cDNA was generated using the RevertAid H Minus First Strand cDNA Synthesis Kit (Thermo Fisher, cat. K1632). Real-time PCR reactions were performed using respective primers (Table S2), Applied Biosystems PowerUp SYBR Green Master Mix (Thermo Fisher, cat. A25776) in a 7500 Fast Real-Time PCR system (Applied Biosystems, Foster City, CA). Relative gene expression was normalized to *GAPDH*, and fold-induction calculated relative to an uninfected and untreated condition.

Enzyme-linked immunosorbent assay (ELISA): 786-0 cells were treated with respective drugs for 4 hours and infected with VSVΔ51. After 24 hours, supernatants of cells were collected and analyzed for CXCL10 concentration using the Human CXCL10/IP-10 DuoSet

Assay kit (R&D Systems, cat. DY266). The assay was performed according to manufacturer's protocol with a 1:30 dilution. Absorbance was read using the Multiskan Ascent Microplate Reader (MXT Lab Systems) at 450nm and corrected for plate imperfections at 540nm.

Immunoblotting and immunoprecipitation: Samples were washed twice with cold PBS and lysed for 10 minutes at 4°C using 50mM HEPES, 150mM NaCl, 10mM EDTA, 10mM $Na_4P_2O_7$, 100mM NaF, 2mM Na_3VO_4, protease inhibitor cocktail (Roche), phosphatase inhibitor cocktail (Cell Signaling Technology, cat. 5870S) and 1% Triton X-100. Cells were scraped and the collected lysate was centrifuged. For nuclear and cytoplasmic fractionation, the NE-PER Nuclear and Cytoplasmic Extraction Kit (Thermo Fisher Scientific) was used according to manufacturer's protocol. Supernatant was collected the protein quantified using the Pierce BCA Protein Assay Kit (Thermo Fisher, cat. 23225). 20µg was loaded with 4X NuPAGE LDS Sample Buffer (Thermo Fisher, cat. NP0007) into 4-15% Mini-PROTEAN Gels (Bio-Rad, Mississauga, ON), electrophoresed using the Mini Trans-Blot Cell system (Bio-Rad, Mississauga, ON) and transferred onto nitrocellulose membrane using the Trans-Blot Turbo RTA Mini Transfer Kit according to manufacturer's protocol (Bio-Rad, cat. 1704270). Blots were subsequently blocked with 5% Bovine Serum Albumin (BSA) and probed with respective primary and secondary antibodies as listed in the Key Resources Table (Table S1). Bands were visualized using Clarity Western ECL Substrate (Bio-Rad, cat. 1705061) on a ChemiDoc Touch Imaging System (Bio-Rad, Mississauga, ON).

Immunocytochemistry: Cells were seeded on 12mm glass round coverslips (Thomas Scientific, cat. 64-0712), then treated with specified reagents. After washing twice with PBS* (PBS with 1mM $CaCl_2$ and 500µM $MgCl_2$), cells were fixed using 4% paraformaldehyde for 30 minutes, permeabilized using a 0.2% Triton-X 100 in 200mM glycine/PBS* solution for 8

minutes, then quenched in 200mM glycine/PBS*. Samples were then blocked using 5% BSA/PBS* for 1 hour at room temperature, then incubated with respective primary antibody overnight in a humidified chamber at 4℃ as listed in the Key Resources Table (Table S2.1). Corresponding secondary antibodies were applied for 1 hour, then samples were mounted onto glass slides and counterstained using Prolong gold anti-fade with 4',6-diamidino-2-phenyl-indole (Molecular Probes). Slides were imaged using Zeiss Axiocam HRM Inverted fluorescent microscope (Zeiss, Toronto, Canada) and Axiovision 4.0 software. Images were processed using ImageJ. Nuclear: cytoplasmic signal quantification processes were performed using CellProfiler (Massachusetts Institute of Technology, Cambridge, USA).

Ex Vivo Tumor Model*:* 8-week-old healthy, female Balb/c mice were implanted with subcutaneous CT26WT cells. Mice were sacrificed after reaching a tumor volume of 1000mm^3. Tumor tissues were extracted from the mice, cut into 2-mm slices and 2mm x 2mm cores were taken using a punch biopsy tool. Cores were maintained in humidified incubators at 37°C, 5% CO_2 in DMEM supplemented with 10% serum, 30mM HEPES, 1% (v/v) penicillin-streptomycin and 0.25mg/L amphotericin B. Cores were treated with their respective drugs at indicated timepoints, then infected with VSVΔ51-GFP (3e4 pfu/core for CT26WT). Fluorescence images were taken 24hpi and supernatant stored at -80°C 48hpi for viral titer plaque assay.

In vivo Tumor Models*:* Female 8-week-old Balb/c mice (Charles River Laboratories) were implanted subcutaneously with CT26WT cells and allowed to progress to 100mm^3, about 11 days. Tumors were treated intratumorally with vanadyl sulfate (50mg/kg) and/or gefitinib (100mg/kg) at various time points. Tumors were then injected with VSVΔ51-FLuc (1e8 pfu/tumor) intratumorally. After 24 hours, mice were anesthetized and imaged using a live in

vivo imaging system (Perkin Elmer). Bioluminescent signal intensity was quantified and analyzed using Living Image v2.50.1 software. All experiments were performed in accordance with the University of Ottawa Animal Care and Veterinary Service guidelines for animal care under the protocols OHRI-2264 and ORI-2265.

Quantification and statistical analysis: Statistical analyses were performed using Prism 8 (GraphPad, San Diego, CA) software. Experiments involving viral titer, absolute luminescence and relative mRNA expression were log-transformed prior Statistical tests were performed as indicated by Fig. legends including Student's t-test, one-way and two-way ANOVA according to experimental conditions. Error bars represent the standard error from the mean (SEM). A P-value less than 0.05 was considered statistically significant.

2.6 Acknowledgements

The graphical abstract schematic was created using BioRender.com (Toronto, ON, Canada) licensed to Boaz Wong (agreement #EC22Z6360S). The authors would like to thank Michael Phan (University of Ottawa), Naveen Haribabu and Dr. Julien Yockell-Lelievre (Ottawa Hospital Research Institute) for their assistance with the reverse kinase screen, Dr. William Stanford and Rina Al-awar (Ontario Institute for Cancer Research) for supplying the kinase inhibitor library, Serge Neault (University of Ottawa) for his expertise with the measles virus, and Dr. Guy Ungerechts (Ottawa Hospital Research Institute) for his generous provision of the measles virus for their use in this study. We would also like to thank Dr. Debbie C. Crans (Colorado State University) for helpful discussions surrounding vanadium chemistry.

J.S.D. is supported by the Terry Fox Research Institute (TFF 122868), the Canadian Institutes of Health Research (CIHR, INI-147824 and grant #705952), and the Canadian Cancer Society supported by the Lotte & John Hecht Memorial Foundation (703014). B.W. is

supported by the Ontario Graduate Scholarships (OGS) and CIHR Doctoral Fellowship (CGS-D). A.B was supported by the Hans K. Uhthoff Graduate Fellowship and Queen Elizabeth II Graduate Scholarships in Science and Technology (QEII-GSST).

Chapter 3. High throughput screen identifies lysosomal acid phosphatase 2 (ACP2) to regulate IFN-1 responses to potentiate oncolytic VSVΔ51 activity

Boaz Wong[1,2], Rayanna Birtch[1,2], Anabel Bergeron[1,2], Kristy Ng[1], Glib Maznyi[1], Marcus Spinelli[1], Andrew Chen[1], Rozanne Arulanandam[1], Carolina S. Ilkow[1,2], Jean-Simon Diallo[1,2]*

[1]Centre for Innovative Cancer Research, Ottawa Hospital Research Institute; Ottawa, Ontario, Canada, K1H 8L6. [2]Department of Biochemistry, Microbiology and Immunology, Faculty of Medicine, University of Ottawa; Ottawa, Ontario, Canada, K1H 8M5. * denotes corresponding author.

Submitted October 2023 to *Scientific Reports*

3.1 Abstract

Strategies in genetic and pharmacological modulation of various cellular processes are being explored to overcome the inherent limitations in clinical therapeutic activity of oncolytic virotherapy (OV) against cancer. We have recently characterized the ability for vanadium-based compounds, a class of pan-phosphatase (PP) inhibitors, to potentiate OVs. We next sought to identify PPs that could be targeted to enhance OVs, akin to vanadium. By conducting a high-throughput screen of a library of silencing RNA (siRNA) targeting human PPs, we uncovered several PPs that robustly enhanced infectivity and oncolysis of the oncolytic vesicular stomatitis virus (VSVΔ51). Knockdown of our top validated hit, lysosomal acid phosphatase 2 (ACP2), increased VSVΔ51 viral titers by over 20-fold. *In silico* analysis by RNA sequencing revealed ACP2 to interfere with antiviral type I interferon (IFN-1) signaling and repress downstream IFN-1 effectors, similar to vanadium. To further exploit this mechanism for therapeutic gain, we encoded a short-hairpin RNA (shRNA) against ACP2 into oncolytic vesicular stomatitis virus (VSVΔ51) under a miR-30 promoter. This bioengineered OV demonstrated expression of the miR-30 promoter, knockdown of ACP2, repression and ultimately, showed markedly enhanced viral VSVΔ51 particle production compared to its non-targeting control counterpart. Altogether, this study identifies IFN-1 regulating PP targets, namely ACP2, that may prove instrumental in increasing the therapeutic efficacy of OVs. Furthermore, this study also serves as a proof of concept that these targets can be exploited using RNA interference expressing OVs.

3.2 Introduction

Since its discovery as a potent anti-tumor agent in the 1950s, the development of viruses as a cancer immunotherapy has escalated in recent decades highlighted by the clinical approval of talimogene laherparepvec (T-VEC) for the treatment of melanoma in 2015 (25, 27). Through genetic engineering, oncolytic virotherapy (OV) promises potent cancer cell killing and the development of robust anti-tumor immunological memory, all while leaving physiological tissue unharmed (28). This efficacy hinges upon the innate type 1 interferon (IFN-1) response, which orchestrates the initial propagation of cellular antiviral programs and bridging to inflammatory processes (198). While most tumors have been thought to be deficient in this IFN-1 response as a byproduct of malignant transformation, residual IFN-1 responses have been blamed for therapeutic resistance to OV regimens (199). Thus, the genetic or pharmacological modulation of cellular processes that ultimately impinge upon the IFN-1 response represents a logical strategy to improve the therapeutic gain of OVs (78, 86). To this end, our group identified vanadium-based compounds, among others, to improve the viral spread, bystander killing and anti-tumor efficacy of OVs, such as the oncolytic vesicular stomatitis virus (VSVΔ51), when administered in combination (106). This mechanism was eventually found to be secondary to activation of the epidermal growth factor receptor (EGFR) subsequently leading to changes in STAT phosphorylation and NF-κB signaling to subvert IFN-1 responses towards more of an IFN-2 phenotype (200). However, given the well-known pan-protein phosphatase (PP) inhibitory activity of vanadium, the exact PPs responsible for this phenomenon remains elusive.

Protein phosphorylation represents a major post-translational regulatory mechanism; therefore, its imbalance typically results in disruption of key cellular functions. The covalent

addition of a phosphate group by kinases triggers conformational changes to its respective substrate thereby changing its response, typically towards activation (109). PPs are responsible for the removal of phosphatases to reverse this regulation, therefore, their inhibition often culminates in substrate hyperactivation, as in the case of constitutive EGFR activity upon vanadium treatment (200). Given their extensive regulation across a plethora of cellular processes, interception of a few PPs has unsurprisingly been demonstrated to both enhance and antagonize IFN-1 responses. Through dephosphorylation of IFN-binding receptors, protein tyrosine phosphatase 1B (PTP1B) stimulates their endocytic turnover to repress antiviral response and defenses (201). On the other hand, there is evidence that phosphatase slingshot homolog protein 1 (SHP-1) controls the secretion of IFN-1 effectors and pro-inflammatory cytokines (202). Without the use of a high-throughput screening approach, there are undoubtedly many more involved PP targets to be discovered.

In an attempt to increase OV potency and selectivity, various payloads have been encoded into the genomic backbone of viral vectors (203). These typically consist of immunomodulatory transgenes, such as interferon gamma (IFN-ɣ) or interleukin-12, intended to elicit stronger anti-tumor immune responses (72, 204). The use of RNA interference (RNAi) has recently led to the investigation of another potential class of payloads for delivery by viral vectors for cancer therapy. Through the delivery of RNAi effectors which include silencing RNA (siRNA) and microRNA (miRNA), the expression of specific gene transcripts can be dramatically reduced for therapeutic gain. Broadly, these RNAi effectors can elicit similar effects as virus encoded transgenes from immunomodulation to induction of tumor cell apoptosis to direct oncogene silencing (116). Although the majority of *in vivo* tested viral-delivered RNAi are by replication incompetent vectors, the synergy between RNAi effectors

and the inherent oncolytic ability of replication-competent viruses represents a promising avenue for investigation.

The objective of this study was to identify PP targets that could mimic the OV-enhancing effects of vanadium and its respective mechanism of action in regulating the innate antiviral response. Upon successful identification of a OV-enhancing PP target, we then aimed to express RNAi against the identified PP as a payload using a VSVΔ51 vector to develop a bioengineered OV with increased viral infectivity and oncolytic activity.

3.3 Results

High-throughput siRNA phosphatase screen identifies candidates for OV enhancement

To identify protein phosphatases (PP) that play a regulatory role in the cellular antiviral defense, we employed a high-throughput screening (HTS) approach using the MISSION® silencing RNA (siRNA) Human Phosphatase Library targeting 303 phosphatase genes using an arsenal of 1,131 total siRNA. 786-0 cells were seeded in 96well plates and transfected with respective siRNA at a concentration of 0.2μM using Invitrogen's Lipofectamine® RNAiMAX reagent, then infected with oncolytic vesicular stomatitis virus (VSVΔ51) tagged with firefly luciferase (FLuc). Following 48 hours of incubation, samples were titered using a previously established high-throughput method and relative cell viability was established using resazurin metabolic dye (Fig. 3.1A) (147). Each siRNA was assigned calculated values expressed as (1) fold-change in viral titer over infected cells transfected with a universal negative control and (2) oncolysis enhancing factor defined as the logarithm of the viability of transfected cells

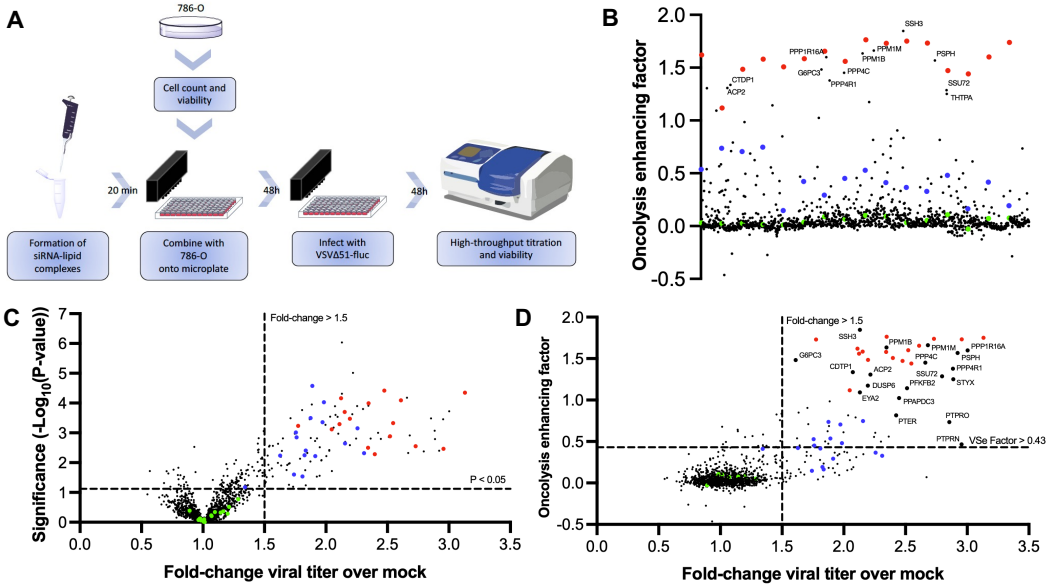

Fig 3.1. High throughput screen reveals PP targets that enhance oncolytic VSVΔ51. (A) Schematic diagram representing the workflow of the high-throughput screen. (B-E) Human 786-0 cells were seeded in 96-well plates, transfected with RNA from the MISSION® silencing RNA (siRNA) Human Phosphatase Library or corresponding controls for 48 hours. Cells were then infected with VSVΔ51 tagged with firefly luciferase (VSVΔ51-fluc) at a multiplicity of infection of 0.05. Blue dots indicate cell treated with vanadate. Red dots indicated cells transfected with RIG-I siRNA. Green dots indicate cells transfected with scramble siRNA. (B) Oncolysis enhancing factor was calculated as described in the methods and plotted. Candidates of interest are labeled as shown. (C) Supernatant was assessed for viral titer by high-throughput titration 48hpi and expressed a fold-change over infected-only cells, and by significance from average infectivity of infected-only cells by unpaired t-test assuming unequal variance. (D) Oncolysis enhancing factor of candidates were plotted against fold-change viral titer. Top candidates of interest are labeled as shown.

divided by the viability of transfected infected cells. As a positive control, siRNA against retinoic acid-inducible gene I (RIG-I), central to innate antiviral interferon (IFN) signaling (205), and cells treated with vanadate were used.

Each siRNA target was plotted for its viability when combined with VSVΔ51 and significance in p-value when compared to cells treated only with control siRNA (Fig. S3.2). A total of 232 of the 1,131 tested targets were able to significantly decrease the cell viability below 40% with a P-value less than 0.05 (upper left quadrant). To score viability, an *oncolysis enhancing factor* was assigned to each library siRNA target which considers the cytotoxicity generated from the siRNA in the absence of VSVΔ51 infection and gives a positive score to targets that synergize with VSVΔ51 for increased oncolysis. Given that the average oncolysis enhancing factor for vanadate treated samples is 0.43 (blue points in Fig. 3.1B), a total of 54 PP targets scored higher than vanadate with the highest hit being slingshot homolog 3 (SSH3). Similarly, in Fig. 1C, the fold-change in VSVΔ51 viral titer with PP siRNA transfection was plotted for each target against significance in p-value compared to cells treated with control siRNA. The HTS found 78 targets situated in the upper right quadrant with viral titer fold-change greater than 1.5 and P-value less than 0.05. The HTS found that the target with the greatest increase in viral titer was protein phosphatase 1, regulatory subunit 16A (PPP1R16A) which increased VSVΔ51 by about 3-fold. To combine the results of both measures to determine the top candidates of the HTS, oncolysis enhancing factor and fold-change in viral titer were plotted together in Fig. 3.1D. Using the previously selected cutoffs of oncolysis enhancing factor greater than 0.43 and fold-change in viral titer greater than 1.5, this identified 38 hits, which are shown in Table 3.1. These candidates were subsequently selected for validation.

Table 3.1. Top hits from the high-throughput siRNA phosphatase screen

Target	FC Viral Titer	Oncolysis enhancing factor	Gene ID	Gene Name	Accession #
PTP1C2	1.62	0.54	ACP2	acid phosphatase 2, lysosomal	NM_001610
PTP1C3	2.22	1.31	ACYP1	acylphosphatase 1, erythrocyte (common) type	NM_203488
PTP1F11	2.13	1.09	EYA2	eyes absent homolog 2 (Drosophila)	NM_005244
PTP2C2	2.21	1.31	ACP2	acid phosphatase 2, lysosomal	NM_001610
PTP2D5	2.07	1.34	CTDP1	CTD (carboxy-terminal domain, RNA polymerase II, polypeptide A) phosphatase, subunit 1	NM_004715
PTP2D8	1.71	0.71	DUSP26	dual specificity phosphatase 26 (putative)	NM_024025
PTP2E5	2.09	0.79	CTDSP1	CTD (carboxy-terminal domain, RNA polymerase II, polypeptide A) small phosphatase 1	NM_021198
PTP3A9	1.89	0.98	DUSP6	dual specificity phosphatase 6	NM_001946
PTP3D2	1.88	0.69	ACP5	acid phosphatase 5, tartrate resistant	NM_001111034
PTP3E10	1.87	0.62	ENPP7	ectonucleotide pyrophosphatase/phosphodiesterase 7	NM_178543
PTP3F11	1.87	0.47	EYA2	eyes absent homolog 2 (Drosophila)	NM_005244
PTP4D3	2.24	0.56	ILKAP	integrin-linked kinase-associated serine/threonine phosphatase	NM_176799
PTP4D9	2.51	1.14	PFKFB2	6-phosphofructo-2-kinase/fructose-2,6-biphosphatase 2	NM_001018053

PTP4D10	1.85	0.50	PHOSPHO2	phosphatase, orphan 2	NM_001008489
PTP4H9	1.63	0.85	PGAM4	phosphoglycerate mutase family member 4	XM_930828
PTP6E4	1.75	0.45	INPP5E	inositol polyphosphate-5-phosphatase, 72 kDa	NM_019892
PTP6F5	2.36	0.56	LHPP	phospholysine phosphohistidine inorganic pyrophosphate phosphatase	NM_022126
PTP6F11	2.45	1.02	PPAPDC3	phosphatidic acid phosphatase type 2 domain containing 3	NM_032728
PTP6H2	1.61	1.48	G6PC3	glucose 6 phosphatase, catalytic, 3	NM_138387
PTP7A7	3.00	1.60	PPP1R16A	protein phosphatase 1, regulatory subunit 16A	NM_032902
PTP7B11	2.88	1.38	PPP4R1	protein phosphatase 4, regulatory subunit 1	NM_005134
PTP7H10	2.66	1.45	PPP4C	protein phosphatase 4, catalytic subunit	NM_002720
PTP8H2	2.35	1.64	PPM1B	protein phosphatase, Mg2+/Mn2+ dependent, 1B	NM_001033556
PTP9B5	2.19	1.17	PPP1R10	protein phosphatase 1, regulatory subunit 10	NM_002714
PTP9C6	1.64	0.45	PPP1R14A	protein phosphatase 1, regulatory (inhibitor) subunit 14A	NM_033256
PTP9C11	2.03	0.81	PPP4R1L	protein phosphatase 4, regulatory subunit 1-like	NM_018498
PTP9D4	2.68	1.66	PPM1M	protein phosphatase,	NM_144641

				Mg2+/Mn2+ dependent, 1M	
PTP9D9	2.25	0.60	PPP2R2C	protein phosphatase 2, regulatory subunit B, gamma	NM_020416
PTP10E6	1.70	0.91	PTPN6	protein tyrosine phosphatase, non-receptor type 6	NM_002831
PTP10G10	2.13	1.85	SSH3	slingshot homolog 3 (Drosophila)	NM_018276
PTP12D2	2.92	1.57	PSPH	phosphoserine phosphatase	NM_004577
PTP12F2	2.42	0.82	PTER	phosphotriesterase related	NM_001001484
PTP12F8	2.95	0.46	PTPN7	protein tyrosine phosphatase, non-receptor type 7	NM_002832
PTP12H10	2.80	1.29	SSU72	SSU72 RNA polymerase II CTD phosphatase homolog (S. cerevisiae)	NM_014188
PTP12H11	2.89	1.25	THTPA	thiamine triphosphatase	NR_023314
PTP13G3	2.30	0.50	ENTPD2	ectonucleoside triphosphate diphosphohydrolase 2	NM_203468
PTP14B8	2.00	0.61	PTPN20A	protein tyrosine phosphatase, non-receptor type 20A	XM_931711
PTP16F4	2.86	0.74	PTPRO	protein tyrosine phosphatase, receptor type, O	NM_030668

FC = Fold-change

Knockdown of ACP2 enhances VSVΔ51 infectivity and oncolysis

For the validation of top PP targets in Table 3.1, we transfected cherry-picked siRNA from the library into 786-0 cells, then infected with VSVΔ51 tagged with green fluorescent protein (GFP) to directly visualize the viral enhancing impact of the siRNA. Fluorescent foci were counted and fold change was calculated relative to control cells treated with scramble siRNA. The validation demonstrated that only two hits were able to increase VSVΔ51 greater than vanadate: lysosomal acid phosphatase 2 (ACP2) and phosphoserine phosphatase (PSPH) by 19.5 and 17.5-fold respectively (Fig. 3.2A). We ultimately selected to proceed with ACP2 given its greatest increase in VSVΔ51 viral titer on validation. To confirm its genetic knockdown using custom sequence siRNA (outlined in Supplemental Table S3.3), 786-0 cells transfected with ACP2 siRNA and infected with VSVΔ51 were probed by real-time quantitative polymerase chain reaction (qPCR) for ACP2 RNA transcripts. Indeed, we confirmed that the siRNA reduced ACP2 transcription by roughly 10-fold both in the presence and absence of infection (Fig. 3.2B).

Given the successful knockdown using our ACP2 siRNA, we quantified the increase in VSVΔ51 viral titer using standard plaque assay (Fig. 3.2C). Moreover, we demonstrated its ability to increase tagged VSVd51-GFP expression by florescence microscopy (Fig. 3.2D) and VSV-M RNA expression by qPCR, both indicating increased VSVΔ51 (Fig. 3.2E). To evaluate cell viability, resazurin metabolic dye was used and showed that knockdown of ACP2 increased the oncolytic activity of VSVΔ51, akin to the results of the screen. Transfection with ACP2 siRNA alone decreased the viability of the cells to 85%, while the further addition of VSVΔ51 significantly reduced viability to 60% 72 hours post-infection. Together, these results confirm ACP2 as a suitable target of interest to enhance oncolytic VSVΔ51.

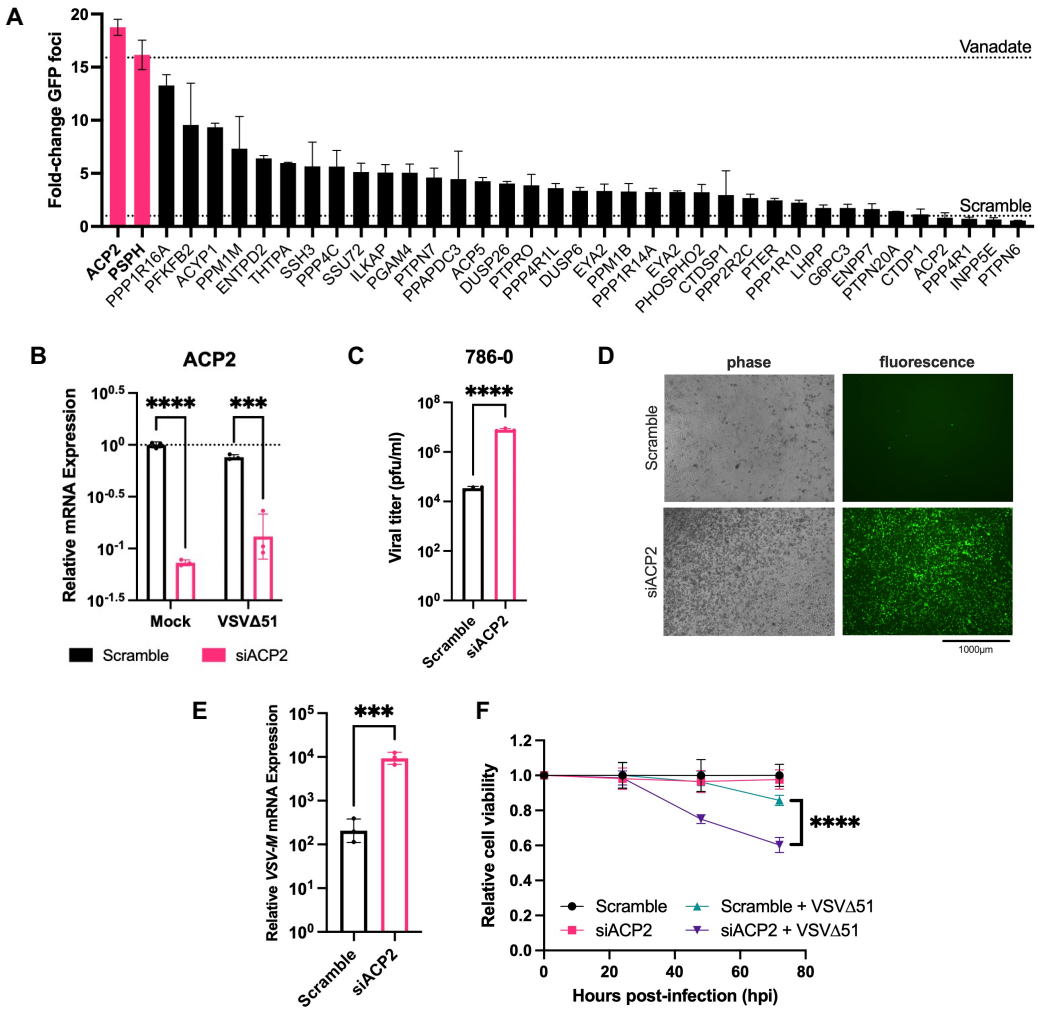

Fig 3.2. ACP2 knockdown increases VSVΔ51 infectivity and oncolysis. (A) Top hits from the high-throughput screen were validated in 786-0 cells using a similar protocol. Cells were transfected with PP-targeting siRNA for 48 hours, then infected with VSVΔ51 tagged with green fluorescent protein (VSVΔ51-GFP) at a multiplicity of infection of 0.05. Fluorescent foci were counted 24 hours post infection (hpi) and expressed as fold-change over the infected-only condition (n=3, mean). (B-F) 786-0 cells were transfected with siRNA targeting ACP2 for 6 hours, then the media was replaced. 48 hours later, cells were infected with VSVΔ51-GFP (MOI 0.01). (B) Cells were lysed 24hpi for RNA extraction and analyzed for ACP2 transcripts by qPCR (n=3, mean ± SD; ***P<0.001, ****P<0.0001 by two-way ANOVA). (C) Supernatant was taken 24hpi and analyzed for viral titer by plaque assay (n=3, mean ± SD; ****P<0.0001 by unpaired t-test). (D) Representative fluorescent images were taken 24hpi.

(E) Infected cells were lysed 24hpi for RNA extraction and analyzed for VSV-M transcripts by qPCR (n=3, mean ± SD; ***P<0.001 by unpaired t-test). (F) Relative viability was measured by resazurin metabolic dye over mock transfected, uninfected controls at indicated timepoints (n=3, mean ± SD; ****P<0.0001 by two-way ANOVA).

Regulation of the type I interferon response by ACP2

Asides from roles in neurodevelopment in mice (206, 207), ACP2 was mainly established to be instrumental in lysosomal activity for the processing of cellular degradation products (208, 209). There are previous reports suggesting a role for ACP2 in regulating herpes-simplex virus (HSV) cellular entry (210), but none directly describing its role in regulating the antiviral defense response. Therefore, to investigate this potential new role for ACP2, we performed *in silico* analysis via RNA sequencing. RNA from 786-0 cells transfected with siRNA against ACP2 was extracted after 24 hours of infection with VSVΔ51, then sequenced for whole transcriptome changes and gene expression profiles calculated between experimental conditions. Between uninfected cells transfected with scramble siRNA or siRNA against ACP2, 1,080 genes were significantly upregulated ($P < 0.05$, $\log_2$-fold change >1) and 1,813 genes were significantly downregulated (Fig. 3.3A). Analysis of involved gene ontology (GO) terms using the GOrilla tool revealed significant downregulation of antiviral-related terms including “type I interferon signaling pathway” and “defense response to virus” (211, 212) (Fig. 3.3B). A heatmap with differential expression of all genes related to the “type I signaling pathway” GO term was plotted which overall demonstrates repression of related genes upon transfection with siACP2, in both the absence and presence of VSVΔ51 infection (Fig. 3.3C, S3.3).

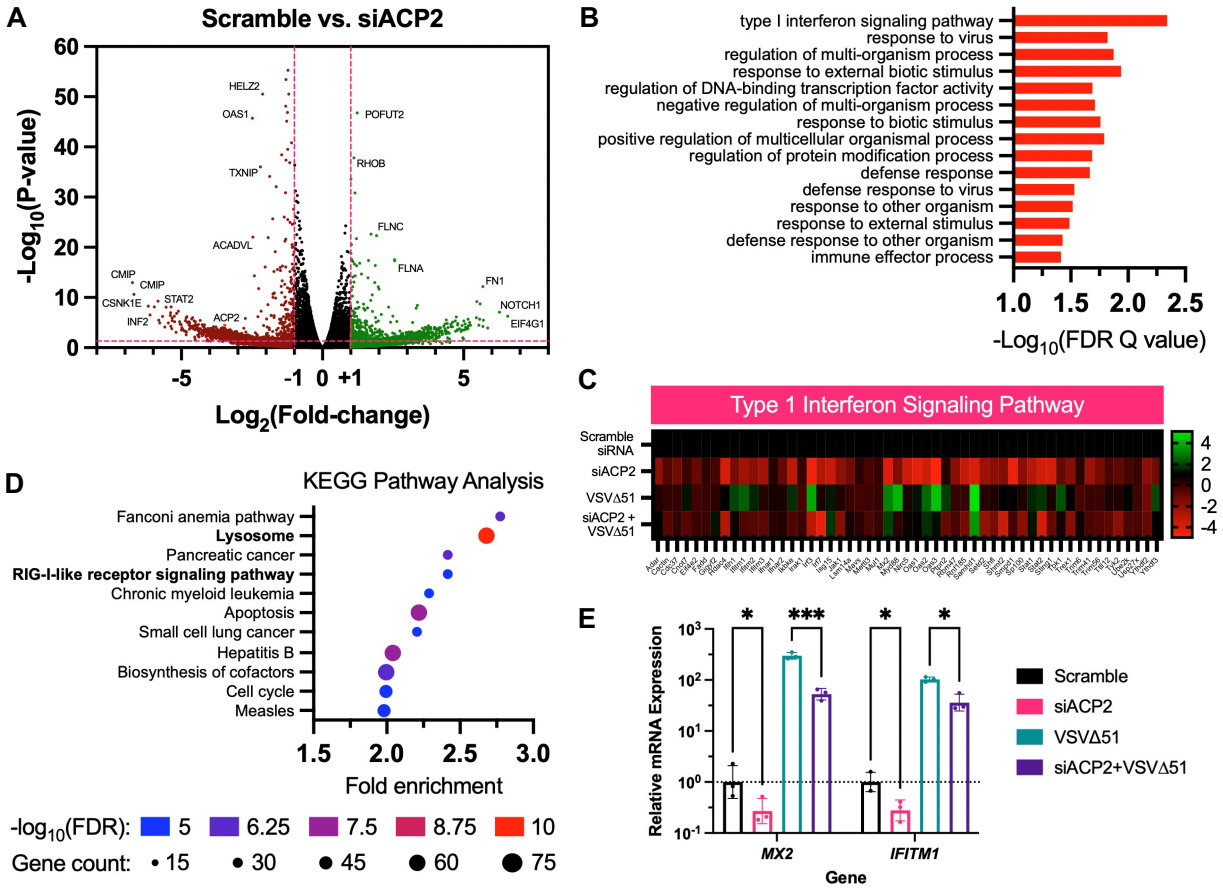

Fig 3.3. ACP2 is involved in the IFN-1 response. (A-D) 786-0 cells were transfected with siRNA targeting ACP2 for 6 hours, then the media was replaced. 48 hours later, cells were infected with VSVΔ51-GFP (MOI 0.01). RNA was then extracted 24 hours post infection (hpi) and sequenced in two biological replicates. Processing by KALLISTO pseudo-alignment and SLEUTH yielded normalized log2-fold change in differential gene expression and P-values. (A) Each gene was plotted for fold-change and P-value in a volcano plot, notable hits were labeled. (B) Significantly downregulated (>2 log2-fold change) gene expressions were processed by Gorilla to identify relevant gene ontology (GO) terms. FDR = False Discovery Rate. (C) A heatmap of the fold-change expression of gene related to the "Type 1 Interferon Signaling Pathway" GO term was plotted. (D) Significantly downregulated genes were input into the Graphite and CliPPER tools to determine relevant Kyoto Encyclopedia of Genes and Genomes (KEGG) pathways. (E) 786-0 cells were transfected with siRNA targeted ACP2, then infected with VSVΔ51 (MOI 0.05). Cells were lysed 24 hours later and RNA was

extracted. MX2 and IFITM1 mRNA transcripts were quantified by qPCR (n=3, mean ± SD; *P<0.05, ***P<0.001 by two-way ANOVA).

Furthermore, when downregulated ranked gene lists between cells transfected with scramble siRNA and siRNA against ACP2 were analyzed using Kyoto Encyclopedia of Genes and Genomes (KEGG) pathways to link the sequencing data to involved cellular processes, we identified relevant pathways including the lysosome pathway and the RIG-I-like receptor signaling pathway (Fig. 3.3D). The former hit validates our knockdown method given that ACP2 is responsible for regulating lysosomal pathways (209), while the latter further implicates innate antiviral immunity to be a new repressed pathway upon ACP2 knockdown (Fig. S3.4, S3.5). Given that our *in silico* analyses support the repression of IFN-1 pathways, we wanted to confirm the suppression of IFN-1 effectors by ACP2 knockdown. Indeed, quantification of mRNA 24 hours after infection showed that transfection with siRNA against ACP2 significantly reduced transcription of the antiviral IFN-1 effectors, MX2 and IFITM1 (Fig. 3.3E).

VSVΔ51 expressing shACP2 has increased viral infectivity in human tumor models

The second objective of this study was to test the feasibility of cloning RNAi into a VSVΔ51 vector against a PP target for improved infectivity. The cloning plan for the viral backbone is outlined in Fig. 3.4A. After generating a pre-miR-30 short hairpin cassette with our predetermined siRNA sequence against ACP2 flanked by XhoI and NheI restriction, we digested the oligonucleotide sequence into a VSVΔ51 plasmid between the G and L proteins.

To confirm the knockdown efficacy of the resulting bioengineered virus, we infected 786-0 cells with either VSVΔ51 against non-targeting control (VSVΔ51-NTC) or shACP2 (VSVΔ51-shACP2) and analyzed their lysate for miR-30 expression and ACP2 mRNA. Indeed, our analysis by qPCR with primers against miR-shACP2 foci found increased expression by VSVΔ51-shACP2 at both multiplicities of infection (MOI) 0.01 and 0.1 as soon as 12 hours after infection (Fig. 3.4B). Moreover, our data found about 30% repression of ACP2 transcription in cells infected with VSVΔ51-shACP2 (Fig. 3.4C) relative to the control. These data confirm proper expression of our desired miR-30 cassette and effective knockdown of our target gene, ACP2, in infected cells.

After establishing the functionality of VSVΔ51-shACP2, we wanted to test its efficacy in increasing viral infectivity. Upon infection of 786-0 cells with VSVd51-shACP2 or VSVd51-NTC at different MOI, resulting titers showed significant increases with VSVΔ51-shACP2 at higher MOI, supporting increased viral output per infected cell (Fig. 3.4D). In testing the growth kinetics of VSVΔ51-shACP2, we found that VSVΔ51-shACP2 was able to enhance viral output in both the single- and multistep growth curves performed in 786-0 cells which suggest that VSVΔ51-shACP2 exhibits increased viral spread and replication over the control (Fig. 3.4E). To confirm that our novel bioengineered virus has increased infectivity across multiple tumor contexts, we tested both VSVΔ51-NTC and VSVΔ51-shACP2 in several cell lines. Indeed, we found that VSVΔ51-shACP2 had greater viral titers after 24 hours of infection in human *in vitro* models of lung, breast, and sarcoma tumors (Fig. 3.4F). VSVΔ51-shACP2 also showed increased cytotoxicity relative to the control across all tested cell lines at the same MOI (Fig. 3.4G).

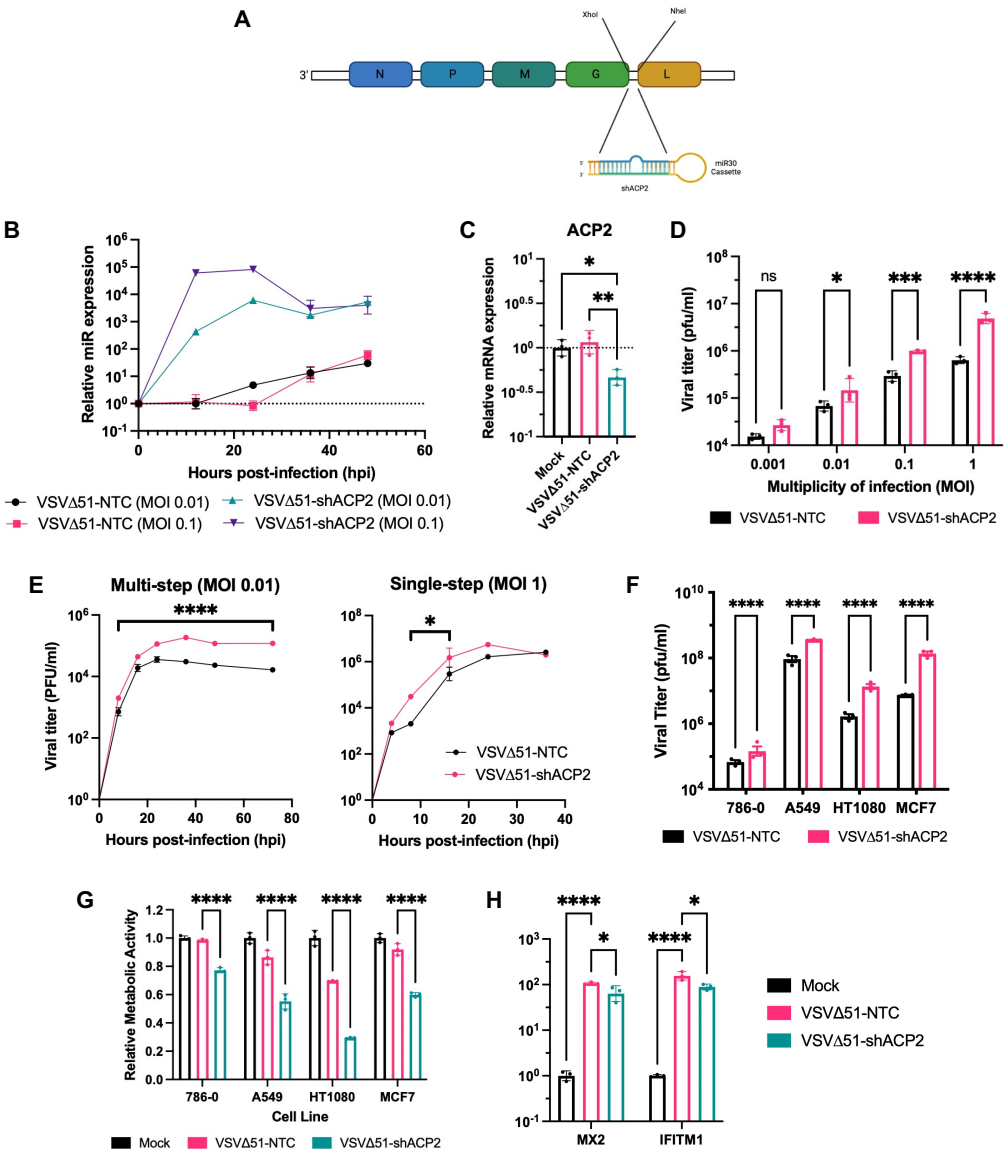

Fig 3.4. VSV expressing shRNA against ACP2 has improved infectivity and oncolysis. (A) Schematic detailing the viral backbone of VSVΔ51-shACP2. (B-D) 786-0 cells were infected with either VSVΔ51-non targeting control (NTC) or VSVΔ51-shACP2 (with indicated multiplicity of infection, MOI). (B) Cells were lysed, miRNA was extracted at indicated timepoints, then probed for miR-30 and shRNA against ACP2 cassette expression. (C) Lysates were extracted from cells 24 hpi and RNA was extracted. *ACP2* mRNA transcript levels were probed by qPCR (n=3, mean ± SD; *P<0.05, **P<0.01 by one-way ANOVA). (D) Supernatant of infected cells with different MOI were assessed for VSVΔ51 viral titer 24 hpi by viral plaque

assay (n=3, mean ± SD; *P<0.05, ***P<0.001, ****P<0.0001 by two-way ANOVA). (E) Multi-step and single-step growth curves of 786-0 infected with VSVΔ51-NTC or VSVΔ51-shACP2 (MOI 0.01 or 3). Supernatants were quantified by viral plaque assay at specified timepoints (n=3, mean ± SD; *P<0.05, ****P<0.0001 by one-way ANOVA. (F-G) Various cell lines were infected with VSVΔ51-NTC or VSVΔ51-shACP2 (MOI 0.01). (F) Supernatant was analyzed for VSVΔ51 viral titer 24 hpi by viral plaque assay (n=3, mean ± SD; ****P<0.0001 by two-way ANOVA). (G) Cell viability was measured by resazurin metabolic dye 48 hpi, normalized to the uninfected condition (n=3, mean ± SD; ****P<0.0001 by two-way ANOVA). (H) RNA was extracted from 786-0 cells infected with VSVΔ51-NTC or VSVΔ51-shACP2 24 hpi, then probed for *MX2* and *IFITM1* mRNA transcripts by qPCR (n=3, mean ± SD; *P<0.05, ****P<0.0001 by two-way ANOVA).

Finally, to confirm the proposed mechanism of action of IFN-1 repression by our novel VSVΔ51-shACP2, we analyzed 786-0 cell lysates infected for 24 hours with VSVΔ51-shACP2 for IFN-1 effectors, MX2 and IFITM1. While the magnitude was not large, VSVΔ51-shACP2 was still able to show significant repression of MX2 and IFITM1 transcription (Fig. 3.4H), similar to what was observed in 3E with the silencing RNA against ACP2. Taken altogether, this data supports that VSVΔ51-shACP2 has more potent infectivity and cytotoxicity in tumor cells compared to the control VSVΔ51 vector and operates via repression of the IFN-1 axis.

3.4 Discussion

Here, we demonstrate that multiple PPs have intimate roles in regulating the antiviral response through a high-throughput screening approach. Knockdown of some PP transcripts confer enhanced VSVΔ51 infectivity and/or oncolysis. Further molecular analysis of our top

hit, ACP2, confirmed its VSVΔ51 enhancing activity and found that its mechanism of action hinges upon repression of IFN-1 signaling and its downstream antiviral effectors. We then secondarily demonstrated that upon cloning of an ACP2-targeting shRNA into a VSVΔ51 backbone, the resulting VSVΔ51-shACP2 virus exhibited increased infectivity and cytotoxicity over its non-targeting control counterpart in multiple cancer cell lines.

Balance of the protein phosphatome is crucial to the regulation of innate cellular process including the antiviral response. The targeting of kinases using small molecular inhibitors to favor dephosphorylated states has been shown to influence the interferon signalling and resistance to infection in a multitude of ways. For example, in light of the recent SARS-CoV-2 (COVID-19) pandemic, high-specificity kinase inhibitors have been explored as a clinical therapeutic to repress SARA-CoV-2 infection (213). On the other hand, phosphatases are much harder to target with specificity given that 1) a highly conserved active tissue or phosphatase binding pocket makes specificity difficult, and 2) the positively charged active site challenges cell membrane permeability (111, 112). For these reasons, it is more feasible to execute specific PP inhibition via gene knockdown using RNAi as opposed to using small molecules (116). Accordingly, we applied this strategy with our HTS using the MISSION® silencing RNA (siRNA) Human Phosphatase Library to identify relevant PP targets to enhancing OV infectivity.

Aside from ACP2, our HTS yielded some interesting insights into the roles of other PPs that simultaneously enhanced VSVΔ51 infectivity and oncolysis (Fig. 3.1E). Eyes absent (EYA) proteins are haloacid dehalogenase PPs that have been implicated to interact with signal transducers of innate antiviral immunity including MAVS, STING and NLRX1. Transduction of EYA1-4 into murine embryonic fibroblasts has been reported to show increased IFN-β and

pro-inflammatory CXCL10 production when stimulated with pattern-associated molecular patterns (214). In our HTS, knockdown of both EYA2 and EYA4 significantly increased VSVΔ51 viral titers (Fig. 3.1D). Secondly, we found that knockdown of both regulatory and catalytic subunits of the phosphoprotein phosphatases family (PP1R16A, PPP4R1, PPP4C, PPP1R10, PPP1R14A, PPP4R1L, and PPP2R2C) conferred VSVΔ51 enhancing activity. Phosphoprotein phosphatases such as PP1 and PP2A have been shown to inactivate interferon response factors (IRF) to ultimately impede IFN responses in response to viral infection (215–217). In the case of PP1, the target PPP1R14A is responsible for negative control of the PP1 catalytic subunit; therefore, its knockdown allows for dysregulated PP1 activity and impedance of the IFN response to ultimately allow for increased viral infection (218).

On the other hand, some identified hits run counterintuitive to literature. PPP4C and PPP4R1, the two dimeric components of PP4, were part of the short list of 38 hits we identified to simultaneously increase VSVΔ51 infectivity and oncolysis upon genetic knockdown (Table 3.1). However, PP4 activity has been implicated to dephosphorylate and deactivate TBK1 to disrupt IFN-1 production via IRF3 repression. The same study found that knockdown of PPP4C in macrophages increased IFN-β production and thus reduced VSV replication (219). This discordance therefore raises two assertions: 1) the need for validation of these hits to remove false positives, or 2) the elucidation of different roles of the same PP across different contexts (*e.g.,* in immune vs. tumor cells). In both scenarios, further investigation is warranted to cement the role of each respective PP in the IFN pathway and further our understanding of how the phosphatome interacts with the natural anti-viral response.

Nonetheless, in this study we were successful in identifying the role of ACP2 in the innate antiviral response. Given the roles of ACP2 in regulating lysosome and endosome

trafficking, knockout of ACP2 was previously shown to compromise influenza A virus membrane fusion, thereby halting viral entry (210). In the context of VSVΔ51, it appears that ACP2 knockdown is not involved in VSV trafficking (220), but rather ACP2 may be necessary for intracellular viral detection given the identification of repression of the "RIG-I-like receptor signalling pathway" KEGG pathway term on *in silico* analysis (Fig. 3.3D, S3.3, S3.4). One working hypothesis for this interference may depend on the required localization of toll-like receptors (TLR) to endosomes during viral detection, which may be compromised without functional ACP2 (221). A secondary explanation could involve compromise of the JAK-STAT signalling pathway, whose components, like STAT2, were shown to be downregulated upon ACP2 knockdown from our transcriptome analysis (Fig. 3.3C). Interference of signal transduction following IFN-β binding could potentially explain our observed decreases in downstream antiviral effectors such as *MX2* and *IFITM1* (Fig. 3.3E).

The design of our RNAi-expressing VSVΔ51 vector (Fig. 3.4A) is based upon previous studies establishing the utility of a miR-30 promoter for the expression of shRNA (222). The resulting VSVΔ51-shACP2 primarily represents a proof-of-concept that PPs can be targeted using RNAi expressed by an OV vector for beneficial effects. Indeed, our VSVΔ51-shACP2 demonstrates improved viral infectivity and oncolysis through its predicted mechanism of action of IFN-1 repression (Fig. 3.4). However, there remain several limitations to this approach before it can be considered for therapeutic use. Firstly, while our knockdown efficacy was significant, it was only capable of modestly reducing ACP2 transcripts by less than 2-fold, compared to 10-fold using direct siRNA transfection. This translated to weaker inhibition of downstream IFN-1 effectors (Fig. 3.4H). Another important consideration is that upon infection of healthy tissues, the off-target gene silencing does not compromise the safety profile

of the virus. Strategies like placing RNAi effectors under tissue-specific promoters could help mitigate unwanted gene knockdown events. Finally, the immediate clinical utility of VSV is limited given lack of experience in human clinical trials; therefore, exploration of the relationship between PP knockdown and its ability to potentiate other viral vectors further along in clinical trial pipelines (*i.e., HSV-1*) represent intriguing avenues of investigation. Comprehensive strategies on addressing each of these limitations: efficacy, safety, and vector selection are outlined in a related review by our group (116).

The development of innovative strategies to improve efficacy are paramount for the continued success of oncolytic virotherapy. Altogether, this study represents a proof-of-concept for incorporating RNAi targeting PPs for increased viral infectivity and oncolysis. Next steps for this experimental series would be to validate and clone several other PP targets into VSV and test their impact on OV infectivity and oncolysis. Casting a wider net could pave the way for unexpected therapeutic synergies and hopefully, a better chance at clinical impact by OVs.

3.5 Material and Methods

Study Design

In this controlled laboratory study, the hypothesis was initially formulated upon the previous observation that vanadium-based compounds, which operate as pan-phosphatase (PP) inhibitors, increases VSVΔ51 infectivity and oncolysis. Subsequently, the objective was to identify PPs that could mimic this oncolytic virus enhancing effect. An *in vitro* approach was taken by employing a high throughput screen using the MISSION® siRNA Human

Phosphatase Library to identify PP targets, that when knocked down, could confer OV enhancement. Upon identification of top candidates, subsequent hypotheses led us to investigate their mechanism of action and its potential exploitation for further therapeutic gain.

Drugs and Chemical Reagents

Sodium orthovanadate (vanadate, Na_3VO_4), the main vanadium-based compound used in the study, was obtained from Sigma-Aldrich (cat. 450243). To prepare the sodium orthovanadate, the compounds was dissolved in water, pH-adjusted to 10, boiled until translucent, then allowed to cool to room temperature to ensure formation of stable monomeric vanadate (223). The remainder of drugs, chemical and cytokines along with their supplies, catalog numbers and solvent are listed in Supplemental Table S3.1.

Cell Lines

A complete list of the cell lines (species, tissue type, supplier) can be found in Table S1. Cells were maintained in Dulbecco's modified Eagle's medium (DMEM; HyClone cat.10-013) supplemented with 1% (v/v) penicillin-streptomycin (Gibco), 30mM HEPES buffer, and 10% (v/v) serum composed of 3-parts HyClone newborn calf serum (Thermo Fisher, cat. SH3011803) and 1-part Fetal Bovine Serum (Gibco, cat. 12483020). Cells were incubated at 37°C and 5% CO_2 conditions in a humidified incubator. Phase and fluorescence images were taken using the EVOS Live Cell Imaging System (Thermo Fisher).

Oncolytic Viruses

The Indiana serotype of vesicular stomatitis virus harboring a deletion of methionine 51 in the M protein (VSVΔ51) and insertion of green fluorescence protein (GFP) or firefly luciferase (FLuc) were used throughout this study (38). All viruses were propagated on Vero

cells and purified on 5-50% OptiPrep (Sigma-Aldrich, St. Louis, MO) gradients. Viral titers were determined by high-throughput titration according to published protocol(147), or standard plaque assay on Vero cells according to published protocol(197).

The oncolytic VSVΔ51 virus backbone and propagation protocols have been previously described (38). To generate replication-competent shRNA-expressing VSVΔ51 viruses, a non-targeting control (NTC) or a siRNA targeting ACP2, incorporated in a pre-miR-30-based short hairpin cassette flanked by XhoI and NheI restriction sites, were obtained from Integrated DNA Technology (IDT). The VSVΔ51 plasmid was digested with XhoI and NheI (NEB), and the shRNA inserts were ligated individually into the VSVΔ51 empty vector at the gene junction between the G and L proteins, following established protocols. Sanger sequencing (performed at StemCore Laboratories, Ottawa, ON) was conducted to confirm the constructs' integrity. The viruses were generated using an infection-transfection method, as previously described (222).

High Throughput siRNA Screen

The entire experimental workflow is graphically summarized as Figure 3.1A. The phosphatase library used for the high-throughput screen was taken from the MISSION® siRNA Human Phosphatase Library (cat. SI03200) targeting 303 phosphatase genes (1131 siRNA total) was acquired from Millipore Sigma and reconstituted by diluting in molecular grade RNase, DNase, protease-free water (Sigma, cat. W4502) to a final stock concentration of 2.5μM and stored at -20°C until use. Immediately prior to transfection, a working plate was derived from each library plate by diluting phosphatase siRNA (siPP) in molecular grade water to a working concentration of 0.2μM. Human 786-0 renal cell carcinoma cells were seeded at a final cell density of 1.6 x 10^4 cells/well in 96-well microplates and transfected with siRNA

using Lipofectamine® RNAiMax (Invitrogen, cat. 13778150). RNAiMax Lipofectamine was first prepared by mixing into serum-free Opti-MEM I Medium (Thermo Fisher Scientific, cat. 31985070) and allowed to incubate for 5 minutes. Respective siRNAs were then diluted into this solution and incubated for 20 minutes to allow for formation of siRNA-lipid complexes, then mixed into the cell suspension at a final siRNA concentration of 20nM. All dilutions were performed using the BioTek™ Precision™ Microplate Pipetting System (Thermo Fisher Scientific) and solutions were dispensed using the MicroFlo Select™ Microplate Dispenser (Biotek™). After 48 hours incubation in standard conditions, cells were subsequently infected with VSVΔ51-FLuc (MOI 0.05) using the manual Liquidator 96 Pipetting System (Mettler Toledo).

Infectious viral particles were quantified by high-throughput titration 48 hours post infection (hpi) and relative metabolic activity assessed by resazurin metabolic dye (Millipore Sigma, cat. SI03200). The dye was added to samples at a 1:10 dilution and incubated for 2 hours. Using a BioTek Microplate Reader (Norgen BioTek Corp, Ontario, Canada) and Gen5 2.07 software, fluorescence was measured at 590 nm upon excitation at 530 nm. Readings were normalized to the average of the uninfected, mock treated condition. To calculate *oncolysis enhancing factor* (formerly *viral sensitizing factor* (93)) for ranking of primary hits based on viability, the following equation was used.

$$Oncolysis\ enhancing\ factor = Log_{10}\left(\frac{Viability\ siPP\ alone}{Viability\ siPP + VSV\Delta 51}\right)$$

Each microplate, performed in triplicate, consisted of 80 wells of tested siRNA, two scramble siRNA controls (Mission® siRNA Universal Negative Control #1, Sigma, cat.

SIC001), two vanadate-treated wells (125μM) and two RIG-I (Millipore Sigma, cat. NM_014314, siRNA ID SASI_Hs01_00047980) knockdowns acting as transfection control. This plate layout is graphically represented as Figure S3.1B.

Small-interfering RNA (siRNA) transfection

786-0 cells were seeded at 40% density in 24-well plates in serum-free DMEM overnight. Transfections were performed using control, scramble RNA (ON-TARGETplus Non-targeting Control Pool, #D-001810-10-05, Horizon Discovery), custom siRNA against lysosomal acid phosphatase 2 (ACP2) (Thermo Fisher). Custom siRNA sequences are listed in Table S2. Transfection was performed using Lipofectamine™ RNAiMAX Transfection Reagent (Thermo Fisher, cat. 13778075) according to manufacturer's protocol in Opti-MEM™ I Reduced Serum Medium (Thermo Fisher, cat. 31985062). After 6 hours, media containing siRNA was replaced with DMEM supplemented with 1% (v/v) penicillin-streptomycin (Gibco), 30mM HEPES buffer and 10% (v/v) serum composed of 3-parts HyClone newborn calf serum (Thermo Fisher, cat. SH3011803) and 1-part Fetal Bovine Serum (Gibco, cat. 12483020). Upon reaching approximately 80% confluency, cells were treated with reagents or infected with VSVΔ51 as specified.

Quantitative Real-time Polymerase Chain Reaction

To first homogenize cells for RNA yield, cells were lysed using the QIAshredder (Qiagen, cat. 79656). RNA was then extracted using the QIAGEN RNeasy kit (Qiagen, cat. 74106) according to manufacturer's protocol and quantified using a NanoDrop™ One Microvolume UV-Vis Spectrophotometer (Thermo Fisher Scientific, Rockford, IL). The RevertAid H-Minus First Strand cDNA Synthesis Kit (Thermo Fisher, cat. K1632) was used to generate corresponding cDNA from extracted RNA. To isolate miRNA, RNA extractions

were performed using TRIzol™ reagent as per manufacturer protocol (Invitrogen). The miRNA 1st-Strand cDNA Synthesis Kit was used according to manufacturer protocol (Agilent, cat. 600036).

Resulting nucleic acid was subject to quantitative real-time PCR using primers outlined in Table S2, Applied Biosystems PowerUp SYBR Green Master Mix (Thermo Fisher, cat. A25776) in a 7500 Fast Real-Time PCR system (Applied Biosystems, Foster City, CA). Gene expression was calculated using the Pfaffl method (224). For miRNA qPCR, the universal poly-A tail (Agilent) was used as the reverse primer.

RNA-Sequencing Analysis

RNA was extracted from cell lysates as described in the previous section. Upon quantification and quality assurance, samples were shipped to the Donnelly Sequencing Centre (University of Toronto) and mRNA-seq libraries were generated using the NEB NEBNext Ultra II Directional RNA library prep kit according to manufacturer's protocol. Libraries were sequenced using the Illumina NovaSeq with paired-end 150bp reads. After sequencing, resulting Fastq files were checked for quality using FastQC (Babraham Bioinformatics, United Kingdom). Pseudo alignment and transcript quantification were performed with KALLISTO(225), and differential expression was determined using SLEUTH (226). Gene ontology analysis was performed using the Gene Ontology enrichment analysis and visualization tool (GOrilla) (211, 212). Signaling pathway topology analyses were performed using Graphite and CliPPER (Department of Biology, University of Padova, Italy) (227, 228). Finally, Kyoto Encyclopedia of Genes and Genomes (KEGG) pathway analyses was performed using the ShinyGO version 0.77 tool (South Dakota State University, United States of America) (229).

Statistics

All statistical analyses and visualization of data was performed using Prism 9 (GraphPad, San Diego, CA) software. Statistical tests were performed as indicated by figure legends including Student's t-test, one-way analysis of variance (ANOVA) with Tukey's multiple comparisons test, and two-way ANOVA. Two-tailed testing was used unless otherwise specified, and error bars represent the standard error from the mean (SEM). A P-value less than 0.05 was considered statistically significant throughout this study.

3.6 Acknowledgements

Any graphical models were created using BioRender.com (Toronto, ON, Canada) licensed to Boaz Wong (agreement #YV234Y2B6F). The authors would like to thank Dr. David Cook (University of Ottawa) for his guidance throughout the RNA sequencing analysis. The authors would also like to acknowledge Donnelly Sequencing Centre (http://ccbr.utoronto.ca/donnelly-sequencing-centre) for their efficiency and professionalism in providing their RNA-sequencing service.

Chapter 4. Pevonedistat, a First in-class NEDD8-activating Enzyme Inhibitor, sensitizes cancer cells to VSVΔ51 Oncolytic Virotherapy

Boaz Wong[1,2], Anabel Bergeron[1,2], Glib Maznyi[1], Kristy Ng[1], Anna Jirovec[1,2], Harsimrat K. Birdi[1,2], Daniel Serrano[1], Marcus Spinelli[1], Max Thomson[1], Zaid Taha[1,2], Akram Alwithenani[1,2], Andrew Chen[1], Ian Lorimer[1], Barbara Vanderhyden[1], Rozanne Arulanandam[1]*, Jean-Simon Diallo[1,2]*

[1]Centre for Innovative Cancer Research, Ottawa Hospital Research Institute; Ottawa, Ontario, Canada, K1H 8L6. [2]Department of Biochemistry, Microbiology and Immunology, Faculty of Medicine, University of Ottawa; Ottawa, Ontario, Canada, K1H 8M5. * denotes corresponding author and equal contribution.

Published on September 26, 2023 in *Molecular Therapy*

4.1 Abstract

The clinical efficacy of VSVΔ51 oncolytic virotherapy has been limited by tumor resistance to viral infection, thus strategies to transiently repress antiviral defenses are warranted. Pevonedistat is a first in-class NEDD8-activating enzyme (NAE) inhibitor currently tested in clinical trial for its antitumor potential. In this study, we demonstrate that pevonedistat sensitizes human and murine cancer cells to increase oncolytic VSVΔ51 infection, increase tumor cell death, and improve therapeutic outcomes in resistant syngeneic murine cancer models. Increased VSVΔ51 infectivity was also observed in clinical human tumor samples. We further identify the mechanism of this effect to operate via blockade of the type 1 interferon (IFN-1) response through neddylation-dependent interferon-stimulated growth factor 3 (ISGF3) repression and neddylation-independent inhibition of NF-κB nuclear translocation. Together, our results identify a role for neddylation in regulating the innate immune response and demonstrate that pevonedistat can improve the therapeutic outcomes of strategies employing oncolytic virotherapy.

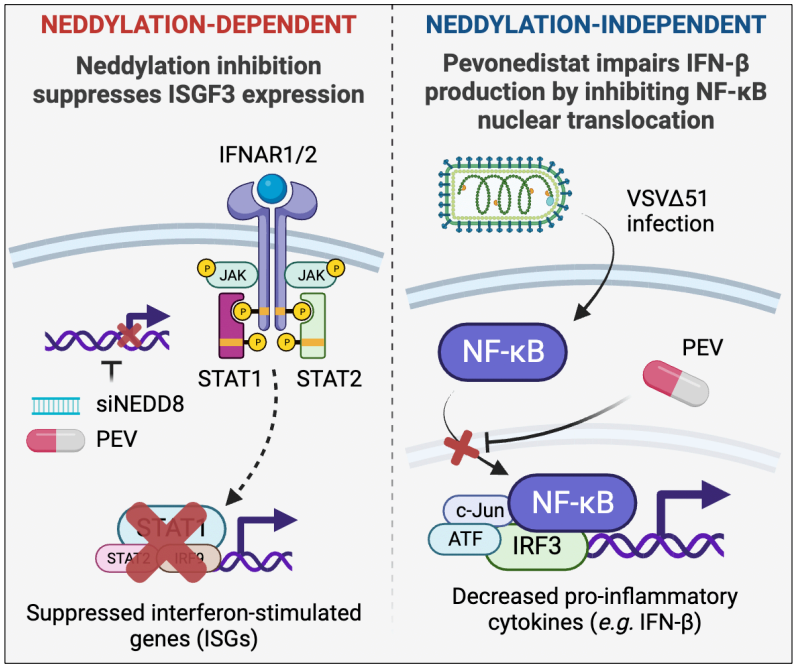

4.2 Introduction

Since the clinical approval of talimogene laherparepvec (T-VEC) for the treatment of melanoma in 2015 (27), the success of oncolytic virotherapy as a viable cancer therapeutic has seen limited advances. Describing a broad class of cancer immunotherapy, oncolytic viruses (OV) have the unique ability to selectively infect, replicate within, and kill tumor cells to not only directly reduce tumor burden, but also to orchestrate a potent antitumor response by the patient's own immune system (38, 86, 140). However, challenges pertaining to incomplete tumor infection, large variabilities in resistance to OV infectivity, and subsequent poor patient responses remain at the forefront of questions to be answered. The development of innovative solutions to overcome these barriers have become imperative to establishing the efficacy of this budding immunotherapy.

Of particular focus is the interferon (IFN) signaling pathway, which mediates the initial cellular response to infection and the production of antiviral products (230). While cancer cells are typically deficient in IFN reactivity as a byproduct of neoplastic transformation, some tumors actually demonstrate an upregulation of IFN signaling (84, 199). Consequently, strategies targeting the reduction or blockade of IFNs have shown to be effective in improving the OV response, particularly in combination with the oncolytic vesicular stomatitis virus (VSVΔ51). Using a broad pharmacological screening approach, our group has previously identified and characterized several small molecules that are effective in modulating IFN signaling to augment VSVΔ51 infectivity, spread, and tumor cell killing (93, 95, 96, 106). A common denominator between these compounds is their ability to decrease type I IFN (IFN-1) production, responsible for triggering pleiotropic effects of antiviral cytokine production, curbing cell proliferation, and adaptive immune cell activation (67, 230). This ultimately

allows for a transient window of opportunity for the OV to gain a foothold within the resistant tumor and orchestrate its full antitumor effect.

Pevonedistat, or MLN4924, is a first in-class small molecule NEDD8 (neural precursor cell expressed developmentally downregulated protein 8)-activating enzyme (NAE) inhibitor. Pevonedistat represents a first in-class tool to inhibit neddylation, a post-translational proteome regulatory process that has previously been implicated to be inappropriately upregulated in tumors and their respective microenvironments (129, 231). NAE, which is a heterodimer composed of amyloid-β precursor protein binding protein 1 (APPBP1) and ubiquitin-activating enzyme 3 (UBA3), first uses adenosine triphosphate (ATP) to attach NEDD8 to an active site cysteine residue. A subsequent transthiolation reaction attaches NEDD8 to an E2 conjugating enzyme, which is then transferred to target substrate proteins by E3 conjugating enzymes (232). As an adenosine mimetic, pevonedistat is used by NAE to create an irreversible, covalent bond with NEDD8. This complex subsequently halts the neddylation process as it cannot be used in its respective downstream processes (126).

The cellular effects of pevonedistat primarily hinge upon its ability to disrupt cullin-RING ligases (CRL) to ubiquinate target proteins for proteasome-dependent degradation. As neddylation is required for CRL activation, accumulation of targeted substrates consequently dysregulate processes of tumor suppression, damage stress responses, and inhibit NF-κB signal transduction (129, 233). At the forefront of clinical application are its antitumor effects through DNA damage-induced apoptosis (122, 234, 235). Several phase 1-3 clinical trials testing pevonedistat in combination with chemotherapy are currently underway in hematological and solid tumor cancers (236, 237). Given its antitumor potential and ability to alter cellular targets involved in IFN signaling, the objective of this study was to characterize the potentiating

effects of pevonedistat on oncolytic VSVΔ51 virotherapy and to elucidate the mechanism of action by which it confers these immunomodulatory properties.

4.3 Results

Pevonedistat sensitizes cancer cells to oncolytic VSVΔ51 infectivity

In a previously performed high-throughput screen of kinase inhibitors in combination with rhabdovirus VSVΔ51 infection, pevonedistat (Fig. 4.1A) was identified among several classes of kinase inhibitors capable of increasing VSVΔ51 infectivity and oncolysis (200). To first characterize the viral sensitizing properties of pevonedistat, human renal 786-0 carcinoma cells, a model naturally refractory to VSVΔ51 infection were used to distinctly emphasize any pharmacological viral enhancing activity. Cells were first pre-treated with a standard dose of 1μM for 4 hours, then infected with VSVΔ51 tagged with green fluorescent protein (VSVΔ51-GFP) at a low multiplicity of infection (MOI). At 24 hours post infection (hpi), we were able to demonstrate a marked increase in viral GFP transgene expression by fluorescent microscopy (Fig. 4.1B) and flow cytometry (Fig. 4.1C), supporting the robust enhancement of VSVΔ51 infectivity by pevonedistat. Further investigation by high-throughput titration using a wide concentration range of pevonedistat revealed that pevonedistat was able to significantly increase viral titer compared to VSVΔ51-infected only cells across a range of approximately 180nM to 120μM (Fig. 4.1D and S4.1A). Moreover, we demonstrate that administration of pevonedistat as early as 24 hours prior until 4 hours after infection was capable of increasing VSVΔ51 viral titer highlighting its rapid uptake and extended pro-viral mechanism of action (Fig. S4.1B). To confirm increased levels of VSVΔ51, RNA extracted from these cells waanalyzed for VSV genome expression by quantitative polymerase chain reaction (qPCR).

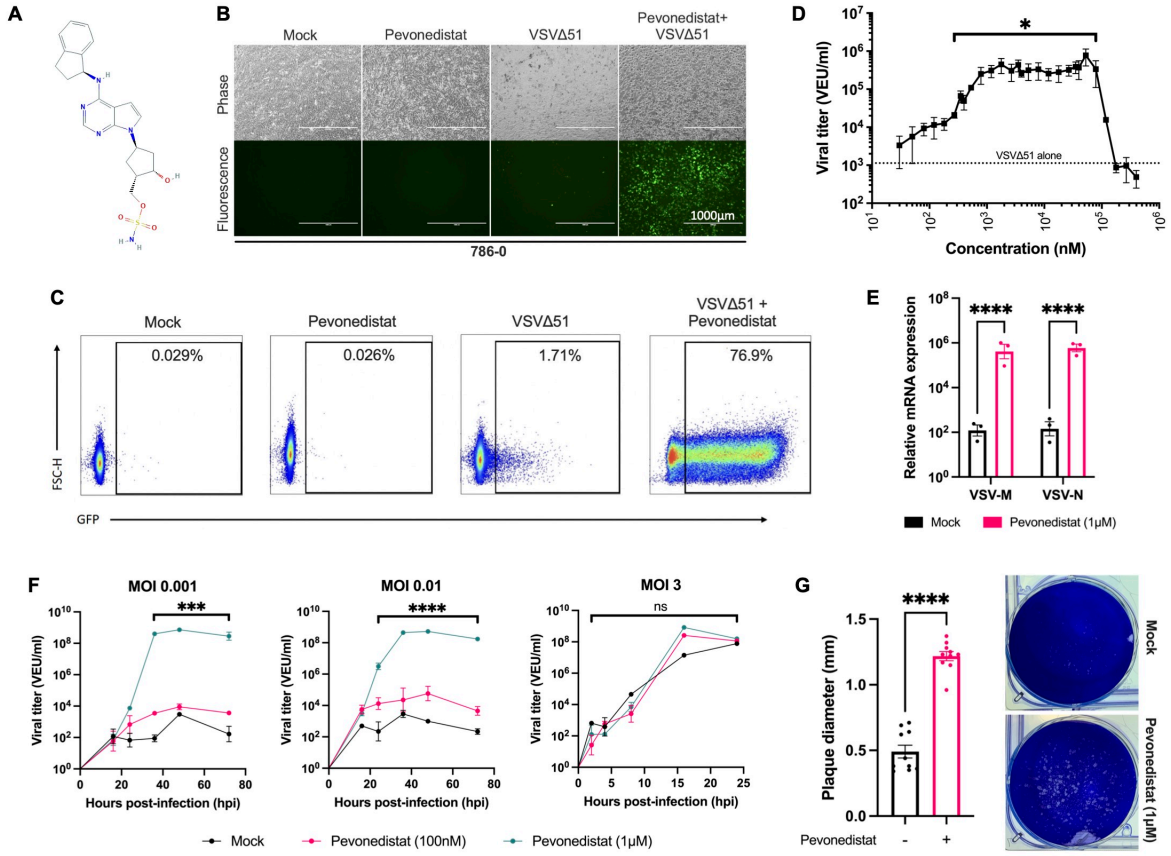

Fig. 4.1. Pevonedistat confers potent viral sensitizing activity. (A) Structure of pevonedistat (MLN4924). (B-G) Human 786-0 cells were pre-treated for 4 hours with pevonedistat (30nM – 400μM), then infected with VSVΔ51 expressing green fluorescent protein (GFP) or firefly luciferase (FLuc) at MOI 0.01. (B) Representative phase and fluorescent images were taken 24 hours post infection (hpi) (scale bar = 1000μm). (C) Cells were collected 24hpi and quantified for green fluorescence protein (GFP) expression by flow cytometry, FSC-H = forward scatter height. (D) Supernatants were quantified by high-throughput titration 24hpi (n=2, *P<0.05 by two-tailed t-test to mock treated, infected cells). (E) RNA was extracted from cells at 24hpi, then expression of *VSV-M* and *VSV-N* genes quantified by qPCR (n=3, mean ± SD; ****P<0.0001 by Student's t-test). (F) Multi-step and single-step growth curves of 786-0 treated with pevonedistat, then infected with VSVΔ51-FLuc (MOI 0.001, 0.01, 3). Supernatants were quantified by high-throughput titration at specified timepoints (n=3, mean ± SD; ***P<0.001, ****P<0.0001 by one-way ANOVA compared to the mock treated, mock infected condition). (G) 786-0 were treated with pevonedistat (1μM), then infected with

VSVΔ51 (MOI 0.0001). After 1 hour, an agarose overlay was added. At 48hpi, cells were then stained with Coomassie blue and plaque diameters were measured at random (n=10, mean ± SD; ****P<0.0001 by two-tailed t-test).

Expectedly, messenger RNA (mRNA) levels of VSV matrix protein (M) and nuclear protein (N) were significantly increased in pevonedistat-treated cells compared to their untreated counterparts (Fig. 4.1E).

Further investigation into the ability of pevonedistat to potentiate viral infectivity was explored by comparing multi-step to single-step growth curves. Pevonedistat was able to robustly enhance VSVΔ51 when infected at a low MOI of 0.001 or 0.01, but not at a high MOI of 3 by high-throughput titration (Fig. 4.1F). This suggests that pevonedistat promotes viral spread to increase its growth. However, given that pevonedistat was able to increase the spread of wild-type VSV, we cannot exclude that pevonedistat may also have some impact on VSV replication or viral entry (Fig. S4.1D). Nevertheless, analysis of viral spread by plaque expansion assay demonstrated that pevonedistat significantly increased the average plaque diameter of each viral foci in a monolayer of 786-0 cells as visualized by Coomassie blue stain (Fig. 4.1G).

Pevonedistat confers VSVΔ51 viral sensitization across a variety of tumor models

Given that pevonedistat is currently under clinical investigation for its antitumor effect (236, 237), we sought to establish its viral sensitizing ability across a large variety of cancer types. In both human and murine models, we successfully demonstrate that pevonedistat

increases VSVΔ51-GFP viral titer across different solid and hematological cancer cell lines (Fig. 4.2A). Fluorescent microscopy confirms increased VSVΔ51-GFP transgene expression in these cell lines (Fig. S4.2A). This trend was also observed in human ovarian (OVAPT) and glioma (PriGO) patient-derived cell lines where pevonedistat also significantly increased VSVΔ51 viral titer as determined by viral plaque assay (Fig. 4.2B). Moreover, pevonedistat does not increase viral replication in isolated primary murine hepatocytes, demonstrating that tumor selectivity is maintained (Fig. 4.2C). Pevonedistat also increased VSV infection of isolated human T-cell lymphocytes (Fig. S4.2B).

To test this phenomenon in an *ex vivo* model, murine CT26WT colon carcinoma cells were implanted into BALB/c mice. Mice were culled upon reaching a tumor volume of 1500mm^3. Normal brain, lung, spleen and muscle cores, and tumor cores were extracted, pre-treated with 10μM pevonedistat, then infected with VSVΔ51-GFP. Fluorescent images 24hpi confirm that pevonedistat has significant viral sensitizing properties in tumors *ex vivo*, but not in physiological tissue (Fig. 4.2D). In fact, pevonedistat was able to increase VSVΔ51 viral titer by over 30-fold in the CT26WT model as indicated by viral plaque assay. Similar results were also obtained in *ex vivo* 76-9 rhabdomyosarcoma cores in C57BL/6 mice (Fig. S4.2C and fig. S4.2D). When tested in primary human *ex vivo* clinical samples, pevonedistat was also able to increase VSVΔ51 infection across the large variety of tumor types acquired for our assays including from breast, colon, lung, rectal and renal as demonstrated by viral plaque assay and fluorescent microscopy (Fig. 4.2E). In the rectal cancer sample, pevonedistat increased the viral titer by over 15-fold. Along with Fig. 4.2B using patient-derived *in vitro* models, these results provide rationale for testing pevonedistat and VSVΔ51 combinational therapy in a clinical setting.

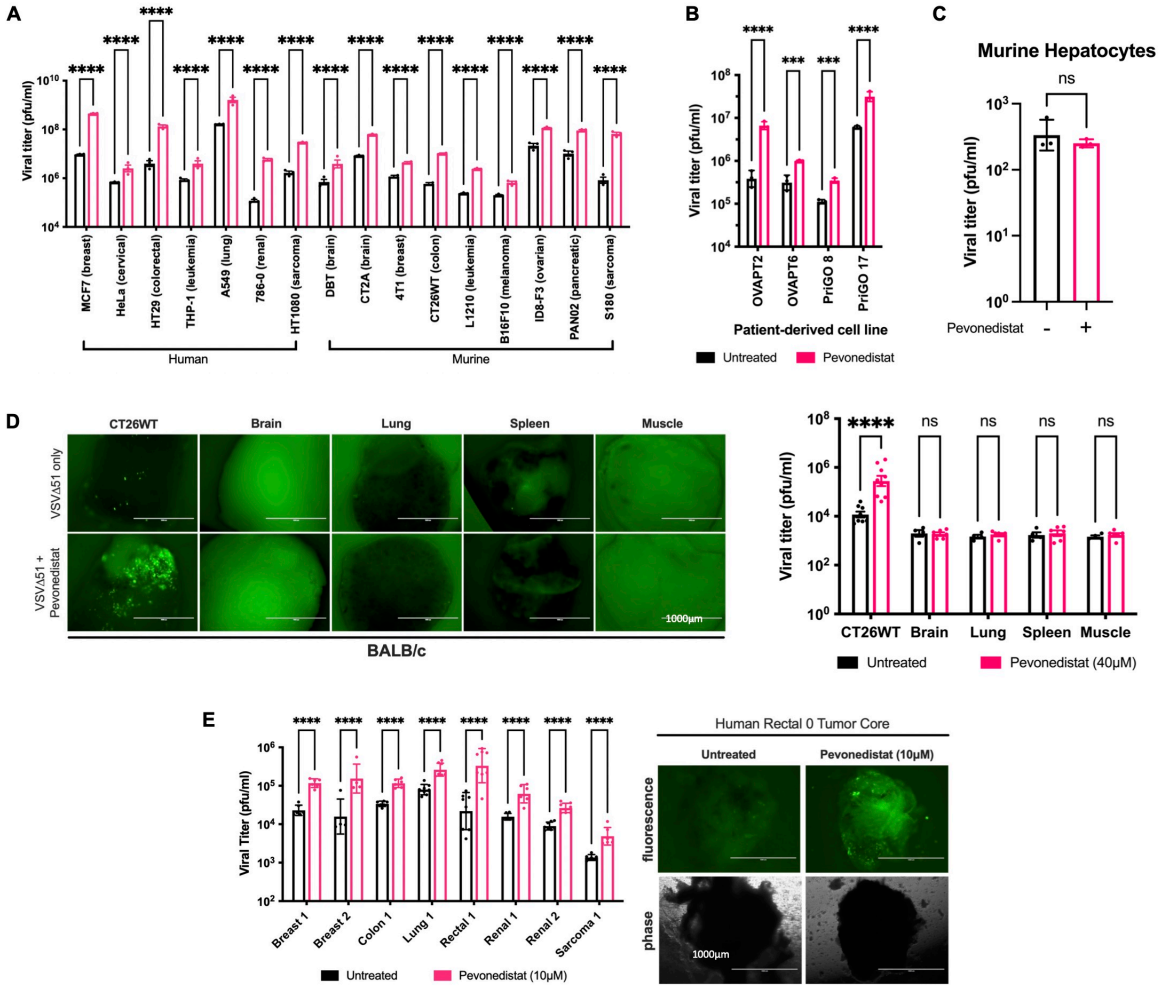

Fig. 4.2. Pevonedistat sensitizes human and murine tumor types to VSVΔ51. (A) Various human and murine cell lines were pre-treated ± pevonedistat (1μM), then infected with VSVΔ51-GFP (MOI 0.01). At 24 hours post infection (hpi), supernatants were quantified for viral titer by plaque assay (n=3, mean ± SD; ****P<0.0001 by two-tailed t-test). (B) Patient-derived ovarian (OVAPT) and glioma (PriGO) cells were pre-treated ± pevonedistat (1μM), then infected with VSVΔ51-GFP (MOI 0.01). At 48hpi, supernatants were quantified for viral titer (n=3, mean ± SD; ***P<0.001, ****P<0.0001 by two-tailed t-test). (C) Primary murine hepatocytes were isolated, cultured, treated ± pevonedistat (1μM) for 4 hours, then infected with VSVΔ51-Fluc (MOI 0.05). At 40hpi, supernatants were quantified for viral titer (n=3, mean ± SD). (D) CT26WT colon tumors were grown subcutaneously in BALB/c mice, then excised and cored upon reaching 1500mm^3. Normal brain, lung, spleen, and muscle tissues

were also obtained and cored. (E) Clinical human samples were obtained and cored. (D,E) Cores were treated with pevonedistat (10μM) for 4 hours, then infected with VSVΔ51-GFP (3 x 10^4 pfu/core). At 24hpi, representative fluorescent images were obtained (scale bar = 1000μm). Supernatants were taken 48hpi and quantified for viral titer (n>6, mean ± SD; ns = no significance, *P< 0.05, ****P<0.0001 by two-tailed t-test).

Pevonedistat increases VSVΔ51-mediated oncolysis through apoptotic pathways

Similar to other small molecules with viral sensitizing properties, we hypothesized that pevonedistat could also synergize with VSVΔ51 to increase apoptosis-mediated oncolysis (238, 239). 786-0 cells were pre-treated with various concentrations of pevonedistat for 4 hours and infected with VSVΔ51 (MOI 0.01). Cell viability was then assayed using resazurin metabolic dye 48hpi. While pevonedistat on its own had a calculated median lethal dose (LD50) of 109.6μM, the addition of VSVΔ51 robustly reduced the LD50 to 7.36μM with significant differences detected at a concentration as low as 120nM (Fig. 4.3A). This synergistic cytotoxicity phenomenon can be generalized across different solid and hematological tumor types using sub-lethal doses of pevonedistat (Fig. 4.3B). Conversely, isolated primary murine hepatocytes treated with pevonedistat and infected with VSVΔ51 showed no significant viability differences from hepatocytes treated only with pevonedistat (Fig. S4.3A).

Next, to establish the role of apoptosis, 786-0 cells treated in combination with pevonedistat and VSVΔ51 (MOI 0.1) were lysed 48hpi and probed for downstream effectors of apoptosis by western blot (Fig. 4.3C). As expected, cells treated with the combination

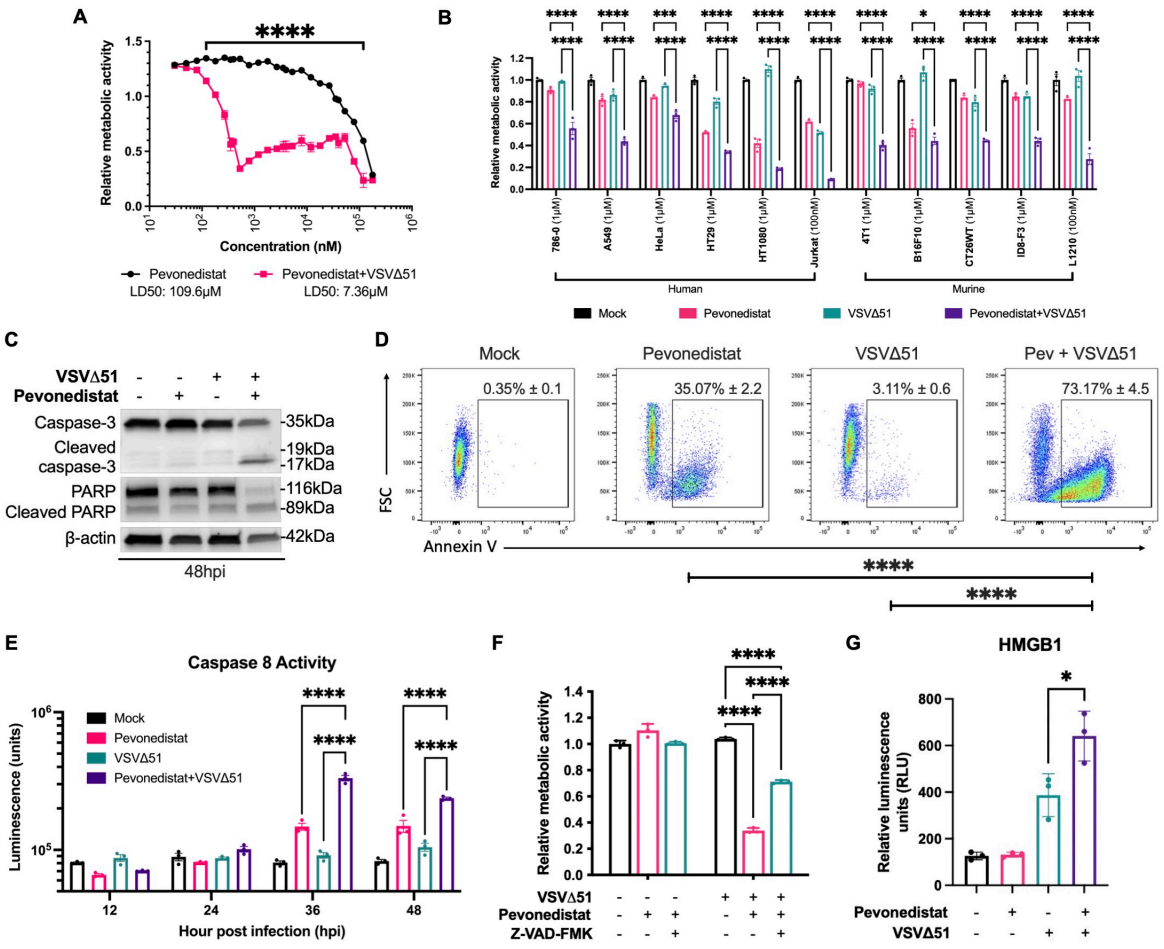

Fig. 4.3. Pevonedistat synergizes with VSVΔ51 to induce apoptosis via TNF-α pathways. (A) Human renal 786-0 carcinoma cells were pre-treated with pevonedistat (30nM – 175μM), then infected with VSVΔ51 (MOI 0.01). At 48 hours post infection (hpi), cells were measured for cell viability using resazurin metabolic dye normalized to untreated, uninfected cells. Lethal dose (LD50) was calculated (n=3, mean ± SD; ****P<0.0001 by two-tailed t-test). (B) Indicated cell lines were pre-treated ± pevonedistat (1μM), then infected ± VSVΔ51 (MOI 0.01). Cell viability was measured at 48hpi (n=3, mean ± SD; **P<0.01, ****P<0.0001 by one-way ANOVA). (C-E) 786-0 cells pre-treated with pevonedistat (1μM) for 4 hours and infected with VSVΔ51 (MOI 0.01). (C) At 48hpi, cells were lysed and probed for caspase-3, PARP, and β-actin by western blot. (D) Cells collected 48hpi were stained for Annexin V by flow cytometry, FSC = forward scatter area (n=3, mean ± SD; ****P<0.0001 by one-way ANOVA). (E) At indicated timepoints, 786-0 cells were measured for caspase-8 activity using

a luciferase-based assay (n=3, mean ± SD; ****P<0.0001 by one-way ANOVA). (F) 786-0 cells were treated ± pevonedistat (1μM) ± Z-VAD-FMK (10μM) for four hours, then infected ± VSVΔ51 (MOI 0.01). Cell viability was measured 48hpi (n=3, mean ± SD; ****P<0.0001 by two-way ANOVA). (G) 786-0 cells were pre-treated with pevonedistat (1μM), then infected with VSVΔ51 (MOI 0.01) 4 hours later. HMGB1 levels were assessed using a luminescence-based assay 48 hpi (n=3, mean ± SD; *P<0.05 by one-way ANOVA).

---

showed markedly higher levels of cleaved caspase-3 and decreased levels of full-length poly (ADP-ribose) polymerase (PARP), indicating their increased activation. Similarly, flow cytometry analysis of these cells following Annexin V staining demonstrated a significantly greater proportion of positive cells in the combination treatment compared to either monotherapy, suggesting increased apoptosis in this population (Fig. 4.3D). We then sought to assess the activity of caspase 8, the subsequent initiator to the extrinsic apoptotic cascade, which was analyzed via luciferase assay. Our data revealed that caspase-8 activity in cells treated in combination with pevonedistat and VSVΔ51 peaked at 36hpi and remained significantly increased 48hpi compared to all other conditions (Fig. 4.3E). Moreover, the addition of the broad-spectrum caspase inhibitor Z-VAD-FMK was able to significantly rescue cell viability in cells co-treated with pevonedistat and VSVΔ51 from 33% to 71%, supporting that the oncolytic impact of pevonedistat ultimately operates through caspase-dependent apoptotic mechanisms (Fig. 4.3F).

We then wanted to investigate the impact of pevonedistat on immunogenic modes of cell death. To do this, we looked at mobility group box 1 protein (HMGB1), which is a damage-associated molecular pattern released to activate the innate immune system (240). We assessed

HMGB1 secretion using a luminescence-based assay as a surrogate for immunogenic cell death (ICD). The data revealed that 786-0 cells treated in combination with pevonedistat and VSVΔ51 increased secretion of HMGB1 compared to cells only infected with VSVΔ51, suggesting increased ICD in combination with pevonedistat (Fig. 4.3G).

Pevonedistat improves oncolytic VSVΔ51 therapeutic efficacy in vivo

Upon establishing the potentiation of VSVΔ51 oncolytic efficacy by pevonedistat, we wondered whether this combinational treatment regimen would improve the anti-cancer therapeutic efficacy of oncolytic VSVΔ51 therapy in mouse models of cancer. Syngeneic murine colon CT26WT or mammary 4T1 carcinoma cells, both of which demonstrated marked viral sensitization responses *in vitro*, were subcutaneously implanted into 6-week-old BALB/c mice and allowed to progress to 100mm^3. Mice were then injected intratumorally with pevonedistat (90mg/kg), then 1 x 10^8 pfu of VSVΔ51 4 hours later for a total of three treatments spaced one day apart (day 0, 2 and 4). When mice were imaged using a live in vivo imaging (IVIS) system 7 days after treatment, tumors exhibited greater luminescence suggesting increased concentration of VSVΔ51 (Fig. S4.4B). Luminescence was minimal in other physiological tissues supporting the tumor selectivity of our treatment. Mice given the combination therapy were successfully able to suppress tumor progression as tumor volumes taken post-treatment were significantly smaller when compared to either monotherapy (Fig. 4.4A, 4.4B). For survival studies, mice were culled according to animal care guidelines when tumor volumes reached 1500mm^3. In accordance with the greater tumor control observed in mice receiving the combination treatment, 4/15 (27%) mice bearing CT26WT tumors achieved

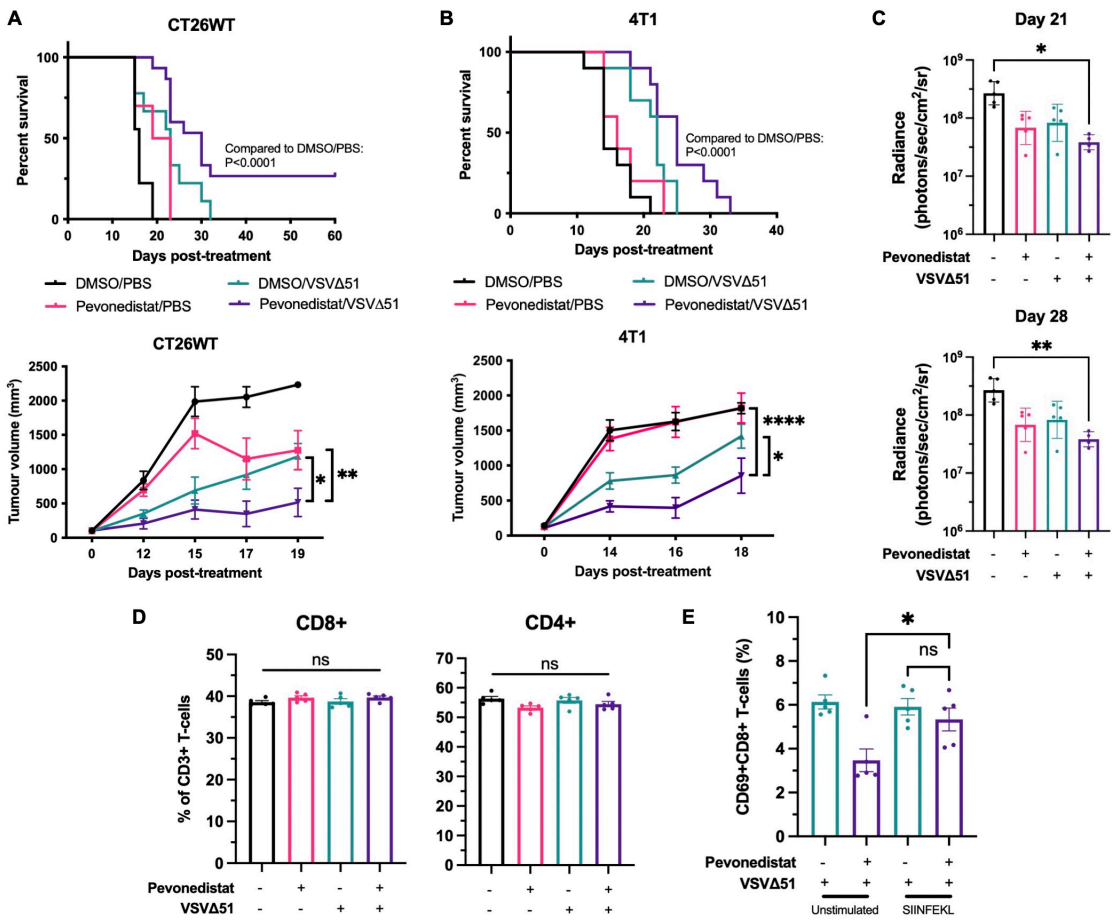

Fig. 4.4. Pevonedistat improves VSVΔ51 therapeutic efficacy in murine *in vivo* tumor models. (A) Colon CT26WT and (B) mammary 4T1 tumors were implanted into the right flank of BALB/c mice. Upon reaching sufficient size, tumors were injected intratumorally with pevonedistat (90mg/kg). Four hours later, tumors were then injected intratumorally with VSVΔ51 (1 x 10^8 pfu/tumor). Tumor volumes were monitored every 2-3 days (n > 10, mean ± SEM; *P<0.05, **P<0.01 by one-way ANOVA). Mice were culled when tumor volumes reached 1500mm^3 for survival analysis. Kaplan-Meier curves were plotted and compared using the log-rank (Mantel-Cox) test (n=10 to 15). (C) Ovarian ID8-Tp53-/- (F3) cells were injected intraperitoneally and allowed to achieve sufficient tumor burden. Mice were then injected intraperitoneally with pevonedistat (90mg/kg), then VSVΔ51 (1 x 10^8 pfu) three times, spaced one day apart. Tumor burden was assessed by luminescence signal measurements taken with the *in vivo* imaging system (IVIS) and quantified at day 21 and 28 after first treatment (n=4-5, mean ± SEM; *P<0.05, **P<0.01 by two-way ANOVA, all other comparisons not significant).

(D,E) Melanoma B16 tumors overexpressing OVA antigen (B16-OVA) were implanted into the right flank of C57BL/6 mice. When tumor volume reached 100mm^3, mice were injected intratumorally with three doses of pevonedistat (90mg/kg), then VSVΔ51 (1 x 10^8 pfu/tumor), spaced one day apart. (D) 7 days after implantation, blood was harvested and analyzed by flow cytometry for proportions of CD4+ and CD8+ T-cells (n=5, mean ± SD; ns = no significance by one-way ANOVA). (E) Splenocytes were also independently stimulated using a CD8-OVA specific peptide (SIINFEKL) and assessed for CD69+CD8+ T-cell populations (n=5, mean ± SD; *P<0.05, **P<0.01 by one-way ANOVA) by flow.

---

complete remission whereas all other mice receiving placebo or monotherapies succumbed to their tumor burden (Fig. 4.4A; P=0.001 vs. Pevonedistat group, P=0.03 vs. VSVΔ51 group). In the more aggressive 4T1 model, the pevonedistat + VSVΔ51 combination also significantly prolonged survival compared to all other conditions (Fig. 4.4B; P=0.0009 vs. Pevonedistat group, P=0.04 vs. VSVΔ51 group). These results demonstrate that pevonedistat in combination with VSVΔ51 therapy confers improved therapeutic benefit when compared to mice receiving placebo or either monotherapy.

We then wanted to investigate the efficacy of systemically administered pevonedistat combination therapy in a disseminated model of intra-abdominal cancer. Murine ID8-Tp53-/- (F3) ovarian cancer cells were tagged with firefly luciferase, injected into the peritoneum of C57BL/6 mice, and monitored using IVIS. When sufficient tumor burden was achieved (7d post implantation), mice were injected intraperitoneally with pevonedistat (90mg/kg), then 1 x 10^8 pfu VSVΔ51 4 hours later. Compared to mice receiving placebo treatment, mice receiving combinational treatment demonstrated significantly reduced tumor burden as measured by luciferase signal, which was notably not significant for either monotherapy (Fig. 4.4C).

Finally, to investigate the in vivo immunological response to pevonedistat + VSVΔ51 combinational therapy, we performed a descriptive analysis of T- cell populations. Using the murine B16 melanoma model expressing OVA-antigen (B16-OVA), tumors were established in C57BL/6 mice and treated intratumorally with pevonedistat (90mg/kg) and VSVΔ51 (1 x 10^8 pfu) for three doses, then blood was collected 7 days after first treatment for flow cytometry. The results revealed that pevonedistat alone decreased circulating CD3+ immune cell populations (Fig. S4.4C) but maintained similar proportions of CD4+ and CD8+ T-cells (Fig. 4.4D). More importantly, when bulk splenocytes from VSV-treated or pevonedistat + VSVΔ51 combination treated mice were stimulated using an OVA-specific peptide (SIINFEKL), no significant difference in the proportion of activated CD69+CD8+ T-cells was observed (Fig. 4.4E). These data together support comparable cytotoxic T-cell anti-tumor immunological response induced by combined VSVΔ51 and pevonedistat, but conversely suggest that differences in tumor-specific T-cells may not be the main driver of increased efficacy *in vivo*.

Pevonedistat impairs the antiviral type 1 interferon response

To take an unbiased approach in elucidating the viral sensitizing mechanism of pevonedistat, we first employed RNA-sequencing to analyze whole transcriptome changes in response to pevonedistat and VSVΔ51 combinational therapy. RNA was extracted from 786-0 cells pre-treated with or without pevonedistat (1μM) for 4 hours and infected with or without VSVΔ51 (MOI 0.01) after 24 hours. After sequencing, gene expression profiles between cells infected with VSVΔ51 treated with or without pevonedistat identified 3,038 genes that were significantly upregulated ($P < 0.05$, $\log_2$-fold change >2) and 3,326 genes that were

significantly downregulated (Fig. 4.5A). Gene ontology (GO) enrichment analyses were performed on ranked lists using the GOrilla tool (211, 212), which confirmed upregulation of previously established processes of pevonedistat including cellular processes of DNA metabolism, cell cycle regulation and stress responses (Fig. S4.5A) (130, 241, 242). More importantly, the GO analysis identified defense responses to virus, immune response and the IFN-1 signaling as being significantly downregulated in both the presence and absence of infection (Fig. 4.5B and Fig. S4.5B). Upon closer inspection of the genes related to the "Defense response to virus" GO term, almost all genes were downregulated upon addition of pevonedistat with the promyelocytic leukemia protein (PML) gene being downregulated by approximately 79-fold (Fig. 4.5C). Moreover, graphing the $\log_2$-fold change of all genes related to the IFN-1 GO term revealed that these genes were significantly downregulated upon the addition of pevonedistat, even in the absence of VSVΔ51 infection (Fig. 4.5D). These findings support that pevonedistat behaves similarly to many other viral-sensitizing compounds by impairing the IFN-1 response to increase VSVΔ51 sensitivity (86). However, not only does pevonedistat impair the cellular ability to respond to viral infection but it continues to suppress the antiviral response even in the absence of infection.

Neddylation inhibition confers viral sensitizing activity through ISGF3 repression

To gain insight into which transcription factors were modulated in response to pevonedistat during VSVΔ51 infection, we first analyzed our RNA sequencing dataset by inputting significantly downregulated genes upon addition of pevonedistat using the published TFactS tool in 786-0 cells (151). Our *in silico* results identified that STAT1 is inhibited with

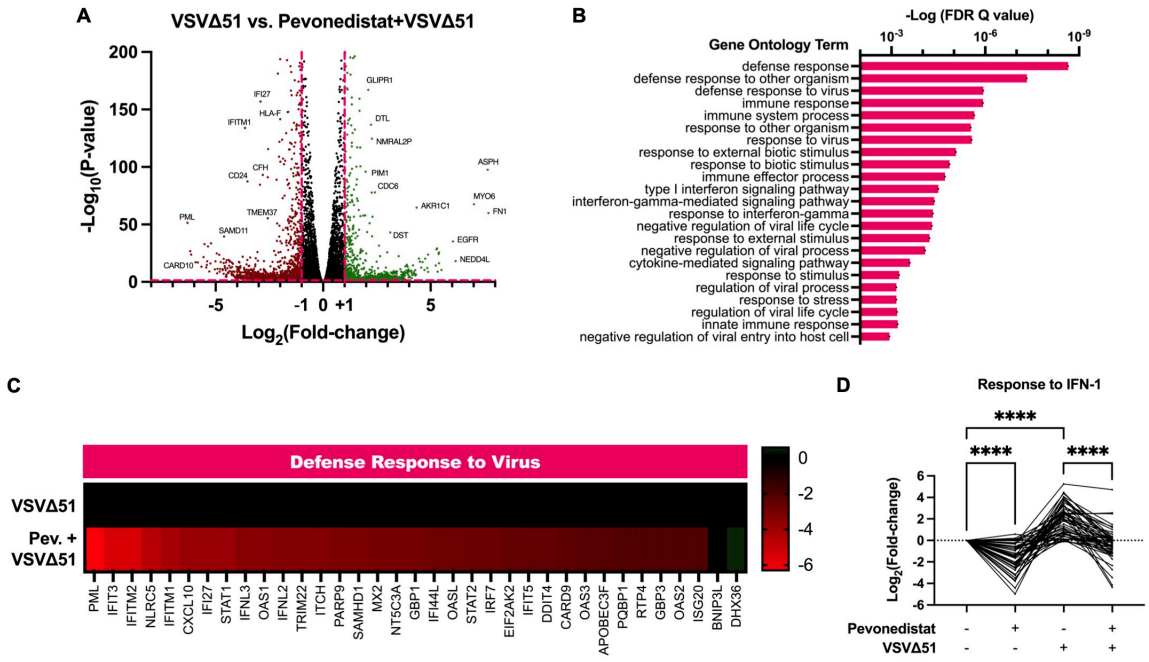

Fig. 4.5. Pevonedistat impairs the IFN-1 response. (A-D) Two biological replicates of 786-0 cells were pre-treated ± pevonedistat (1μM) for 4 hours, then infected ± VSVΔ51 (MOI 0.01) for 24 hours. RNA was extracted and sequenced. Processing by KALLISTO pseudo-alignment and SLEUTH yielded normalized $\log_2$-fold change in differential gene expression and P-values between the VSVΔ51 infected condition vs. the pevonedistat + VSVΔ51 condition (225, 226). (A) Each gene was plotted on a volcano plot, and notable hits were named. (B) Significantly downregulated (>2 $\log_2$-fold change) gene expressions were processed by GOrilla to identify relevant gene ontology (GO) terms. (C) Heat map of differential gene expressions related to the "Defense response to virus" GO term normalized to the mock treated, uninfected control condition. (D) Log_2-fold changes of genes related to the "Response to type 1 interferon" GO term between conditions were plotted. Overall gene expressions levels were compared (n=2; ****P<0.0001 by one-way ANOVA).

pevonedistat both in the absence and presence of VSVΔ51 infection (Fig. 4.6A). Indeed, a heatmap of STAT1 regulated genes demonstrates a global reduction in RNA transcripts upon pevonedistat treatment (Fig. 4.6B). Cells respond to IFN cytokines via activation of the JAK (Janus activated kinase) / STAT (signal transducer and activator of transcription) pathway. Therefore, STAT1 represents a crucial player in the IFN-1 response given its role in the interferon-stimulated growth factor complex 3 (ISGF3), along with STAT2 and interferon regulatory factor 9 (IRF9), which propagates transcription of downstream interferon-stimulated genes (ISGs) by binding to the interferon-stimulated response element (31). To investigate this relationship, whole and fractionated cell lysates were probed for the components of ISGF3: STAT1, STAT2 and IRF9. We show that pevonedistat causes a global reduction in protein availability of ISGF3 components (Fig. 4.6C ad fig. S4.6A). Different concentrations of pevonedistat were unable to markedly influence phosphorylation levels of STAT1 and STAT2 in response to IFN-β treatment (Fig. S4.6B). On the RNA level, we found that pevonedistat significantly decreased transcription of STAT1 and its ISGF3 counterparts, as well as several of its downstream ISGs (IRF7, MX2, IFTM1) relative to both mock and VSVΔ51 only conditions (Fig. 4.6D and fig. S4.6C).

Pevonedistat confers most of its cellular effects by inhibiting neddylation activity; therefore, we wondered whether inhibiting the neddylation pathway via silencing RNA (siRNA) could recapitulate the same viral sensitizing effects. 786-0 cells were transfected with siRNA targeting NEDD8 or UBA3, key components of the neddylation mechanism, and successful knockdown was validated at both the protein and RNA level (Fig. 4.6E,F and fig. S4.6D,E). Transfected cells were subject to the same treatment regimen of pevonedistat pre-

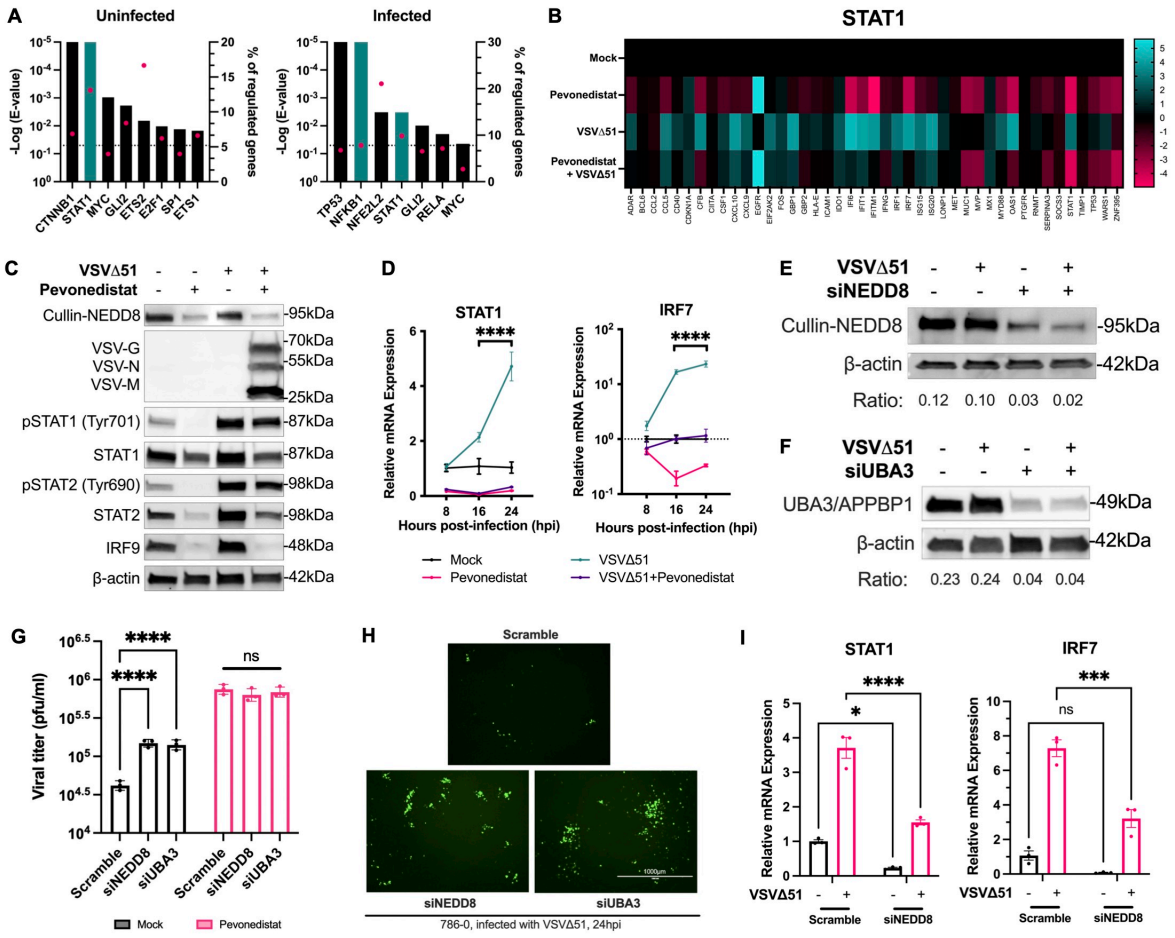

Fig. 4.6. Neddylation inhibition confers some viral sensitizing activity by repressing ISGF3. (A) Differential gene expressions from performed RNA-sequencing between the mock vs. pevonedistat condition (uninfected) and between the VSVΔ51 infected condition vs. the pevonedistat + VSVΔ51 condition (infected) were input into TFactS to predict involved transcription factors (151). E-value and percentage of regulated genes were plotted. (B) Heatmap of log_2-fold change of genes regulated by the STAT1 transcription factor. (C,D) Human renal 786-0 carcinoma cells were pre-treated ± pevonedistat (1μM) for 4 hours, then infected ± VSVΔ51 (MOI 0.1). (C) At 24 hours post infection (hpi), cells were lysed and probed for proteins as indicated by western blot. (D) Cells were lysed at 8, 16, and 24hpi and expression of *STAT1* and *IRF7* were quantified by qPCR (n=3, mean ± SD; ****P<0.0001 by one-way ANOVA between the VSVΔ51 infected condition vs. pevonedistat + VSVΔ51 condition). (E-I) 786-0 cells were transfected either with scramble, control siRNA or siRNA

targeting NEDD8 or UBA3. Transfected cells were then pre-treated ± pevonedistat (1μM) for 4 hours, then infected ± VSVΔ51 (MOI 0.05). (E,F) Cells were lysed at 24hpi and probed for NEDD8 or UBA3 protein expression by western blot. (G) Supernatant was taken 24hpi and quantified for viral titer by plaque assay (n=3, mean ± SD; ns = no significance, ****P<0.0001 by two-way ANOVA). (H) Representative fluorescent images were taken 24hpi (scale bar = 1000μm). (I) Lysates taken at 24hpi were probed for *STAT1* and *IRF7* expression by qPCR (n=3, mean ± SD; *P<0.05, ****P<0.0001 by two-way ANOVA).

---

treatment for 4 hours, then infection with VSVΔ51-GFP (MOI 0.01). Supernatant analyzed for viral titer by plaque assay demonstrates an increase in VSVΔ51 viral titer with pevonedistat upon NEDD8 or UBA3 knockdown (Fig. 4.6G). This finding was confirmed by representative fluorescent images taken 24hpi, which display increased tagged GFP expression upon knockdown of NEDD8 and UBA3 (Fig. 4.6H). Moreover, analysis of mRNA from treated, transfected cells 24hpi by qPCR demonstrated that siRNA against neddylation components on their own were able to inhibit transcription of STAT1 and downstream IRF7 (Fig. 4.6I and fig. S4.6F). Interestingly, this phenomenon did not apply in normal MRC5 lung fibroblasts (Fig. S4.6G). Together, these data support that pevonedistat's viral sensitizing ability is, at least in part, mediated by a neddylation-dependent suppression of ISGF3 signaling that was reproduced using a genetic approach to neddylation knockdown.

Pevonedistat inhibits NF-κB independently of neddylation to block the primary IFN-1 response

Given that neddylation inhibition on its own was unable to recapitulate the full viral sensitizing effect of pevonedistat, we sought to identify a second mechanism of action. Another

notable observation from the TFactS analysis was the inhibition of NF-κB transcriptional activity by pevonedistat in VSVΔ51 infected cells. Pevonedistat has previously been reported in the literature to inhibit NF-κB nuclear translocation (243), and to repress pro-inflammatory cytokine production (133, 244). We therefore sought to confirm this effect in our pevonedistat + VSVΔ51 combination therapy. Indeed, nuclear/cytoplasmic fractionated lysates of 786-0 cells pre-treated with pevonedistat and infected with VSVΔ51 for 24 hours showed markedly less NF-κB protein expression, but not IRF3, in nuclear fractions compared to cells infected only with VSVΔ51 (Fig. 4.7A). The inhibition of NF-κB nuclear translocation in response to VSVΔ51 infection and TNF-α stimulation was also observed by immunofluorescence (Fig. 4.7B,C, fig. S4.7A,B). As expected, treated cells showed repressed transcription of pro-inflammatory cytokines controlled by NF-κB signaling (Fig. 4.7D) including the central IFN-1 cytokine, IFN-β as early as 16hpi (Fig. S4.7D). Quantification of IFN-β secretion 24hpi by enzyme-linked immunosorbent assay (ELISA) followed a similar trend (Fig. 4.7E).

Next, we wondered if neddylation inhibition via gene silencing would be able to recapitulate these same phenomena. Our results demonstrate that siRNA targeting NEDD8 was in fact unable to abrogate induced NF-κB nuclear translocation (Fig. 4.7F and fig. S4.7E), impair IFN-β transcription (Fig. 4.7G), nor impair the secretion of IFN-β in response to VSVΔ51 (Fig. S4.7H). This same nuclear NF-κB inhibiting phenomenon was confirmed in cells treated with siRNA against UBA3 (Fig. S4.7F,G). Together, these results suggest that pevonedistat's ability to inhibit NF-κB nuclear translocation and abrogate IFN-β production may be independently conferred from its ability to inhibit neddylation. Moreover, further investigation demonstrates that pevonedistat is still able to increase viral titers (Fig. S4.7I) while inhibiting the transcription of STAT1 and downstream IRF7 (Fig. 4.7H and fig. S4.7J),

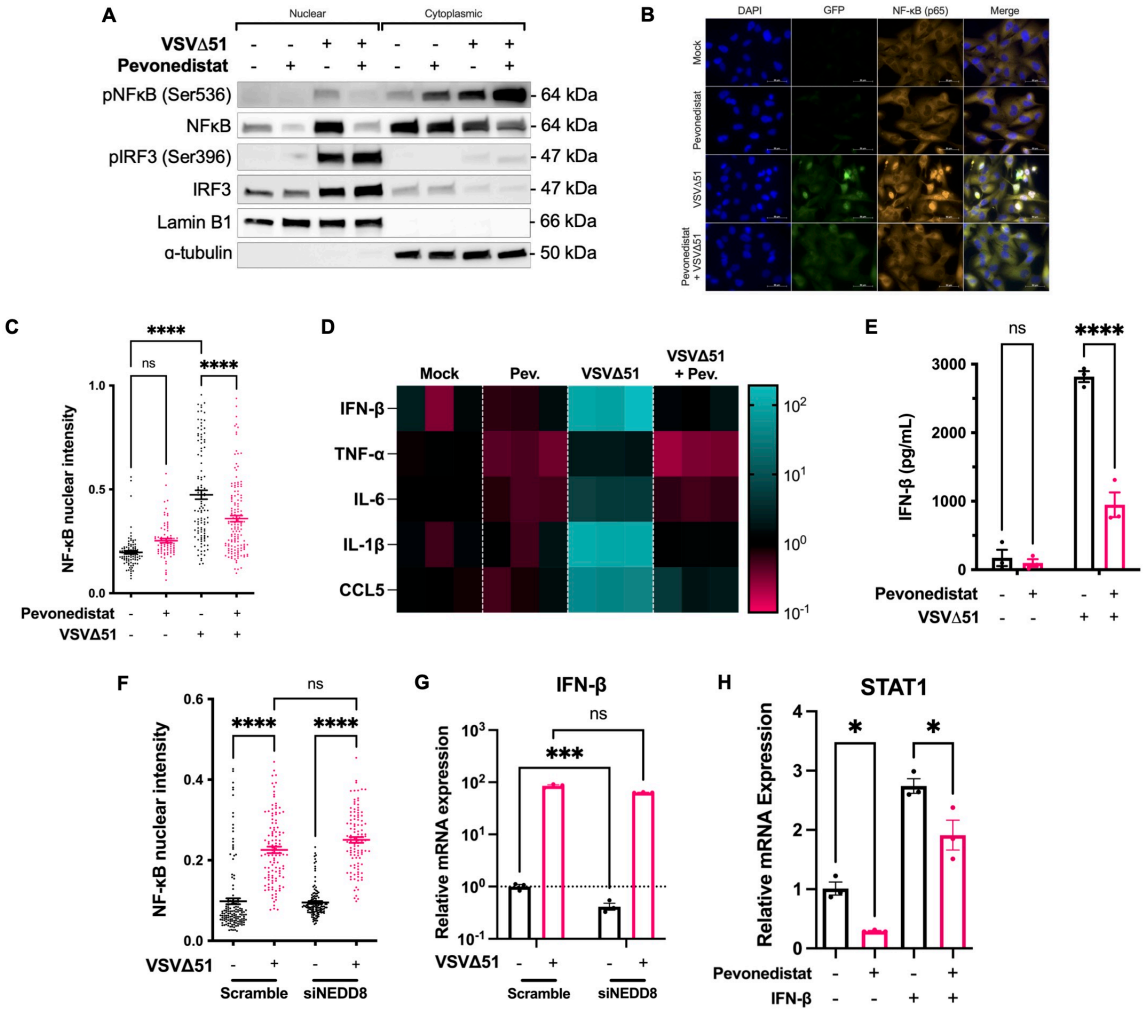

Fig. 4.7. Pevonedistat inhibits NF-κB to suppress IFN-β in a neddylation-independent manner. (A) Human renal 786-0 carcinoma cells were pre-treated for 4 hours with pevonedistat (1μM), then infected with VSVΔ51 (MOI 0.01). At 24 hours post infection (hpi), cells were lysed and fractionated to separate nuclear and cytoplasmic proteins, then probed for indicated proteins by western blot. (B,C) 786-0 cells were seeded on glass coverslips, pre-treated for 4 hours with pevonedistat (10μM). After treatment, cells were then infected with VSVΔ51 (MOI 1) for 6 hours. Cells were fixed and immunostained for NF-κB and nuclei (DAPI). (B) Representative fluorescent images were taken. (C) Nuclear NF-κB intensity was quantified (n=3, mean ± SD; ****P<0.0001). (D,E) 786-0 cells pre-treated ± pevonedistat (1μM) for 4 hours, then infected ± VSVΔ51 (MOI 0.01). (D) RNA was extracted from cells 24hpi and probed for indicated genes by qPCR. Relative mRNA expression was plotted on a

heatmap. (E) At 24hpi, supernatants were quantified for IFN-β secretion by ELISA (n=3, mean ± SD; ****P<0.0001 by two-way ANOVA). (F,G) 786-0 cells were transfected either with scramble siRNA or siRNA targeting NEDD8. (F) Cells were pre-treated ± pevonedistat (10μM), then infected ± VSVΔ51-GFP (MOI 1) for 6 hours, fixed and immunostained for NF-κB and nuclei (DAPI). Images were quantified for mean nuclear NF-κB signal (n=3, mean ± SD; ns = no significance, ****P<0.0001 by one-way ANOVA). (G) Cells were pre-treated with pevonedistat (1μM) for 4 hours, then infected with VSVΔ51 (MOI 0.01). RNA was extracted 24hpi and probed for *IFN-β* gene expression by qPCR (n=3, mean ± SD; ns = no significance, ***P<0.001 by one-way ANOVA). (H) 786-0 cells were pre-treated for 4 hours with pevonedistat (1μM), then treated with human IFN-β (1000 U/mL) for 6 hours. RNA was extracted and probed for *STAT1* gene expression (n=3, mean ± SD; *P<0.05 by one-way ANOVA).

---

even in the presence of exogenous IFN-α and IFN-β. These data support our findings that pevonedistat's identified mechanisms in repressing ISGF3 factor expression and inhibiting NF-κB nuclear translocation are not co-dependent.

4.4 Discussion

The outstanding promise of tumor selectivity, self-amplifying therapeutic effects, and long-term antitumor immunity by oncolytic virotherapy make it an attractive area of investigation in the fight against cancer. Despite this, there are still many barriers obstructing more OV products from reaching the clinic, namely heterogenous tumor resistance to viral infection through retention of the antiviral IFN-1 response (28, 38, 83, 245). In this study, we identify and characterize the viral sensitizing properties of pevonedistat, a first in-class NAE

inhibitor, and its application to enhance oncolytic virotherapy. Many combinational therapies between cellular modulators and oncolytic viruses have previously been identified and reviewed (246). We tout that compared to previously established viral-enhancing compounds, pevonedistat demonstrates superior potency, achieving similar if not higher levels of VSVΔ51 enhancement at a fraction of the concentration required by the other drugs, as well as a broader and sustained activity range (Fig. S4.4.1E) (94, 96, 106). Through mechanisms of IFN-1 inhibition, pevonedistat increases the viral spread, cytotoxicity, and therapeutic efficacy of VSVΔ51 OV treatments across a broad range of tumor types (Fig. 2), including some primary human samples, while sparing physiological tissue (Fig. 4.2B,E, S4.6G). Pevonedistat was also successful in reducing tumor burden in several *in vivo* models when administered both locally and systemically, indicating broader clinical applicability (Fig. 4.4). Moreover, we successfully identify pevonedistat's viral sensitizing mechanism to operate through neddylation-dependent repression of ISGF3 and neddylation-independent inhibition of NF-κB signaling.

Pevonedistat is currently being investigated as an anti-cancer agent, namely in an ongoing phase 3 clinical trial in combination with standard chemotherapy (azacytidine) in patients with myelodysplastic syndromes, chronic myelomonocytic leukemia (CMML) or acute myelogenous leukemia (AML) (128). In accordance with our gene ontology analysis (Fig. S4.5A), pevonedistat induces the DNA damage stress response towards apoptosis in tumor cells (122). Additionally, by inhibiting CRL ubiquitin activity, pevonedistat is able to stabilize members of the extrinsic apoptotic pathway such as Bcl-2 homologous antagonist/killer (BAK) (247, 248). While pevonedistat monotherapies have demonstrated success in murine models of cancer (249), they typically require intensive treatment regimens

with high drug dosages and/or frequent administration. With our proposed combination of pevonedistat and the VSVΔ51 OV, we were able to induce tumor cell killing at much lower doses (Fig. 4.3), likely translating into decreased off-target toxicity and subsequent side effects.

Several viruses such as Kaposi's Sarcoma-Associated Herpesvirus (KSHV) have evolved dependency on neddylation as part of their lifecycle, while other viruses hijack CRL activity for their own survival (120, 250, 251). Subsequently, pevonedistat has previously been characterized to have potent, antiviral activity against several families of viruses including *Herpesviridae* (HSV-1, cytomegalovirus)(250), *Adenoviridae* (Ad5) (252), and *Orthomyxoviridae* (influenza), some of which we also observed (Fig. S4.1C) (253). For example, the influenza virus induces increased neddylation of CRL-1 at an early stage to help propagate its proteins and uses neddylation to help stabilize basic protein 2 (PB2), an essential viral replication component (254). By inhibiting neddylation of these components, pevonedistat was able to block the early replication capability of influenza. Additionally, this mechanism of viral suppression is thought to be independent from the IFN system as pevonedistat impaired cytomegalovirus growth even in the absence of IFNAR1 (252). Given that we can confidently establish that pevonedistat operates through IFN-1 (Fig. 4.5), it becomes intuitive that only oncolytic virotherapy strategies employing IFN-sensitive viruses such as VSVΔ51 benefit (38, 255). This narrow specificity could prove beneficial in ensuring that patients undergoing this treatment regimen do not become vulnerable to unintended infection by other viruses.

The response to the IFN-1 axis is centrally controlled by the JAK/STAT pathway, where reception of IFN-β to the interferon-alpha/beta receptor (IFNAR) triggers phosphorylation and heterodimerization of STAT1 and STAT2 to transcribe downstream IFN-1 genes. As such,

many characterized viral sensitizing compounds classically inhibit STAT1 or STAT2 phosphorylation, compromising ISGF3 complex formation to impair the subsequent IFN-1 response (95, 96, 106). However, we surprisingly found that pevonedistat did not similarly influence STAT phosphorylation (Fig. S6B), but for the first time to our knowledge, we report a neddylation-dependent inhibition of both baseline and VSV-induced ISGF3 expression by pevonedistat (Fig. 4.6C,D). In latent cells, constitutive expression of STAT1 allows for cells to quickly respond to IFN cytokines (256); therefore, any reduction in these baseline levels compromise the cellular ability to activate IFN processes, including positive feedback upregulation of all ISGF3 components (69, 257, 258). Accordingly, we demonstrate that the silencing of neddylation by siRNA could confer some viral sensitizing activity by repressing STAT1 expression (Fig. 4.6I, fig. S4.6I). The exact mechanism by which this occurs could be of interest in developing the relationship between neddylation and innate immunity.

In the case of VSVΔ51 infection, viral single-stranded RNA or glycoproteins are first picked up by Toll-like receptor 3 (TLR3) and retinoic-acid induced gene I (RIG-I) to initiate the IFN-β promoter stimulator (IPS-1) signaling cascade (259). The downstream result is phosphorylation of interferon regulatory factor 3 (IRF3) and nuclear translocation of NF-κB, both of which are crucial components of the enhanceosome complex at the IFN-β promoter, stimulating IFN-β production and secretion (260, 261). The inhibition of NF-κB nuclear translocation to block the IFN-1 response is used by wild-type VSV via its functional M protein (262), and has also been identified as the main mechanism of action of other viral sensitizing compounds (93, 96). Here, we demonstrate that pevonedistat impairs pro-inflammatory cytokine production (Fig. 4.7D), including IFN-β transcription and secretion (Fig. S4.7D and fig. 4.7E) presumably by relying on this same mechanism of NF-κB inhibition (Fig. 4.7A-C).

While we found that this mechanism is independent of neddylation inhibition (Fig. 4.7F,G), which runs counterintuitive to the established mechanism in literature of CRL-1 deactivation and stabilization of IκB-α to sequester NF-κB in the cytoplasm (Fig. S4.7C) (263), few other studies have also found that genetic silencing of neddylation could not impact levels of IFN-β in response to viral infection (133, 264). Indeed, we demonstrate that despite increasing IκB-α abundance (Fig. S4.7C), siRNA-mediated knockdown of UBA3 was unable to inhibit NF-κB activation (Fig. S4.7F,G). Finally, while some compounds that inhibit NF-κB indirectly (e.g. bortezomib (265)) have been reported to enhance the activity of VSV, we also consider that many others are unable to sensitize cancer cells to VSVΔ51 infection (188, 189). This suggests that depending on the mechanism involved, blocking the NF-κB pathway alone does not necessarily confer viral sensitization. Based on our observations, we further hypothesize that the cooperation of both neddylation-dependent and independent mechanisms is required for pevonedistat to achieve its full, potent viral sensitizing effect.

The limitations associated with this combinational approach pertain to the apparent immunosuppressive role of pevonedistat (244, 266). This notion is supported by our data demonstrating the repression of pro-inflammatory cytokines by pevonedistat (Fig. 4.7D), which could potentially impair induction of immunological memory (267, 268). However, tumor-specific T-cell activation appears to be unchanged with pevonedistat (Fig. 4.4E), suggesting that T-cell activation is not impaired, but may also not be the main driver of improved efficacy *in vivo*. Given the therapeutic importance of antitumor memory, OV therapies furthest along the clinical development pipeline tend to carry immunostimulatory payloads (269); therefore, it is imperative that in addition to the increased oncolysis (Fig. 4.3), cells undergo an immunogenic cell death mode (immunogenic apoptosis, necrosis, pyroptosis)

to release damage-associated molecular patterns (DAMPs) as suggested by Fig. 4.3G, and tumor-associated antigens (TAAs) into the microenvironment to trigger inflammatory processes (32). We therefore conclude that tumor cell killing is likely a result of both direct and immune-mediated oncolysis. Future studies will be needed to further characterize the immunological landscape established by this combinational therapy in order to maximize its effects, particularly for the treatment of systemic disease. Altogether, our study provides the pre-clinical basis for evaluating pevonedistat in combination with VSV-based oncolytic immunotherapy in a clinical setting.

4.5 Material and Methods

Study Design

In this controlled laboratory study, the hypothesis was initially formulated upon the observation that pevonedistat increased VSVΔ51 infectivity in an unrelated, high-throughput screen. Subsequently, the objective was to characterize pevonedistat's ability to improve the therapeutic efficacy of oncolytic VSVΔ51 virotherapy in a variety of contexts including in cell-culture models, *ex vivo* murine and human patient samples, and *in vivo* tumor models. Hypotheses stemming from the initial objective led us to further investigate and elucidate the mechanism of action by which pevonedistat was able to confer these beneficial effects. For *in vivo* studies, a sample size of 5 – 15 was chosen, and endpoints were defined when tumor volumes reached 1500mm^3. To assign experimental groups, stratified randomization was used so that each group had a comparable mean tumor volume at the time of first treatment. Investigators were not blinded, and no outliers were excluded from data analysis.

Drugs and Chemical Reagents

Pevonedistat (MLN4924), the primary drug of this study, was obtained from Cedarlane Labs (cat. A11260) dissolved in dimethyl sulfoxide (DMSO). The remainder of drugs, chemical and cytokines along with their supplies, catalog numbers and solvent are listed in the Resources Table (Table S4.1).

Cell Lines

Cell lines used in this study along with their species, tissue type, supplier and catalog number are outlined in Table S4.1. Cells either utilized Dulbecco's modified Eagle's medium (DMEM; HyClone cat.10-013) or RPMI 1640 medium (Corning) supplemented with 1% (v/v) penicillin-streptomycin (Gibco), 30mM HEPES buffer, and 10% (v/v) Fetal Bovine Serum (Gibco, cat. 12483020) or 10% (v/v) serum composed of 3-parts HyClone newborn calf serum (Thermo Fisher, cat. SH3011803) and 1-part Fetal Bovine Serum (Gibco, cat. 12483020). Cell lines were maintained in 37°C and 5% CO_2 conditions in a humidified incubator. Phase and fluorescence images were taken using the EVOS Live Cell Imaging System (Thermo Fisher).

Primary murine hepatocytes were generously supplied by Dr. Morgan Fullerton and Conor O'Dwyer (University of Ottawa) and were isolated as previously described (270). Primary ovarian cancer patient-derived cell lines (OVAPT) were derived from patient ascites fluid were obtained from routine paracentesis according to Ottawa Health Science Network Research Ethics Board (OHSN-REB) protocol #20140075-01H. Primary human glioblastoma (PriGO) cells were established from surgically resected tumors from patients at The Ottawa Hospital and were obtained as a generous gift from Dr. Ian Lormier of the Ottawa Hospital Research Institute (Ottawa, Canada). PriGO cells were grown on laminin-coated plates using serum-free Neurobasal A (NA) media supplemented with epidermal growth factor (EGF),

fibroblast growth factor 2 (FGF2), B-27 and N-2, and maintained in 37°C, 5% O_2 and 20% CO_2 conditions in a humidified incubator.

Human T-cells were isolated from frozen PBMCs (STEMCELL cat. 70025) by negative selection following the EasySep Human T-cell Isolation Kit (STEMCELL, cat. 10981) and expanded following manufacturer instructions with ImmunoCult Human CD3/CD28 T-cell activator (STEMCELL, cat. 10981) for at least 3 days prior to treatment and infection.

Oncolytic Viruses

Rhabdovirus: Indiana serotype of VSV wild-type (VSV-WT) or harboring a deletion of methionine 51 in the M protein (VSVΔ51) and insertion of green fluorescence protein (GFP) or firefly luciferase (FLuc) were used throughout this study(38). All viruses were propagated on Vero cells and purified on 5-50% OptiPrep (Sigma-Aldrich, St. Louis, MO) gradients. Viral titers were determined by standard plaque assay on Vero cells according to published protocol(197).

Herpes Simplex Virus: HSV-1 N212 expressing GFP was obtained as a generous gift from Dr. Karen Mossman of McMaster University (Hamilton, Canada). Viral titers were determined by standard plaque assay on Vero cells according to published protocol(81).

Vaccinia Virus: The VV Wyeth strain harboring a disruption of thymidine kinase (TK) and vaccinia growth factors genes, and insertion of GFP (VVdd) was obtained as a generous gift from Dr. Andrea McCart of Mount Sinai Hospital (Toronto, Canada). Viral titers were determined by standard plaque assay on U2OS cells according to published protocol (47).

High Throughput Viral Titration

Vero cells were seeded at a density of 2.5 x 10^4 cells/well in opaque white bottom 96-well microplates (Thermo Fisher, cat. 07-200-628). 20 µL of sample supernatant was transferred to the microplates and incubated for 5 hours. The automated addition of 25 µL of luciferin solution (2mg/mL constituted in sterile PBS, Cedarlane Labs, cat. 122799(PE)) was performed, and mean luminescence read after 30 seconds. Readings were analyzed in comparison to a standard curve. Refer to published protocol for further details (147).

In vivo mouse tumor models

CT26WT: 6-week-old BALB/c mice (Charles River Laboratories) were subcutaneously implanted with a bolus of 100µL PBS containing 3 x 10^5 syngeneic CT26WT colon carcinoma cells in the right flank. After 11 days when tumor volumes reach roughly 100mm^3, tumors were injected intratumorally with pevonedistat (90mg/kg) or vehicle alone. Four hours later, tumors were injected intratumorally with a bolus of 25µL PBS containing 1 x 10^8 pfu of VSVΔ51. This treatment regimen was repeated two more times, spaced one day apart. After 7 days, mice were anesthetized and imaged using a live in vivo imaging system (Perkin Elmer). Bioluminescent signal intensity was analyzed using Living Image v2.50.1 software.

4T1: 6-week-old BALB/c mice (Charles River Laboratories) were subcutaneously implanted with a bolus of 100µL PBS containing 5 x 10^5 4T1 syngeneic 4T1 mammary carcinoma cells in the right flank. After 9 days when tumor volumes reach roughly 100mm^3, tumors were injected intratumorally with pevonedistat (90mg/kg) or vehicle alone. Four hours later, tumors were injected intratumorally with a bolus of 25µL PBS containing 1 x 10^8 pfu of VSVΔ51. This treatment regimen was repeated two more times, spaced one day apart. For

survival studies, mice were end pointed when tumor volumes reached greater than 1500mm^3 or showed significant respiratory distress from lung metastases.

ID8-Tp53-/- tagged with firefly luciferase (F3) were generated as previously described(271). 5 x 10^6 cells were injected intraperitoneally into 8-week-old C57BL/6 mice and allowed to progress for 10 days. Mice were then injected intraperitoneally with pevonedistat (90mg/kg) or vehicle alone, then 1 x 10^8 pfu of VSVΔ51 4 hours later for three treatments, spaced 1 day apart. Tumor burden was measured using the in vivo imaging system (IVIS) for luciferase activity at day 21 and 28. Mice were randomized to different treatment groups according to tumor size prior to the first treatment.

B16-OVA: 6-week-old C57BL/6 mice (Charles River Laboratories) were subcutaneously implanted with 100µL PBS containing 5 x 10^5 syngeneic B16-OVA melanoma cells in the right flank. After 9 days when tumor volumes reached roughly 100mm^3, tumors were injected intratumorally with pevonedistat (90mg/kg) or vehicle alone. Four hours later, tumors were injected intratumorally with a bolus of 25µL PBS containing 1 x 10^8 pfu of VSVΔ51. This treatment regimen was repeated two more times, spaced one day apart. All experiments were performed in accordance with the University of Ottawa Animal Care and Veterinary Service guidelines for animal care, under the protocols OHRI-2264 and OHRI-2265.

Human and Murine Ex Vivo Tumor Models

BALB/c mice were subcutaneously implanted with 3 x 10^5 CT26WT colon carcinoma cells or C57BL/6 mice were subcutaneously implanted with 3 x 10^5 76-9 rhabdomyosarcoma cells. Upon reaching a tumor volume of 1500 mm^3, mice were culled, and tissues of interest were extracted. For human tissue samples, tumor samples were obtained from patients

undergoing surgical resection who provided informed consent in accordance with Declaration of Helsinki guidelines. The global tissue collection program was approved by the OHSN-REB under the protocol numbers OHSN-REB #2003109-01H and OHSN-REB #20120559-01). Tissues were processed into 2mm slices and 2mm diameter circular cores were taken using a punch biopsy tool. Cores were maintained in humidified incubators at 37°C, 5% CO_2 in DMEM supplemented with 10% serum, 30mM HEPES, 1% (v/v) penicillin-streptomycin and 0.25 mg/L amphotericin B. Cores were treated with pevonedistat 4 hours, then infected with VSVΔ51-GFP at 3 x 10^4 pfu/core. After 48hpi, fluorescence images were taken using the EVOS Live Cell Imaging System (Thermo Fisher) and the supernatant was analyzed for viral titer by standard plaque assay as described previously(197).

Quantitative Real-time Polymerase Chain Reaction

RNA from lysed cells were homogenized using the QIAshredder (Qiagen, cat. 79656), then extracted from lysed cells using the QIAGEN Rneasy kit (Qiagen, cat. 74106) according to manufacturer's protocol and quantified using a NanoDrop One Microvolume UV-Vis Spectrophotometer (Thermo Fisher Scientific, Rockford, IL). To generate cDNA, the RevertAid H-Minus First Strand cDNA Synthesis Kit (Thermo Fisher, cat. K1632) was used. Resulting nucleic acid was subject to quantitative real-time PCR using primers outlined in Table S4.2, Applied Biosystems PowerUp SYBR Green Master Mix (Thermo Fisher, cat. A25776) in a 7500 Fast Real-Time PCR system (Applied Biosystems, Foster City, CA). Gene expression was calculated using the Pfaffl method.

Cell Viability Assay

Resazurin metabolic dye (Millipore Sigma, cat. SI03200) was added to samples at a 1:10 dilution and incubated for 2 hours. Using a BioTek Microplate Reader (Norgen BioTek Corp,

Ontario, Canada) and Gen5 2.07 software, fluorescence was measured at 590 nm upon excitation at 530 nm. Readings were expressed relative to the average of the uninfected, mock treated condition.

Luminescence-based Assays

786-0 seeded in a 96-well white plate were subject to treatment with pevonedistat or vehicle, then infection by VSVΔ51 or vehicle four hours later. At the specified time-point of interest, cells were assayed using the Caspase-Glo® 8 Assay System (Promega, cat. G8201) or Lumit™ HMGB1 Human/Mouse Immunoassay (Promega, cat. W6110) according to manufacturer's instructions. Luminescence readings were taken using the BioTek Microplate Reader (Norgen BioTek Corp, Ontario, Canada).

Enzyme-linked Immunosorbent Assay (ELISA)

Supernatant from treated and infected 786-0 cells seeded in a 24-well plate were collected 24hpi and quantified for human IFN-β concentration using the Human IFN Beta ELISA Kit (PBL Assay Science, cat. 41410) according to manufacturer's protocol. Absorbance readings were taken using the BioTek Microplate Reader (Norgen BioTek Corp, Ontario, Canada) at 450nm.

RNA-Sequencing Analysis

Two biological replicates of RNA were extracted from lysates of treated cells and quantified as described above. Pooled samples were then shipped to the Donnelly Sequencing Centre (University of Toronto) and mRNA-seq libraries were generated using the NEB NEBNext Ultra II Directional RNA library prep kit according to manufacturer's protocol. Libraries were sequenced using the Illumina NextSeq500 with single-end 75bp reads. After

sequencing, resulting fastq files were checked for quality using FastQC (Babraham Bioinformatics, United Kingdom). Pseudo alignment and transcript quantification were performed with KALLISTO(225), and differential expression was determined using SLEUTH(226). Gene ontology analysis was performed using the Gene Ontology enrichment analysis and visualization tool (GOrilla) (211, 212). Identification of involved transcription factors was performed using the TfactS tool (de Duve Institute, Université Catholique de Louvain, Brussels, Belgium) (151).

Immunoblotting

Sample were washed twice with cold PBS and lysed for 10 minutes at 4°C using 50 mM HEPES, 150mM NaCl, 10mM EDTA, 10mM $Na_4P_2O_7$, 100mM NaF, 2mM Na_3VO_3, protease inhibitor cocktail (Roche), phosphatase inhibitor cocktail (Cell Signaling Technology, cat. 5870S) and 1% Triton X-100. Resulting cell lysates were centrifuged to remove cellular debris. For nuclear and cytoplasmic fractionation, the NE-PER Nuclear and Cytoplasmic Extraction Kit (Thermo Fisher Scientific) was used according to manufacturer's protocol. Protein concentrations were quantified using the Pierce BCA Protein Assay Kit (Thermo Fisher, cat. 23225). 20 µg was loaded with 4X NuPAGE LDS Sample Buffer (Thermo Fisher, cat. NP0007) into 4-15% Mini-PROTEAN Gels (Bio-Rad, Mississauga, ON), electrophoresed using the Mini Trans-Blot Cell system (Bio-Rad, Mississauga, ON) and transferred onto nitrocellulose membrane using the Trans-Blot Turbo RTA Mini Transfer Kit according to manufacturer's protocol (Bio-Rad, cat. 1704270). Blots were blocked with 5% BSA for 1 hours, then probed with respective primary and secondary antibodies as listed in Table S1. Bands were visualized using Clarity Western ECL Substrate (Bio-Rad, cat. 1705061) on a ChemiDoc Touch Imaging System (Bio-Rad, Mississauga, ON).

Immunocytochemistry

Cells were seeded on 12mm glass round coverslips (Thomas Scientific, cat. 64-0712) in a 12-well format. Following indicated experimental processes, cells were washed twice with PBS* (PBS supplemented with 1mM $CaCl_2$, 500μM $MgCl_2$), fixed using 4% paraformaldehyde (PFA) for 30 minutes, permeabilized using a 0.2% Triton-X 100 in a 200mM glycine/PBS* solution for 7 minutes, then quenched in 200mM glycine/PBS* for 15 minutes. Slides were then blocked using 5% BSA/PBS* for 1 hour at room temperature, then incubated overnight with the respective primary antibody (Table S4.1) in humidified chamber at 4°C. After two washes with PBS*, corresponding secondary antibodies (Table S4.1) were applied for 1 hour, then samples were mounted onto glass slides and counterstained using Prolong gold anti-fade with 4',6-diamidino-2-phenyl-indole (Molecular Probes). Slides were imaged using a Zeiss Axiocam HRM Inverted fluorescent microscope (Zeiss, Toronto, Canada) and images were processed using Axiovision 4.0 software. Quantification of fluorescent intensities were performed using CellProfiler 3.0.0 (Massachusetts Institute of Technology, Cambridge, USA). Each graphed data point represents mean fluorescence from one, individually analyzed nucleus as determined by CellProfiler using the DAPI stain.

Tumour Processing and Flow Cytometry

786-0 cells were treated and infected with VSVΔ51-GFP in a 6-well format. At 24hpi, cells were collected, washed, and stained with propidium iodide (PI) (Biolegend, cat. 421301) or Annexin V (Cedarlane labs, cat. 640934) according to manufacturer's protocol. Samples were then analyzed for PI staining and GFP signal by flow cytometry on a BD LSRFortessa. Acquired data was analyzed using FlowJo software.

For OVA-specific T-cell responses were measured in the blood at day 7 by intra-orbital bleed using anti-CD3, CD4 and CD8 antibodies. To assess SIINFEKL-specific CD8+ T cell *in vitro* restimulation, 1×10^6 splenocytes were harvested on day 7, then incubated in RPMI medium, supplemented with 10% FBS and 5% pen-strep containing 10 μM of SIINFEKL peptide overnight, and brefeldin A (Golgi plug) was added for the last 6 hours. Cells were then stained with V510 viability dye (1:1000) in PBS for 15 min at RT. Following washes, cells were incubated with anti-CD16/32 in 0.5% BSA/PBS at 4°C to block nonspecific antibody interaction with Fc receptors. Subsequently, anti- CD8, and CD69 antibodies were added to cells and incubated for 30 min (4°C). After staining, cells were washed with FACS buffer and fixed in 1% paraformaldehyde. Cells were acquired on Becton Dickinson (BD) flow cytometry (Fortessa), and analyses were performed using FlowJo software version (v.9).

Small-interfering RNA (siRNA)

786-0 cells were seeded at 40% density in 24-well plates in serum-free DMEM overnight. Cells were then transfected either with control, scramble RNA (ON-TARGETplus Non-targeting Control Pool, #D-001810-10-05, Horizon Discovery) or a SMARTpool of siRNA targeting NEDD8 (ON-TARGETplus NEDD8 siRNA, #L-020081-00-0005, Horizon Discovery) or targeting UBA3 (ON-TARGETplus UBA3 siRNA, #L-005249-00-0005, Horizon Discovery) using the Lipofectamine™ RNAiMAX Transfection Reagent (Thermo Fisher, cat. 13778075) according to manufacturer's protocol in Opti-MEM™ I Reduced Serum Medium (Thermo Fisher, cat. 31985062). After 6 hours, media containing siRNA was replaced with DMEM supplemented with 10% (v/v) serum composed of 3-parts HyClone newborn calf serum (Thermo Fisher, cat. SH3011803) and 1-part Fetal Bovine Serum (Gibco, cat.

12483020). Upon reaching approximately 80% confluency, cells were treated with reagents or infected with VSVΔ51 as specified.

Statistics

Statistical analyses were performed using Prism 9 (GraphPad, San Diego, CA) software. Viral titer and mRNA expression values were log-transformed prior to analysis. Viability measures were normalized to untreated, uninfected cells as indicated in figure legends. Statistical tests were performed as indicated by figure legends including Student's t-test, one-way analysis of variance (ANOVA) with Tukey's multiple comparisons test, and two-way ANOVA. Two-tailed testing was used unless otherwise specified. Kaplan-Meier curves were graphed for survival studies and differences detected using the log-rank test. Error bars represent the standard error from the mean (SEM). A P-value less than 0.05 was considered statistically significant.

4.6 Acknowledgements

The graphical abstract of pevonedistat's mechanism of action was created using BioRender.com (Toronto, ON, Canada) licensed to Boaz Wong (agreement #YV234Y2B6F). The authors would like to thank Michael Phan (University of Ottawa) for his assistance with the RNA work, Dr. William Stanford and Rina Al-awar (Ontario Institute for Cancer Research) for supplying the kinase inhibitor library, Dr. Sylvie Lavictoire (Ottawa Hospital Research Institute) for her assistance with using the PriGO cells, and Dr. David Cook (University of Ottawa) for his guidance throughout the RNA sequencing analysis. The authors would also like to acknowledge Donnelly Sequencing Centre (http://ccbr.utoronto.ca/donnelly-

sequencing-centre) for their efficiency and professionalism in providing their RNA-sequencing service. This study was funded by: Terry Fox Research Institute, TFF-122868 (JSD), Canadian Institutes of Health Research, grant INI-147824 and #705952 (JSD), and by the Canadian Cancer Society supported by the Lotte & John Hecht Memorial Foundation, grant #703014 (JSD). BW is supported by a Canadian Institutes of Health Research, Canada Graduate Scholarship Doctoral Award.

Chapter 5. General Discussion

5.1 Dependency of OV efficacy on the IFN response

While significant progress has been made in the recent decade, a comprehensive understanding of the sheer complexity of malignant transformation processes remains out of reach. Cellular processes that were assumed to be detrimental for malignancy are not always eliminated, rather are context-dependent and can instead be exploited to favour growth of the tumour (272). One relevant example, the antiviral IFN response can be seen as an obstacle to overcome for cancer immunoediting. The natural anti-tumour role of IFNs to inhibit cellular proliferation, arrest cell cycle, and alert nearby immune defenses deems this process as one that should be suppressed in malignancy (273). Indeed, in a number of different tumour types, IFN signaling is blocked at various points to favour tumour progression, with evidence being found for STAT1 (274), IFNAR1/2 (275, 276), and suppressor of cytokine signaling (SOCS) (277). This has also been demonstrated in the epigenetics of cancer cells, where 46% of genes that were downregulated via methylation following cellular immortalization were involved in IFN signaling in some capacity (278).

However, the entire transformation picture goes beyond simple insensitivity to IFN as later stages of immunoediting paradoxically may use IFNs in pro-tumorigenic roles. Prolonged IFN exposure in surviving IFN-sensitive cells promotes immune escape by inducing expression of immune checkpoint ligands such as PD-L1 (279). Still in certain cancer types, increased IFN signaling promotes metastasis via switching to more invasive phenotypes (280, 281). That is to say that deficiency in antiviral IFN responses may not be present in all tumour types. Given that the efficacy of many OV therapies hinges upon this same response, the level

of heterogeneity in IFN system "wiring" becomes a large determinant of OV success (34). To combat this, strategies aimed at the suppression of functional antiviral responses have been explored. Our group and others have successfully characterized the use of multiple compounds capable of potentiating OV infectivity and local oncolysis particularly through IFN-1 inhibition (144). In this thesis, we looked to further dissect cellular mechanisms that regulate IFN-1 and exploit them to improve OV therapeutic regimens. In Chapter 2, we elucidate in depth cell signaling events linking EGFR activation to suppression of the antiviral response while in Chapters 3 and 4, we uncover new posttranslational mechanisms and identify novel protein targets (*i.e.,* ACP2, neddylation) that regulate IFN-1 pathways and that can be exploited for enhancing oncolytic VSV and potentially other OVs (Fig. 5).

5.2 Overlapping target pathways for OV potentiation

All chapters of this thesis pertain to cellular modification of some aspect of the IFN-1 signal transduction pathway to potentiate oncolytic virotherapy. Using a global transcriptome approach, *in silico* results from microarray and RNA sequencing experiments each confirm downregulation of the gene ontology terms "defense response to virus" and "type 1 interferon signaling pathway" upon pevonedistat treatment or ACP2 knockdown with VSVΔ51 infection. Specifically, our established viral sensitizing compounds intercept this pathway at two major points: inhibition of the IFN-β enhanceosome (including NF-κB, IRF3), or blockade of JAK/STAT signaling to compromise downstream ISG production. The aforementioned *in silico* approaches also agree with this observation as STAT1 and NF-κB come up among top

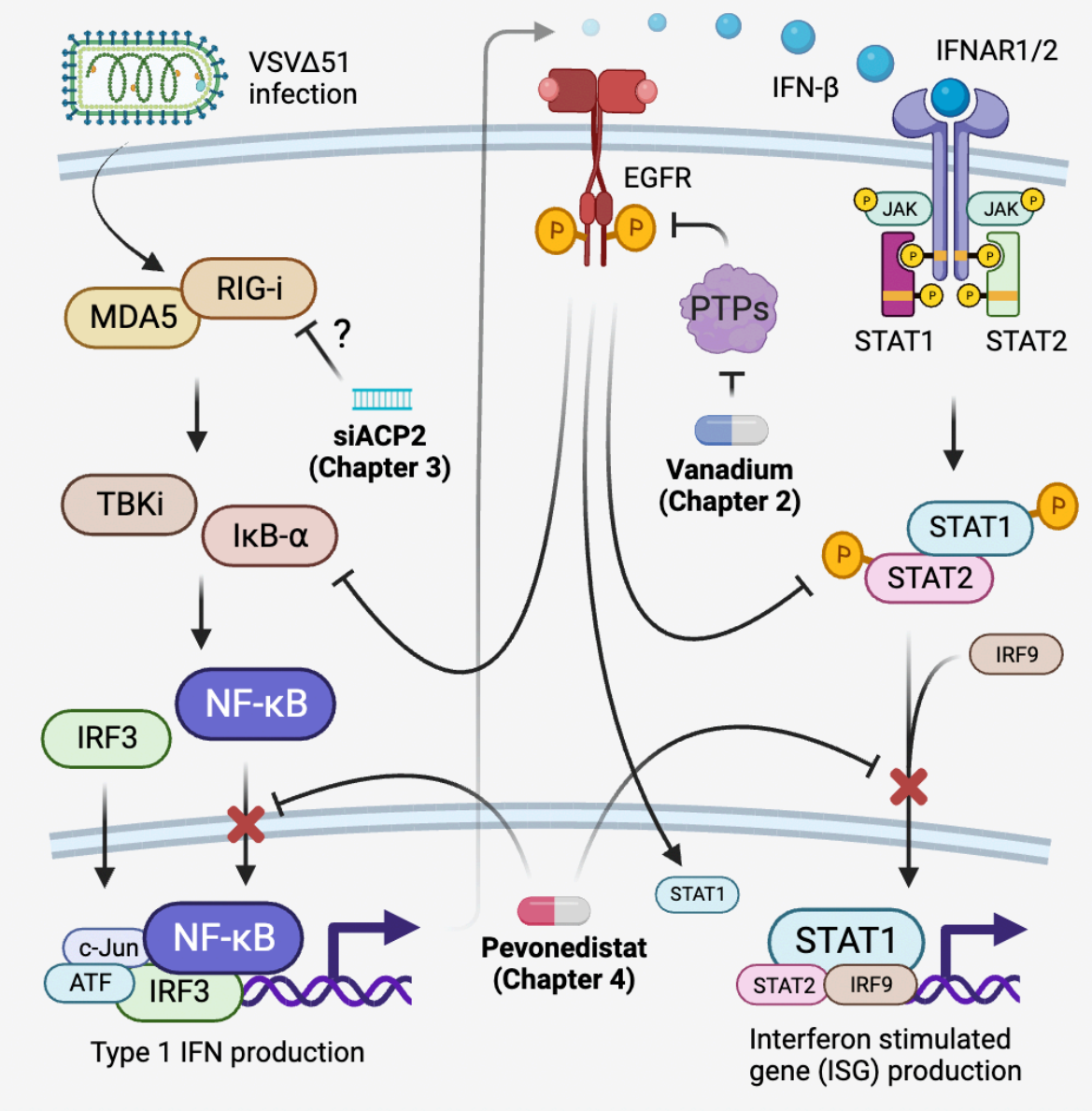

Fig. 5. Summary of main cellular pathways implicated in this thesis. As demonstrated by several chapters of this thesis, some genetic or pharmacological antagonism of the IFN-1 response can enhance oncolytic virotherapy. In chapter 2, we demonstrate that vanadium-based compounds through EGFR activation helps subvert IFN-1 into IFN-2 responses. In chapter 3, we demonstrate that knockdown of ACP2 impedes the early IFN-1 response. In chapter 4, we demonstrate that pevonedistat co-impairs both JAK/STAT and NF-κB pathways to dampen IFN-1.

hits of downregulated transcription factors upon treatment with vanadate or pevonedistat, upon infection (Fig. 2.4A, 4.6A). Still other pathways including PI3K and MAPK have been shown in literature to also be contributory to IFN production and regulation (31).

5.2.1 Antagonizing the JAK/STAT pathway

Inhibition of the JAK/STAT pathway has already been established as a strategy to potentiate oncolytic virotherapy. Knockout models of STAT1 and STAT2 show impaired IFN-1 signaling and susceptibility to oncolytic virus infection (282, 283). To mimic this effect using pharmacological strategies, several drugs targeting the JAK/STAT pathway have already been demonstrated to this effect. Ruxolitinib, an approved JAK1/2 inhibitor for the treatment of myelofibrosis, was found to sensitize head and neck squamous cell carcinoma cell lines to VSV infection (88). In sarcoma tumors, thought to have naturally high resistance to oncolytic viral infectivity due to their high basal levels of IFN, JAK1 inhibition by valproate was capable of increasing their susceptibility to oncolytic VSV and Sindbis virus infection (284). These findings are in line with our findings in Chapter 2, where we demonstrate EGFR activation by vanadium to directly repress JAK/STAT phosphorylation and signaling (Fig. 2.3), as well as Chapter 4, where we demonstrate pevonedistat's ability to transcriptionally suppress STATs to consequently block downstream ISGs through a neddylation-dependent mechanism (Fig. 4.6).

However, studies by our group suggest that is important to distinguish the role of STAT1 compared to STAT2, especially in how they play into downstream IFN-1 vs. IFN-2 responses. In the case of vanadium, we found that STAT2 phosphorylation was inhibited, but not STAT1, which allowed for intact pro-inflammatory cytokine production (Fig. 2.3D, 2.4F).

Retaining STAT1 homodimers for IFN-2 signaling is a key distinguishing feature of vanadium compared to other viral-enhancing compounds (86), which by more broadly blocking IFN-1 production and response may not initially promote immune responses in the tumour microenvironment. Our group has recently characterized the immune landscape of tumours treated in combination with vanadium and VSVΔ51. Indeed, we found that vanadium further boosts IFN-2 in animals and enhances antigen-specific anti-tumour responses which may translate into more complete and durable anti-cancer treatments (285).

5.2.2 Antagonizing the NF-κB pathway

The NF-κB axis hosts downstream effects with implications in almost all the hallmarks of cancer including inflammation, cellular transformation, and invasion. Aberrant NF-κB signaling is therefore typically seen to be a driver of malignancy and its blockade should be beneficial for cancer therapy (286). However, NF-κB has been discovered to be pleomorphic, where its activation supports both pro- and anti-tumorigenic processes (287). A good example of this is found when we contrast the mechanism of vanadium to pevonedistat. We demonstrate that vanadium activates EGFR to promote NF-κB signaling (Fig. 2.4D), while pevonedistat treatment clearly inhibits the nuclear localization of NF-κB (Fig. 4.7). Despite this, both compounds have viral enhancing activity, and from this we can formulate two hypotheses. The first is that sensitivity to OV may generally be predominantly controlled by JAK/STAT signaling. In one study, the authors tested a panel of 16 small molecules that were known to enhance OVs and found that the most potent candidates commonly impaired JAK (189). Indeed, vanadium compounds show that antagonizing STAT alone is sufficient for potent VSV viral enhancement via repression of ISG effectors despite increased NF-κB activity (106). This

intact NF-κB axis was later found to be required for the production of pro-inflammatory CXCL10 to promote anti-tumor immune responses by vanadium (Fig. 2.4F, G).

The second hypothesis is that careful consideration of the cellular context by which NF-κB is regulated is key for viral enhancement. This is reasonable given the multitude of regulatory mechanisms that control NF-κB through canonical and non-canonical pathways (288). In turn, the dependency of the IFN response on NF-κB signaling will certainly be different between different tumour types, ultimately altering the impact of inhibiting NF-κB on oncolytic virus enhancement. For example, BMS-34551 is a specific inhibitor of NF-κB activation through IKK inhibition (289). In glioma cells, BMS-34551 inhibited CXCL8 transcription via NF-κB antagonism to enhance VSV infection (188). However, in the U266 and 5TGM1 multiple myeloma cell lines, the study demonstrated that NF-κB activity was in fact required for the VSV lifecycle and treatment with BMS-34551 inhibited VSV replication and spread (265). Relating this question back in the context of this thesis, NF-κB is a key transcription factor as part of the IFN-β enhanceosome, thus its inhibition is likely contributory to improved OV infectivity through reduced production of IFN-β. This mechanism is also common for other viral enhancing compounds including dimethyl fumarate and VSe1 (93, 96). As we found in Chapter 4, the full viral enhancing effect of pevonedistat appeared to require inhibition of both JAK/STAT and NF-κB pathways (Fig. 4.6, 4.7).

5.2.3 Regulation of IFN production by phosphatases

The initial objective of the kinase inhibitor and siRNA PP high-throughput screens were to identify the exact PPs by which vanadium confers its viral sensitizing effect. In addition to leading to discovering the involvement of the EGFR pathway in Chapter 2, this screen also led

us identify PPs that have their own IFN-modulating effects in Chapter 3 and further to the identification of Pevonedistat which was further studied in Chapter 4. PPs have already been demonstrated to regulate JAK/STAT signaling, for example via the slingshot homolog proteins 1 and 2 (SHP-1 and SHP-2) (290). Mouse fibroblasts lacking SHP-2 had prolonged STAT phosphorylation, resulting in IFN secretion (291) While we did not analyze the exact mechanism by which ACP2, the top hit from our high-throughput siPP screen, regulated the IFN pathway, we can make two inferences based upon our data.

First, our RNA sequencing *in silico* analysis identified the RIG-I signaling pathway as being impacted by ACP2 knockdown. This suggests that ACP2 may be involved in the early phases of the viral response to initiate production of IFN-1 cytokines given the involvement of RIG-I (292, 293). Disruption of RIG-I cumulatively led to a decrease in downstream anti-viral ISGs (Fig. 4.3C, E). Secondly, this phenomenon may involve a virus-specific mechanism. In some preliminary experiments, ACP2 knockdown by siRNA was unable to enhance other viruses (data not shown). Given that ACP2 is involved in lysosome and endosomal trafficking, one hypothesis is that ACP2 knockdown impairs endosomal toll-like receptor 7 (TLR-7) detection of viral nucleic acids and the downstream anti-viral response (294). Indeed, ACP2 has been implicated in viral entry for HSV-1 (210). Admittedly the connection between ACP2 and IFN is not immediately obvious, therefore further characterization is required before announcing ACP2 as a target for oncolytic virotherapy.

5.3 Beyond targeting IFN for OV resistance

The biggest caveat to the strategies outlined by this thesis is that IFN antagonism may not be the only pattern of resistance against oncolytic virotherapy, and in fact, may not even

correlate with therapeutic efficacy in some cases. Firstly, at its current stage of development, delivery of IFN-targeting compounds is often still required to be done directly into tumour for sufficient efficacy. While we have some data supporting efficacy following systemic administration of pevonedistat and VSVΔ51 (Fig. 4.4C), there are certainly many other factors contributing to therapeutic resistance, including the tumour microenvironment, that must be overcome in addition to high IFN responses (295). Investigation into strategies to target viral enhancing compounds to the tumour are also underway for example through antibody-drug conjugates (ADC) (296).

Secondly, IFN signaling inhibits tumour growth by arresting cell cycling and inducing apoptosis, and thus its pharmacological inhibition may not always be desirable (297). In this thesis, all the chapters have mainly used VSV as the prototype OV, which is known to be particularly sensitive to IFN resistance (297, 298). Along with reovirus and NDV (299, 300), these represent viruses that are susceptible to IFN and may be good candidates for combinational therapy with IFN-antagonizing compounds. Conversely, vanadate and pevonedistat (Chapter 4) were unable to enhance the viral titer of DNA viruses like HSV-1 and vaccinia which are further along in clinical development pipelines (106).

Additionally, decreasing IFN may compromise recruitment of immune cells to the tumour cells and subsequently, may reduce the formation of anti-cancer immunological memory (301). Depending on the method by which IFN is blocked and the cancer subtype, this may prove to be a crucial consideration. T-VEC has actually been shown to increase IFN-1, which appears to run counterintuitive to increased viral infectivity proposed by our thesis (302). This is all to say that there are multiple, important factors to be considered before IFN

antagonism can definitively be relied upon as a possible solution to resistance to oncolytic virotherapy in the clinic.

5.4 Involving anti-tumour immunological memory

From our findings, it generally appears that in some cases, inhibition of STAT1 of the JAK/STAT pathway permits OV infectivity, while NF-κB helps tune the inflammatory response depending on the cellular context. As demonstrated by the mechanism of action of vanadium compounds, the retention of pro-inflammatory signals can be beneficial for mounting the anti-tumour immune response (Fig. 2.4F) (106), which may be a critical effect and benefit of oncolytic virotherapy. Looking at successful therapies in the clinic, involvement of the immune system appears paramount. The goal of modern cancer therapy has seemingly shifted from trying to directly eradicate cancer cells towards boosting the body's natural immune response against tumours for a more durable cure. For example, immune checkpoint inhibitors in metastatic melanoma have drastically improved median survival from approximately 6 months to 6 years, while showing milder side effects (303). Accordingly, the goal of oncolytic virotherapy should not only be direct tumor lysis, but the amplification of anti-tumour immunity. Accordingly, some viral enhancing compounds and combinations represent better candidates than others towards this objective. We demonstrate that pevonedistat may unfortunately fall in the latter category as we show that pevonedistat does not particularly benefit immune T-cell populations (Fig. 4.4D), while vanadium-based drugs may be better candidates given their ability to induce pro-inflammatory cytokine secretion and to increase recruitment of immune cells to the tumour site (106, 285).

5.4.1 Arming viruses with therapeutic payloads

T-VEC, the only clinically approved oncolytic virus in the United States, is armed with GM-CSF, with the specific intention of increasing tumour-specific immune recruitment (304). As we explored in Chapter 3, arming oncolytic viruses with payloads can help antagonize IFN to lower antiviral cellular defenses or stimulate the immune response. For example, VSV can directly be encoded to express IFN cytokines such as IFN-β and IFN-ɣ to augment pro-inflammatory cytokine production to drive anti-tumour immunity (72, 305). The therapeutic effect of these encoded cytokines is lost in immunodeficient mice models, confirming dependency on the immune response. Additionally, our group has shown that VSV armed with interleukin 12 (IL-12) combined with vanadium further improved therapeutic outcomes (285). On the other hand, in our review (Appendix A), we broadly describe 4 categories of RNAi effector payloads for the potentiation of oncolytic virotherapy: increasing tumour lysis, drug sensitivity, immunomodulation and oncogenic silencing. With respect to IFN pathways, siRNA against suppressor of cytokine signaling (SOCS-1), when delivered into dendritic cells, has been shown to enhance cytokine production to help mount an anti-tumour response (306).

We demonstrate in Chapter 3 that siRNA can be used to temporarily suppress IFN-1 to improve viral titer when delivered by VSV. However, we would assert that this study serves more as a proof-of-concept for viral delivery of RNAi than a direct avenue of investigation given how little is known about ACP2. As with all transgene-encoding viruses, this strategy faces challenges in efficacy given that the viral infection event has to take place prior to the payload being released. Thus, these viruses still face initial resistance to infection and may still require transient IFN knockdown by pharmacological compounds. This hypothesis may explain why our VSVΔ51-shACP2 only showed a marginal increase in viral titer compared to

its non-targeting control counterpart as both were challenged by initial tumour resistance to infection (Fig. 3.4E). This strategy may therefore be better suited for tumour types with already low basal expression of IFN and natural resistance to infectivity, allowing for the RNAi to be expressed and further enhance the OV's effects.

5.5 Conclusion

Oncolytic virotherapy has made progress over the last decade towards approval in the clinic; however, it also continues to face several hurdles, primarily relating to insufficient efficacy in patients. Indeed, while T-VEC was approved by regulators for treatment of melanoma, it has since been abandoned commercially since more effective and more easily administered options are now available. High resistance to infection, which is controlled by the IFN pathways, represents one of the hurdles to efficacious OV therapy, particularly for IFN-sensitive viruses like VSV. This thesis focused on pharmacological and genetic strategies to repress IFN-1 to enhance OVs (Fig. 5).

In Chapter 2, we identified the mechanism by which vanadium suppresses IFN-1, which is through activation of the EGFR pathway to modulate JAK/STAT and NF-κB signaling.

In Chapter 3, as a finding of our recent human phosphatase siRNA library high-throughput screen, we identified ACP2 as a novel regulating PP on IFN-1, and bioengineered VSV to carry siACP2, which demonstrates improved infectivity.

Finally in Chapter 4, we identified and characterized pevonedistat, a first in-class neddylation inhibitor, as a viral enhancing compound through impedance of the STAT1 and NF-κB pathways. We found that these strategies were indeed able to increase susceptibility of

tumours to VSVΔ51 and improved *in vivo* therapeutic outcomes compared to VSVΔ51 therapy alone.

As discussed in this thesis, these strategies hold promise in advancing oncolytic virotherapy into the clinic, but further investigation is needed. Long-term inhibition of IFN-1 is likely not a definite solution to OV resistance as it may compromise the secondary action of oncolytic virotherapy, which is orchestration of long-lasting anti-tumour immunological memory. Follow-up studies to this thesis should choose to investigate whether certain properties of IFN-1 inhibition can be harnessed to allow for OV uptake within the tumour without impeding the downstream, pro-inflammatory role of IFN. Altogether, this thesis deepens our mechanistic understanding of the cellular intricacies that govern the IFN-1 response to boost the efficacy of OV treatment strategies and to exploit them towards improved cancer treatment options in the future.

Contributions of Collaborators

Chapter 2: Dependency of EGFR activation in Vanadium-based Sensitization to Oncolytic Virotherapy

Contribution: Conceptualization, B.W., A.B. and J.S.D.; Methodology, B.W., A.B., J.S.D.; Investigation, B.W., A.B., R.A., N.A., G.M. and A.C.; Writing – Original Draft, B.W., R.A. and J.S.D.; Writing – Review & Editing, B.W., A.B., R.A. and J.S.D.; Funding Acquisition, J.S.D.; Supervision, R.A. and J.S.D.

Table 2: BW and AB were responsible for this table with the assistance of GM and RA.

Figure 2.1: AB was responsible for the visualization of Fig. 2.1A. BW was responsible for Fig. 2.1B-D with the assistance of AB and RA.

Figure 2.2: BW was responsible for all figures. GM and RA assisted with Fig. 2.2B,C,F,G.

Figure 2.3: BW was responsible for all figures.

Figure 2.4: BW was responsible for all figures. GM and RA assisted with Fig. 2.4B,C.

BW wrote majority (over 90%) of the original manuscript.

Chapter 3: High throughput screen identifies lysosomal acid phosphatase 2 (ACP2) to regulate IFN-1 responses to potentiate oncolytic VSVΔ51 activity

Contribution: Conceptualization: BW, AB, RA, JSD, Methodology: BW, RB, AB, RA, CI, JSD, Investigation: BW, RB, AB, KN, GM, MS, AC, RA, Visualization: BW, KN, Funding

acquisition: CI, JSD, Project administration: BW, RA, JSD, Supervision: RA, CI, JSD, Writing – original draft: BW, RB, RA, Writing – review & editing: BW, RB, RA, CI, JSD

Table 3: BW and AB were responsible for this table with the assistance of GM and RA.

Figure 3.1: BW and AB were responsible for Fig. 4.1B-D, and were assisted by GM and RA. AB generated Fig. 4.1A.

Figure 3.2: BW was responsible for all figures. MS assisted with Fig. 3.2F.

Figure 3.3: BW and KN were responsible for Fig. 3.3A-D. BW was responsible for Fig. 3.3E.

Figure 3.4: BW and RB were responsible for all figures. RB generated the tools for all figures and visualized Fig. 3.4A. AC assisted with Fig. 3.4F,G.

BW wrote majority (over 90%) of the original manuscript except for method sections pertaining to the generation of the VSVΔ51-shACP2, which was written by RB.

Chapter 4: Pevonedistat, a First in-class NEDD8-activating Enzyme Inhibitor, sensitizes cancer cells to VSVΔ51 Oncolytic Virotherapy

Conceptualization: BW, AB, RA, JSD; Methodology: BW, AB, RA, JSD; Investigation: all authors; Visualization: BW, KN; Funding acquisition: JSD; Project administration: BW, RA, JSD; Supervision: RA, JSD; Writing – original draft: BW, RA; Writing – review & editing: BW, RA, JSD

Figure 4.1: BW was responsible for all figures except for Fig. 4.1C (performed by HKB), and received help for Fig. 4.1D from GM and RA.

Figure 4.2: BW was responsible for all figures except for Fig. 4.2C (performed by AB). IL and BV provided tools for the generation of Fig. 4.2B.

Figure 4.3: BW was responsible for all figures except for Fig. 4.3D (performed by HKB)

Figure 4.4: BW was responsible for all figures except for Fig. 4.4D-E (performed by AJ). AC and RA assisted with Fig. 4A-C. ZT provided tools for the generation of Fig. 4.4C.

Figure 4.5: BW and KN were responsible for all figures.

Figure 4.6: BW was responsible for all figures.

Figure 4.7: BW was responsible for figures. DS assisted in generating Fig. 4.7B.

BW wrote majority (over 90%) of the manuscript with the exception of methods pertaining to flow cytometry and a paragraph pertaining to analysis of immune cell populations under *Pevonedistat improves oncolytic VSVΔ51 therapeutic efficacy in vivo*, which were written by AJ.

Appendix A: Optimal Delivery of RNA interference by viral vectors for cancer therapy

Contribution: All authors were involved in the writing and editing of this manuscript. BW, RB, RR and CSI were involved in the initial conceptualization of this review. JSD and CSI were involved in funding acquisition and study supervision.

BW and RB each approximately wrote 50% of the content included in the original manuscript. BW was responsible for Figure A1 and A2. RB was responsible for Table A1.

RR and MC each contributed 1-2 paragraphs to the original manuscript.

References

1. Bray F, Ferlay J, Soerjomataram I, Siegel RL, Torre LA, Jemal A. 2018. Global cancer statistics 2018: GLOBOCAN estimates of incidence and mortality worldwide for 36 cancers in 185 countries. CA Cancer J Clin 68:394–424.
2. Canadian Cancer Statistics Advisory Committee. 2018. Canadian Cancer Statistics 2018. Can Cancer Soc.
3. Xie A, Semenciw R, Mery L. 2015. Cancer incidence in Canada: trends and projections (1983-2032). Health Promot Chronic Dis Perv Can 35:1–187.
4. Garaszczuk R, Yong JHE, Sun Z, de Oliveira C. 2022. The Economic Burden of Cancer in Canada from a Societal Perspective. Curr Oncol Tor Ont 29:2735–2748.
5. Hanahan D, Weinberg RA. 2000. The Hallmarks of Cancer. Cell 100:57–70.
6. Hanahan D, Weinberg RA. 2011. Hallmarks of Cancer: The Next Generation. Cell 144:646–674.
7. Biswas S, Rao CM. 2017. Epigenetics in cancer: Fundamentals and Beyond. Pharmacol Ther 173:118–134.
8. Kandoth C, McLellan MD, Vandin F, Ye K, Niu B, Lu C, Xie M, Zhang Q, McMichael JF, Wyczalkowski MA, Leiserson MDM, Miller CA, Welch JS, Walter MJ, Wendl MC, Ley TJ, Wilson RK, Raphael BJ, Ding L. 2013. Mutational landscape and significance across 12 major cancer types. Nature 502:333–339.
9. Wang M, Zhao J, Zhang L, Wei F, Lian Y, Wu Y, Gong Z, Zhang S, Zhou J, Cao K, Li X, Xiong W, Li G, Zeng Z, Guo C. 2017. Role of tumor microenvironment in tumorigenesis. J Cancer 8:761–773.
10. Ilkow CS, Marguerie M, Batenchuk C, Mayer J, Ben Neriah D, Cousineau S, Falls T, Jennings VA, Boileau M, Bellamy D, Bastin D, de Souza CT, Alkayyal A, Zhang J, Le Boeuf F, Arulanandam R, Stubbert L, Sampath P, Thorne SH, Paramanthan P, Chatterjee A, Strieter RM, Burdick M, Addison CL, Stojdl DF, Atkins HL, Auer RC, Diallo J-S, Lichty BD, Bell JC. 2015. Reciprocal cellular cross-talk within the tumor microenvironment promotes oncolytic virus activity. Nat Med 21:530–536.

11. Koebel CM, Vermi W, Swann JB, Zerafa N, Rodig SJ, Old LJ, Smyth MJ, Schreiber RD. 2007. Adaptive immunity maintains occult cancer in an equilibrium state. Nature 450:903–907.
12. Ho V, Heslin MJ, Yun H, Howard L. 2006. Trends in Hospital and Surgeon Volume and Operative Mortality for Cancer Surgery. Ann Surg Oncol 13:851–858.
13. Hunt MA, Pastrana G, Amols HI, Killen A, Alektiar K. 2012. The Impact of New Technologies on Radiation Oncology Events and Trends in the Past Decade: An Institutional Experience. Int J Radiat Oncol 84:925–931.
14. Bendzsak AM, Baxter NN, Darling GE, Austin PC, Urbach DR. 2017. Regionalization and Outcomes of Lung Cancer Surgery in Ontario, Canada. J Clin Oncol 35:2772–2780.
15. Miller KD, Nogueira L, Mariotto AB, Rowland JH, Yabroff KR, Alfano CM, Jemal A, Kramer JL, Siegel RL. 2019. Cancer treatment and survivorship statistics, 2019. CA Cancer J Clin 69:363–385.
16. DeVita VT, Chu E. 2008. A History of Cancer Chemotherapy. Cancer Res 68:8643–8653.
17. Schirrmacher V. 2019. From chemotherapy to biological therapy: A review of novel concepts to reduce the side effects of systemic cancer treatment (Review). Int J Oncol 13.
18. Gerber DE. 2008. Targeted therapies: a new generation of cancer treatments. Am Fam Physician 77:311–319.
19. Adams GP, Weiner LM. 2005. Monoclonal antibody therapy of cancer. Nat Biotechnol 23:1147–1157.
20. Pérez-Herrero E, Fernández-Medarde A. 2015. Advanced targeted therapies in cancer: Drug nanocarriers, the future of chemotherapy. Eur J Pharm Biopharm 93:52–79.
21. Khalil DN, Smith EL, Brentjens RJ, Wolchok JD. 2016. The future of cancer treatment: immunomodulation, CARs and combination immunotherapy. Nat Rev Clin Oncol 13:273–290.
22. Farkona S, Diamandis EP, Blasutig IM. 2016. Cancer immunotherapy: the beginning of the end of cancer? BMC Med 14:73.
23. Suda K, Mitsudomi T. 2014. Successes and Limitations of Targeted Cancer Therapy in Lung Cancer, p. 62–77. *In* Peters, S, Stahel, RA (eds.), Progress in Tumor Research. S. KARGER AG, Basel.

24. Sharma P, Allison JP. 2015. Immune Checkpoint Targeting in Cancer Therapy: Toward Combination Strategies with Curative Potential. Cell 161:205–214.
25. Kelly E, Russell SJ. 2007. History of Oncolytic Viruses: Genesis to Genetic Engineering. Mol Ther 15:651–659.
26. Pol J, Kroemer G, Galluzzi L. 2016. First oncolytic virus approved for melanoma immunotherapy. OncoImmunology 5:e1115641.
27. Rehman H, Silk AW, Kane MP, Kaufman HL. 2016. Into the clinic: Talimogene laherparepvec (T-VEC), a first-in-class intratumoral oncolytic viral therapy. J Immunother Cancer 4:53.
28. Russell SJ, Peng K-W, Bell JC. 2012. Oncolytic virotherapy. Nat Biotechnol 30:658–670.
29. Twumasi-Boateng K, Pettigrew JL, Kwok YYE, Bell JC, Nelson BH. 2018. Oncolytic viruses as engineering platforms for combination immunotherapy. Nat Rev Cancer 18:419–432.
30. Lawler SE, Speranza M-C, Cho C-F, Chiocca EA. 2017. Oncolytic Viruses in Cancer Treatment: A Review. JAMA Oncol 3:841.
31. Platanias LC. 2005. Mechanisms of type-I- and type-II-interferon-mediated signalling. Nat Rev Immunol 5:375–386.
32. Guo ZS, Liu Z, Bartlett DL. 2014. Oncolytic Immunotherapy: Dying the Right Way is a Key to Eliciting Potent Antitumor Immunity. Front Oncol 10:74.
33. Seymour LW, Fisher KD. 2016. Oncolytic viruses: finally delivering. Br J Cancer 114:357–361.
34. Lichty BD, Power AT, Stojdl DF, Bell JC. 2004. Vesicular stomatitis virus: re-inventing the bullet. Trends Mol Med 10:210–216.
35. Dinh PX, Das A, Pattanaik AK. 2016. Host Cell Functions In Vesicular Stomatitis Virus Replication. UNL Digital Commons, Biology and Pathogenesis of Rhabdo and Filoviruses.
36. Morris MC, Russell TM, Lyman CA, Wong WK, Broderick G, Ferran MC. 2022. Computational prediction of intracellular targets of wild-type or mutant vesicular stomatitis matrix protein. PLOS ONE 17:e0263065.
37. Shinozaki K, Ebert O, Suriawinata A, Thung SN, Woo SLC. 2005. Prophylactic Alpha Interferon Treatment Increases the Therapeutic Index of Oncolytic Vesicular Stomatitis

Virus Virotherapy for Advanced Hepatocellular Carcinoma in Immune-Competent Rats. J Virol 79:13705–13713.

38. Stojdl DF, Lichty BD, tenOever BR, Paterson JM, Power AT, Knowles S, Marius R, Reynard J, Poliquin L, Atkins H, Brown EG, Durbin RK, Durbin JE, Hiscott J, Bell JC. 2003. VSV strains with defects in their ability to shutdown innate immunity are potent systemic anti-cancer agents. Cancer Cell 4:263–275.
39. Patel MR, Jacobson BA, Ji Y, Drees J, Tang S, Xiong K, Wang H, Prigge JE, Dash AS, Kratzke AK, Mesev E, Etchison R, Federspiel MJ, Russell SJ, Kratzke RA. 2015. Vesicular stomatitis virus expressing interferon-β is oncolytic and promotes antitumor immune responses in a syngeneic murine model of non-small cell lung cancer. Oncotarget 6:33165–33177.
40. Heiber JF, Barber GN. 2011. Vesicular Stomatitis Virus Expressing Tumor Suppressor p53 Is a Highly Attenuated, Potent Oncolytic Agent. J Virol 85:10440–10450.
41. Shin EJ, Wanna GB, Choi B, Aguila D, Ebert O, Genden EM, Woo SL. 2007. Interleukin-12 Expression Enhances Vesicular Stomatitis Virus Oncolytic Therapy in Murine Squamous Cell Carcinoma. The Laryngoscope 117:210–214.
42. Roberts A, Buonocore L, Price R, Forman J, Rose JK. 1999. Attenuated Vesicular Stomatitis Viruses as Vaccine Vectors. J Virol 73:3723–3732.
43. Felt SA, Grdzelishvili VZ. 2017. Recent advances in vesicular stomatitis virus-based oncolytic virotherapy: a 5-year update. J Gen Virol 98:2895–2911.
44. Kaur B, Antonio Chiocca E, P. Cripe T. 2012. Oncolytic HSV-1 Virotherapy: Clinical Experience and Opportunities for Progress. Curr Pharm Biotechnol 13:1842–1851.
45. Koch M, Lawler S, Chiocca E. 2020. HSV-1 Oncolytic Viruses from Bench to Bedside: An Overview of Current Clinical Trials. Cancers 12:3514.
46. Pelin A, Boulton S, Tamming LA, Bell JC, Singaravelu R. 2020. Engineering vaccinia virus as an immunotherapeutic battleship to overcome tumor heterogeneity. Expert Opin Biol Ther 20:1083–1097.
47. Breitbach CJ, Burke J, Jonker D, Stephenson J, Haas AR, Chow LQM, Nieva J, Hwang T-H, Moon A, Patt R, Pelusio A, Le Boeuf F, Burns J, Evgin L, De Silva N, Cvancic S, Robertson T, Je J-E, Lee Y-S, Parato K, Diallo J-S, Fenster A, Daneshmand M, Bell JC,

Kirn DH. 2011. Intravenous delivery of a multi-mechanistic cancer-targeted oncolytic poxvirus in humans. Nature 477:99–102.

48. Liu T-C, Galanis E, Kirn D. 2007. Clinical trial results with oncolytic virotherapy: a century of promise, a decade of progress. Nat Clin Pract Oncol 4:101–117.
49. Seth RB, Sun L, Chen ZJ. 2006. Antiviral innate immunity pathways. Cell Res 16:141–147.
50. Kotenko SV, Durbin JE. 2017. Contribution of type III interferons to antiviral immunity: location, location, location. J Biol Chem 292:7295–7303.
51. Schoggins JW. 2019. Interferon-Stimulated Genes: What Do They All Do? Annu Rev Virol 6:567–584.
52. Staeheli P, Pavlovic J. 1991. Inhibition of vesicular stomatitis virus mRNA synthesis by human MxA protein. J Virol 65:4498–4501.
53. Diamond MS, Farzan M. 2013. The broad-spectrum antiviral functions of IFIT and IFITM proteins. Nat Rev Immunol 13:46–57.
54. Alber D, Staeheli P. 1996. Partial Inhibition of Vesicular Stomatitis Virus by the Interferon-Induced Human 9-27 Protein. J Interferon Cytokine Res 16:375–380.
55. Rihn SJ, Aziz MA, Stewart DG, Hughes J, Turnbull ML, Varela M, Sugrue E, Herd CS, Stanifer M, Sinkins SP, Palmarini M, Wilson SJ. 2019. TRIM69 Inhibits Vesicular Stomatitis Indiana Virus. J Virol 93:e00951-19.
56. Yamamoto M, Sato S, Mori K, Hoshino K, Takeuchi O, Takeda K, Akira S. 2002. Cutting Edge: A Novel Toll/IL-1 Receptor Domain-Containing Adapter That Preferentially Activates the IFN-β Promoter in the Toll-Like Receptor Signaling. J Immunol 169:6668–6672.
57. Ramos HJ, Gale M. 2011. RIG-I like receptors and their signaling crosstalk in the regulation of antiviral immunity. Curr Opin Virol 1:167–176.
58. Wang J, Basagoudanavar SH, Wang X, Hopewell E, Albrecht R, García-Sastre A, Balachandran S, Beg AA. 2010. NF-ϰB RelA Subunit Is Crucial for Early IFN-β Expression and Resistance to RNA Virus Replication. J Immunol 185:1720–1729.
59. Reus JB, Rex EA, Gammon DB. 2022. How to Inhibit Nuclear Factor-Kappa B Signaling: Lessons from Poxviruses. Pathogens 11:1061.

60. Taniguchi K, Karin M. 2018. NF-κB, inflammation, immunity and cancer: coming of age. Nat Rev Immunol 18:309–324.

61. Karin M, Greten FR. 2005. NF-κB: linking inflammation and immunity to cancer development and progression. Nat Rev Immunol 5:749–759.

62. Beg AA, Ruben SM, Scheinman RI, Haskill S, Rosen CA, Baldwin AS. 1992. I kappa B interacts with the nuclear localization sequences of the subunits of NF-kappa B: a mechanism for cytoplasmic retention. Genes Dev 6:1899–1913.

63. Dev A, Iyer S, Razani B, Cheng G. 2010. NF-κB and Innate Immunity, p. 115–143. *In* Karin, M (ed.), NF-kB in Health and Disease. Springer Berlin Heidelberg, Berlin, Heidelberg.

64. Deb A, Haque SJ, Mogensen T, Silverman RH, Williams BRG. 2001. RNA-Dependent Protein Kinase PKR Is Required for Activation of NF-κB by IFN-γ in a STAT1-Independent Pathway. J Immunol 166:6170–6180.

65. Pfeffer LM. 2011. The Role of Nuclear Factor κB in the Interferon Response. J Interferon Cytokine Res 31:553–559.

66. Gaddy DF, Lyles DS. 2007. Oncolytic Vesicular Stomatitis Virus Induces Apoptosis via Signaling through PKR, Fas, and Daxx. J Virol 81:2792–2804.

67. Ivashkiv LB, Donlin LT. 2014. Regulation of type I interferon responses. Nat Rev Immunol 14:36–49.

68. Bereczky S, Lindegren G, Karlberg H, Akerstrom S, Klingstrom J, Mirazimi A. 2010. Crimean-Congo hemorrhagic fever virus infection is lethal for adult type I interferon receptor-knockout mice. J Gen Virol 91:1473–1477.

69. Meraz MA, White JM, Sheehan KCF, Bach EA, Rodig SJ, Dighe AS, Kaplan DH, Riley JK, Greenlund AC, Campbell D, Carver-Moore K, DuBois RN, Clark R, Aguet M, Schreiber RD. 1996. Targeted Disruption of the Stat1 Gene in Mice Reveals Unexpected Physiologic Specificity in the JAK–STAT Signaling Pathway. Cell 84:431–442.

70. Yoshimura A, Naka T, Kubo M. 2007. SOCS proteins, cytokine signalling and immune regulation. Nat Rev Immunol 7:454–465.

71. Wynn TA. 2015. Type 2 cytokines: mechanisms and therapeutic strategies. Nat Rev Immunol 15:271–282.

72. Bourgeois-Daigneault M-C, Roy DG, Falls T, Twumasi-Boateng K, St-Germain LE, Marguerie M, Garcia V, Selman M, Jennings VA, Pettigrew J, Amos S, Diallo J-S, Nelson B, Bell JC. 2016. Oncolytic vesicular stomatitis virus expressing interferon-γ has enhanced therapeutic activity. Mol Ther 11.

73. Paulson M, Pisharody S, Pan L, Levy DE, Guadagno S, Mui AL. 1999. Stat Protein Transactivation Domains Recruit p300/CBP through Widely Divergent Sequences. J Biol Chem 274:25343–25349.

74. Ferluga S, Baiz D, Hilton DA, Adams CL, Ercolano E, Dunn J, Bassiri K, Kurian KM, Hanemann CO. 2020. Constitutive activation of the EGFR–STAT1 axis increases proliferation of meningioma tumor cells. Neuro-Oncol Adv 2:vdaa008.

75. Collins-McMillen D, Stevenson EV, Kim JH, Lee B-J, Cieply SJ, Nogalski MT, Chan GC, Frost RW, Spohn CR, Yurochko AD. 2017. Human Cytomegalovirus Utilizes a Nontraditional Signal Transducer and Activator of Transcription 1 Activation Cascade via Signaling through Epidermal Growth Factor Receptor and Integrins To Efficiently Promote the Motility, Differentiation, and Polarization of Infected Monocytes. J Virol 91.

76. Critchley-Thorne RJ, Simons DL, Yan N, Miyahira AK, Dirbas FM, Johnson DL, Swetter SM, Carlson RW, Fisher GA, Koong A, Holmes S, Lee PP. 2009. Impaired interferon signaling is a common immune defect in human cancer. Proc Natl Acad Sci 106:9010–9015.

77. Parker BS, Rautela J, Hertzog PJ. 2016. Antitumour actions of interferons: implications for cancer therapy. Nat Rev Cancer 16:131–144.

78. Forbes NE, Abdelbary H, Lupien M, Bell JC, Diallo J-S. 2013. Exploiting tumor epigenetics to improve oncolytic virotherapy. Front Genet 4.

79. Schirrmacher. 2009. Expression of RIG-I, IRF3, IFN-β and IRF7 determines resistance or susceptibility of cells to infection by Newcastle Disease Virus. Int J Oncol 34.

80. Zhang K, Matsui Y, Hadaschik BA, Lee C, Jia W, Bell JC, Fazli L, So AI, Rennie PS. 2010. Down-regulation of type I interferon receptor sensitizes bladder cancer cells to vesicular stomatitis virus-induced cell death. Int J Cancer NA-NA.

81. Sobol PT, Boudreau JE, Stephenson K, Wan Y, Lichty BD, Mossman KL. 2011. Adaptive Antiviral Immunity Is a Determinant of the Therapeutic Success of Oncolytic Virotherapy. Mol Ther 19:335–344.

82. Berchtold S, Lampe J, Weiland T, Smirnow I, Schleicher S, Handgretinger R, Kopp H-G, Reiser J, Stubenrauch F, Mayer N, Malek NP, Bitzer M, Lauer UM. 2013. Innate Immune Defense Defines Susceptibility of Sarcoma Cells to Measles Vaccine Virus-Based Oncolysis. J Virol 87:3484–3501.

83. Moerdyk-Schauwecker M, Shah NR, Murphy AM, Hastie E, Mukherjee P, Grdzelishvili VZ. 2013. Resistance of pancreatic cancer cells to oncolytic vesicular stomatitis virus: Role of type I interferon signaling. Virology 436:221–234.

84. Liu Y-P, Suksanpaisan L, Steele MB, Russell SJ, Peng K-W. 2013. Induction of antiviral genes by the tumor microenvironment confers resistance to virotherapy. Sci Rep 3:2375.

85. Fulci G, Dmitrieva N, Gianni D, Fontana EJ, Pan X, Lu Y, Kaufman CS, Kaur B, Lawler SE, Lee RJ, Marsh CB, Brat DJ, van Rooijen N, Rachamimov AS, Hochberg FH, Weissleder R, Martuza RL, Chiocca EA. 2007. Depletion of Peripheral Macrophages and Brain Microglia Increases Brain Tumor Titers of Oncolytic Viruses. Cancer Res 67:9398–9406.

86. Forbes NE, Krishnan R, Diallo J-S. 2014. Pharmacological Modulation of Anti-Tumor Immunity Induced by Oncolytic Viruses. Front Oncol 4:191.

87. Ghonime MG, Cassady KA. 2018. Combination Therapy Using Ruxolitinib and Oncolytic HSV Renders Resistant MPNSTs Susceptible to Virotherapy. Cancer Immunol Res 6:1499–1510.

88. Escobar-Zarate D, Liu Y-P, Suksanpaisan L, Russell SJ, Peng K-W. 2013. Overcoming cancer cell resistance to VSV oncolysis with JAK1/2 inhibitors. Cancer Gene Ther 20:582–589.

89. Otsuki A, Patel A, Kasai K, Suzuki M, Kurozumi K, Antonio Chiocca E, Saeki Y. 2008. Histone Deacetylase Inhibitors Augment Antitumor Efficacy of Herpes-based Oncolytic Viruses. Mol Ther 16:1546–1555.

90. Nguyen TL-A, Abdelbary H, Arguello M, Breitbach C, Leveille S, Diallo J-S, Yasmeen A, Bismar TA, Kirn D, Falls T, Snoulten VE, Vanderhyden BC, Werier J, Atkins H, Vaha-Koskela MJV, Stojdl DF, Bell JC, Hiscott J. 2008. Chemical targeting of the innate antiviral response by histone deacetylase inhibitors renders refractory cancers sensitive to viral oncolysis. Proc Natl Acad Sci 105:14981–14986.

91. Colina R, Costa-Mattioli M, Dowling RJO, Jaramillo M, Tai L-H, Breitbach CJ, Martineau Y, Larsson O, Rong L, Svitkin YV, Makrigiannis AP, Bell JC, Sonenberg N. 2008. Translational control of the innate immune response through IRF-7. Nature 452:323–328.
92. Alain T, Lun X, Martineau Y, Sean P, Pulendran B, Petroulakis E, Zemp FJ, Lemay CG, Roy D, Bell JC, Thomas G, Kozma SC, Forsyth PA, Costa-Mattioli M, Sonenberg N. 2010. Vesicular stomatitis virus oncolysis is potentiated by impairing mTORC1-dependent type I IFN production. Proc Natl Acad Sci 107:1576–1581.
93. Diallo J-S, Boeuf FL, Lai F, Cox J, Vaha-Koskela M, Abdelbary H, MacTavish H, Waite K, Falls T, Wang J, Brown R, Blanchard JE, Brown ED, Kirn DH, Hiscott J, Atkins H, Lichty BD, Bell JC. 2010. A High-throughput Pharmacoviral Approach Identifies Novel Oncolytic Virus Sensitizers. Mol Ther 18:1123–1129.
94. Dornan MH, Krishnan R, Macklin AM, Selman M, El Sayes N, Son HH, Davis C, Chen A, Keillor K, Le PJ, Moi C, Ou P, Pardin C, Canez CR, Le Boeuf F, Bell JC, Smith JC, Diallo J-S, Boddy CN. 2016. First-in-class small molecule potentiators of cancer virotherapy. Sci Rep 6:26786.
95. Arulanandam R, Batenchuk C, Varette O, Zakaria C, Garcia V, Forbes NE, Davis C, Krishnan R, Karmacharya R, Cox J, Sinha A, Babawy A, Waite K, Weinstein E, Falls T, Chen A, Hamill J, De Silva N, Conrad DP, Atkins H, Garson K, Ilkow C, Kærn M, Vanderhyden B, Sonenberg N, Alain T, Le Boeuf F, Bell JC, Diallo J-S. 2015. Microtubule disruption synergizes with oncolytic virotherapy by inhibiting interferon translation and potentiating bystander killing. Nat Commun 6:6410.
96. Selman M, Ou P, Rousso C, Bergeron A, Krishnan R, Pikor L, Chen A, Keller BA, Ilkow C, Bell JC, Diallo J-S. 2018. Dimethyl fumarate potentiates oncolytic virotherapy through NF-κB inhibition. Sci Transl Med 10:eaao1613.
97. Rehder D. 2016. Perspectives for vanadium in health issues. Future Med Chem 8:325–338.
98. Elsa Irving, Andrew Stoker. 2017. Vanadium Compounds as PTP Inhibitors. Molecules 22:2269.
99. McLauchlan CC, Peters BJ, Willsky GR, Crans DC. 2015. Vanadium–phosphatase complexes: Phosphatase inhibitors favor the trigonal bipyramidal transition state geometries. Coord Chem Rev 301–302:163–199.

100. Fawcett JP, Farquhar SJ, Walker RJ, Thou T, Lowe G, Goulding A. 1996. The Effect of Oral Vanadyl Sulfate on Body Composition and Performance in Weight-Training Athletes. Int J Sport Nutr 6:382–390.
101. Ścibior A, Pietrzyk Ł, Plewa Z, Skiba A. 2020. Vanadium: Risks and possible benefits in the light of a comprehensive overview of its pharmacotoxicological mechanisms and multi-applications with a summary of further research trends. J Trace Elem Med Biol 61:126508.
102. Mohammad A, Wang J, McNeill JH. 2002. [No title found]. Mol Cell Biochem 229:125–128.
103. Thompson HJ, Chasteen ND, Meeker LD. 1984. Dietary vanadyl(IV) sulfate inhibits chemically-induced mammary carcinogenesis. Carcinogenesis 5:849–851.
104. Ray RS, Ghosh B, Rana A, Chatterjee M. 2007. Suppression of cell proliferation, induction of apoptosis and cell cycle arrest: Chemopreventive activity of vanadiumin vivo andin vitro. Int J Cancer 120:13–23.
105. Bishayee A, Waghray A, Patel MA, Chatterjee M. 2010. Vanadium in the detection, prevention and treatment of cancer: The in vivo evidence. Cancer Lett 294:1–12.
106. Selman M, Rousso C, Bergeron A, Son HH, Krishnan R, El-Sayes NA, Varette O, Chen A, Le Boeuf F, Tzelepis F, Bell JC, Crans DC, Diallo J-S. 2018. Multi-modal Potentiation of Oncolytic Virotherapy by Vanadium Compounds. Mol Ther 26:56–69.
107. Tsave O, Petanidis S, Kioseoglou E, Yavropoulou MP, Yovos JG, Anestakis D, Tsepa A, Salifoglou A. 2016. Role of Vanadium in Cellular and Molecular Immunology: Association with Immune-Related Inflammation and Pharmacotoxicology Mechanisms. Oxid Med Cell Longev 2016:1–10.
108. McAusland TM, van Vloten JP, Santry LA, Guilleman MM, Rghei AD, Ferreira EM, Ingrao JC, Arulanandam R, Major PP, Susta L, Karimi K, Diallo J-S, Bridle BW, Wootton SK. 2021. Combining vanadyl sulfate with Newcastle disease virus potentiates rapid innate immune-mediated regression with curative potential in murine cancer models. Mol Ther - Oncolytics 20:306–324.
109. Vlastaridis P, Kyriakidou P, Chaliotis A, Van de Peer Y, Oliver SG, Amoutzias GD. 2017. Estimating the total number of phosphoproteins and phosphorylation sites in eukaryotic proteomes. GigaScience 6.

110. Attwood MM, Fabbro D, Sokolov AV, Knapp S, Schiöth HB. 2021. Trends in kinase drug discovery: targets, indications and inhibitor design. Nat Rev Drug Discov 20:839–861.
111. Zhang Z-Y. 2017. Drugging the Undruggable: Therapeutic Potential of Targeting Protein Tyrosine Phosphatases. Acc Chem Res 50:122–129.
112. Mullard A. 2018. Phosphatases start shedding their stigma of undruggability. Nat Rev Drug Discov 17:847–849.
113. Wu SY, Lopez-Berestein G, Calin GA, Sood AK. 2014. RNAi Therapies: Drugging the Undruggable. Sci Transl Med 6.
114. Strand MS, Krasnick BA, Pan H, Zhang X, Bi Y, Brooks C, Wetzel C, Sankpal N, Fleming T, Goedegebuure SP, DeNardo DG, Gillanders WE, Hawkins WG, Wickline SA, Fields RC. 2019. Precision delivery of RAS-inhibiting siRNA to KRAS driven cancer via peptide-based nanoparticles. Oncotarget 10:4761–4775.
115. Pecot CV, Wu SY, Bellister S, Filant J, Rupaimoole R, Hisamatsu T, Bhattacharya R, Maharaj A, Azam S, Rodriguez-Aguayo C, Nagaraja AS, Morelli MP, Gharpure KM, Waugh TA, Gonzalez-Villasana V, Zand B, Dalton HJ, Kopetz S, Lopez-Berestein G, Ellis LM, Sood AK. 2014. Therapeutic Silencing of KRAS Using Systemically Delivered siRNAs. Mol Cancer Ther 13:2876–2885.
116. Wong B, Birtch R, Rezaei R, Jamieson T, Crupi M, Diallo J-S, Ilkow CS. 2023. Optimal delivery of RNA interference by viral vectors for cancer therapy. Mol Ther S1525001623004999.
117. Relph KL, Harrington KJ, Pandha H. 2005. Adenoviral Strategies for the Gene Therapy of Cancer. Semin Oncol 32:573–582.
118. Poulin KL, Lanthier RM, Smith AC, Christou C, Risco Quiroz M, Powell KL, O'Meara RW, Kothary R, Lorimer IA, Parks RJ. 2010. Retargeting of Adenovirus Vectors through Genetic Fusion of a Single-Chain or Single-Domain Antibody to Capsid Protein IX. J Virol 84:10074–10086.
119. Shulak L, Beljanski V, Chiang C, Dutta SM, Van Grevenynghe J, Belgnaoui SM, Nguyên TL-A, Di Lenardo T, Semmes OJ, Lin R, Hiscott J. 2014. Histone Deacetylase Inhibitors Potentiate Vesicular Stomatitis Virus Oncolysis in Prostate Cancer Cells by Modulating NF-κB-Dependent Autophagy. J Virol 88:2927–2940.

120. Zou T, Zhang J. 2021. Diverse and pivotal roles of neddylation in metabolism and immunity. FEBS J 288:3884–3912.
121. Zhao Y, Morgan MA, Sun Y. 2014. Targeting Neddylation Pathways to Inactivate Cullin-RING Ligases for Anticancer Therapy. Antioxid Redox Signal 21:2383–2400.
122. Soucy TA, Smith PG, Milhollen MA, Berger AJ, Gavin JM, Adhikari S, Brownell JE, Burke KE, Cardin DP, Critchley S, Cullis CA, Doucette A, Garnsey JJ, Gaulin JL, Gershman RE, Lublinsky AR, McDonald A, Mizutani H, Narayanan U, Olhava EJ, Peluso S, Rezaei M, Sintchak MD, Talreja T, Thomas MP, Traore T, Vyskocil S, Weatherhead GS, Yu J, Zhang J, Dick LR, Claiborne CF, Rolfe M, Bolen JB, Langston SP. 2009. An inhibitor of NEDD8-activating enzyme as a new approach to treat cancer. Nature 458:732–736.
123. Lu Y, Yang X. 2020. The pivotal roles of neddylation pathway in immunoregulation. Immun Inflamm Dis 8:782–792.
124. Chairatvit K, Ngamkitidechakul C. 2007. Control of cell proliferation via elevated NEDD8 conjugation in oral squamous cell carcinoma. Mol Cell Biochem 306:163–169.
125. Salon C, Brambilla E, Brambilla C, Lantuejoul S, Gazzeri S, Eymin B. 2007. Altered pattern of Cul-1 protein expression and neddylation in human lung tumours: relationships with CAND1 and cyclin E protein levels. J Pathol 213:303–310.
126. Xu GW, Toth JI, da Silva SR, Paiva S-L, Lukkarila JL, Hurren R, Maclean N, Sukhai MA, Bhattacharjee RN, Goard CA, Gunning PT, Dhe-Paganon S, Petroski MD, Schimmer AD. 2014. Mutations in UBA3 Confer Resistance to the NEDD8-Activating Enzyme Inhibitor MLN4924 in Human Leukemic Cells. PLoS ONE 9:e93530.
127. Sekeres MA, Watts J, Radinoff A, Sangerman MA, Cerrano M, Lopez PF, Zeidner JF, Campelo MD, Graux C, Liesveld J, Selleslag D, Tzvetkov N, Fram RJ, Zhao D, Bell J, Friedlander S, Faller DV, Adès L. 2021. Randomized phase 2 trial of pevonedistat plus azacitidine versus azacitidine for higher-risk MDS/CMML or low-blast AML. Leukemia 35:2119–2124.
128. Sekeres MA, Fram RJ, Hua Z, Ades L. 2018. Phase 3 study of first line pevonedistat (PEV) + azacitidine (AZA) versus single-agent AZA in patients with higher-risk myelodysplastic syndromes (HR MDS), chronic myelomonocytic leukemia (CMML) or low-blast acute myelogenous leukemia (AML). J Clin Oncol 36:TPS7077–TPS7077.

129. Nawrocki ST, Griffin P, Kelly KR, Carew JS. 2012. MLN4924: a novel first-in-class inhibitor of NEDD8-activating enzyme for cancer therapy. Expert Opin Investig Drugs 21:1563–1573.
130. Swords RT, Kelly KR, Smith PG, Garnsey JJ, Mahalingam D, Medina E, Oberheu K, Padmanabhan S, O'Dwyer M, Nawrocki ST, Giles FJ, Carew JS. 2010. Inhibition of NEDD8-activating enzyme: a novel approach for the treatment of acute myeloid leukemia. Blood 115:3796–3800.
131. Milhollen MA, Traore T, Adams-Duffy J, Thomas MP, Berger AJ, Dang L, Dick LR, Garnsey JJ, Koenig E, Langston SP, Manfredi M, Narayanan U, Rolfe M, Staudt LM, Soucy TA, Yu J, Zhang J, Bolen JB, Smith PG. 2010. MLN4924, a NEDD8-activating enzyme inhibitor, is active in diffuse large B-cell lymphoma models: rationale for treatment of NF-κB–dependent lymphoma. Blood 116:1515–1523.
132. Jin J, Jing Z, Ye Z, Guo L, Hua L, Wang Q, Wang J, Cheng Q, Zhang J, Xu Y, Wei L. 2018. MLN4924 suppresses lipopolysaccharide-induced proinflammatory cytokine production in neutrophils in a dose-dependent manner. Oncol Lett https://doi.org/10.3892/ol.2018.8333.
133. Song H, Huai W, Yu Z, Wang W, Zhao J, Zhang L, Zhao W. 2016. MLN4924, a First-in-Class NEDD8-Activating Enzyme Inhibitor, Attenuates IFN-β Production. J Immunol 196:3117–3123.
134. Mao H, Sun Y. 2020. Neddylation-Independent Activities of MLN4924, p. 363–372. *In* Sun, Y, Wei, W, Jin, J (eds.), Cullin-RING Ligases and Protein Neddylation. Springer Singapore, Singapore.
135. Yu Q, Jiang Y, Sun Y. 2020. Anticancer drug discovery by targeting cullin neddylation. Acta Pharm Sin B 10:746–765.
136. Lukkarila JL, da Silva SR, Ali M, Shahani VM, Xu GW, Berman J, Roughton A, Dhe-Paganon S, Schimmer AD, Gunning PT. 2011. Identification of NAE Inhibitors Exhibiting Potent Activity in Leukemia Cells: Exploring the Structural Determinants of NAE Specificity. ACS Med Chem Lett 2:577–582.
137. Yoshimura C, Muraoka H, Ochiiwa H, Tsuji S, Hashimoto A, Kazuno H, Nakagawa F, Komiya Y, Suzuki S, Takenaka T, Kumazaki M, Fujita N, Mizutani T, Ohkubo S. 2019. TAS4464, A Highly Potent and Selective Inhibitor of NEDD8-Activating Enzyme,

Suppresses Neddylation and Shows Antitumor Activity in Diverse Cancer Models. Mol Cancer Ther 18:1205–1216.

138. Jones TM, Carew JS, Bauman JE, Nawrocki ST. 2021. Targeting NEDDylation as a Novel Approach to Improve the Treatment of Head and Neck Cancer. Cancers 13:3250.
139. Barski MS, Minnell JJ, Maertens GN. 2021. PP2A Phosphatase as an Emerging Viral Host Factor. Front Cell Infect Microbiol 11:725615.
140. Lichty BD, Breitbach CJ, Stojdl DF, Bell JC. 2014. Going viral with cancer immunotherapy. Nat Rev Cancer 14:559–567.
141. Pikor LA, Bell JC, Diallo J-S. 2015. Oncolytic Viruses: Exploiting Cancer's Deal with the Devil. Trends Cancer 1:266–277.
142. Ilkow CS, Swift SL, Bell JC, Diallo J-S. 2014. From Scourge to Cure: Tumour-Selective Viral Pathogenesis as a New Strategy against Cancer. PLoS Pathog 10:e1003836.
143. Parato KA, Senger D, Forsyth PAJ, Bell JC. 2005. Recent progress in the battle between oncolytic viruses and tumours. Nat Rev Cancer 5:965–976.
144. Phan M, Watson MF, Alain T, Diallo J-S. 2018. Oncolytic Viruses on Drugs: Achieving Higher Therapeutic Efficacy. ACS Infect Dis 4:1448–1467.
145. Bergeron A, Kostenkova K, Selman M, Murakami HA, Owens E, Haribabu N, Arulanandam R, Diallo J-S, Crans DC. 2019. Enhancement of oncolytic virotherapy by vanadium(V) dipicolinates. Biometals Int J Role Met Ions Biol Biochem Med 32:545–561.
146. Evangelou AM. 2002. Vanadium in cancer treatment. Crit Rev Oncol Hematol 42:249–265.
147. Garcia V, Krishnan R, Davis C, Batenchuk C, Le Boeuf F, Abdelbary H, Diallo J-S. 2014. High-throughput Titration of Luciferase-expressing Recombinant Viruses. J Vis Exp 51890.
148. Herbst RS. 2004. Review of epidermal growth factor receptor biology. Int J Radiat Oncol 59:S21–S26.
149. Lupberger J, Duong FHT, Fofana I, Zona L, Xiao F, Thumann C, Durand SC, Pessaux P, Zeisel MB, Heim MH, Baumert TF. 2013. Epidermal growth factor receptor signaling impairs the antiviral activity of interferon-alpha: Hepatology. Hepatology 58:1225–1235.

150. Quesnelle KM, Boehm AL, Grandis JR. 2007. STAT-mediated EGFR signaling in cancer. J Cell Biochem 102:311–319.
151. Essaghir A, Toffalini F, Knoops L, Kallin A, van Helden J, Demoulin J-B. 2010. Transcription factor regulation can be accurately predicted from the presence of target gene signatures in microarray gene expression data. Nucleic Acids Res 38:e120–e120.
152. Brown K, Park S, Kanno T, Franzoso G, Siebenlist U. 1993. Mutual regulation of the transcriptional activator NF-kappa B and its inhibitor, I kappa B-alpha. Proc Natl Acad Sci 90:2532–2536.
153. Sun L, Carpenter G. 1998. Epidermal growth factor activation of NF-κB is mediated through IκBα degradation and intracellular free calcium. Oncogene 16:2095–2102.
154. Shostak K, Chariot A. 2015. EGFR and NF-κB: partners in cancer. Trends Mol Med 21:385–393.
155. Lawrence T. 2009. The Nuclear Factor NF- B Pathway in Inflammation. Cold Spring Harb Perspect Biol 1:a001651–a001651.
156. Hiroi M, Ohmori Y. 2003. The Transcriptional Coactivator CREB-binding Protein Cooperates with STAT1 and NF-κB for Synergistic Transcriptional Activation of the CXC Ligand 9/Monokine Induced by Interferon-γ Gene. J Biol Chem 278:651–660.
157. Clarke DL, Clifford RL, Jindarat S, Proud D, Pang L, Belvisi M, Knox AJ. 2010. TNFα and IFNγ Synergistically Enhance Transcriptional Activation of CXCL10 in Human Airway Smooth Muscle Cells via STAT-1, NF-κB, and the Transcriptional Coactivator CREB-binding Protein. J Biol Chem 285:29101–29110.
158. Hoang H-D, Graber TE, Alain T. 2018. Battling for Ribosomes: Translational Control at the Forefront of the Antiviral Response. J Mol Biol 430:1965–1992.
159. Thompson KH, Orvig C. 2006. Vanadium in diabetes: 100 years from Phase 0 to Phase I. J Inorg Biochem 100:1925–1935.
160. Rozzo C, Sanna D, Garribba E, Serra M, Cantara A, Palmieri G, Pisano M. 2017. Antitumoral effect of vanadium compounds in malignant melanoma cell lines. J Inorg Biochem 174:14–24.
161. Naso LG, Badiola I, Marquez Clavijo J, Valcarcel M, Salado C, Ferrer EG, Williams PAM. 2016. Inhibition of the metastatic progression of breast and colorectal cancer in

vitro and in vivo in murine model by the oxidovanadium(IV) complex with luteolin. Bioorg Med Chem 24:6004–6011.

162. Wu Y, Ma Y, Xu Z, Wang D, Zhao B, Pan H, Wang J, Xu D, Zhao X, Pan S, Liu L, Dai W, Jiang H. 2014. Sodium orthovanadate inhibits growth of human hepatocellular carcinoma cells in vitro and in an orthotopic model in vivo. Cancer Lett 351:108–116.
163. Kim Y-R, Cha H-Y, Lim K, Hwang B-D, Hoe K-L, Namgung U, Park S-K. 2003. Activation of epidermal growth factor receptor is responsible for pervanadate-induced phospholipase D activation. Exp Mol Med 35:118–124.
164. Lahusen T, Fereshteh M, Oh A, Wellstein A, Riegel AT. 2007. Epidermal Growth Factor Receptor Tyrosine Phosphorylation and Signaling Controlled by a Nuclear Receptor Coactivator, Amplified in Breast Cancer 1. Cancer Res 67:7256–7265.
165. Wieduwilt MJ, Moasser MM. 2008. The epidermal growth factor receptor family: Biology driving targeted therapeutics. Cell Mol Life Sci 65:1566–1584.
166. Uchida H, Marzulli M, Nakano K, Goins WF, Chan J, Hong C-S, Mazzacurati L, Yoo JY, Haseley A, Nakashima H, Baek H, Kwon H, Kumagai I, Kuroki M, Kaur B, Chiocca EA, Grandi P, Cohen JB, Glorioso JC. 2013. Effective Treatment of an Orthotopic Xenograft Model of Human Glioblastoma Using an EGFR-retargeted Oncolytic Herpes Simplex Virus. Mol Ther 21:561–569.
167. Piao Y, Jiang H, Alemany R, Krasnykh V, Marini FC, Xu J, Alonso MM, Conrad CA, Aldape KD, Gomez-Manzano C, Fueyo J. 2009. Oncolytic adenovirus retargeted to Delta-EGFR induces selective antiglioma activity. Cancer Gene Ther 16:256–265.
168. Zaoui K, Bossow S, Grossardt C, Leber MF, Springfeld C, Plinkert PK, von Kalle C, Ungerechts G. 2012. Chemovirotherapy for head and neck squamous cell carcinoma with EGFR-targeted and CD/UPRT-armed oncolytic measles virus. Cancer Gene Ther 19:181–191.
169. Ueki IF, Min-Oo G, Kalinowski A, Ballon-Landa E, Lanier LL, Nadel JA, Koff JL. 2013. Respiratory virus–induced EGFR activation suppresses IRF1-dependent interferon λ and antiviral defense in airway epithelium. J Exp Med 210:1929–1936.
170. Mitchell HD, Eisfeld AJ, Stratton KG, Heller NC, Bramer LM, Wen J, McDermott JE, Gralinski LE, Sims AC, Le MQ, Baric RS, Kawaoka Y, Waters KM. 2019. The Role of

EGFR in Influenza Pathogenicity: Multiple Network-Based Approaches to Identify a Key Regulator of Non-lethal Infections. Front Cell Dev Biol 7:200.

171. Yang L, Xu J, Guo L, Guo T, Zhang L, Feng L, Chen H, Wang Y. 2018. Porcine Epidemic Diarrhea Virus-Induced Epidermal Growth Factor Receptor Activation Impairs the Antiviral Activity of Type I Interferon. J Virol 92:e02095-17, /jvi/92/8/e02095-17.atom.
172. Diao J, Pantua H, Ngu H, Komuves L, Diehl L, Schaefer G, Kapadia SB. 2012. Hepatitis C Virus Induces Epidermal Growth Factor Receptor Activation via CD81 Binding for Viral Internalization and Entry. J Virol 86:10935–10949.
173. Beerli C, Yakimovich A, Kilcher S, Reynoso GV, Fläschner G, Müller DJ, Hickman HD, Mercer J. 2019. Vaccinia virus hijacks EGFR signalling to enhance virus spread through rapid and directed infected cell motility. Nat Microbiol 4:216–225.
174. Wang C, Wang X, Veleeparambil M, Kessler PM, Willard B, Chattopadhyay S, Sen GC. 2020. EGFR-mediated tyrosine phosphorylation of STING determines its trafficking route and cellular innate immunity functions. EMBO J 39.
175. Lulli D, Carbone ML, Pastore S. 2016. Epidermal growth factor receptor inhibitors trigger a type I interferon response in human skin. Oncotarget 7:47777–47793.
176. Gong K, Guo G, Panchani N, Bender ME, Gerber DE, Minna JD, Fattah F, Gao B, Peyton M, Kernstine K, Mukherjee B, Burma S, Chiang C-M, Zhang S, Amod Sathe A, Xing C, Dao KH, Zhao D, Akbay EA, Habib AA. 2020. EGFR inhibition triggers an adaptive response by co-opting antiviral signaling pathways in lung cancer. Nat Cancer 1:394–409.
177. Qureshi SA, Leung S, Kerr IM, Stark GR, Darnell JE. 1996. Function of Stat2 protein in transcriptional activation by alpha interferon. Mol Cell Biol 16:288–293.
178. Blaszczyk K, Nowicka H, Kostyrko K, Antonczyk A, Wesoly J, Bluyssen HAR. 2016. The unique role of STAT2 in constitutive and IFN-induced transcription and antiviral responses. Cytokine Growth Factor Rev 29:71–81.
179. Park C, Li S, Cha E, Schindler C. 2000. Immune Response in Stat2 Knockout Mice. Immunity 13:795–804.
180. Christian SL, Collier TW, Zu D, Licursi M, Hough CM, Hirasawa K. 2009. Activated Ras/MEK Inhibits the Antiviral Response of Alpha Interferon by Reducing STAT2 Levels. J Virol 83:6717–6726.

181. Noser JA, Mael AA, Sakuma R, Ohmine S, Marcato P, WK Lee P, Ikeda Y. 2007. The RAS/Raf1/MEK/ERK Signaling Pathway Facilitates VSV-mediated Oncolysis: Implication for the Defective Interferon Response in Cancer Cells. Mol Ther 15:1531–1536.
182. Han W, Carpenter RL, Cao X, Lo H-W. 2013. STAT1 gene expression is enhanced by nuclear EGFR and HER2 via cooperation With STAT3: STAT1 REGULATION BY NUCLEAR EGFR AND STAT3. Mol Carcinog 52:959–969.
183. Andersen P, Pedersen MW, Woetmann A, Villingshøj M, Stockhausen M-T, Ødum N, Poulsen HS. 2008. EGFR induces expression of IRF-1 via STAT1 and STAT3 activation leading to growth arrest of human cancer cells: EGFR Mediated IRF-1 Expression Through STAT Activation. Int J Cancer 122:342–349.
184. Cheng C, Lin H, Tsai K, Chiang Y, Lim K, Chen CG, Su Y, Peng C, Ho A, Huang L, Chang Y, Lin H, Chang J, Chang Y. 2018. Epidermal growth factor induces STAT1 expression to exacerbate the IFNr-mediated PD-L1 axis in epidermal growth factor receptor-positive cancers. Mol Carcinog 57:1588–1598.
185. Wu TR, Hong YK, Wang X-D, Ling MY, Dragoi AM, Chung AS, Campbell AG, Han Z-Y, Feng G-S, Chin YE. 2002. SHP-2 Is a Dual-specificity Phosphatase Involved in Stat1 Dephosphorylation at Both Tyrosine and Serine Residues in Nuclei. J Biol Chem 277:47572–47580.
186. Wang S, Zheng G, Zhao L, Xu F, Qian J. 2015. Shp-2 contributes to anti-RSV activity in human pulmonary alveolar epithelial cells by interfering with the IFN-α-induced Jak/Stat1 pathway. J Cell Mol Med 19:2432–2440.
187. Wang Q, Pan W, Wang S, Pan C, Ning H, Huang S, Chiu S-H, Chen J-L. 2020. Protein Tyrosine Phosphatase SHP2 Suppresses Host Innate Immunity against Influenza A Virus by Regulating EGFR-Mediated Signaling. J Virol 95:e02001-20, /jvi/95/6/JVI.02001-20.atom.
188. Du Z, Whitt MA, Baumann J, Garner JM, Morton CL, Davidoff AM, Pfeffer LM. 2012. Inhibition of Type I Interferon-Mediated Antiviral Action in Human Glioma Cells by the IKK Inhibitors BMS-345541 and TPCA-1. J Interferon Cytokine Res 32:368–377.

189. Cataldi M, Shah NR, Felt SA, Grdzelishvili VZ. 2015. Breaking resistance of pancreatic cancer cells to an attenuated vesicular stomatitis virus through a novel activity of IKK inhibitor TPCA-1. Virology 485:340–354.
190. Ohmori Y, Schreiber RD, Hamilton TA. 1997. Synergy between Interferon-γ and Tumor Necrosis Factor-α in Transcriptional Activation Is Mediated by Cooperation between Signal Transducer and Activator of Transcription 1 and Nuclear Factor κB. J Biol Chem 272:14899–14907.
191. Shelton JG, Steelman LS, Abrams SL, Bertrand FE, Franklin RA, McMahon M, McCubrey JA. 2005. The epidermal growth factor receptor gene family as a target for therapeutic intervention in numerous cancers: what's genetics got to do with it? Expert Opin Ther Targets 9:1009–1030.
192. Sigismund S, Avanzato D, Lanzetti L. 2018. Emerging functions of the EGFR in cancer. Mol Oncol 12:3–20.
193. Jutten B, Keulers TG, Schaaf MBE, Savelkouls K, Theys J, Span PN, Vooijs MA, Bussink J, Rouschop KMA. 2013. EGFR overexpressing cells and tumors are dependent on autophagy for growth and survival. Radiother Oncol 108:479–483.
194. Liccardi G, Hartley JA, Hochhauser D. 2011. EGFR Nuclear Translocation Modulates DNA Repair following Cisplatin and Ionizing Radiation Treatment. Cancer Res 71:1103–1114.
195. Tao Y, Song X, Deng X, Xie D, Lee LM, Liu Y, Li W, Li L, Deng L, Wu Q, Gong J, Cao Y. 2005. Nuclear accumulation of epidermal growth factor receptor and acceleration of G1/S stage by Epstein–Barr-encoded oncoprotein latent membrane protein 1. Exp Cell Res 303:240–251.
196. Arulanandam R, Batenchuk C, Angarita FA, Ottolino-Perry K, Cousineau S, Mottashed A, Burgess E, Falls TJ, De Silva N, Tsang J, Howe GA, Bourgeois-Daigneault M-C, Conrad DP, Daneshmand M, Breitbach CJ, Kirn DH, Raptis L, Sad S, Atkins H, Huh MS, Diallo J-S, Lichty BD, Ilkow CS, Le Boeuf F, Addison CL, McCart JA, Bell JC. 2015. VEGF-Mediated Induction of PRD1-BF1/Blimp1 Expression Sensitizes Tumor Vasculature to Oncolytic Virus Infection. Cancer Cell 28:210–224.
197. Diallo J-S, Vähä-Koskela M, Le Boeuf F, Bell J. 2012. Propagation, Purification, and In Vivo Testing of Oncolytic Vesicular Stomatitis Virus Strains 797:127–40.

198. Katze MG, He Y, Gale M. 2002. Viruses and interferon: a fight for supremacy. Nat Rev Immunol 2:675–687.
199. Matveeva OV, Chumakov PM. 2018. Defects in interferon pathways as potential biomarkers of sensitivity to oncolytic viruses. Rev Med Virol 28:6.
200. Wong B, Bergeron A, Alluqmani N, Maznyi G, Chen A, Arulanandam R, Diallo J-S. 2022. Dependency of EGFR activation in vanadium-based sensitization to oncolytic virotherapy. Mol Ther - Oncolytics 25:146–159.
201. Carbone CJ, Zheng H, Bhattacharya S, Lewis JR, Reiter AM, Henthorn P, Zhang Z-Y, Baker DP, Ukkiramapandian R, Bence KK, Fuchs SY. 2012. Protein tyrosine phosphatase 1B is a key regulator of IFNAR1 endocytosis and a target for antiviral therapies. Proc Natl Acad Sci 109:19226–19231.
202. An H, Hou J, Zhou J, Zhao W, Xu H, Zheng Y, Yu Y, Liu S, Cao X. 2008. Phosphatase SHP-1 promotes TLR- and RIG-I-activated production of type I interferon by inhibiting the kinase IRAK1. Nat Immunol 9:542–550.
203. Martin NT, Bell JC. 2018. Oncolytic Virus Combination Therapy: Killing One Bird with Two Stones. Mol Ther 26:1414–1422.
204. Veinalde R, Grossardt C, Hartmann L, Bourgeois-Daigneault M-C, Bell JC, Jäger D, von Kalle C, Ungerechts G, Engeland CE. 2017. Oncolytic measles virus encoding interleukin-12 mediates potent antitumor effects through T cell activation. OncoImmunology 6:e1285992.
205. Rehwinkel J, Gack MU. 2020. RIG-I-like receptors: their regulation and roles in RNA sensing. Nat Rev Immunol 20:537–551.
206. Mannan AU, Roussa E, Kraus C, Rickmann M, Maenner J, Nayernia K, Krieglstein K, Reis A, Engel W. 2004. Mutation in the gene encoding lysosomal acid phosphatase (Acp2) causes cerebellum and skin malformation in mouse. Neurogenetics 5:229–238.
207. Bailey K, Rahimi Balaei M, Mehdizadeh M, Marzban H. 2013. Spatial and Temporal Expression of Lysosomal Acid Phosphatase 2 (ACP2) Reveals Dynamic Patterning of the Mouse Cerebellar Cortex. The Cerebellum 12:870–881.
208. Waheed A, Van Etten RL, Gieselmann V, Von Figura K. 1985. Immunological characterization of human acid phosphatase gene products. Biochem Genet 23:309–319.

209. Makrypidi G, Damme M, Müller-Loennies S, Trusch M, Schmidt B, Schlüter H, Heeren J, Lübke T, Saftig P, Braulke T. 2012. Mannose 6 Dephosphorylation of Lysosomal Proteins Mediated by Acid Phosphatases Acp2 and Acp5. Mol Cell Biol 32:774–782.
210. Lee J, Kim J, Son K, d'Alexandry d'Orengiani A-LPH, Min J-Y. 2017. Acid phosphatase 2 (ACP2) is required for membrane fusion during influenza virus entry. Sci Rep 7:43893.
211. Eden E, Navon R, Steinfeld I, Lipson D, Yakhini Z. 2009. GOrilla: a tool for discovery and visualization of enriched GO terms in ranked gene lists. BMC Bioinformatics 10:48.
212. Eden E, Lipson D, Yogev S, Yakhini Z. 2007. Discovering Motifs in Ranked Lists of DNA Sequences. PLoS Comput Biol 3:e39.
213. Naik RR, Shakya AK, Aladwan SM, El-Tanani M. 2022. Kinase Inhibitors as Potential Therapeutic Agents in the Treatment of COVID-19. Front Pharmacol 13:806568.
214. Okabe Y, Sano T, Nagata S. 2009. Regulation of the innate immune response by threonine-phosphatase of Eyes absent. Nature 460:520–524.
215. Gu M, Zhang T, Lin W, Liu Z, Lai R, Xia D, Huang H, Wang X. 2014. Protein phosphatase PP1 negatively regulates the Toll-like receptor- and RIG-I-like receptor-triggered production of type I interferon by inhibiting IRF3 phosphorylation at serines 396 and 385 in macrophage. Cell Signal 26:2930–2939.
216. Wang L, Zhao J, Ren J, Hall KH, Moorman JP, Yao ZQ, Ning S. 2016. Protein phosphatase 1 abrogates IRF7-mediated type I IFN response in antiviral immunity. Eur J Immunol 46:2409–2419.
217. Shanker V, Trincucci G, Heim HM, Duong HTF. 2013. Protein phosphatase 2A impairs IFNα-induced antiviral activity against the hepatitis C virus through the inhibition of STAT1 tyrosine phosphorylation. J Viral Hepat 20:612–621.
218. Koyama M, Ito M, Feng J, Seko T, Shiraki K, Takase K, Hartshorne DJ, Nakano T. 2000. Phosphorylation of CPI-17, an inhibitory phosphoprotein of smooth muscle myosin phosphatase, by Rho-kinase. FEBS Lett 475:197–200.
219. Zhan Z, Cao H, Xie X, Yang L, Zhang P, Chen Y, Fan H, Liu Z, Liu X. 2015. Phosphatase PP4 Negatively Regulates Type I IFN Production and Antiviral Innate Immunity by Dephosphorylating and Deactivating TBK1. J Immunol 195:3849–3857.
220. Sun X, Roth SL, Bialecki MA, Whittaker GR. 2010. Internalization and fusion mechanism of vesicular stomatitis virus and related rhabdoviruses. Future Virol 5:85–96.

221. Katze MG, Fornek JL, Palermo RE, Walters K-A, Korth MJ. 2008. Innate immune modulation by RNA viruses: emerging insights from functional genomics. Nat Rev Immunol 8:644–654.
222. Chang K, Marran K, Valentine A, Hannon GJ. 2013. Creating an miR30-Based shRNA Vector. Cold Spring Harb Protoc 2013:pdb.prot075853.
223. Gordon JA. 1991. [41] Use of vanadate as protein-phosphotyrosine phosphatase inhibitor, p. 477–482. *In* Methods in Enzymology. Elsevier.
224. Pfaffl MW. 2001. A new mathematical model for relative quantification in real-time RT-PCR. Nucleic Acids Res 29:45e–445.
225. Bray NL, Pimentel H, Melsted P, Pachter L. 2016. Near-optimal probabilistic RNA-seq quantification. Nat Biotechnol 34:525–527.
226. Pimentel H, Bray NL, Puente S, Melsted P, Pachter L. 2017. Differential analysis of RNA-seq incorporating quantification uncertainty. Nat Methods 14:687–690.
227. Sales G, Calura E, Cavalieri D, Romualdi C. 2012. graphite - a Bioconductor package to convert pathway topology to gene network. BMC Bioinformatics 13:20.
228. Martini P, Sales G, Massa MS, Chiogna M, Romualdi C. 2013. Along signal paths: an empirical gene set approach exploiting pathway topology. Nucleic Acids Res 41:e19–e19.
229. Ge SX, Jung D, Yao R. 2020. ShinyGO: a graphical gene-set enrichment tool for animals and plants. Bioinformatics 36:2628–2629.
230. Alsharifi M, Müllbacher A, Regner M. 2008. Interferon type I responses in primary and secondary infections. Immunol Cell Biol 86:239–245.
231. Zhou L, Jiang Y, Luo Q, Li L, Jia L. 2019. Neddylation: a novel modulator of the tumor microenvironment. Mol Cancer 18:77.
232. Enchev RI, Schulman BA, Peter M. 2015. Protein neddylation: beyond cullin–RING ligases. Nat Rev Mol Cell Biol 16:30–44.
233. Merlet J, Burger J, Gomes J-E, Pintard L. 2009. Regulation of cullin-RING E3 ubiquitin-ligases by neddylation and dimerization. Cell Mol Life Sci 66:1924–1938.
234. Tong S, Si Y, Yu H, Zhang L, Xie P, Jiang W. 2017. MLN4924 (Pevonedistat), a protein neddylation inhibitor, suppresses proliferation and migration of human clear cell renal cell carcinoma. Sci Rep 7:5599.

235. Wang Y, Luo Z, Pan Y, Wang W, Zhou X, Jeong LS, Chu Y, Liu J, Jia L. 2015. Targeting protein neddylation with an NEDD8-activating enzyme inhibitor MLN4924 induced apoptosis or senescence in human lymphoma cells. Cancer Biol Ther 16:420–429.
236. Swords RT, Coutre S, Maris MB, Zeidner JF, Foran JM, Cruz J, Erba HP, Berdeja JG, Tam W, Vardhanabhuti S, Pawlikowska-Dobler I, Faessel HM, Dash AB, Sedarati F, Dezube BJ, Faller DV, Savona MR. 2018. Pevonedistat, a first-in-class NEDD8-activating enzyme inhibitor, combined with azacitidine in patients with AML. Blood 131:1415–1424.
237. Sarantopoulos J, Shapiro GI, Cohen RB, Clark JW, Kauh JS, Weiss GJ, Cleary JM, Mahalingam D, Pickard MD, Faessel HM, Berger AJ, Burke K, Mulligan G, Dezube BJ, Harvey RD. 2016. Phase I Study of the Investigational NEDD8-Activating Enzyme Inhibitor Pevonedistat (TAK-924/MLN4924) in Patients with Advanced Solid Tumors. Clin Cancer Res 22:847–857.
238. Felt SA, Moerdyk-Schauwecker MJ, Grdzelishvili VZ. 2015. Induction of apoptosis in pancreatic cancer cells by vesicular stomatitis virus. Virology 474:163–173.
239. Gaddy DF, Lyles DS. 2005. Vesicular Stomatitis Viruses Expressing Wild-Type or Mutant M Proteins Activate Apoptosis through Distinct Pathways. J Virol 79:4170–4179.
240. Andersson U, Tracey KJ. 2011. HMGB1 Is a Therapeutic Target for Sterile Inflammation and Infection. Annu Rev Immunol 29:139–162.
241. Bailly A, Perrin A, Bou Malhab LJ, Pion E, Larance M, Nagala M, Smith P, O'Donohue M-F, Gleizes P-E, Zomerdijk J, Lamond AI, Xirodimas DP. 2016. The NEDD8 inhibitor MLN4924 increases the size of the nucleolus and activates p53 through the ribosomal-Mdm2 pathway. Oncogene 35:415–426.
242. Lin JJ, Milhollen MA, Smith PG, Narayanan U, Dutta A. 2010. NEDD8-Targeting Drug MLN4924 Elicits DNA Rereplication by Stabilizing Cdt1 in S Phase, Triggering Checkpoint Activation, Apoptosis, and Senescence in Cancer Cells. Cancer Res 70:10310–10320.
243. Godbersen JC, Humphries LA, Danilova OV, Kebbekus PE, Brown JR, Eastman A, Danilov AV. 2014. The Nedd8-Activating Enzyme Inhibitor MLN4924 Thwarts Microenvironment-Driven NF-κB Activation and Induces Apoptosis in Chronic Lymphocytic Leukemia B Cells. Clin Cancer Res 20:1576–1589.

244. Chang F-M, Reyna SM, Granados JC, Wei S-J, Innis-Whitehouse W, Maffi SK, Rodriguez E, Slaga TJ, Short JD. 2012. Inhibition of Neddylation Represses Lipopolysaccharide-induced Proinflammatory Cytokine Production in Macrophage Cells. J Biol Chem 287:35756–35767.
245. Stojdl DF, Lichty B, Knowles S, Marius R, Atkins H, Sonenberg N, Bell JC. 2000. Exploiting tumor-specific defects in the interferon pathway with a previously unknown oncolytic virus. Nat Med 6:821–825.
246. Zhu Z, McGray AJR, Jiang W, Lu B, Kalinski P, Guo ZS. 2022. Improving cancer immunotherapy by rationally combining oncolytic virus with modulators targeting key signaling pathways. Mol Cancer 21:196.
247. Torka P, Mavis C, Kothari S, Belliotti S, Gu J, Sundaram S, Barth M, Hernandez-Ilizaliturri FJ. 2020. Pevonedistat, a NEDD8-activating enzyme inhibitor, induces apoptosis and augments efficacy of chemotherapy and small molecule inhibitors in pre-clinical models of diffuse large B-cell lymphoma. eJHaem 1:122–132.
248. Czuczman NM, Barth MJ, Gu J, Neppalli V, Mavis C, Frys SE, Hu Q, Liu S, Klener P, Vockova P, Czuczman MS, Hernandez-Ilizaliturri FJ. 2016. Pevonedistat, a NEDD8-activating enzyme inhibitor, is active in mantle cell lymphoma and enhances rituximab activity in vivo. Blood 127:1128–1137.
249. Wong KM, Micel LN, Selby HM, Tan AC, Pitts TM, Bagby SM, Spreafico A, Klauck PJ, Blakemore SJ, Smith PF, McDonald A, Berger A, Tentler JJ, Eckhardt SG. 2017. Targeting the protein ubiquitination machinery in melanoma by the NEDD8-activating enzyme inhibitor pevonedistat (MLN4924). Invest New Drugs 35:11–25.
250. Hughes DJ, Wood JJ, Jackson BR, Baquero-Pérez B, Whitehouse A. 2015. NEDDylation Is Essential for Kaposi's Sarcoma-Associated Herpesvirus Latency and Lytic Reactivation and Represents a Novel Anti-KSHV Target. PLOS Pathog 11:e1004771.
251. Ramirez PW, DePaula-Silva AB, Szaniawski M, Barker E, Bosque A, Planelles V. 2015. HIV-1 Vpu utilizes both cullin-RING ligase (CRL) dependent and independent mechanisms to downmodulate host proteins. Retrovirology 12:65.
252. Le-Trilling VTK, Megger DA, Katschinski B, Landsberg CD, Rückborn MU, Tao S, Krawczyk A, Bayer W, Drexler I, Tenbusch M, Sitek B, Trilling M. 2016. Broad and potent antiviral activity of the NAE inhibitor MLN4924. Sci Rep 6:19977.

253. Sun H, Yao W, Wang K, Qian Y, Chen H, Jung Y-S. 2018. Inhibition of neddylation pathway represses influenza virus replication and pro-inflammatory responses. Virology 514:230–239.
254. Zhang T, Ye Z, Yang X, Qin Y, Hu Y, Tong X, Lai W, Ye X. 2017. NEDDylation of PB2 Reduces Its Stability and Blocks the Replication of Influenza A Virus. Sci Rep 7:43691.
255. Ryman KD, Klimstra WB, Nguyen KB, Biron CA, Johnston RE. 2000. Alpha/Beta Interferon Protects Adult Mice from Fatal Sindbis Virus Infection and Is an Important Determinant of Cell and Tissue Tropism. J Virol 74:3366–3378.
256. Gough DJ, Messina NL, Hii L, Gould JA, Sabapathy K, Robertson APS, Trapani JA, Levy DE, Hertzog PJ, Clarke CJP, Johnstone RW. 2010. Functional Crosstalk between Type I and II Interferon through the Regulated Expression of STAT1. PLoS Biol 8:e1000361.
257. Wong LH, Krauer KG, Hatzinisiriou I, Estcourt MJ, Hersey P, Tam ND, Edmondson S, Devenish RJ, Ralph SJ. 1997. Interferon-resistant Human Melanoma Cells Are Deficient in ISGF3 Components, STAT1, STAT2, and p48-ISGF3γ. J Biol Chem 272:28779–28785.
258. Durbin JE, Hackenmiller R, Simon MC, Levy DE. 1996. Targeted Disruption of the Mouse Stat1 Gene Results in Compromised Innate Immunity to Viral Disease. Cell 84:443–450.
259. Kumar H, Kawai T, Kato H, Sato S, Takahashi K, Coban C, Yamamoto M, Uematsu S, Ishii KJ, Takeuchi O, Akira S. 2006. Essential role of IPS-1 in innate immune responses against RNA viruses. J Exp Med 203:1795–1803.
260. Kim TK, Maniatis T. 1997. The Mechanism of Transcriptional Synergy of an In Vitro Assembled Interferon-β Enhanceosome. Mol Cell 1:119–129.
261. Munshi N, Yie J, Merika M, Senger K, Lomvardas S, Agalioti T, Thanos D. 1999. The IFN- Enhancer: A Paradigm for Understanding Activation and Repression of Inducible Gene Expression. Cold Spring Harb Symp Quant Biol 64:149–160.
262. Varble AJ, Ried CD, Hammond WJ, Marquis KA, Woodruff MC, Ferran MC. 2016. The vesicular stomatitis virus matrix protein inhibits NF-ϰB activation in mouse L929 cells. Virology 499:99–104.

263. Ehrentraut SF, Curtis VF, Wang RX, Saeedi BJ, Ehrentraut H, Onyiah JC, Kelly CJ, Campbell EL, Glover LE, Kominsky DJ, Colgan SP. 2016. Perturbation of neddylation-dependent NF-κB responses in the intestinal epithelium drives apoptosis and inhibits resolution of mucosal inflammation. Mol Biol Cell 27:3687–3694.
264. Zhao M, Zhang Y, Yang X, Jin J, Shen Z, Feng X, Zou T, Deng L, Cheng D, Zhang X, Qin C, Niu C, Ye Z, Zhang X, He J, Hou C, Li G, Han G, Cheng Q, Wang Q, Wei L, Dong J, Zhang J. 2021. Myeloid neddylation targets IRF7 and promotes host innate immunity against RNA viruses. PLOS Pathog 17:e1009901.
265. Yarde DN, Nace RA, Russell SJ. 2013. Oncolytic vesicular stomatitis virus and bortezomib are antagonistic against myeloma cells in vitro but have additive anti-myeloma activity in vivo. Exp Hematol 41:1038–1049.
266. Pai C-CS, Khuat LT, Chen M, Murphy WJ, Abedi M. 2017. Therapeutic Effects of a NEDD8-Activating Enzyme Inhibitor, Pevonedistat, on Sclerodermatous Graft-versus-Host Disease in Mice. Biol Blood Marrow Transplant 23:30–37.
267. Marelli G, Howells A, Lemoine NR, Wang Y. 2018. Oncolytic Viral Therapy and the Immune System: A Double-Edged Sword Against Cancer. Front Immunol 9:866.
268. Cervera-Carrascon V, Quixabeira DCA, Havunen R, Santos JM, Kutvonen E, Clubb JHA, Siurala M, Heiniö C, Zafar S, Koivula T, Lumen D, Vaha M, Garcia-Horsman A, Airaksinen AJ, Sorsa S, Anttila M, Hukkanen V, Kanerva A, Hemminki A. 2020. Comparison of Clinically Relevant Oncolytic Virus Platforms for Enhancing T Cell Therapy of Solid Tumors. Mol Ther - Oncolytics 17:47–60.
269. Chaurasiya S, Fong Y, Warner SG. 2021. Oncolytic Virotherapy for Cancer: Clinical Experience. Biomedicines 9:419.
270. Fullerton MD, Hakimuddin F, Bonen A, Bakovic M. 2009. The Development of a Metabolic Disease Phenotype in CTP:Phosphoethanolamine Cytidylyltransferase-deficient Mice. J Biol Chem 284:25704–25713.
271. Walton J, Blagih J, Ennis D, Leung E, Dowson S, Farquharson M, Tookman LA, Orange C, Athineos D, Mason S, Stevenson D, Blyth K, Strathdee D, Balkwill FR, Vousden K, Lockley M, McNeish IA. 2016. CRISPR/Cas9-Mediated *Trp53* and *Brca2* Knockout to Generate Improved Murine Models of Ovarian High-Grade Serous Carcinoma. Cancer Res 76:6118–6129.

272. Fouad YA, Aanei C. 2017. Revisiting the hallmarks of cancer. Am J Cancer Res 7:1016–1036.

273. Chen H, Tanaka N, Mitani Y, Oda E, Nozawa H, Chen J, Yanai H, Negishi H, Choi MK, Iwasaki T, Yamamoto H, Taniguchi T, Takaoka A. 2009. Critical role for constitutive type I interferon signaling in the prevention of cellular transformation. Cancer Sci 100:449–456.

274. Widschwendter A, Tonko-Geymayer S, Welte T, Daxenbichler G, Marth C, Doppler W. 2002. Prognostic significance of signal transducer and activator of transcription 1 activation in breast cancer. Clin Cancer Res Off J Am Assoc Cancer Res 8:3065–3074.

275. Gao J, Shi LZ, Zhao H, Chen J, Xiong L, He Q, Chen T, Roszik J, Bernatchez C, Woodman SE, Chen P-L, Hwu P, Allison JP, Futreal A, Wargo JA, Sharma P. 2016. Loss of IFN-γ Pathway Genes in Tumor Cells as a Mechanism of Resistance to Anti-CTLA-4 Therapy. Cell 167:397-404.e9.

276. Zaretsky JM, Garcia-Diaz A, Shin DS, Escuin-Ordinas H, Hugo W, Hu-Lieskovan S, Torrejon DY, Abril-Rodriguez G, Sandoval S, Barthly L, Saco J, Homet Moreno B, Mezzadra R, Chmielowski B, Ruchalski K, Shintaku IP, Sanchez PJ, Puig-Saus C, Cherry G, Seja E, Kong X, Pang J, Berent-Maoz B, Comin-Anduix B, Graeber TG, Tumeh PC, Schumacher TNM, Lo RS, Ribas A. 2016. Mutations Associated with Acquired Resistance to PD-1 Blockade in Melanoma. N Engl J Med 375:819–829.

277. Zitzmann K, Brand S, De Toni EN, Baehs S, Göke B, Meinecke J, Spöttl G, Meyer HHHD, Auernhammer CJ. 2007. SOCS1 Silencing Enhances Antitumor Activity of Type I IFNs by Regulating Apoptosis in Neuroendocrine Tumor Cells. Cancer Res 67:5025–5032.

278. Kulaeva OI, Draghici S, Tang L, Kraniak JM, Land SJ, Tainsky MA. 2003. Epigenetic silencing of multiple interferon pathway genes after cellular immortalization. Oncogene 22:4118–4127.

279. Blank C, Brown I, Peterson AC, Spiotto M, Iwai Y, Honjo T, Gajewski TF. 2004. PD-L1/B7H-1 Inhibits the Effector Phase of Tumor Rejection by T Cell Receptor (TCR) Transgenic CD8+ T Cells. Cancer Res 64:1140–1145.

280. Bakhoum SF, Ngo B, Laughney AM, Cavallo J-A, Murphy CJ, Ly P, Shah P, Sriram RK, Watkins TBK, Taunk NK, Duran M, Pauli C, Shaw C, Chadalavada K, Rajasekhar VK,

Genovese G, Venkatesan S, Birkbak NJ, McGranahan N, Lundquist M, LaPlant Q, Healey JH, Elemento O, Chung CH, Lee NY, Imielenski M, Nanjangud G, Pe'er D, Cleveland DW, Powell SN, Lammerding J, Swanton C, Cantley LC. 2018. Chromosomal instability drives metastasis through a cytosolic DNA response. Nature 553:467–472.

281. Yan R, van Meurs M, Popa ER, Jongman RM, Zwiers PJ, Niemarkt AE, Kuiper T, Kamps JA, Heeringa P, Zijlstra JG, Molema G, Moser J. 2017. Endothelial Interferon Regulatory Factor 1 Regulates Lipopolysaccharide-Induced VCAM-1 Expression Independent of NFκB. J Innate Immun 9:546–560.
282. Dehler CE, Lester K, Della Pelle G, Jouneau L, Houel A, Collins C, Dovgan T, Machat R, Zou J, Boudinot P, Martin SAM, Collet B. 2019. Viral Resistance and IFN Signaling in STAT2 Knockout Fish Cells. J Immunol 203:465–475.
283. Suzuki M, Chiocca EA, Saeki Y. 2007. Early STAT1 Activation After Systemic Delivery of HSV Amplicon Vectors Suppresses Transcription of The Vector-encoded Transgene. Mol Ther 15:2017–2026.
284. Paglino JC, van den Pol AN. 2011. Vesicular Stomatitis Virus Has Extensive Oncolytic Activity against Human Sarcomas: Rare Resistance Is Overcome by Blocking Interferon Pathways. J Virol 85:9346–9358.
285. Alluqmani N, Jirovec A, Taha Z, Varette O, Chen A, Serrano D, Maznyi G, Khan S, Forbes NE, Arulanandam R, Auer RC, Diallo J-S. 2022. Vanadyl sulfate-enhanced oncolytic virus immunotherapy mediates the antitumor immune response by upregulating the secretion of pro-inflammatory cytokines and chemokines. Front Immunol 13:1032356.
286. Struzik J, Szulc-Dąbrowska L. 2018. NF-κB Signaling in Targeting Tumor Cells by Oncolytic Viruses—Therapeutic Perspectives. Cancers 10:426.
287. Pires B, Silva R, Ferreira G, Abdelhay E. 2018. NF-kappaB: Two Sides of the Same Coin. Genes 9:24.
288. Oeckinghaus A, Ghosh S. 2009. The NF-kappaB family of transcription factors and its regulation. Cold Spring Harb Perspect Biol 1:a000034.
289. Burke JR, Pattoli MA, Gregor KR, Brassil PJ, MacMaster JF, McIntyre KW, Yang X, Iotzova VS, Clarke W, Strnad J, Qiu Y, Zusi FC. 2003. BMS-345541 is a highly selective

inhibitor of I kappa B kinase that binds at an allosteric site of the enzyme and blocks NF-kappa B-dependent transcription in mice. J Biol Chem 278:1450–1456.

290. Xu D, Qu C-K. 2008. Protein tyrosine phosphatases in the JAK/STAT pathway. Front Biosci J Virtual Libr 13:4925–4932.
291. You M, Yu D-H, Feng G-S. 1999. Shp-2 Tyrosine Phosphatase Functions as a Negative Regulator of the Interferon-Stimulated Jak/STAT Pathway. Mol Cell Biol 19:2416–2424.
292. Xu L, Wang W, Li Y, Zhou X, Yin Y, Wang Y, de Man RA, van der Laan LJW, Huang F, Kamar N, Peppelenbosch MP, Pan Q. 2017. RIG-I is a key antiviral interferon-stimulated gene against hepatitis E virus regardless of interferon production. Hepatol Baltim Md 65:1823–1839.
293. Kell AM, Hemann EA, Turnbull JB, Gale M. 2020. RIG-I-like receptor activation drives type I IFN and antiviral signaling to limit Hantaan orthohantavirus replication. PLOS Pathog 16:e1008483.
294. Lind NA, Rael VE, Pestal K, Liu B, Barton GM. 2022. Regulation of the nucleic acid-sensing Toll-like receptors. Nat Rev Immunol 22:224–235.
295. Vähä-Koskela M, Hinkkanen A. 2014. Tumor Restrictions to Oncolytic Virus. Biomedicines 2:163–194.
296. Arulanandam R, Taha Z, Garcia V, Selman M, Chen A, Varette O, Jirovec A, Sutherland K, Macdonald E, Tzelepis F, Birdi H, Alluqmani N, Landry A, Bergeron A, Vanderhyden B, Diallo J-S. 2020. The strategic combination of trastuzumab emtansine with oncolytic rhabdoviruses leads to therapeutic synergy. Commun Biol 3:254.
297. Li Q, Tan F, Wang Y, Liu X, Kong X, Meng J, Yang L, Cen S. 2022. The gamble between oncolytic virus therapy and IFN. Front Immunol 13:971674.
298. Dold C, Rodriguez Urbiola C, Wollmann G, Egerer L, Muik A, Bellmann L, Fiegl H, Marth C, Kimpel J, Von Laer D. 2016. Application of interferon modulators to overcome partial resistance of human ovarian cancers to VSV-GP oncolytic viral therapy. Mol Ther - Oncolytics 3:16021.
299. Adair RA, Scott KJ, Fraser S, Errington-Mais F, Pandha H, Coffey M, Selby P, Cook GP, Vile R, Harrington KJ, Toogood G, Melcher AA. 2013. Cytotoxic and immune-mediated killing of human colorectal cancer by reovirus-loaded blood and liver mononuclear cells. Int J Cancer 132:2327–2338.

300. Santos MR, Xavier PLP, Pires PRL, Rochetti AL, Rosim DF, Scagion GP, De Campos Zuccari DAP, Munir M, Ferreira HL, Fukumasu H. 2021. Oncolytic effect of Newcastle disease virus is attributed to interferon regulation in canine mammary cancer cell lines. Vet Comp Oncol 19:593–601.
301. Gao Y, Bergman I. 2018. Potent Antitumor T-Cell Memory Is Generated by Curative Viral Oncolytic Immunotherapy But Not Curative Chemotherapy. Anticancer Res 38:6621–6629.
302. Bommareddy PK, Shettigar M, Kaufman HL. 2018. Integrating oncolytic viruses in combination cancer immunotherapy. Nat Rev Immunol 18:498–513.
303. Knight A, Karapetyan L, Kirkwood JM. 2023. Immunotherapy in Melanoma: Recent Advances and Future Directions. Cancers 15:1106.
304. Kaufman HL, Shalhout SZ, Iodice G. 2022. Talimogene Laherparepvec: Moving From First-In-Class to Best-In-Class. Front Mol Biosci 9:834841.
305. Moglan AM, Albaradie OA, Alsayegh FF, Alharbi HM, Samman YM, Jalal MM, Saeedi NH, Mahmoud AB, Alkayyal AA. 2023. Preclinical efficacy of oncolytic VSV-IFNβ in treating cancer: A systematic review. Front Immunol 14:1085940.
306. Subramanya S, Armant M, Salkowitz JR, Nyakeriga AM, Haridas V, Hasan M, Bansal A, Goepfert PA, Wynn KK, Ladell K, Price DA, Manjunath N, Kan-Mitchell J, Shankar P. 2010. Enhanced Induction of HIV-specific Cytotoxic T Lymphocytes by Dendritic Cell-targeted Delivery of SOCS-1 siRNA. Mol Ther 18:2028–2037.
307. Fire A, Xu S, Montgomery MK, Kostas SA, Driver SE, Mello CC. 1998. Potent and specific genetic interference by double-stranded RNA in Caenorhabditis elegans. Nature 391:806–811.
308. Montgomery MK. 2004. RNA Interference, p. 3–21. *In* Gott, JM (ed.), RNA Interference, Editing, and Modification. Humana Press, Totowa, NJ.
309. Stram Y, Kuzntzova L. 2006. Inhibition of Viruses by RNA Interference. Virus Genes 32:299–306.
310. Elbashir SM, Harborth J, Lendeckel W, Yalcin A, Weber K, Tuschl T. 2001. Duplexes of 21-nucleotide RNAs mediate RNA interference in cultured mammalian cells. Nature 411:494–498.

311. Taxman DJ, Moore CB, Guthrie EH, Huang MT-H. 2010. Short Hairpin RNA (shRNA): Design, Delivery, and Assessment of Gene Knockdown, p. 139–156. *In* Sioud, M (ed.), RNA Therapeutics. Humana Press, Totowa, NJ.
312. Rao DD, Vorhies JS, Senzer N, Nemunaitis J. 2009. siRNA vs. shRNA: Similarities and differences. Adv Drug Deliv Rev 61:746–759.
313. McAnuff MA, Rettig GR, Rice KG. 2007. Potency of siRNA versus shRNA mediated knockdown in vivo. J Pharm Sci 96:2922–2930.
314. Lam JKW, Chow MYT, Zhang Y, Leung SWS. 2015. siRNA Versus miRNA as Therapeutics for Gene Silencing. Mol Ther - Nucleic Acids 4:e252.
315. Fernandes LGV, Guaman LP, Vasconcellos SA, Heinemann MB, Picardeau M, Nascimento ALTO. 2019. Gene silencing based on RNA-guided catalytically inactive Cas9 (dCas9): a new tool for genetic engineering in Leptospira. Sci Rep 9:1839.
316. Ouyang JPT, Folkmann A, Bernard L, Lee C-Y, Seroussi U, Charlesworth AG, Claycomb JM, Seydoux G. 2019. P Granules Protect RNA Interference Genes from Silencing by piRNAs. Dev Cell 50:716-728.e6.
317. Hoy SM. 2018. Patisiran: First Global Approval. Drugs 78:1625–1631.
318. Zhang MM, Bahal R, Rasmussen TP, Manautou JE, Zhong X. 2021. The growth of siRNA-based therapeutics: Updated clinical studies. Biochem Pharmacol 189:114432.
319. Ahmadzada T, Reid G, McKenzie DR. 2018. Fundamentals of siRNA and miRNA therapeutics and a review of targeted nanoparticle delivery systems in breast cancer. Biophys Rev 10:69–86.
320. Li CX, Parker A, Menocal E, Xiang S, Borodyansky L, Fruehauf JH. 2006. Delivery of RNA Interference. Cell Cycle 5:2103–2109.
321. Song E, Zhu P, Lee S-K, Chowdhury D, Kussman S, Dykxhoorn DM, Feng Y, Palliser D, Weiner DB, Shankar P, Marasco WA, Lieberman J. 2005. Antibody mediated in vivo delivery of small interfering RNAs via cell-surface receptors. Nat Biotechnol 23:709–717.
322. Hamblett KJ, Senter PD, Chace DF, Sun MMC, Lenox J, Cerveny CG, Kissler KM, Bernhardt SX, Kopcha AK, Zabinski RF, Meyer DL, Francisco JA. 2004. Effects of Drug Loading on the Antitumor Activity of a Monoclonal Antibody Drug Conjugate. Clin Cancer Res 10:7063–7070.

323. Lorenzer C, Dirin M, Winkler A-M, Baumann V, Winkler J. 2015. Going beyond the liver: Progress and challenges of targeted delivery of siRNA therapeutics. J Controlled Release 203:1–15.
324. Bulcha JT, Wang Y, Ma H, Tai PWL, Gao G. 2021. Viral vector platforms within the gene therapy landscape. Signal Transduct Target Ther 6:53.
325. Schaffer DV, Koerber JT, Lim K. 2008. Molecular Engineering of Viral Gene Delivery Vehicles. Annu Rev Biomed Eng 10:169–194.
326. Kim M, Williamson CT, Prudhomme J, Bebb DG, Riabowol K, Lee PWK, Lees-Miller SP, Mori Y, Rahman MM, McFadden G, Johnston RN. 2010. The viral tropism of two distinct oncolytic viruses, reovirus and myxoma virus, is modulated by cellular tumor suppressor gene status. Oncogene 29:3990–3996.
327. MacKenzie TC, Kobinger GP, Kootstra NA, Radu A, Sena-Esteves M, Bouchard S, Wilson JM, Verma IM, Flake AW. 2002. Efficient Transduction of Liver and Muscle after in Utero Injection of Lentiviral Vectors with Different Pseudotypes. Mol Ther 6:349–358.
328. Ungerechts G, Bossow S, Leuchs B, Holm PS, Rommelaere J, Coffey M, Coffin R, Bell J, Nettelbeck DM. 2016. Moving oncolytic viruses into the clinic: clinical-grade production, purification, and characterization of diverse oncolytic viruses. Mol Ther - Methods Clin Dev 3:16018.
329. Zhao Z, Anselmo AC, Mitragotri S. 2022. Viral vector-based gene therapies in the clinic. Bioeng Transl Med 7.
330. Rouha H, Thurner C, Mandl CW. 2010. Functional microRNA generated from a cytoplasmic RNA virus. Nucleic Acids Res 38:8328–8337.
331. Pijlman GP, Suhrbier A, Khromykh AA. 2006. Kunjin virus replicons: an RNA-based, non-cytopathic viral vector system for protein production, vaccine and gene therapy applications. Expert Opin Biol Ther 6:135–145.
332. Vargas JE, Chicaybam L, Stein RT, Tanuri A, Delgado-Cañedo A, Bonamino MH. 2016. Retroviral vectors and transposons for stable gene therapy: advances, current challenges and perspectives. J Transl Med 14:288.

333. Cunningham AP, Andrews LG, Tollefsbol TO. 2007. Retrovirus-Mediated RNA Interference, p. 39–46. *In* Andrews, LG, Tollefsbol, TO (eds.), Telomerase Inhibition. Humana Press, Totowa, NJ.

334. Brummelkamp TR, Bernards R, Agami R. 2002. A System for Stable Expression of Short Interfering RNAs in Mammalian Cells. Science 296:550–553.

335. Yu SS, Han E, Hong Y, Lee J-T, Kim S, Kim S. 2003. Construction of a retroviral vector production system with the minimum possibility of a homologous recombination. Gene Ther 10:706–711.

336. Zufferey R, Dull T, Mandel RJ, Bukovsky A, Quiroz D, Naldini L, Trono D. 1998. Self-Inactivating Lentivirus Vector for Safe and Efficient In Vivo Gene Delivery. J Virol 72:9873–9880.

337. Cavazza A, Cocchiarella F, Bartholomae C, Schmidt M, Pincelli C, Larcher F, Mavilio F. 2013. Self-inactivating MLV vectors have a reduced genotoxic profile in human epidermal keratinocytes. Gene Ther 20:949–957.

338. Raoul C, Abbas-Terki T, Bensadoun J-C, Guillot S, Haase G, Szulc J, Henderson CE, Aebischer P. 2005. Lentiviral-mediated silencing of SOD1 through RNA interference retards disease onset and progression in a mouse model of ALS. Nat Med 11:423–428.

339. Drouet V, Ruiz M, Zala D, Feyeux M, Auregan G, Cambon K, Troquier L, Carpentier J, Aubert S, Merienne N, Bourgois-Rocha F, Hassig R, Rey M, Dufour N, Saudou F, Perrier AL, Hantraye P, Déglon N. 2014. Allele-Specific Silencing of Mutant Huntingtin in Rodent Brain and Human Stem Cells. PLoS ONE 9:e99341.

340. Sapru MK, Yates JW, Hogan S, Jiang L, Halter J, Bohn MC. 2006. Silencing of human α-synuclein in vitro and in rat brain using lentiviral-mediated RNAi. Exp Neurol 198:382–390.

341. Horvath L, van Marion I, Taï K, Nielsen TT, Lundberg C. 2011. Knockdown of GAD67 protein levels normalizes neuronal activity in a rat model of Parkinson's disease. J Gene Med 13:188–197.

342. Singer O, Marr RA, Rockenstein E, Crews L, Coufal NG, Gage FH, Verma IM, Masliah E. 2005. Targeting BACE1 with siRNAs ameliorates Alzheimer disease neuropathology in a transgenic model. Nat Neurosci 8:1343–1349.

343. Piedrahita D, Hernandez I, Lopez-Tobon A, Fedorov D, Obara B, Manjunath BS, Boudreau RL, Davidson B, LaFerla F, Gallego-Gomez JC, Kosik KS, Cardona-Gomez GP. 2010. Silencing of CDK5 Reduces Neurofibrillary Tangles in Transgenic Alzheimer's Mice. J Neurosci 30:13966–13976.

344. Pfeifer A, Eigenbrod S, Al-Khadra S, Hofmann A, Mitteregger G, Moser M, Bertsch U, Kretzschmar H. 2006. Lentivector-mediated RNAi efficiently suppresses prion protein and prolongs survival of scrapie-infected mice. J Clin Invest 116:3204–3210.

345. White MD, Farmer M, Mirabile I, Brandner S, Collinge J, Mallucci GR. 2008. Single treatment with RNAi against prion protein rescues early neuronal dysfunction and prolongs survival in mice with prion disease. Proc Natl Acad Sci 105:10238–10243.

346. Zhou H-X, Li X-Y, Li F-Y, Liu C, Liang Z-P, Liu S, Zhang B, Wang T-Y, Chu T-C, Lu L, Ning G-Z, Kong X-H, Feng S-Q. 2014. Targeting RPTPσ with lentiviral shRNA promotes neurites outgrowth of cortical neurons and improves functional recovery in a rat spinal cord contusion model. Brain Res 1586:46–63.

347. DiGiusto DL, Krishnan A, Li L, Li H, Li S, Rao A, Mi S, Yam P, Stinson S, Kalos M, Alvarnas J, Lacey SF, Yee J-K, Li M, Couture L, Hsu D, Forman SJ, Rossi JJ, Zaia JA. 2010. RNA-Based Gene Therapy for HIV with Lentiviral Vector–Modified CD34 $^{+}$ Cells in Patients Undergoing Transplantation for AIDS-Related Lymphoma. Sci Transl Med 2.

348. Anderson J, Li M-J, Palmer B, Remling L, Li S, Yam P, Yee J-K, Rossi J, Zaia J, Akkina R. 2007. Safety and Efficacy of a Lentiviral Vector Containing Three Anti-HIV Genes—CCR5 Ribozyme, Tat-rev siRNA, and TAR Decoy—in SCID-hu Mouse–Derived T Cells. Mol Ther 15:1182–1188.

349. Li M, Rossi JJ. 2005. Lentiviral Vector Delivery of siRNA and shRNA Encoding Genes into Cultured and Primary Hematopoietic Cells, p. 261–272. *In* RNA Silencing. Humana Press, New Jersey.

350. Banerjea A, Li M-J, Bauer G, Remling L, Lee N-S, Rossi J, Akkina R. 2003. Inhibition of HIV-1 by lentiviral vector-transduced siRNAs in T lymphocytes differentiated in SCID-hu mice and CD34+ progenitor cell-derived macrophages. Mol Ther 8:62–71.

351. Li M-J, Kim J, Li S, Zaia J, Yee J-K, Anderson J, Akkina R, Rossi JJ. 2005. Long-Term Inhibition of HIV-1 Infection in Primary Hematopoietic Cells by Lentiviral Vector

Delivery of a Triple Combination of Anti-HIV shRNA, Anti-CCR5 Ribozyme, and a Nucleolar-Localizing TAR Decoy. Mol Ther 12:900–909.

352. Anderson J, Akkina R. 2005. CXCR4 and CCR5 shRNA transgenic CD34+ cell derived macrophages are functionally normal and resist HIV-1 infection. Retrovirology 2:53.
353. An DS, Donahue RE, Kamata M, Poon B, Metzger M, Mao S-H, Bonifacino A, Krouse AE, Darlix J-L, Baltimore D, Qin FX-F, Chen ISY. 2007. Stable reduction of CCR5 by RNAi through hematopoietic stem cell transplant in non-human primates. Proc Natl Acad Sci 104:13110–13115.
354. Barclay SL, Yang Y, Zhang S, Fong R, Barraza A, Nolta JA, Torbett BE, Abedi M, Bauer G, Anderson JS. 2015. Safety and Efficacy of a tCD25 Preselective Combination Anti-HIV Lentiviral Vector in Human Hematopoietic Stem and Progenitor Cells. Stem Cells 33:870–879.
355. Kumar P, Lee SK, Shankar P, Manjunath N. 2006. A Single siRNA Suppresses Fatal Encephalitis Induced by Two Different Flaviviruses. PLoS Med 3:e96.
356. Kumar P, Wu H, McBride JL, Jung K-E, Hee Kim M, Davidson BL, Kyung Lee S, Shankar P, Manjunath N. 2007. Transvascular delivery of small interfering RNA to the central nervous system. Nature 448:39–43.
357. Kim Y-J, Ahn J, Jeung S-Y, Kim D-S, Na H-N, Cho Y-J, Yun S-H, Jee Y, Jeon E-S, Lee H, Nam J-H. 2008. Recombinant lentivirus-delivered short hairpin RNAs targeted to conserved coxsackievirus sequences protect against viral myocarditis and improve survival rate in an animal model. Virus Genes 36:141–146.
358. Gu W, Putral L, Hengst K, Minto K, Saunders NA, Leggatt G, McMillan NAJ. 2006. Inhibition of cervical cancer cell growth in vitro and in vivo with lentiviral-vector delivered short hairpin RNA targeting human papillomavirus E6 and E7 oncogenes. Cancer Gene Ther 13:1023–1032.
359. Zhou J, Li B, Peng C, Wang F, Fu Z, Zhou C, Hong D, Ye F, Lü W, Xie X. 2013. Inhibition of cervical cancer cell growth in vitro and in vivo by lentiviral-vector mediated shRNA targeting the common promoter of HPV16 E6 and E7 oncogenes. Antiviral Res 98:305–313.
360. Dittgen T, Nimmerjahn A, Komai S, Licznerski P, Waters J, Margrie TW, Helmchen F, Denk W, Brecht M, Osten P. 2004. Lentivirus-based genetic manipulations of cortical

neurons and their optical and electrophysiological monitoring *in vivo*. Proc Natl Acad Sci 101:18206–18211.

361. Morris KV, Rossi JJ. 2006. Lentiviral-mediated delivery of siRNAs for antiviral therapy. Gene Ther 13:553–558.
362. Burns JC, Friedmann T, Driever W, Burrascano M, Yee JK. 1993. Vesicular stomatitis virus G glycoprotein pseudotyped retroviral vectors: concentration to very high titer and efficient gene transfer into mammalian and nonmammalian cells. Proc Natl Acad Sci 90:8033–8037.
363. Finkelshtein D, Werman A, Novick D, Barak S, Rubinstein M. 2013. LDL receptor and its family members serve as the cellular receptors for vesicular stomatitis virus. Proc Natl Acad Sci 110:7306–7311.
364. Cronin J, Zhang X-Y, Reiser J. 2005. Altering the Tropism of Lentiviral Vectors through Pseudotyping. Curr Gene Ther 5:387–398.
365. Lei Y, Joo K-I, Zarzar J, Wong C, Wang P. 2010. Targeting lentiviral vector to specific cell types through surface displayed single chain antibody and fusogenic molecule. Virol J 7:35.
366. Jiang A, Chu T-HT, Nocken F, Cichutek K, Dornburg R. 1998. Cell-Type-Specific Gene Transfer into Human Cells with Retroviral Vectors That Display Single-Chain Antibodies. J Virol 72:10148–10156.
367. Jiang A, Dornburg R, Dornburg R. 1999. In vivo cell type-specific gene delivery with retroviral vectors that display single chain antibodies. Gene Ther 6:1982–1987.
368. Bupp K, Roth MJ. 2002. Altering Retroviral Tropism Using a Random-Display Envelope Library. Mol Ther 5:329–335.
369. Szécsi J, Drury R, Josserand V, Grange M-P, Boson B, Hartl I, Schneider R, Buchholz CJ, Coll J-L, Russell SJ, Cosset F-L, Verhoeyen E. 2006. Targeted retroviral vectors displaying a cleavage site-engineered hemagglutinin (HA) through HA–protease interactions. Mol Ther 14:735–744.
370. Duerner LJ, Schwantes A, Schneider IC, Cichutek K, Buchholz CJ. 2008. Cell entry targeting restricts biodistribution of replication-competent retroviruses to tumour tissue. Gene Ther 15:1500–1510.

371. Seamon JA, Jones KS, Miller C, Roth MJ. 2002. Inserting a Nuclear Targeting Signal into a Replication-Competent Moloney Murine Leukemia Virus Affects Viral Export and Is Not Sufficient for Cell Cycle-Independent Infection. J Virol 76:8475–8484.
372. Roe T, Reynolds TC, Yu G, Brown PO. 1993. Integration of murine leukemia virus DNA depends on mitosis. EMBO J 12:2099–2108.
373. Lewis PF, Emerman M. 1994. Passage through mitosis is required for oncoretroviruses but not for the human immunodeficiency virus. J Virol 68:510–516.
374. Kawasaki Y, Tamamoto A, Takagi-Kimura M, Maeyama Y, Yamaoka N, Terada N, Okamura H, Kasahara N, Kubo S. 2011. Replication-competent retrovirus vector-mediated prodrug activator gene therapy in experimental models of human malignant mesothelioma. Cancer Gene Ther 18:571–578.
375. Logg CR, Tai C-K, Logg A, Anderson WF, Kasahara N. 2001. A Uniquely Stable Replication-Competent Retrovirus Vector Achieves Efficient Gene Delivery *in Vitro* and in Solid Tumors. Hum Gene Ther 12:921–932.
376. Hiraoka K, Kimura T, Logg CR, Tai C-K, Haga K, Lawson GW, Kasahara N. 2007. Therapeutic Efficacy of Replication-Competent Retrovirus Vector–Mediated Suicide Gene Therapy in a Multifocal Colorectal Cancer Metastasis Model. Cancer Res 67:5345–5353.
377. Tai C-K. 2012. Replicating retroviral vectors for oncolytic virotherapy of experimental hepatocellular carcinoma. Oncol Rep https://doi.org/10.3892/or.2012.1789.
378. Tai C-K, Wang WJ, Chen TC, Kasahara N. 2005. Single-Shot, Multicycle Suicide Gene Therapy by Replication-Competent Retrovirus Vectors Achieves Long-Term Survival Benefit in Experimental Glioma. Mol Ther 12:842–851.
379. Wang WJ, Tai C-K, Kasahara N, Chen TC. 2003. Highly Efficient and Tumor-Restricted Gene Transfer to Malignant Gliomas by Replication-Competent Retroviral Vectors. Hum Gene Ther 14:117–127.
380. Logg CR, Robbins JM, Jolly DJ, Gruber HE, Kasahara N. 2012. Retroviral Replicating Vectors in Cancer, p. 199–228. *In* Methods in Enzymology. Elsevier.
381. Athanasopoulos T, Munye MM, Yáñez-Muñoz RJ. 2017. Nonintegrating Gene Therapy Vectors. Hematol Oncol Clin North Am 31:753–770.

382. Uren AG, Kool J, Berns A, van Lohuizen M. 2005. Retroviral insertional mutagenesis: past, present and future. Oncogene 24:7656–7672.
383. Patel K, Kilfoil G, Wyles DL, Naggie S, Lawitz E, Bradley S, Lindell P, Suhy D. 2016. Phase I/IIa Study of TT-034, a DNA-Directed RNA Interference (ddRNAi) Agent Delivered as a Single Administration for the Treatment of Subjects with Chronic Hepatitis C Virus (HCV). Mol Ther 24:S102.
384. Zhang Y-A, Nemunaitis J, Samuel SK, Chen P, Shen Y, Tong AW. 2006. Antitumor Activity of an Oncolytic Adenovirus-Delivered Oncogene Small Interfering RNA. Cancer Res 66:9736–9743.
385. Saydam O, Glauser DL, Heid I, Turkeri G, Hilbe M, Jacobs AH, Ackermann M, Fraefel C. 2005. Herpes Simplex Virus 1 Amplicon Vector-Mediated siRNA Targeting Epidermal Growth Factor Receptor Inhibits Growth of Human Glioma Cells in Vivo. Mol Ther 12:803–812.
386. Hu JCC, Coffin RS. 2003. Gene Therapy with Virus Vectors for specific Disease of the Nervous System, p. 165–184. *In* International Review of Neurobiology. Elsevier.
387. Post D, Fulci G, Chiocca E, Van Meir E. 2004. Replicative Oncolytic Herpes Simplex Viruses in Combination Cancer Therapies. Curr Gene Ther 4:41–51.
388. Grandi P. 2004. Targeting HSV amplicon vectors. Methods 33:179–186.
389. Grandi P, Wang S, Schuback D, Krasnykh V, Spear M, Curiel DT, Manservigi R, Breakefield XO. 2004. HSV-1 Virions Engineered for Specific Binding to Cell Surface Receptors. Mol Ther 9:419–427.
390. Sabbioni S, Callegari E, Manservigi M, Argnani R, Corallini A, Negrini M, Manservigi R. 2007. Use of herpes simplex virus type 1-based amplicon vector for delivery of small interfering RNA. Gene Ther 14:459–464.
391. Lee CS, Bishop ES, Zhang R, Yu X, Farina EM, Yan S, Zhao C, Zeng Z, Shu Y, Wu X, Lei J, Li Y, Zhang W, Yang C, Wu K, Wu Y, Ho S, Athiviraham A, Lee MJ, Wolf JM, Reid RR, He T-C. 2017. Adenovirus-mediated gene delivery: Potential applications for gene and cell-based therapies in the new era of personalized medicine. Genes Dis 4:43–63.

392. Narvaiza I, Aparicio O, Vera M, Razquin N, Bortolanza S, Prieto J, Fortes P. 2006. Effect of Adenovirus-Mediated RNA Interference on Endogenous MicroRNAs in a Mouse Model of Multidrug Resistance Protein 2 Gene Silencing. J Virol 80:12236–12247.
393. Carette JE, Overmeer RM, Schagen FHE, Alemany R, Barski OA, Gerritsen WR, van Beusechem VW. 2004. Conditionally Replicating Adenoviruses Expressing Short Hairpin RNAs Silence the Expression of a Target Gene in Cancer Cells. Cancer Res 64:2663–2667.
394. Doloff JC, Waxman DJ, Jounaidi Y. 2008. Human Telomerase Reverse Transcriptase Promoter-Driven Oncolytic Adenovirus with E1B-19 kDa and E1B-55 kDa Gene Deletions. Hum Gene Ther 19:1383–1399.
395. Zhang J, Ramesh N, Chen Y, Li Y, Dilley J, Working P, Yu D-C. 2002. Identification of human uroplakin II promoter and its use in the construction of CG8840, a urothelium-specific adenovirus variant that eliminates established bladder tumors in combination with docetaxel. Cancer Res 62:3743–3750.
396. Tanimoto T, Tazawa H, Ieda T, Nouso H, Tani M, Oyama T, Urata Y, Kagawa S, Noda T, Fujiwara T. 2020. Elimination of MYCN-Amplified Neuroblastoma Cells by Telomerase-Targeted Oncolytic Virus via MYCN Suppression. Mol Ther Oncolytics 18:14–23.
397. Mao L, Zhang J, Liu N, Fan L, Yang D, Xue B, Shan Y, Zheng J. 2015. Oncolytic virus carrying shRNA targeting SATB1 inhibits prostate cancer growth and metastasis. Tumor Biol 36:9073–9081.
398. Yoo JY, Kim J-H, Kim J, Huang J-H, Zhang SN, Kang Y-A, Kim H, Yun C-O. 2008. Short hairpin RNA-expressing oncolytic adenovirus-mediated inhibition of IL-8: effects on antiangiogenesis and tumor growth inhibition. Gene Ther 15:635–651.
399. Luo Q, Basnet S, Dai Z, Li S, Zhang Z, Ge H. 2016. A novel E1B55kDa-deleted oncolytic adenovirus carrying microRNA-143 exerts specific antitumor efficacy on colorectal cancer cells. Am J Transl Res 8:3822–3830.
400. Li Y, Zhang B, Zhang H, Zhu X, Feng D, Zhang D, Zhuo B, Li L, Zheng J. 2013. Oncolytic adenovirus armed with shRNA targeting MYCN gene inhibits neuroblastoma cell proliferation and in vivo xenograft tumor growth. J Cancer Res Clin Oncol 139:933–941.

401. Chen J, Yang L, Chen H, Yuan T, Liu M, Chen P. 2014. Recombinant adenovirus encoding FAT10 small interfering RNA inhibits HCC growth in vitro and in vivo. Exp Mol Pathol 96:207–211.
402. Yoo JY, Kim J-H, Kwon Y-G, Kim E-C, Kim NK, Choi HJ, Yun C-O. 2007. VEGF-specific Short Hairpin RNA–expressing Oncolytic Adenovirus Elicits Potent Inhibition of Angiogenesis and Tumor Growth. Mol Ther 15:295–302.
403. Machitani M, Yamaguchi T, Shimizu K, Sakurai F, Katayama K, Kawabata K, Mizuguchi H. 2011. Adenovirus Vector-Derived VA-RNA-Mediated Innate Immune Responses. Pharmaceutics 3:338–353.
404. Sakurai H, Kawabata K, Sakurai F, Nakagawa S, Mizuguchi H. 2008. Innate immune response induced by gene delivery vectors. Int J Pharm 354:9–15.
405. Zhu J, Huang X, Yang Y. 2007. Innate Immune Response to Adenoviral Vectors Is Mediated by both Toll-Like Receptor-Dependent and -Independent Pathways. J Virol 81:3170–3180.
406. Mast TC, Kierstead L, Gupta SB, Nikas AA, Kallas EG, Novitsky V, Mbewe B, Pitisuttithum P, Schechter M, Vardas E, Wolfe ND, Aste-Amezaga M, Casimiro DR, Coplan P, Straus WL, Shiver JW. 2010. International epidemiology of human pre-existing adenovirus (Ad) type-5, type-6, type-26 and type-36 neutralizing antibodies: Correlates of high Ad5 titers and implications for potential HIV vaccine trials. Vaccine 28:950–957.
407. Somanathan S, Breous E, Bell P, Wilson JM. 2010. AAV Vectors Avoid Inflammatory Signals Necessary to Render Transduced Hepatocyte Targets for Destructive T Cells. Mol Ther 18:977–982.
408. Zaiss A-K, Liu Q, Bowen GP, Wong NCW, Bartlett JS, Muruve DA. 2002. Differential Activation of Innate Immune Responses by Adenovirus and Adeno-Associated Virus Vectors. J Virol 76:4580–4590.
409. Wang D, Tai PWL, Gao G. 2019. Adeno-associated virus vector as a platform for gene therapy delivery. Nat Rev Drug Discov 18:358–378.
410. Zhao X, Zhang C, Le Z, Zeng S, Pan C, Shi J, Wang J, Zhao X. 2018. Telomerase reverse transcriptase interference synergistically promotes tumor necrosis factor-related apoptosis-inducing ligand-induced oral squamous cell carcinoma apoptosis and

suppresses proliferation in□vitro and in□vivo. Int J Mol Med https://doi.org/10.3892/ijmm.2018.3721.

411. Bhere D, Tamura K, Wakimoto H, Choi SH, Purow B, Debatisse J, Shah K. 2018. microRNA-7 upregulates death receptor 5 and primes resistant brain tumors to caspase-mediated apoptosis. Neuro-Oncol 20:215–224.
412. Bhere D, Arghiani N, Lechtich ER, Yao Y, Alsaab S, Bei F, Matin MM, Shah K. 2020. Simultaneous downregulation of miR-21 and upregulation of miR-7 has anti-tumor efficacy. Sci Rep 10:1779.
413. Kattenhorn LM, Tipper CH, Stoica L, Geraghty DS, Wright TL, Clark KR, Wadsworth SC. 2016. Adeno-Associated Virus Gene Therapy for Liver Disease. Hum Gene Ther 27:947–961.
414. Xu G, Luo L, Tai PWL, Qin W, Xiao Y, Wang C, Su Q, Ma H, He R, Wei Y, Gao G. 2016. High-Throughput Sequencing of AAV Proviral Libraries from the Human Population Reveals Novel Variants with Unprecedented Intra-and Inter-Tissue Diversity. Mol Ther 24:S4.
415. Wang D, Li S, Gessler DJ, Xie J, Zhong L, Li J, Tran K, Van Vliet K, Ren L, Su Q, He R, Goetzmann JE, Flotte TR, Agbandje-McKenna M, Gao G. 2018. A Rationally Engineered Capsid Variant of AAV9 for Systemic CNS-Directed and Peripheral Tissue-Detargeted Gene Delivery in Neonates. Mol Ther - Methods Clin Dev 9:234–246.
416. Tse LV, Klinc KA, Madigan VJ, Castellanos Rivera RM, Wells LF, Havlik LP, Smith JK, Agbandje-McKenna M, Asokan A. 2017. Structure-guided evolution of antigenically distinct adeno-associated virus variants for immune evasion. Proc Natl Acad Sci 114.
417. Wooley DP, Sharma P, Weinstein JR, Kotha Lakshmi Narayan P, Schaffer DV, Excoffon KJDA. 2017. A directed evolution approach to select for novel Adeno-associated virus capsids on an HIV-1 producer T cell line. J Virol Methods 250:47–54.
418. Deverman BE, Pravdo PL, Simpson BP, Kumar SR, Chan KY, Banerjee A, Wu W-L, Yang B, Huber N, Pasca SP, Gradinaru V. 2016. Cre-dependent selection yields AAV variants for widespread gene transfer to the adult brain. Nat Biotechnol 34:204–209.
419. Usme-Ciro JA, Campillo-Pedroza N, Almazán F, Gallego-Gomez JC. 2013. Cytoplasmic RNA viruses as potential vehicles for the delivery of therapeutic small RNAs. Virol J 10:185.

420. Hastie E, Grdzelishvili VZ. 2012. Vesicular stomatitis virus as a flexible platform for oncolytic virotherapy against cancer. J Gen Virol 93:2529–2545.
421. Lundstrom K. 2017. Oncolytic Alphaviruses in Cancer Immunotherapy. Vaccines 5:9.
422. Shapiro JS, Schmid S, Aguado LC, Sabin LR, Yasunaga A, Shim JV, Sachs D, Cherry S, tenOever BR. 2014. Drosha as an interferon-independent antiviral factor. Proc Natl Acad Sci 111:7108–7113.
423. Hussain M, Torres S, Schnettler E, Funk A, Grundhoff A, Pijlman GP, Khromykh AA, Asgari S. 2012. West Nile virus encodes a microRNA-like small RNA in the 3' untranslated region which up-regulates GATA4 mRNA and facilitates virus replication in mosquito cells. Nucleic Acids Res 40:2210–2223.
424. Parameswaran P, Sklan E, Wilkins C, Burgon T, Samuel MA, Lu R, Ansel KM, Heissmeyer V, Einav S, Jackson W, Doukas T, Paranjape S, Polacek C, dos Santos FB, Jalili R, Babrzadeh F, Gharizadeh B, Grimm D, Kay M, Koike S, Sarnow P, Ronaghi M, Ding S-W, Harris E, Chow M, Diamond MS, Kirkegaard K, Glenn JS, Fire AZ. 2010. Six RNA Viruses and Forty-One Hosts: Viral Small RNAs and Modulation of Small RNA Repertoires in Vertebrate and Invertebrate Systems. PLoS Pathog 6:e1000764.
425. Shapiro JS, Varble A, Pham AM, tenOever BR. 2010. Noncanonical cytoplasmic processing of viral microRNAs. RNA 16:2068–2074.
426. Langlois RA, Shapiro JS, Pham AM, tenOever BR. 2012. In Vivo Delivery of Cytoplasmic RNA Virus-derived miRNAs. Mol Ther 20:367–375.
427. tenOever BR. 2013. RNA viruses and the host microRNA machinery. Nat Rev Microbiol 11:169–180.
428. Wedge M-E, Jennings VA, Crupi MJF, Poutou J, Jamieson T, Pelin A, Pugliese G, de Souza CT, Petryk J, Laight BJ, Boileau M, Taha Z, Alluqmani N, McKay HE, Pikor L, Khan ST, Azad T, Rezaei R, Austin B, He X, Mansfield D, Rose E, Brown EEF, Crawford N, Alkayyal A, Surendran A, Singaravelu R, Roy DG, Migneco G, McSweeney B, Cottee ML, Jacobus EJ, Keller BA, Yamaguchi TN, Boutros PC, Geoffrion M, Rayner KJ, Chatterjee A, Auer RC, Diallo J-S, Gibbings D, tenOever BR, Melcher A, Bell JC, Ilkow CS. 2022. Virally programmed extracellular vesicles sensitize cancer cells to oncolytic virus and small molecule therapy. Nat Commun 13:1898.
429. Danial NN, Korsmeyer SJ. 2004. Cell Death. Cell 116:205–219.

430. Yin L, Keeler GD, Zhang Y, Hoffman BE, Ling C, Qing K, Srivastava A. 2021. AAV3-miRNA vectors for growth suppression of human hepatocellular carcinoma cells in vitro and human liver tumors in a murine xenograft model in vivo. Gene Ther 28:422–434.
431. Lou W, Chen Q, Ma L, Liu J, Yang Z, Shen J, Cui Y, Bian X, Qian C. 2013. Oncolytic adenovirus co-expressing miRNA-34a and IL-24 induces superior antitumor activity in experimental tumor model. J Mol Med 91:715–725.
432. Luo Q, Song H, Deng X, Li J, Jian W, Zhao J, Zheng X, Basnet S, Ge H, Daniel T, Xu B, Fang L. 2020. A Triple-Regulated Oncolytic Adenovirus Carrying MicroRNA-143 Exhibits Potent Antitumor Efficacy in Colorectal Cancer. Mol Ther - Oncolytics 16:219–229.
433. Mu Y, Wang Q, Tan L, Lin L, Zhang B. 2020. microRNA-144 inhibits cell proliferation and invasion by directly targeting TIGAR in esophageal carcinoma. Oncol Lett 19:3079–3088.
434. Kota J, Chivukula RR, O'Donnell KA, Wentzel EA, Montgomery CL, Hwang H-W, Chang T-C, Vivekanandan P, Torbenson M, Clark KR, Mendell JR, Mendell JT. 2009. Therapeutic microRNA Delivery Suppresses Tumorigenesis in a Murine Liver Cancer Model. Cell 137:1005–1017.
435. Lin L, Wang D, Qu S, Zhao H, Lin Y. 2020. miR-370-3p Alleviates Ulcerative Colitis-Related Colorectal Cancer in Mice Through Inhibiting the Inflammatory Response and Epithelial-Mesenchymal Transition. Drug Des Devel Ther Volume 14:1127–1141.
436. Nordentoft I, Birkenkamp-Demtroder K, Agerbæk M, Theodorescu D, Ostenfeld MS, Hartmann A, Borre M, Ørntoft TF, Dyrskjøt L. 2012. miRNAs associated with chemo-sensitivity in cell lines and in advanced bladder cancer. BMC Med Genomics 5:40.
437. Ma D, Qin M, Shi L, Ding X. 2019. MicroRNA-6077 enhances the sensitivity of patients-derived lung adenocarcinoma cells to anlotinib by repressing the activation of glucose transporter 1 pathway. Cell Signal 64:109391.
438. Robert C. 2020. A decade of immune-checkpoint inhibitors in cancer therapy. Nat Commun 11:3801.
439. Jenkins RW, Barbie DA, Flaherty KT. 2018. Mechanisms of resistance to immune checkpoint inhibitors. Br J Cancer 118:9–16.

440. Wang G, Kang X, Chen KS, Jehng T, Jones L, Chen J, Huang XF, Chen S-Y. 2020. An engineered oncolytic virus expressing PD-L1 inhibitors activates tumor neoantigen-specific T cell responses. Nat Commun 11:1395.
441. Hamilton JR, Vijayakumar G, Palese P. 2018. A Recombinant Antibody-Expressing Influenza Virus Delays Tumor Growth in a Mouse Model. Cell Rep 22:1–7.
442. Vijayakumar G, McCroskery S, Palese P. 2020. Engineering Newcastle Disease Virus as an Oncolytic Vector for Intratumoral Delivery of Immune Checkpoint Inhibitors and Immunocytokines. J Virol 94.
443. Zheng X, Koropatnick J, Li M, Zhang X, Ling F, Ren X, Hao X, Sun H, Vladau C, Franek JA, Feng B, Urquhart BL, Zhong R, Freeman DJ, Garcia B, Min W-P. 2006. Reinstalling Antitumor Immunity by Inhibiting Tumor-Derived Immunosuppressive Molecule IDO through RNA Interference. J Immunol 177:5639–5646.
444. Kim JH, Kang TH, Noh KH, Bae HC, Ahn Y-H, Lee Y-H, Choi EY, Chun K-H, Lee S-J, Kim TW. 2011. Blocking the immunosuppressive axis with small interfering RNA targeting interleukin (IL)-10 receptor enhances dendritic cell-based vaccine potency: IL-10 receptor siRNA enhances DC-based vaccine potency. Clin Exp Immunol 165:180–189.
445. Sondka Z, Bamford S, Cole CG, Ward SA, Dunham I, Forbes SA. 2018. The COSMIC Cancer Gene Census: describing genetic dysfunction across all human cancers. Nat Rev Cancer 18:696–705.
446. Li Y, Zhang H, Zhu X, Feng D, Zhang D, Zhuo B, Zheng J. 2015. Oncolytic adenovirus-mediated short hairpin RNA targeting MYCN gene induces apoptosis by upregulating RKIP in neuroblastoma. Tumor Biol 36:6037–6043.
447. Uehara N, Otsuki N, Kubo M, Kitamoto J, Kojima Y, Teshima M, Shinomiya H, Shirakawa T, Nibu K. 2020. Oncolytic effect of Midkine promoter–based conditionally replicating adenoviruses expressing EGFR siRNA in head and neck squamous cancer cell line T891. Cancer Rep 3.
448. Sun A, Tang J, Terranova PF, Zhang X, Thrasher JB, Li B. 2010. Adeno-associated virus–delivered short hairpin-structured RNA for androgen receptor gene silencing induces tumor eradication of prostate cancer xenografts in nude mice: A preclinical study. Int J Cancer 126:764–774.

449. Shen W, Wang C-Y, Wang X-H, Fu Z-X. 2009. Oncolytic adenovirus mediated Survivin knockdown by RNA interference suppresses human colorectal carcinoma growth in vitro and in vivo. J Exp Clin Cancer Res 28:81.
450. Han Z, Lee S, Je S, Eom C-Y, Choi HJ, Song JJ, Kim J-H. 2016. Survivin silencing and TRAIL expression using oncolytic adenovirus increase anti-tumorigenic activity in gemcitabine-resistant pancreatic cancer cells. Apoptosis 21:351–364.
451. Ye H, Zhang X, Chen Y, Liu Q, Wei J. 2016. Ranking novel cancer driving synthetic lethal gene pairs using TCGA data. Oncotarget 7:55352–55367.
452. Chan SM, Thomas D, Corces-Zimmerman MR, Xavy S, Rastogi S, Hong W-J, Zhao F, Medeiros BC, Tyvoll DA, Majeti R. 2015. Isocitrate dehydrogenase 1 and 2 mutations induce BCL-2 dependence in acute myeloid leukemia. Nat Med 21:178–184.
453. Rovira-Rigau M, Raimondi G, Marín MÁ, Gironella M, Alemany R, Fillat C. 2019. Bioselection Reveals miR-99b and miR-485 as Enhancers of Adenoviral Oncolysis in Pancreatic Cancer. Mol Ther 27:230–243.
454. Chen X, Zhou Y, Wang J, Wang J, Yang J, Zhai Y, Li B. 2015. Dual silencing of Bcl-2 and Survivin by HSV-1 vector shows better antitumor efficacy in higher PKR phosphorylation tumor cells in vitro and in vivo. Cancer Gene Ther 22:380–386.
455. Yamakuchi M, Ferlito M, Lowenstein CJ. 2008. miR-34a repression of SIRT1 regulates apoptosis. Proc Natl Acad Sci 105:13421–13426.
456. Tomar RS, Matta H, Chaudhary PM. 2003. Use of adeno-associated viral vector for delivery of small interfering RNA. Oncogene 22:5712–5715.
457. Grimm D, Streetz KL, Jopling CL, Storm TA, Pandey K, Davis CR, Marion P, Salazar F, Kay MA. 2006. Fatality in mice due to oversaturation of cellular microRNA/short hairpin RNA pathways. Nature 441:537–541.
458. Grimm D. 2011. The dose can make the poison: lessons learned from adverse in vivo toxicities caused by RNAi overexpression. Silence 2:8.
459. Cornetta K, Lin T-Y, Pellin D, Kohn DB. 2023. Meeting FDA Guidance recommendations for replication-competent virus and insertional oncogenesis testing. Mol Ther - Methods Clin Dev 28:28–39.
460. Connolly JB. 2002. Lentiviruses in gene therapy clinical research. Gene Ther 9:1730–1734.

461. Nie L, Thakur MD, Wang Y, Su Q, Zhao Y, Feng Y. 2010. Regulation of U6 Promoter Activity by Transcriptional Interference in Viral Vector-Based RNAi. Genomics Proteomics Bioinformatics 8:170–179.
462. Mäkinen PI, Koponen JK, Kärkkäinen A-M, Malm TM, Pulkkinen KH, Koistinaho J, Turunen MP, Ylä-Herttuala S. 2006. Stable RNA interference: comparison of U6 and H1 promoters in endothelial cells and in mouse brain. J Gene Med 8:433–441.
463. Goguen RP, Del Corpo O, Malard CMG, Daher A, Alpuche-Lazcano SP, Chen MJ, Scarborough RJ, Gatignol A. 2021. Efficacy, accumulation, and transcriptional profile of anti-HIV shRNAs expressed from human U6, 7SK, and H1 promoters. Mol Ther - Nucleic Acids 23:1020–1034.
464. Xia XG. 2003. An enhanced U6 promoter for synthesis of short hairpin RNA. Nucleic Acids Res 31:100e–1100.
465. Ong ST, Li F, Du J, Tan YW, Wang S. 2005. Hybrid Cytomegalovirus Enhancer–H1 Promoter-Based Plasmid and Baculovirus Vectors Mediate Effective RNA Interference. Hum Gene Ther 16:1404–1412.
466. Giering JC, Grimm D, Storm TA, Kay MA. 2008. Expression of shRNA From a Tissue-specific pol II Promoter Is an Effective and Safe RNAi Therapeutic. Mol Ther 16:1630–1636.
467. Nielsen TT, Marion I van, Hasholt L, Lundberg C. 2009. Neuron-specific RNA interference using lentiviral vectors. J Gene Med 11:559–569.
468. Hu P-Y, Fan X-M, Zhang Y-N, Wang S-B, Wan W-J, Pan H-Y, Mou X-Z. 2021. The limiting factors of oncolytic virus immunotherapy and the approaches to overcome them. Appl Microbiol Biotechnol 105:5257–5257.
469. Singh PK, Doley J, Kumar GR, Sahoo AP, Tiwari AK. 2012. Oncolytic viruses & their specific targeting to tumour cells. Indian J Med Res 136:571–584.
470. Jo MH, Shin S, Jung S-R, Kim E, Song J-J, Hohng S. 2015. Human Argonaute 2 Has Diverse Reaction Pathways on Target RNAs. Mol Cell 59:117–124.
471. Ludwig N, Leidinger P, Becker K, Backes C, Fehlmann T, Pallasch C, Rheinheimer S, Meder B, Stähler C, Meese E, Keller A. 2016. Distribution of miRNA expression across human tissues. Nucleic Acids Res 44:3865–3877.

472. Kelly EJ, Hadac EM, Greiner S, Russell SJ. 2008. Engineering microRNA responsiveness to decrease virus pathogenicity. Nat Med 14:1278–1283.
473. Ylösmäki E, Hakkarainen T, Hemminki A, Visakorpi T, Andino R, Saksela K. 2008. Generation of a Conditionally Replicating Adenovirus Based on Targeted Destruction of E1A mRNA by a Cell Type-Specific MicroRNA. J Virol 82:11009–11015.
474. Edge RE, Falls TJ, Brown CW, Lichty BD, Atkins H, Bell JC. 2008. A let-7 MicroRNA-sensitive Vesicular Stomatitis Virus Demonstrates Tumor-specific Replication. Mol Ther 16:1437–1443.
475. Leber MF, Baertsch M-A, Anker SC, Henkel L, Singh HM, Bossow S, Engeland CE, Barkley R, Hoyler B, Albert J, Springfeld C, Jäger D, von Kalle C, Ungerechts G. 2018. Enhanced Control of Oncolytic Measles Virus Using MicroRNA Target Sites. Mol Ther - Oncolytics 9:30–40.
476. Paroo Z, Liu Q, Wang X. 2007. Biochemical mechanisms of the RNA-induced silencing complex. Cell Res 17:187–194.
477. Börner K, Niopek D, Cotugno G, Kaldenbach M, Pankert T, Willemsen J, Zhang X, Schürmann N, Mockenhaupt S, Serva A, Hiet M-S, Wiedtke E, Castoldi M, Starkuviene V, Erfle H, Gilbert DF, Bartenschlager R, Boutros M, Binder M, Streetz K, Kräusslich H-G, Grimm D. 2013. Robust RNAi enhancement via human Argonaute-2 overexpression from plasmids, viral vectors and cell lines. Nucleic Acids Res 41:e199–e199.
478. Yi R. 2005. Overexpression of Exportin 5 enhances RNA interference mediated by short hairpin RNAs and microRNAs. RNA 11:220–226.
479. Grimm D, Wang L, Lee JS, Schürmann N, Gu S, Börner K, Storm TA, Kay MA. 2010. Argonaute proteins are key determinants of RNAi efficacy, toxicity, and persistence in the adult mouse liver. J Clin Invest 120:3106–3119.
480. Liu YP, Schopman NCT, Berkhout B. 2013. Dicer-independent processing of short hairpin RNAs. Nucleic Acids Res 41:3723–3733.
481. Thomson DW, Dinger ME. 2016. Endogenous microRNA sponges: evidence and controversy. Nat Rev Genet 17:272–283.
482. Li X, Su Y, Sun B, Ji W, Peng Z, Xu Y, Wu M, Su C. 2016. An Artificially Designed Interfering lncRNA Expressed by Oncolytic Adenovirus Competitively Consumes

OncomiRs to Exert Antitumor Efficacy in Hepatocellular Carcinoma. Mol Cancer Ther 15:1436–1451.

483. Su Y, Sun B, Lin X, Zhao X, Ji W, He M, Qian H, Song X, Yang J, Wang J, Chen J. 2016. Therapeutic strategy with artificially-designed i-lncRNA targeting multiple oncogenic microRNAs exhibits effective antitumor activity in diffuse large B-cell lymphoma. Oncotarget 7:49143–49155.
484. Rossbach O. 2019. Artificial Circular RNA Sponges Targeting MicroRNAs as a Novel Tool in Molecular Biology. Mol Ther - Nucleic Acids 17:452–454.
485. Yan N, Chen ZJ. 2012. Intrinsic antiviral immunity. Nat Immunol 13:214–222.
486. Jiang L, Wei C, Li Y. 2012. Viral suppression of RNA silencing. Sci China Life Sci 55:109–118.
487. Bailey L, Newman JFE, Porterfield JS. 1975. The Multiplication of Nodamura Virus in Insect and Mammalian Cell Cultures. J Gen Virol 26:15–20.
488. Bailey L, Scott HA. 1973. The Pathogenicity of Nodamura Virus for Insects. Nature 241:545–545.
489. Chao JA, Lee JH, Chapados BR, Debler EW, Schneemann A, Williamson JR. 2005. Dual modes of RNA-silencing suppression by Flock House virus protein B2. Nat Struct Mol Biol 12:952–957.
490. Körber S, Shaik Syed Ali P, Chen JC-H. 2009. Structure of the RNA-Binding Domain of Nodamura Virus Protein B2, a Suppressor of RNA Interference,. Biochemistry 48:2307–2309.
491. Maillard PV, Ciaudo C, Marchais A, Li Y, Jay F, Ding SW, Voinnet O. 2013. Antiviral RNA Interference in Mammalian Cells. Science 342:235–238.
492. Lu Y, Wambach M, Katze MG, Krug RM. 1995. Binding of the Influenza Virus NS1 Protein to Double-Stranded RNA Inhibits the Activation of the Protein Kinase That Phosphorylates the eIF-2 Translation Initiation Factor. Virology 214:222–228.
493. Bucher E, Hemmes H, de Haan P, Goldbach R, Prins M. 2004. The influenza A virus NS1 protein binds small interfering RNAs and suppresses RNA silencing in plants. J Gen Virol 85:983–991.
494. Cárdenas WB, Loo Y-M, Gale M, Hartman AL, Kimberlin CR, Martínez-Sobrido L, Saphire EO, Basler CF. 2006. Ebola Virus VP35 Protein Binds Double-Stranded RNA

and Inhibits Alpha/Beta Interferon Production Induced by RIG-I Signaling. J Virol 80:5168–5178.

495. Haasnoot J, de Vries W, Geutjes E-J, Prins M, de Haan P, Berkhout B. 2007. The Ebola Virus VP35 Protein Is a Suppressor of RNA Silencing. PLoS Pathog 3:e86.
496. Bennasser Y, Jeang K-T. 2006. HIV-1 Tat interaction with Dicer: requirement for RNA. Retrovirology 3:95.
497. Bennasser Y, Le S-Y, Benkirane M, Jeang K-T. 2005. Evidence that HIV-1 Encodes an siRNA and a Suppressor of RNA Silencing. Immunity 22:607–619.
498. Backes S, Shapiro JS, Sabin LR, Pham AM, Reyes I, Moss B, Cherry S, tenOever BR. 2012. Degradation of host microRNAs by poxvirus poly(A) polymerase reveals terminal RNA methylation as a protective antiviral mechanism. Cell Host Microbe 12:200–210.
499. Li Y, Basavappa M, Lu J, Dong S, Cronkite DA, Prior JT, Reinecker H-C, Hertzog P, Han Y, Li W-X, Cheloufi S, Karginov FV, Ding S-W, Jeffrey KL. 2017. Induction and suppression of antiviral RNA interference by influenza A virus in mammalian cells. Nat Microbiol 2:16250.
500. Bastin D, Aitken AS, Pelin A, Pikor LA, Crupi MJF, Huh MS, Bourgeois-Daigneault M-C, Bell JC, Ilkow CS. 2018. Enhanced susceptibility of cancer cells to oncolytic rhabdovirotherapy by expression of Nodamura virus protein B2 as a suppressor of RNA interference. J Immunother Cancer 6:62.
501. Doerner J, Sallard E, Zhang W, Solanki M, Liu J, Ehrke-Schulz E, Zirngibl H, Lieber A, Ehrhardt A. 2022. Novel group C oncolytic adenoviruses carrying a microRNA inhibitor demonstrate enhanced oncolytic activity in vitro and in vivo. Mol Cancer Ther molcanther.MCT-21-0240-A.2021.
502. Le Boeuf F, Diallo J-S, McCart JA, Thorne S, Falls T, Stanford M, Kanji F, Auer R, Brown CW, Lichty BD, Parato K, Atkins H, Kirn D, Bell JC. 2010. Synergistic Interaction Between Oncolytic Viruses Augments Tumor Killing. Mol Ther 18:888–895.

Appendix A. Optimal Delivery of RNA interference by viral vectors for cancer therapy

Boaz Wong[1,2*], Rayanna Birtch[1,2*], Reza Rezaei[1,2], Taylor Jamieson[1,2], Mathieu Crupi[1,2], Jean-Simon Diallo[1,2], Carolina S. Ilkow[1,2#]

[1]Centre for Innovative Cancer Research, Ottawa Hospital Research Institute; Ottawa, Ontario, Canada, K1H 8L6. [2]Department of Biochemistry, Microbiology and Immunology, Faculty of Medicine, University of Ottawa; Ottawa, Ontario, Canada, K1H 8M5. * denotes equal contribution, # denotes corresponding author.

Published September 20, 2023 in *Molecular Therapy*

A.1 Abstract

In recent years, there has been a surge in the innovative modification and application of the viral vector-based gene therapy field. Significant and consistent improvements in the engineering, delivery and safety of viral vectors have set the stage for their application as RNAi delivery tools. Viral vector-based delivery of RNAi has made remarkable breakthroughs in the treatment of several debilitating diseases and disorders (e.g., neurological diseases); however, their novelty has yet to be fully applied and utilized for the treatment of cancer. This review highlights the most promising and emerging viral vector delivery tools for RNAi therapeutics while discussing the variables limiting their success and suitability for cancer therapy. Specifically, we outline different integrating and non-integrating viral platforms used for gene delivery, currently employed RNAi targets for anti-cancer effect, and various strategies used to optimize the safety and efficacy of these RNAi therapeutics. Most importantly, we provide great insight into what challenges exist in their application as cancer therapeutics and how these challenges can be effectively navigated to advance the field.

A.2 Main Text

An introduction to RNA interference mechanisms and delivery methods

What is RNA interference?

RNA interference (RNAi) describes the mechanism of gene expression knockdown by disrupting cellular messenger RNA (mRNA) levels using short sequences of non-coding RNA. This phenomenon was first described by Andrew Fire & Craig C. Mello in 1998 where they described genetic interference via the injection of double-stranded RNA (dsRNA) in a *C.*

elegans nematode model (307). In the following years, the silencing mechanism was slowly elucidated including the discovery of silencing intermediates such as small interfering RNA (siRNA), identification of enzymes responsible for RNA cleavage and other regulatory pathways (308). In a physiological setting, endogenous RNAi effectors are used in the immune response, particularly in antiviral defence to knockdown essential viral proteins, thereby limiting virus propagation (309). When applied to the current research landscape, RNAi has since become the standard for transient gene knockdown studies.

The three most common types of RNAi species are silencing RNA (siRNA), short-hairpin RNA (shRNA) and microRNA (miRNA), each type differing in features including base-pair length, structure, and mechanism of gene regulation (308). When dealing with single gene knockdown, siRNA is typically used given that it is almost fully complementary to its target mRNA thus conferring maximum specificity. These 21-23 nucleotide RNA sequences, with a 2-nucleotide overhang at the 3' end, result either from the cellular processing of double-stranded RNA by Dicer, a specialized ribonuclease III-like enzyme, or can directly be artificially synthesized (310). Similarly, shRNA is typically 50-70 base-pairs with double-stranded RNA bridged by a single-strand loop with a 3' overhang (311). This effector also inhibits protein translation through the same direct mRNA-degrading mechanism but is significantly more efficient (312, 313). On the other hand, miRNA species exist endogenously, they are first processed within the nucleus, and then exported to the cytoplasm where they are further processed by the Dicer complex. Unlike siRNA, mature miRNA effectors are capable of silencing multiple mRNA targets via partial complementation to the 3' untranslated region to repress its translation (314). Among these, there also exist other RNAi effectors such as

piwi-interacting RNA (piRNA) or guide RNA for CRISPR-Cas9 applications (dCas9-gRNA) (315, 316).

The development of RNAi therapeutics

Since its discovery, the therapeutic potential of RNAi has always been highly touted. Given that its target specificity is largely based upon genetic sequence, short sequences of non-coding RNA can be designed against virtually any cellular target, including targets without an available pharmacological inhibitor (113). As such, the concept of versatile, post-translational knockdown therapeutics was poised to revolutionize the entire field of gene therapy and become a powerful tool for targeting the 'undruggable' targets. Despite challenges related to site-specific delivery, knockdown efficacy and potential off-target toxicities, the United States Food and Drug Administration (FDA) approved the first RNAi-based therapeutic in August 2018. Patrisiran (Onpattro®) uses lipid nanoparticles (LNPs) that deliver a small-interfering RNA (siRNA) to knockdown transthyretin (TTR) gene expression for the treatment of polyneuropathy in patients with hereditary TTR-mediated amyloidosis (317). The FDA has since approved two other RNAi-based therapeutics: Givosiran (Givlaari®) for acute hepatic polyuria in 2019 and Lumasiran (Oxlumno®) for primary hyperoxaluria in 2020. Moreover, currently seven other siRNA-based therapies are undergoing phase 3 clinical trial investigation (318). With respect to cancer therapy, there are many potential therapeutic roles for RNAi. In personalized medicine, genetic screening for overexpressed or overactive cancer driver mutations can identify effective knockdown targets tailored to each tumor. For example, a phase 1 trial of exosome-delivered siRNA targeting *Kras*^{G12D} in KRAS-mutated pancreatic ductal adenocarcinoma is currently underway (NCT03608631).

Preferential delivery of RNAi by viral vectors

Although many therapeutic RNAi delivery strategies have been developed, one of the largest obstacles to their clinical application is the effective delivery of the RNAi effectors enough for potent gene knockdown. A vehicle, such as a viral vector or nanoparticles, is required as naked RNA molecules are rapidly degraded by nucleases present in the extracellular milieu. Accordingly, a competent delivery strategy should encompass the following qualities: (i) the ability to safeguard the RNAi effector in extracellular space, (ii) the ability to seamlessly penetrate the cellular membrane, and (iii) the ability to release the RNAi effector into the cytoplasm when appropriate (319). The simplest delivery vehicle is liposome-mediated transfection or lipofection which describes the packaging of the RNAi effector into a phospholipid bilayer complex that merges with the cellular membrane and releases the effector into the cytoplasm. Representing the simplest form of RNAi delivery, this strategy is very well-established for routine use in experimental applications in laboratory settings. Despite this, its applications are limited by low target specificity and its reduced stability *in vivo*. Meanwhile, nanoparticle-based delivery technologies are being continuingly investigated and improved by using newly developed nanomaterials with greater stability including nanotubes, quantum dots or dextran cages (320).

To further improve cell selectivity, nanoparticles can be conjugated to biomolecules such as peptides or antibodies for targeted delivery of RNAi to specific cell types or diseased cells. In a hallmark study by Song *et al.*, protein-encased siRNA conjugated to Human Immunodeficiency Virus (HIV) type 1 envelope antigen-binding fragments (Fab) demonstrated target specificity to HIV envelope-expressing melanoma cells *in vivo* (321). Similar strategies however are notably reliant on nonspecific electrostatic interactions between

the RNAi carrier and the biomolecule, leaving them prone to aggregation events and subsequently unpredictable pharmacokinetics (322). Majority of these RNAi delivery methods may also be limited by off-site toxicity. For example, nanoparticles fail to extravasate from the blood to the site of interest often end up accumulating in the liver. While recent technological advancements have shown glimpses of accomplishing selective delivery to mitigate toxicities, these strategies have complicated preparation procedures and are often expensive to manufacture (320, 323).

As a simple solution to alleviate these concerns of low stability and specificity, viral vectors represent an intriguing and naturally occurring option (324). Firstly, viruses are stable in extracellular environments and already excel at efficiently delivering genetic material to cellular targets. Viral vectors such as retroviruses, lentiviruses and adenoviruses have well-characterized modes of transmission and gene transfer mechanisms, unlike the aforementioned physical means of RNAi transfection (325). For example, adenoviruses have already been extensively explored in cancer gene therapy, delivering genes that trigger apoptosis (*e.g.,* p53) or to stimulate anti-tumor immune responses (*e.g.,* interleukin 2) (117). Secondly, especially in the field of cancer therapy, several virus types have natural tumor tropisms (28, 326). In the process of attaining neoplasticity, early on cancer cells often lose immunoregulatory mechanisms thus becoming exquisitely susceptible to viral infection. This phenomenon is the basis of oncolytic virotherapy (76). Similar to nanoparticle-antibody conjugation, the tissue selectivity of viral vectors can also be further accomplished through “pseudotyping”, which is the incorporation of envelope material of other viral types to modulate its natural tissue tropism (327) or through “retargeting”, which involves the reprogramming of viral surface-exposed components with single chain variable fragment antibodies (scFvs) or other cell-targeting

moieties (118). Finally, with the recent advances in the field of synthetic biology, the production of genetically engineered viral vectors has become increasingly simple and cost-effective, making it an attractive therapeutic option with the capacity to deliver multiple RNAi species at once (328). In this review (summarized in Figure A1), we present viruses as optimal vectors for RNAi therapeutics and summarize the current strategies employed to target obstacles limiting their success in the clinic.

The versatility of viral vectors for RNAi delivery

Considerations in using viruses as RNAi delivery systems

There has undoubtedly been a recent surge in the innovative modification and application of viral vector-based gene therapy (324). The last decade has seen significant and consistent improvements in the engineering, delivery, and safety of viral vectors as viable RNAi delivery tools in the clinic. Classically, the most common viral-vector gene delivery candidates have proven to be the retroviruses [*e.g.,* gammaretroviruses (γ-retroviruses) and lentiviruses], herpes-simplex viruses (HSV), adenoviruses (AdV) and adeno-associated viruses (AAV) (329). These five main classes of viral vectors can be categorized into two groups according to whether their genomes integrate into host cellular chromatin (*e.g.,* retroviruses and lentiviruses) or persist in the cell nucleus predominantly as extrachromosomal episomes (*e.g.,* AAV, AdV, and HSV). More recently, self-replicating cytoplasm RNA viruses (*e.g.,* Vesicular Stomatitis Virus) have also emerged as promising candidates for gene delivery, especially within the field of oncolytic virotherapy (330, 331). Moreover, some of these classes have already been tested for the delivery of RNAi. Selection for their use in cancer therapy will

depend on differences in key features, namely their efficacy, specificity, stability, and safety. In this section, we will discuss features of the most common viral vector-based RNAi-delivery agents; the integrating and non-integrating viral vectors, as well as introduce the emerging class of self-replicating cytoplasmic RNA viruses as it pertains to their application as RNAi delivery tools, both inside and outside of the field of cancer therapeutics (Table A1).

Retroviruses as integrating viruses for the delivery of RNAi

Characterized by their unique ability to efficiently integrate their viral genome into host cells, retroviruses are a family of enveloped, positive-sense single-stranded (ss) RNA viruses defined by the enzymatic activities of reverse transcriptase and integrase (332). While several retroviruses have been investigated for various gene therapy applications, γ-retroviruses and lentiviruses are the most extensively studied and frequently modified for use as replication-incompetent vectors to deliver RNAi to mammalian cells (333, 334). Their genome is largely non-overlapping, and thus relatively amenable to manipulation while the separation of *cis* (*i.e.,* packaging signal) and *trans* (*i.e., gag, pol, env*) elements generates a simple recombinant retroviral system with up to 8-kb of transgene coding capacity suitable for the easy production of replication-defective recombinant RNAi-retrovirus (332). Great advancements in the engineering of retroviral production systems, notably the advent of self-inactivating (SIN) vectors, have greatly increased the safety profile of these vectors as RNAi delivery tools *in vivo*. Upon their activation, any subsequent spread is abolished and the induction of immune-related responses following transduction are minimized as no viral proteins are synthetized (335, 336). These advancements ultimately result in relatively lower immunogenicity profiles compared to other viral platforms (337).

Retroviruses replicate through a double-stranded (ds) DNA intermediate and integrate their genomes stably into the host cells' DNA, a unique feature that allows for long-term expression of RNAi molecules (332). While the γ-retroviruses [e.g. Murine leukemia virus (MLV)] are only capable of integrating their viral genome into the host cells' genomic DNA during the mitotic phase of the cell cycle, lentiviruses are capable of inducing stable and long-term gene silencing in both dividing and non-dividing cells (332). As such, lentiviral vectors serve as a more attractive option for the delivery of RNAi to the central nervous system (CNS) where they have been shown to efficiently transduce CNS neurons and mediate RNA silencing in the brain and spinal cord *in vivo* to successfully ameliorate several animal models of CNS diseases/disorders. The first studies to use lentiviral-mediated delivery of RNAi to pre-clinically treat CNS disorders, employed an shRNA-based lentiviral approach to silence a disease-causing gene (SOD1) in mouse models of familial amyotrophic lateral sclerosis (ALS). Silencing the expression of SOD1 by lentiviral delivery of shSOD1 to familial ALS mice increased motor neuron survival, improved motor performance, and successfully delayed the onset and slowed down the progression of the disease (338). Indeed, retroviral delivery of RNAi has also shown remarkable pre-clinical success in the treatment of several neurodegenerative diseases and CNS disorders including but not limited to Huntington's disease (HD)(339), Parkinson's disease (PD)(340, 341), Alzheimers disease (AD)(342, 343), Prion disease (344, 345), and spinal cord injury (346).

Lentiviruses offer the potential to transduce stem cells, making them particularly attractive tools for the delivery of RNAi to these non- or slowly proliferating and often difficult to transduce cell types. As such, lentivirus-based RNAi delivery has become a useful tool for the *in vitro* or *ex vivo* engineering of immune cells in the treatment of chronic viral infection.

Hematopoetic stem cells (HSC) can be engineered to resist viral infections through transduction with lentivirus-encoding anti-viral RNAi effector (347, 348). This approach was first pioneered by transplanting human (CD34+) HSCs transduced with a lentivirus expressing an anti-HIV-1 shRNA (shRNA against rev) into thymus and liver grafts in humanized severe combined immunodeficiency disease (SCID) mice (349). These studies demonstrate that transduced T cells and macrophages isolated from mice were shown to resist HIV-1 challenge (349–351). Later this approach was adopted to transduce (CD34+) HSCs with single or bispecific lentiviral constructs expressing shRNAs against the host cell factors, CCR-5 and/or CXCR-4, which subsequently gave rise to progeny macrophages resistant to HIV-1 (352). In non-human primates, a stable reduction of CCR-5 in progeny T cells transduced with shCCR-5 *ex vivo* was observed and shRNA transgene expression was sustained for over a year *in vivo* (353). RNAi has also been combined with other types of gene therapy approaches in a single lentiviral vector (348, 354). For example, people living with HIV-1/AIDS suffering from malignant lymphomas may undergo autologous transplantation with peripheral blood-derived (CD34+) hematopoietic progenitor cells (HPCs) transduced with lentivirus encoding the 3-RNA-based anti-HIV-1 moieties (Tat/Rev shRNA, TAR decoy and CCR5 ribozyme) as treatment. Importantly, it is well documented that the vector persists in multiple cell lineages with prolonged siRNA expression, albeit at low levels, for up to 24 months (347). Using similar approaches, lentiviral RNAi delivery systems have been employed to express anti-viral RNAi mediators for the treatment of many chronic viral infections, including but not limited to encephalitogenic flavivirus (355, 356) and Coxsackie B infections (357), as well as targeting the viral oncogenes E6 and E7 in human papillomavirus (HPV) transformed carcinomas (358, 359).

Despite the recent successes discussed above, the *in vivo* application of retroviral-based RNAi delivery so far has been largely limited to local administration (i.e. treatment of neurological disease) or *ex vivo* approaches (i.e. HSC programming) due to safety and efficacy limitations associated with systemic delivery (360, 361). The irreversible and stable nature of retroviral integration mean that targeting recombinant retroviral particles to desired cell types is essential for safe and effective systemic administration of retroviral-RNAi therapies. Currently, retroviral cell-targeting cannot be accomplished using retroviral vectors pseudotyped with the glycoprotein of Vesicular Stomatitis Virus (VSV-G) given its broad tissue tropism through binding to the ubiquitously expressed cell-surface low-density lipoprotein receptor (LDLR) (362, 363). Several diverse approaches have instead been used to alter retroviral tropism and/or develop highly targeted retroviral delivery systems, including the incorporation of heterologous attachment glycoproteins, single-chain and bi-specific antibody adaptors, and genetic-based systems that alter glycoprotein tropism (364). While these changes improved target cell specificity, in many cases they are also accompanied by reduced transduction efficiency (365–367). Subsequently, developing highly targeted retroviral delivery systems remains one of the largest obstacles for the systemic delivery and clinical applicability of retroviral-based delivery of RNAi in the treatment of many human diseases including cancer.

In the context of treating human malignancies, lentiviruses do not have any natural tumor tropism, therefore they require a targeted delivery strategy for the delivery of RNAi to tumor cells (*e.g.* protease-activated Env proteins) (368–370). However, the γ-retroviruses possess a stringent requirement for cell division to achieve productive infection and preferentially replicate in cells with defective innate immunity making them uniquely well suited for use in

cancer therapy (371–373). By retaining all of the elements necessary for viral replication, retroviral replicating vectors (RRVs) based on γ-retroviruses (*i.e.,* MLV) are capable of transmitting genes via exponential *in situ* amplification and are currently being pursued as therapeutic agents for cancer (374–379). While many other virus types being investigated for this purpose are inherently cytolytic, RRVs confer a considerable degree of natural specificity for tumors without the immediate induction of cytolysis which can contribute to longer-lasting therapeutic efficacy and be particularly advantageous for RNAi therapeutics (380). Furthermore, RRV's non-lytic replication cycle does not trigger immediate anti-viral immune responses, allowing for sustained viral replication and therapeutic transgene expression into the tumor microenvironment (380). These factors alongside a growing safety and drug activity record in humans suggest that these delivery vectors could allow effective use of RNAi strategies in human cancers; however, this potential utility has yet to materialize.

Adenovirus, Adeno-Associated Virus, and Herpes Simplex virus vectors as non-integrating vectors for the delivery of RNAi

While integrating viruses offer the potential for stable, long-term transgene expression though their capacity to integrate in the host cell genome, this unique feature can also pose great genotoxic risk, and in some cases even induce oncogenesis (381, 382). Non-integrating vectors specifically share reduced risk of genotoxicity, offering a safer profile *in vivo* and *in vitro.* In contrast to retroviruses, their genomes exist and replicate efficiently as episomes during infection producing high, yet transient expression of transgenes; however, expression can still be retained for long periods in post-mitotic tissues (381). AdV, AAV, and HSV vectors are three examples of non-integrating viruses that have been employed for RNAi delivery (383–385). All three of these vectors are capable of transducing or infecting dividing and non-

dividing cells, thus offering excellent potential for RNAi delivery to cells in the CNS and other difficult to transduce cell types, such as in stem cells.

Herpesviruses are an important family of dsDNA viruses known for their elaborate and large genome (152 kb), which encodes over 80 gene products. Several genes involved in HSV replication, virulence, and immune evasion are non-essential for the viral life cycle in *in vitro* cell cultures. These genes can be deleted or modified, alone or in combination, to create attenuated and/or safer HSV mutants. In the context of cancer therapy, many of these mutants present with a reduced ability to replicate in normal quiescent cells, but can grow efficiently in tumor or dividing cells setting the stage as cancer therapeutic RNAi delivery vehicles (386, 387). Recent efforts have also been made to further modify the envelope of the HSV-1 virion to target specific receptors that selectively increase infectivity of tumor cells bearing corresponding receptors (388, 389). Although well exploited as an oncolytic virotherapy platform, HSV-1 has unfortunately been less explored as an RNAi delivery vehicle compared to the retroviruses, AdV and AAV. However; HSV amplicon vectors expressing shRNA have been used recently to mediate posttranscriptional silencing of Epidermal Growth Factor Receptor (EGFR), which is frequently activated in human glioblastoma cells (385) and to inhibit the expression of BK polyomavirus (BKV) T antigen and tumorigenicity of BKV-transformed cells *in vitro* (390).

Adenoviruses are nonenveloped viruses containing a dsDNA genome that provide efficient transduction of target cells at a low multiplicity of infection (MOI) and have well-established methods for manipulation and propagation (391). Compared to retroviruses, these vectors have more established manufacturing capabilities (391). A recombinant AdV (rAdV) encoding shRNA (rAdV-shAbcc2) has been employed *in-vivo* to target the murine ATP-

binding cassette multidrug resistance protein 2 (*Abcc2*), a protein involved in the transport of bilirubin out of liver cells and into the bile. C57/BL6 mice injected with rAdV-shAbcc2 showed significant impairment of Abcc2 function for up to 3 weeks, as reflected by high levels of processed shRNA targeting Abcc2, specific reduction of *Abcc2* mRNA, and increased serum bilirubin levels. These results were the first of several to indicate that AdV vectors can be used to express sufficient levels of shRNA capable of silencing target genes in the liver of mice (392).

In the field of cancer gene therapy, AdV has gained considerable attention due to its selective and potent cancer-cell killing properties, amplified transgene expression, an additional therapeutic efficacy by shedding of virus progeny. The first strategy of oncolytic AdV armed with RNAi involved the use of conditionally replicating AdV (CRAdV) encoding shRNA against firefly luciferase. This proof of principle study demonstrated that siRNAs expressed from CRAdV could suppress the expression of firefly luciferase while the efficiency of silencing increased during viral replication (393). Zhang *et al*. later adopted the oncolytic AdV-RNAi platform to achieve siRNA-mediated gene silencing that led to tumor cell death (384). The authors engineered a novel oncolytic AdV carrying a mutant *Kras* siRNA transgene (AdV-siRNA Kras) which demonstrated an additive tumor growth–inhibitory response on human cancer cells through siRNA-mediated *Kras* knockdown and AdV-mediated cancer cell lysis. In a subcutaneous mouse xenograft model of H79 pancreatic cancer, daily intratumoral injections of AdV-siRNA Kras significantly reduced tumor growth (85.5% growth reduction) relative to parental-AdV (47.8% growth reduction) or AdV expressing siRNA targeting GFP (44.1% growth reduction). Tumor were characterized by marked down-regulation of Ras signaling–related gene expression (AKT2, GSK3β, E2F2, and MAP4K5) and cell cycle

blockage reflecting potent siRNA Kras transgene activity (384). Since then, AdV mediated delivery of RNAi effectors with anti-angiogenic (*e.g.,* VEGF, IL-8) and anti-tumor properties (*e.g.,* Ki67, MYCN) as well as the ability to sensitize cancer cells to chemotherapeutics (*e.g.,* Survivin, Akt) have been tested the treatment of breast cancers (394), bladder cancer (395), neuroblastomas (396), prostate cancers (397), pancreatic cancers (384), lung cancers (398), colorectal cancers (398–400), and hepatocellular carcinoma (401, 402) in the pre-clinical setting.

Oncolytic AdV vectors undoubtedly possess the capacity to deliver RNAi species to tumor cells for efficient gene knockdown; however, a major limitation to the clinical use of vectors is the host immune response (403–405). Neutralizing antibodies and preexisting immunity represent two significant barriers to repeated vector administration of AdV based delivery of RNAi (406). Low-level expression of viral vector genes in such settings almost always results in the generation of immune responses directed against AdV-transduced cells and ultimately in the loss of transgene expression. On the other hand, AAV is highly valued for its lack of pathogenicity in multiple vertebrate species, including human and non-human primates (407, 408). Due to their relatively low immunogenicity and their ability to mediate persistent gene expression, AAV vectors are the most actively investigated gene therapy vehicles, currently being tested in several human gene therapy trials (324, 329).

AAVs are a unique group of non-enveloped single stranded DNA viruses characterized by their reliance on helper viruses (*i.e.,* Adenoviruses) to support their propagation. In the most commonly used recombinant AAV (rAAV) systems, all AAV protein-coding sequences are removed to incorporate a payload that is flanked by AAVs inverted terminal repeats (ITRs)(409). When designing vectors for gene replacement therapies, the relatively limited

packaging capacity (~4.7kb) of AAV typically represents a disadvantage; however, this does not apply to RNAi-based applications. Separate or combined packaging constructs containing AAV *rep* and *cap* genes alongside adenoviral helper genes required for replication are provided in *trans* to produce replication-deficient AAV virions. While in quiescent cells, AAV's stable transgene expression can be observed for multiple years, in rapidly dividing cells such as tumor cells, episomal AAV is gradually diluted and in some cases even lost over the repeated rounds of cell division. Of note, the AAV genome cannot replicate along with the host cell DNA leading to loss of the transgene expression (381). Reports on the stability and duration of transgene expression are variable and the exact molecular processes involved in establishing stable gene transduction remain under investigation. As such, it is very difficult to predict with certainty the duration of transgene expression from AAV, particularly in the case of cancers. Nonetheless, AAV is the first RNAi-based gene therapy viral delivery system to be used in humans in clinical settings (NCT01899092). TT-034, an AVV-based RNAi product for the treatment of Hepatitis C virus (HCV) infection, is comprised of an AAV8 vector carrying three different anti-HCV shRNA that cleave the 5' UTR and two coding NS5B regions in the HCV genome. The clinical trial data demonstrates that TT-034 is well tolerated, safe and can effectively transduce hepatocytes and concurrently express three anti-HCV shRNAs in human subjects infected with HCV (383). As a result of the increasing competitive landscape in HCV treatment and the time required to get TT-034 to market, TT-034 has received limited partnering interest preventing its clinical advancement. Despite this fact, TT-034 has provided a great proof of concept AAV based RNAi delivery platform and has built a great foundation for use of viral vector-based RNAi delivery platforms, particularly AAV, in the treatment of human disease.

AAV has also shown pre-clinical promise for the delivery of RNAi therapeutics to treat cancers. For instance, silencing of the human Telomerase Reverse Transcriptase (TERT) using an AAV vector-based approach was shown to restore apoptosis in human oral squamous cells both *in vitro* and *in vivo* (410). Furthermore, expression of endogenous RNAi mediators like miRNA-7 from AAV decreased tumor growth in human glioblastoma mouse xenograft models through downregulation of the growth-promoting EGFR pathway and upregulation of death receptor pathways (411). AAV-based delivery of RNAi has also been employed to target the expression of cancer-promoting miRNAs (e.g., miRNA-21). AAV can mediate stable expression of a shRNA targeting miRNA-21, and thus attenuate HT29 human colon carcinoma and PC3 human prostate tumor growth in mice (412).

One of the main challenges with AAV-based cancer gene therapy is improving the AAV-specific transduction of cancer cells. Efficient targeting of cells and tissues beyond the liver remains a challenge for both AdV and AAV-based RNAi delivery. Systemic administration of AdV and AAV vectors often results in liver retention, thus representing a key barrier when other organs are the intended targets (409, 413). Fortunately, the engineering of novel AAV capsids has been a constant pursuit to improve and expand AAV biodistribution and transduction efficiency (409). To date, 12 different AAV serotypes have been translated into rAAV-based delivery systems. These vectors have variable tropism due to the differential binding of viral capsid proteins to specific cell-surface receptors. Many attempts have also been made to increase the target specificity of rAAV vectors using natural discovery(414), rational design (e.g., capsid/host cell biology) (415, 416), and directed evolution techniques (e.g., error prone PCR) (417, 418) setting the stage for the future of highly targeted rAAV/AdV RNAi delivery systems.

Cytoplasmic RNA Viruses for the delivery of RNAi

Although less explored, self-replicating cytoplasmic RNA viruses (cRNA) represent another valuable option for the delivery of RNAi therapeutics. Unlike retroviruses and lentiviruses, cRNA viruses have a single-stranded RNA genome that replicates without reliance on any DNA intermediates. As such, viral genomic sequences do not integrate into the host cell genome and their transcription and replication are restricted to the cytoplasm. Although many cRNA viruses have proven to have off-target toxicity, several cRNA viruses lack toxicity or can be genetically modified to be used as safe viral vectors for therapeutic delivery(331, 419). Moreover, many cRNA viruses possess an inherent oncolytic capacity, making them an attractive tool for the delivery of RNAi to treat human malignancies (420, 421). Compared to integrating RNA viruses, cRNA viruses ultimately pose less of an oncogenic risk due to the lack of viral sequence integration into the host genome. Due to their high replicative capacity, cRNA viruses such as alphaviruses, flaviviruses, and rhabdoviruses provide both efficient delivery and high-level expression of transgenes (331, 419). These viral vectors are of ample use for delivering therapeutic payloads, including vaccine development and gene therapy-based immunotherapy (331).

Historically, the restriction of cRNA virus transcription to the cytoplasm was initially theorized to prevent the adequate processing of certain RNAi intermediates by preventing access to canonical miRNA processing elements in the nucleus (*e.g.,* Drosha/DGCR8). However, cytoplasmic RNA viruses can to induce the accumulation of RNAi processing machinery (*e.g.,* Drosha) in the cytoplasm (422). The accumulation of Drosha in the cytoplasm following infection with cRNA viruses expressing RNAi species allows Drosha to act on viral RNA in the cytoplasm to produce pre-miRNA that is subsequently processed into double-

stranded RNAi effectors that can engage their target (330). This theory has been supported, for example, by the discovery of several cRNA virus-derived small RNAs and a functional mature miRNA-like structure (KUN-miR-1) expressed from the Kunjin strain of West Nile Virus (WNV_{KUN}) (423). Another potential barrier for cRNA virus delivery of RNAi species is that the potential excision of RNAi precursors from the viral RNA genome can also destroy the viral genome and thus reduce the efficiency of viral replication. However, the presence of a functional and naturally occurring miRNA precursor element in the tick-borne encephalitis virus (TBEV, a cytoplasmic RNA virus) genome was shown to have no measurable negative impact on viral replication (330). To date, multiplexed high-throughput sequencing has revealed populations of small RNAs (10–60 nucleotides long) produced in cells following infection with six different cytoplasmic RNA viruses. While the secondary structure of these RNAs differs from traditional miRNAs, populations of virally-produced small RNAs that exist as duplexed siRNAs have been identified and strand-selective loading of viral siRNAs onto Argonaute complexes observed (424). Although the structure of these small RNAs suggests that miRNA processing may occur through alternative non-canonical pathways, these findings demonstrate that RNAi effectors can be expressed from cRNA viruses. By developing a better understanding of the structure and biogenesis of viral small RNAs, future work may exploit the intrinsic nature of these species for the development of targeted RNAi delivery by cRNA viruses.

Recent discoveries in the field of viral delivery have shown that both positive- and negative-sense cytoplasmic RNA viruses including; TBEV , Sindbis virus (SV), and VSV have been engineered to produce RNAi intermediates and subsequently induce post-transcriptional gene silencing of target genes (330, 425, 426). These replicating viral vectors

represent a safe delivery method for RNAi and a potent strategy for the induction of transcriptional gene silencing due to their capacity to express RNAi species without integrating viral sequences into the host genome (426, 427). Similarly, we recently employed a SV library to perform an *in-vitro* screen based on virus-encoded artificial microRNAs (amiRs) targeting ~16,000 mammalian genes to identify amiRs that can confer a replicative advantage to OV platforms. Results revealed amiRNA, termed amiR-4, targets ARID1A, a protein involved in chromatin remodeling and an important player in mediating resistance to OV replication. An OV backbone armed with amiR-4 enhanced OV replication and survival of tumor-bearing xenograft and immunocompetent murine models (428). While still at early stages of pre-clinical development, recent evidence highlights that replicating cRNA viruses can be employed as delivery vehicles for RNAi-based gene silencing for therapeutic interventions of various diseases, including in treatment of human cancers. More research is needed to unfold the full potential of cRNA viruses as safe delivery vehicles for RNAi therapeutics.

Applying RNAi to cancer therapy

Viral-delivered miRNA targets for cancer therapy

Given the powerful and versatile capabilities of miRNAs as biodrugs, many academic and pharmaceutical research groups are exploring the application of miRNA delivery via viral vectors for the treatment of cancer. The intended application of these different therapeutic miRNAs can be broadly classified into three modes of action: (1) induction of tumor lysis, (2) inhibition of tumor processes, and (3) sensitization to other therapy regimens. Delivery of RNAi effectors against these targets by non-replicating viral vectors has shown promise across

different preclinical cancer models. While only a handful of examples will be covered herein, a list of all recently tested viral vectors delivering RNAi payloads *in vivo* is included in **Figure A2**.

A logical starting point for increasing cancer cell destruction would be to induce inherent cell death programs such as apoptosis, necrosis and pyroptosis. Control of these processes is a delicate balance between the promotion and inhibition of growth and relies on many host-cell factors. miRNAs can influence these pathways at multiple steps, either by silencing anti-apoptotic factors or promoting expression of pro-apoptotic effectors (429). For example, the Bcl-2 family is a commonly targeted family of proteins that operate as guardians to the apoptotic cascade. Delivery of miR-122, known to downregulate the expression of Bcl-2 members, by an AAV vector demonstrated markedly increased cell death in hepatocellular carcinoma cells and increased *in vivo* therapeutic efficacy in human liver mouse xenograft models (430). Similarly, miR-34a delivered by an adenovirus vector also blocked expression of Bcl-2 in liver cancer and multiple myeloma models. In addition, miR-34a-expressing viral vectors showed significant tumor regression in preclinical models using immunodeficient mice (431). Other miRNAs that target apoptotic effectors and can be expressed from viral vectors for cancer therapeutic purposes include miR-143, which targets *Kras* and miR-144, and thus negatively controls the expression of the TP53-inducible glycolysis apoptosis regulator (TIGAR) factor (432, 433).

Delivery of miRNAs by AAV to modulate key components of uncontrolled cellular replication can also be utilized to limit cell growth. For example, in a study by Kota *et al.*, the authors encoded miR-26a, a cell cycle regulatory miRNA, into an AAV vector (AAV-miR-26a)(434). Upon treatment with AAV-miR-26a, while most cells express miR-26a, liver tumor

cells have markedly reduced levels of miR-26a and displayed reduced cell cycle control. Indeed, using AAV-miR-26a as a replacement therapy approach, the authors found that the systemic administration of AAV-delivered miR-26a induced G1 cell-cycle arrest by inhibiting cyclins D2 and E2, which resulted in reduced tumor growth of a hepatocellular carcinoma mouse model. Other targets seek to replace down-regulated tumor-suppressing miRNAs (*e.g.* miR-370-3p) responsible for controlling tumorigenesis and tumor migration (435).

Finally, miRNA can be deployed to modulate processes that sensitize tumor cells to existing chemotherapy drugs or other therapeutic modalities. Expression of a subset of miRNAs (*e.g.,* miR-886, 923, 944, 138) were found to correlate with both response to cisplatin and overall improved survival in bladder cancer (436). Applying a similar proof-of-concept, another group separately identified that miR-6077, through GLUT1 repression, lowered the half maximal inhibitory concentration (IC50) required for anlotinib, a tyrosine kinase inhibitor, to achieve its antitumor effect in patient-derived cell lines of lung adenocarcinoma (437). Accordingly, this addition of novel miRNA-expressing viral appears poised as an avenue to supplement existing current treatment regimens already in clinic.

Viral-delivered siRNA/shRNA targets for cancer therapy

Compared to miRNA, siRNA and shRNA differ by focusing on the knockdown of a single gene target as opposed to multiple. However, like many other single-target therapeutics, the application of siRNA and shRNA can have a profound therapeutic effect with a smaller side effect profile if the right target is selected. Here, we present four categories of explored RNAi targets: (a) immunosuppressive genes, (b) oncogenes, (c) genes promoting cell death,

and (d) other cancer promoting molecules. A comprehensive list of virally delivered siRNAs or shRNAs cancer therapeutics tested in pre-clinical studies can be found in **Figure 2**.

Targeting immunosuppressive molecules. The success of immune checkpoint inhibitors (ICIs) has placed this therapeutic modality at the forefront of modern cancer therapy development. By using monoclonal antibodies to inhibit immune checkpoint proteins, namely PD-1/PD-L1 and CTLA-4, cytotoxic (CD8+) T-lymphocytes are reengaged to recognize and kill cancer cells more efficiently (438). While many patients have successfully shown long-term remission, a fraction of patients remain resistant to ICIs (439). This resistance is mostly attributable to low tumor antigenicity, low infiltration of T cells in the tumor niche or an overall poor immune response. The advantage of delivering ICI molecules using a viral vector is that viral backbones can intrinsically induce immune activation and upregulation of the antigen presentation machinery in the tumor microenvironment. Indeed, the combinational delivery of immune checkpoint blockade via oncolytic viral vectors has demonstrated efficacy in various mouse cancer models (440, 441).

Studies are already underway to incorporate into viral-based platforms RNAi effectors targeting immune checkpoint molecules. For example, the incorporation of RNAi against PD-L1 and CTLA-4 into a Newcastle disease oncolytic virus (NDV) has demonstrated reduced tumor burden and improved overall survival in the poorly immunogenic B16-F10 syngeneic melanoma mouse model (442). Deploying si/shRNA against multiple other immunotargets such as indoleamine 2,3-Dioxygenase (IDO), interleukin-10 (IL-10) and Suppressor Of Cytokine Signaling 1 (SOCS-1) have also demonstrated increased activation of immune cells to stimulate a more robust anti-tumor response (306, 443, 444). Taken together, there is no

shortage of immunosuppressive targets that can be downregulated by viral-mediated delivery of RNAi effectors to improve anti-cancer therapeutic efficacy.

(b) Targeting oncogene addiction. Upon transformation of proto-oncogenes into oncogenes, tumors gain many of the characteristics essential for its pathogenesis, namely increased cell proliferation and survival. Naturally, it is hypothesized that the silencing of these genes would reverse this effect to limit tumor growth or increase cancer sensitivity to chemotherapy. As over 700 oncogenes have been identified to date (445), there are a plethora of targets for viral RNAi-delivery. For example, Li, Y. *et al.* engineered an AAV expressing shRNA against *MYCN*, a known oncogene in 25% of neuroblastoma cases. By decreasing MYCN transcription factor levels and its downstream cell differentiation and proliferation programs, the virally delivered shRNA was shown to significantly reduce tumor burden through apoptosis induction in *in vivo* mouse xenograft neuroblastoma models (400, 446). Additionally, knockdown of other well-established oncogenic markers by viral RNAi delivery have shown promise in pre-clinical studies, including EGFR in head and neck cancer (447), and the androgen receptor (AR) in prostate cancer (448).

(c) Cell death induction. Similar to the miRNA targets mentioned above, si/shRNA can be designed to target core cell components and thus either directly inhibit tumor proliferation and knockdown anti-apoptotic effectors to induce cell death. Among other tested targets, adenovirus-delivered knockdown of Survivin, an established inhibitor of apoptosis, has shown efficacy in reducing tumor burden in murine models of colorectal and pancreatic cancers (449, 450). Of similar interest, synthetic lethal gene pairs describe two unrelated mutations that do not impact the cell on their own but when present together lead to cell death (451). In this context, RNAi has typically been utilized preferentially as a screening tool to identify novel

synthetic lethal gene pairs. For example, in human acute myeloid leukemia (AML) cells, the authors found that the silencing Bcl-2 via lentiviral-delivered shRNA in cells featuring the isocitrate dehydrogenase 1 and 2 (IDH) R132H mutation significantly decreased their viability (452). Exploration of delivery of these synthetic lethal pairs by viral vector represents yet another opportunity for investigation and development of virally expressed RNAi-based therapeutics.

(d) Other RNAi therapeutic targets. In addition to targeting specifically the cancer cells, virus mediated- RNAi delivery has been tested to modify the tumor microenvironment and discourage malignant growth. Multiple studies have previously demonstrated the use of viral vectors to target genes that inhibit angiogenesis. The vascular endothelial growth factor (VEGF) is a central signaling protein to initiate blood vessel formation and orchestrate tumor blood supply. By delivering a VEGF-targeting shRNA using AAV, the strategy demonstrated reduced tumor vascularization, blood vessel density, and blood vessel size. This potent anti-angiogenic effect led to improve overall survival of glioma-bearing mice (402).

Utilizing RNAi to boost the therapeutic efficacy of oncolytic viruses

Most explored RNAi-delivering viral vectors employ viruses without replicating potential, meaning that any therapeutic activity can almost entirely be attributed to the cellular impact of the RNAi effector. While choosing viral vector delivery offers several advantages over other RNAi delivery platforms, herein lies an intriguing opportunity to synergize the effects of RNAi with the inherent killing ability of oncolytic viruses given the multitude of platforms available, as outlined in Section 2. Indeed, several groups have already begun exploring this strategy. A study by Rovira-Rigau *et al.* screened an adenoviral library of 243

human miRNAs in human pancreatic cancers and identified that miR-99b and miR-485 repressed multiple target genes responsible for transcriptional regulation (*e.g., ELF4, MDM2*, and *KLF8*), allowing for the enhanced production of adenoviral proteins (453). Subsequently, when directly expressed by an oncolytic adenovirus, this viral enhancement was able to overwhelm tumor cells leading to increased tumor cytotoxicity and an enhanced anti-tumor effect in various *in vivo* murine cancer models.

Herpes virus simplex-1 (HSV-1) is one of the best characterized oncolytic viral platforms and has been modified to express RNAi effectors. An oncolytic HSV-1 has been engineered to target the apoptotic pathway and disrupt the cancer cell cycle by co-expressing siRNAs against Bcl-2 and Survivin. This recombinant HSV-1 vector showed decreased tumor volume growth in athymic nude mice bearing human breast adenocarcinomas (454). Through a similar mechanism of suppressing pro-survival proteins like Bcl-2 and SIRT1, expression of miR-34a by a tumor-specific oncolytic vaccinia virus (VV-miR-34a) showed increased cytotoxicity in multiple myeloma cells. Although the VV-delivered expression of miR-34a did not show significant improvement in tumor regression alone, its co-administration with a vaccinia virus armed with another apoptosis inducer, SMAC, was able to achieve significantly improved survival of tumor bearing mice (455).

The field of oncolytic virotherapy continues to face obstacles in identifying an optimal combination of payloads to simultaneously increase viral spread and tumor cell killing, all while maintaining the initiation of a potent anti-tumor immune response for a durable cure. Some conventional payloads such as granulocyte-macrophage stimulating factor (GM-CSF) to stimulate the immune system have been used with success (26, 27); however, it is likely that more than one payload may be required to confer curative therapeutic effects. In addition to

cytokines and cytotoxic proteins, RNAi effectors, like the examples outlined in this section, present as a novel class of payloads that can be explored for effective anti-cancer combinations.

Optimizing the viral-RNAi relationship for better safety and efficacy

Safety limitations to the viral-RNAi approach

As with any therapeutic strategy, concerns pertaining to safety and efficacy must be addressed before the therapy is able to move into clinical trials. The delivery of RNAi effectors using viral vectors alleviates many inherent concerns of using RNAi therapeutics including extracellular stability, tissue selectivity, and cellular uptake (456). Despite these advantages, several more breakthroughs are still required to increase the viability of viral-mediated RNAi delivery in cancer therapy. Starting with safety, excess accumulation leading to toxicity remains a concern following systemic delivery, especially in the liver. AAV-mediated *in vivo* delivery of high quantities of various shRNA were found to induce hepatotoxicity and, in some cases, death within two months of treatment (457). This occurs when the amount of exogenously delivered RNAi overwhelms the cell's processing ability, resulting in cytotoxicity (458). Moreover, dose-dependent side effects can also arise at the administration site in response to the virus (17); therefore, a delicate balance is required between reducing toxic side effects and maintaining good gene knockdown efficacy. As in the case of integrating viruses, the capacity for genome integration of lentivirus and retrovirus vectors into healthy host cells have been demonstrated to lead to side-effects of leukoproliferation and malignancy (459, 460). Finally, with any replication-competent, unintended infection of healthy cells could cause necrosis of physiologically vital tissue (*e.g.,* liver toxicity) and downstream adverse

events (28). Fortunately, several innovative strategies exist to optimise the viral-RNAi relationship to improve RNAi processing and tissue selectivity to improve safety profiles of these biotherapeutics.

Strategies to increase tissue selectivity

Strategies that maintain this goldilocks level of RNAi expression over a prolonged period of time has been explored by rationally selecting the "type" of promoter that drives the specific RNAi effector expression. In viral vectors, RNAi effectors are typically expressed under RNA polymerase III promoters, such as H1 or U6 promoters given their simple structure and well-understood features (461–463). In some contexts where expression is suboptimal, promoters with greater activity like the cytomegalovirus (CMV) promoter can be considered (464, 465). Additionally, these promoters can be swapped for tissue-selective promoters and thus increase on-target effects. For instance, the use of a liver-specific RNA polymerase II type promoter (ApoE/hAAT) for AAV-mediated delivery of shRNA *in vivo* showed decreased long-term hepatotoxicity and limited shRNA detection in other tissues (*e.g.* spleen, heart), even at very high doses, compared to the U6 promoter (466). Similar results were obtained from lentiviral-delivered RNAi using a neuron-specific polymerase II enolase promoter (NSE), which limited long-term brain tissue toxicity compared to a conventional CMV promoter in *in vivo* murine models (467). It is worthwhile to discuss that this obstacle may potentially be completely bypassed by the selection of tumor-selective oncolytic viruses with inherent tumor tropism, offering the benefit of less viral backbone modification (468). However, given that some oncolytic viruses rely on targets of apoptosis, rapid transcription, and rapid translation for selectivity, there still may be cell populations with rapid cell tumor where oncolytic virus

infection may be undesirable (469). As such, integration of tumor-specific promoters in these vectors may still be worth investigation as a redundant mechanism for safety.

Another potential strategy for selective targeting employs miRNA response elements (MREs), which are short target sequences typically found on mRNAs that are recognized by specific miRNA species. Superior complementarity pairing between MRE and mRNA leads to a greater likelihood of mRNA cleavage (470). Given that many miRNAs have their expression restricted to specific tissues or even particular cell types (471), MREs can be incorporated into the viral vector to reduce its expression in specific tissues or cells (472, 473). For example, let-7 is a family of miRNA that operates as tumor suppressors and are subsequently downregulated in tumor cells. Indeed, in a study by Edge *et al.*, infection of normal cells with an oncolytic VSV encoding let-7a MREs into the VSV-M gene showed repressed VSV infection in normal GM38 fibroblasts cells, but unaffected activity in lung A549 carcinoma cells, which express minimal let-7a levels. The let-7a engineered VSV platform did not cause weight loss in mice, and its antitumor activity was maintained at a comparable level to control VSV in a murine model of colon carcinoma (474). Modifications in MRE quantity, insertion location, or combinations of different MREs are continued avenues of investigation to ensure enhanced targeting efficacy of the viral vector (475).

Strategies targeting rate of RNAi processing

To successfully knockdown a gene product via RNAi, intensive cooperation of many different cellular components is required. As a quick overview, the introduced RNAi effector is loaded into the RNA-induced silencing complex (RISC) and is used as a guide to identify the target mRNA strand for silencing. Recognition of the respective complementary mRNA

triggers endonucleolytic cleavage by the slicer argonaute-2 (AGO2) to decrease availability of the mRNA transcript for subsequent protein translation (476). Given that the combined kinetics of RISC mRNA recognition and AGO2-mediated RNA degradation is finite, this represents the rate-limiting steps to viral-delivered RNAi efficacy when overwhelmed with exogenous RNAi effectors. In miRNA and shRNA processing, the Dicer enzyme (ribonuclease III) also comes into play to generate the RISC-compatible siRNA for downstream silencing and limits RNAi efficacy (476). Unengaged intracellular RNAi effectors then proceed to compromise cell viability through outcompeting physiological miRNA required for normal cell function for RISC-processing, or the accidental generation of off-target siRNA against vital cellular proteins.

Given these limitations in the physiological processing rate of RNAi effectors, strategies targeted at modifying these protein components can be considered to improve the safety and efficacy of delivered RNAi. The first option involves artificially increasing AGO2 expression to increase processing capacity. Co-expression of AGO2 along with RNAi effectors in the viral vector have been demonstrated to achieve greater knockdown efficacy without the same hepatotoxic effects. The knockdown was observed for five months after viral administration without any increase in circulating liver damage markers (477).

To counteract these excessive RNAi species, the cell uses two major transport karyopherins, exportin-5/XPO5 and exportin-1/CRM1, to reduce levels of RNAi. In theory, by overexpressing these shuttle proteins, the capacity to nuclear export excess siRNA is increased to subsequently decrease any toxicity caused by oversaturation. XPO5 is of particular interest given its use in both shRNA and miRNA export mechanisms. Pioneering studies showed the promise of this approach by demonstrating improved shRNA silencing efficacy in cell lines

stably overexpressing XPO5 (478). However, while delivery of XPO5 overexpression along with the desired shRNA via AAV was found to double the duration of gene silencing in mouse models, its introduction also paradoxically increased mortality (479). The authors hypothesized that the increase in XPO5 precipitated the saturation of another downstream player, AGO2, which could lead to hepatotoxicity. Indeed, RNAi efficacy was found to be best when both XPO5 and AGO2 were co-overexpressed in the same viral vector (479). Thus, the combination of AGO2 and XPO5 remains a potential option to increase RNAi efficacy that warrants further investigation.

Prior to entering the RISC complex for AGO2-mediated splicing, double stranded RNA species, such as pre-miRNA, must undergo pre-processing by the Dicer complex to generate functional siRNAs. Within this processing step, two potential actionable approaches to increase RNAi efficacy could be implemented. The first is to bypass this rate-determining step altogether through "intelligent shRNA design". A study by Liu *et al.* introduces the concept of "agoshRNA", which describes the design of smaller shRNA with small loop sizes that can shunt its processing away from Dicer and become more reliant on the AGO2 endonuclease activity (480). Given its Dicer-independent miRNA processing, not only is RNAi processing efficacy expected to increase, but this approach could lead to a reduction in the levels of antisense RNA species available for off-target toxicity. While delivery of agoshRNA via viral vectors has not yet been explored, consideration of agoshRNA design over conventional shRNA could represent a simple strategy to improve the safety profile of viral vectors delivering RNAi.

RNAi suppression strategies to increase efficacy

As miRNAs function as primary regulatory agents, it does not come as a surprise that the inverse, which is the suppression of RNAi effectors, can also be used to increase the anti-cancer therapeutic efficacy of viral vectors. The competitive endogenous RNA (ceRNA) hypothesis suggests a potential regulatory network between mRNAs, miRNAs, and a set of long non-coding RNAs (lncRNAs) which contain miRNA binding sites and can sequester them (481). This hypothesis propelled effort to use this concept to create more effective "miRNA sponge" strategies utilizing artificial lncRNAs. By delivering an artificial lncRNA designed to "sponge out" different known oncogenic miRNAs via oncolytic adenovirus, the resulting biotherapeutics were able to increase targeted endogenous mRNAs and significantly greater anti-tumor activity in *in vivo* models of hepatocellular carcinoma and diffuse large B-cell lymphoma (482, 483). Furthermore, viral delivery of the recently discovered circular lncRNA (circRNAs), which feature greater stability due to resistance against endonucleolytic cleavage for more efficacious miRNA scavenging ability (484), represents yet another promising option for exploration.

Plants, fungi and invertebrates naturally rely on RNAi to combat RNA and DNA virus infections (485, 486). To counteract this RNAi-mediated antiviral response, many viruses that infect these eukaryotic hosts have evolved virus-encoded suppressors of RNAi (VSRs)(487). One such virus is the Nodamura virus (NoV), which primarily infects insects but is also highly virulent to certain mammals like suckling mice and hamsters (488, 489). NoV encodes a VSR known as B2, which binds double-stranded RNA and inhibits processing by Dicer to prevent the production of antiviral siRNAs (490, 491). Similarly, Influenza A (IAV) encodes the NS1 protein (492, 493), Ebola encodes VP35 (494, 495), HIV-1 encodes Tat (496, 497), Vaccinia virus encodes VP55(498), and Encephalomyocarditis virus (EMCV) encodes 3A (499).

Artificial incorporation of VSRs represents a related opportunity to increase production of their oncolytic virus carriers, thereby increasing oncolytic efficacy. Indeed, several groups, including ours, have demonstrated that expression of VSRs such as B2 or VP55 in VSV (500) or P19 (another plant virus RNAi inhibitor) in adenovirus (501), increases oncolytic virus production and tumor lytic efficacy. In the context of RNAi-expressing viral vectors, we need to acknowledge in future designs that RNAi can attack viral genomes and thus compromise the efficacy of these vectors as therapeutics and vectors to express payloads.

A. 3 Conclusion

Viral vector delivery of RNAi effectors has been successfully used for other therapeutic applications as a powerful tool to knockdown specific genes of interest; however, while exploration of its application for cancer therapy is underway, its clinical application remains limited. The intrigue in its continued exploration lies in the vast opportunity of combinations between different viral vector options, each with unique advantages and disadvantages, with different RNAi effectors. In this review, we outline each of options of viral vectors and tested therapeutic targets to date. Moreover, we also offer innovative strategies that could potentially help overcome challenges faced by this therapeutic class such as modifying RNAi processing or exploitation of newer RNAi species (*e.g.,* lncRNA, agoshRNA). Future directions for this field will continue to focus on identifying an optimal combination of virus and RNAi effectors that meet standards of therapeutic efficacy while retaining safety. Herein, we outline many options available, but a systematic approach to testing these combinations is reasonable for identifying candidates suitable for each clinical application. Nonetheless, from these multitude

of avenues, we immediately foresee expanding RNAi delivery to replication-competent viral vectors with inherent tumor lytic abilities to have the potential for great synergy, and thus, potent therapeutic efficacy. The main limitations to this approach include the natural production of neutralizing antibodies against the virus, inhibiting both its oncolytic and knockdown capacity, as well as sufficient bioavailability of the virus at the tumor site (28, 468). Strategies looking to overcome these obstacles in the form of optimal, context-dependent viral platform selection or combinational therapies with pharmacological compounds ("viral enhancers") are under investigation (86, 502). Nonetheless, given the multitude of options and strategies for researchers to bioengineer a breakthrough in viral vector delivery of RNAi for the treatment of cancer, it is not a matter of whether we will succeed, but when.

A.4 Acknowledgements

BW is supported by the Canadian Institutes of Health Research (CIHR) Doctoral Fellowship (CGS-D). RB is supported by the Ontario Graduate Scholarships (OGS). JSD is supported by the Terry Fox Research Institute (TFF 122868), the Canadian Institutes of Health Research (CIHR, INI-147824 and grant #705952), and the Canadian Cancer Society supported by the Lotte & John Hecht Memorial Foundation (703014). CSI is supported by grants from the Canadian Institutes of Health Research (#377104 and #183812), The Canadian Cancer Society (#840057), and the Canadian Cancer Society Innovation (#705973) and Impact (#IMP-14 and # 706162) grants as well as the generous support from the Ontario Institute for Cancer Research, the Ottawa Regional Cancer Foundation, and the Ottawa Hospital Foundation.

A.5 Tables and Figures

Table A1. List of viral vectors for RNAi delivery

Genus	Main Repres-entative	Genome (sense)	Genome Size	Immuno -genicity	Duration of Expression	Advantages	Disadvantages
Gamma (γ) retrovirus	Murine Leukemia Virus (MLV)	ssRNA (+)	~7-12kb	low	Long term/ Permanent	Persistent gene transfer in most tissues – Broad cell tropism RRV; confer a considerable degree of natural specificity for tumors (cancer therapy) RRV; Non-cytolytic – allowing for persistent gene expression in transduced cells	Integration might induce oncogenesis Unable to transduce non-dividing cells (advantageous for cancer therapy) Site specific delivery *in vivo*
Lentivirus	Human Immunodeficiency Virus (HIV)-1	ssRNA (+)	~10kb	low	Long term/ Permanent	Persistent gene transfer in most tissues – Broad cell tropism Capable of transducing dividing and non-dividing cells Extensive experience optimizing RNAi expression via *ex-vivo* engineering of stem cells	Integration might induce oncogenesis Site specific delivery *in vivo*
Adenovirus	Adenovirus (AdV) - 5	dsDNA	~26-45kb	high	Long term (cell type dependent)	Efficient transduction of target cells at a low multiplicity of infection Selective and potent cancer-cell killing properties (oncolytic)	Immune response to viral proteins (CRAdV) High probability of pre-existing immunity (AdV 1, 2, 5, 6) Liver is often default destination
Adeno-associated Virus	Adeno-associated virus serotype 2	ssDNA	<5kb	low	Long term (cell type dependent)	Low immunogenicity and no pathogenicity Broad cell tropism	Low transduction efficiency Difficult to generate high titers Liver is often default destination
Herpes SimplexVirus	Herpes Simlex Virus Type I	dsDNA	~150kb	high	Short-medium term	Well suited as oncolytic vector and CNS applications (retrograde axonal transport)	Risk of recombination with latently herpes simplex virus-infected cells Suitability as an RNAi delivery tool has been limited to *in vitro* investigations

Vesiculovirus	Vesicular Somatitis Virus	ssRNA (-)	11kb	high	Short term	Cytoplasmic replication allowing high expression levels and potential non-canonical processing of RNAi Apoptosis induction, oncolytic in cancer gene therapy applications Genetic structure allows for easy manipulation High titer production	Very sensitive to the antiviral action of interferon Neurotoxicity associated with viral glycoprotein
Flavivirus	West Nile Viurs (WNV), Tickborne Enchephalitis virus (TBEV)	ssRNA (+)	11kb	medium	Short term	Cytoplasmic replication allowing high expression levels and potential non-canonical processing of RNAi Infect neurons in primary and cell lines, could be good candidates for gene therapy in Central Nervous System (CNS) High titer production	Toxicity (non-cytopathic vectors available) Pre–existing immunity mainly in (sub)tropical countries
Alphavirus	Sindbis Viurs (SINV), Semliki Forest Virus (SFV), Venezuelan Equine Encephalitis Virus (VEE)	ssRNA (+)	11kb	high	Short term	Cytoplasmic replication allowing high expression levels and potential non-canonical processing of RNAi Apoptosis induction, oncolytic in cancer gene therapy applications High titer production	Toxicity due to viral replication (non-cytopathic vectors overcome this limitation)

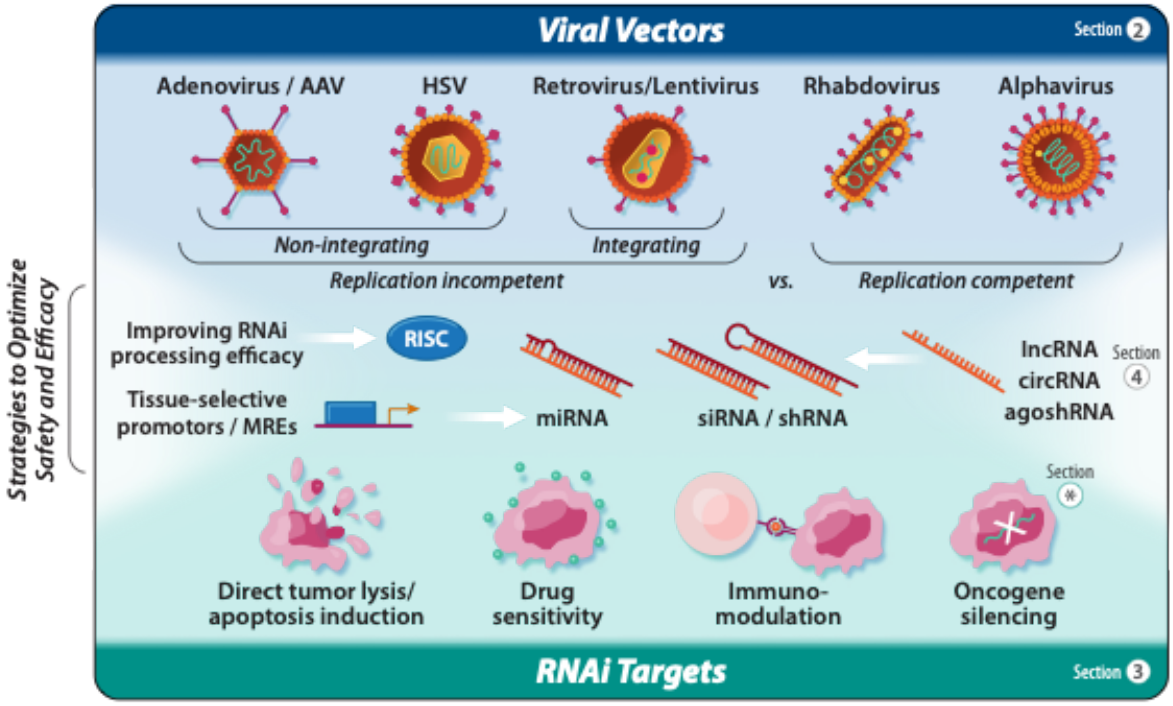

Figure A1. Viruses as optimal vectors for RNA interference delivery. A graphical depiction of the major sections of the review. The selection of different viral vectors is first outlined, which can broadly be divided into replication incompetent vs. competent vectors. Classification of RNA interference targest with anti-cancer effects are then summarized. Finally, strategies to optimize the safety and efficacy of these RNA interference expressing viral vectors is explored.

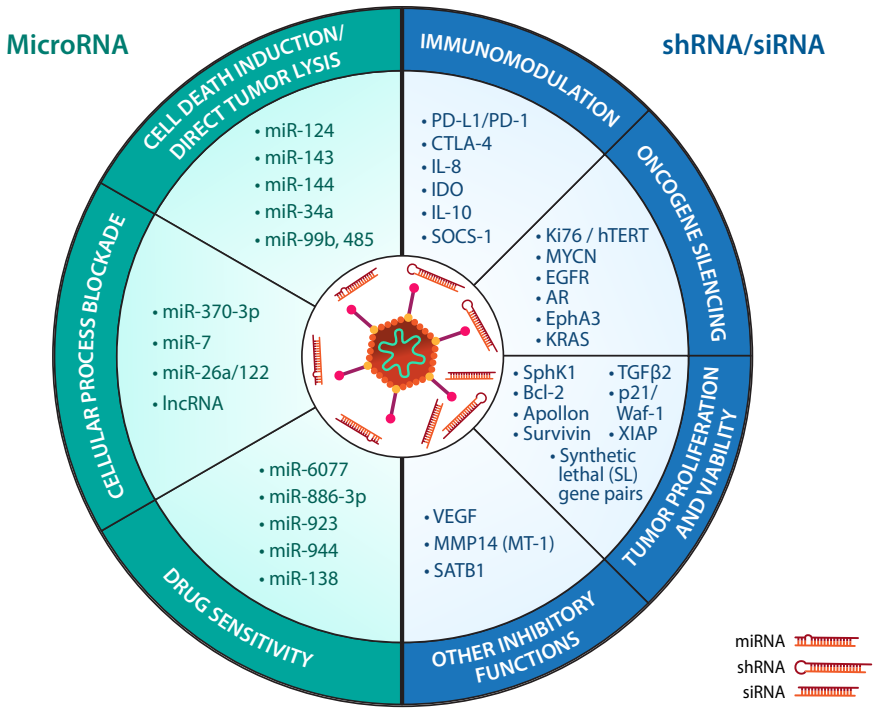

Figure A2. The therapeutic potential of RNAi-species and their link to cancer therapy. (Left) The delivery of microRNA by viral vectors can be divided into three major mechanisms of action: cell death induction / direct tumor lysis, cellular process blockade, and drug sensitivity, each aiming to induce greater cell death and discourage neoplastic growth in the infected tumor cells. The endogenous and multi-targeting nature of microRNA give delivery of this RNAi species tremendous versatility in cancer therapy. **(Right)** The delivery of shRNA/siRNA by viral vectors can be divided into four major mechanisms of action: immunomodulation, oncogene silencing, tumor proliferation and viability, and other inhibitory functions. If the correct gene is chosen, the strength of single gene knockdown by shRNA/siRNA can also confer profound anti-neoplastic activity in infected cancer cells. All targets listed have been experimentally demonstrated to confer therapeutic advantage *in vivo* over their respective unarmed virus controls.

Appendix B. Chapter 2 Supplemental Information

Table S2.1: Key Resources Table

REAGENT or RESOURCE	SOURCE	IDENTIFIER
Antibodies		
Phosphorylated STAT1 (Tyr701), rabbit	Cell Signaling Technology	7649
STAT1, rabbit	Cell Signaling Technology	9172
Phosphorylated STAT2 (Tyr690), rabbit	Cell Signaling Technology	88410
STAT2, rabbit	Cell Signaling Technology	72604
Phosphorylated EGFR (Tyr1068), rabbit	Cell Signaling Technology	2234
EGFR, rabbit	Cell Signaling Technology	4267
Phosphorylated NF-κB/p65 (Ser536), rabbit	Cell Signaling Technology	3033
NF-κB/p65, rabbit	Cell Signaling Technology	8242
IκB-α (Amino-terminal antigen), mouse	Cell Signaling Technology	4814
Lamin B1, rabbit	Cell Signaling Technology	12586
α-tubulin, mouse	Santa Cruz	sc-8035
β-actin, rabbit	Cell Signaling Technology	4970
hFAB™ Rhodamine Anti-Actin	Bio-Rad	12004163
hFAB™ Rhodamine Anti-GAPDH	Bio-Rad	12004168
Anti-rabbit HRP Secondary Antibody	New England Biolabs	7074
Anti-rabbit IgG (H+L) Alexa Fluor® 555	Cell Signaling Technology	4413S
Bacterial and virus strains		
VSVΔ51-Green fluorescent protein (GFP)	Dr. Jean-Simon Diallo	
VSVΔ51ΔG-GFP	Dr. Jean-Simon Diallo	
VSVΔ51-Firefly luciferase (FLuc)	Dr. Jean-Simon Diallo	
Measles virus, Schwartz strain - GFP	Dr. Guy Ungerechts	
Chemicals, peptides, and recombinant proteins		
Gefitinib	BioVision	1589
Erlotinib	BioVision	2048
UO126	Sigma-Aldrich	662005
IMD-0354	Sigma-Aldrich	I3159

SC-514	Sigma-Aldrich	SML0557
Human EGF	R&D Systems	236-EG
Human EGFR (cetuximab) antibody	InvivoGen	hegfr-mab1
Human IFNβ	PBL Assay Science	11415-1
Critical commercial assays		
Human CXCL10/IP-10 DuoSet Assay kit	R&D Systems	DY266
Deposited Data		
All uncropped Western blot images and raw data	Mendeley Data	doi:10.17632/zzpvtnmdw7.1
Experimental models: Cell lines		
786-0, human renal cell carcinoma	ATCC	CRL-1932
CT26WT, murine colon carcinoma	ATCC	CRL-2638
Vero, African green monkey renal cells	ATCC	CRL-81
TC-1, murine lung carcinoma	Dr. Guy Ungerechts	
Experimental models: Organisms/strains		
Female Balb/c mice	Charles River Laboratories	
Oligonucleotides		
Please see supplementary table S2 for oligonucleotides	Thermo Scientific	
Software and algorithms		
Prism 9.0	GraphPad	

Table S2.2: List of primers used in this study.

Model	**Gene**	**Forward primer (5' to 3')**	**Reverse primer (5' to 3')**
VSV	M	ATACTCAGATGTGGCAGCCG	GATCTGCCAATACCGCTGGA
	N	CATGTCACTGCAAGGCCTAAGA	GGCAGTATCGTGAATTCGATGC-3
Human	STAT1	ATGGCAGTCTGGCGGCTGAATT	CCAAACCAGGCTGGCACAATTG
	STAT2	CAGGTCACAGAGTTGCTACAGC	CGGTGAACTTGCTGCCAGTCTT
	GAPDH	ACAGTCAGCCGCATCTTCTT	GTTAAAAGCAGCCCTGGTGA
	IFNβ	CATTACCTGAAGGCCAAGGA	CAGCATCTGCTGGTTGAAGA

	IL-1b	CCACAGACCTTCCAGGAGAATG	GTGCAGTTCAGTGATCGTACAGG
	TNF-α	GCTGCACTTTGGAGTGATCG	GAGGGTTTGCTACAACATGGG
	CCL5	GCAGTCGTCCACAGGTCAAG	TCTTCTCTGGGTTGGCACAC
	IL-6	ACCCCCAATAAATATAGGACTGGA	GAAGGCGCTTGTGGAGAAGG
	CXCL9	AGTGCAAGGAACCCCAGTAG	AGGGCTTGGGGCAAATTGTT
	CXCL10	CTGAGCCTACAGCAGAGGAAC	AGGTACTCCTTGAATGCCACTT
	MX2	GAACGTGCAGCGAGCTTGTC	AAGGCTTGTGGGCCTTAGAC
	IFITM1	CCGTGAAGTCTAGGGACAGG	GGTAGACTGTCACAGAGCCG
Mouse	GAPDH	CATCACTGCCACCCAGAAGACTG	ATGCCAGTGAGCTTCCCGTTCAG
	CXCL9	CAGTGTGGAGTTCGAGGAACC	TTTGTTGCAATTGGGGCTTGG
	CXCL10	ATCATCCCTGCGAGCCTATCCT	GACCTTTTTTGGCTAAACGCTTTC

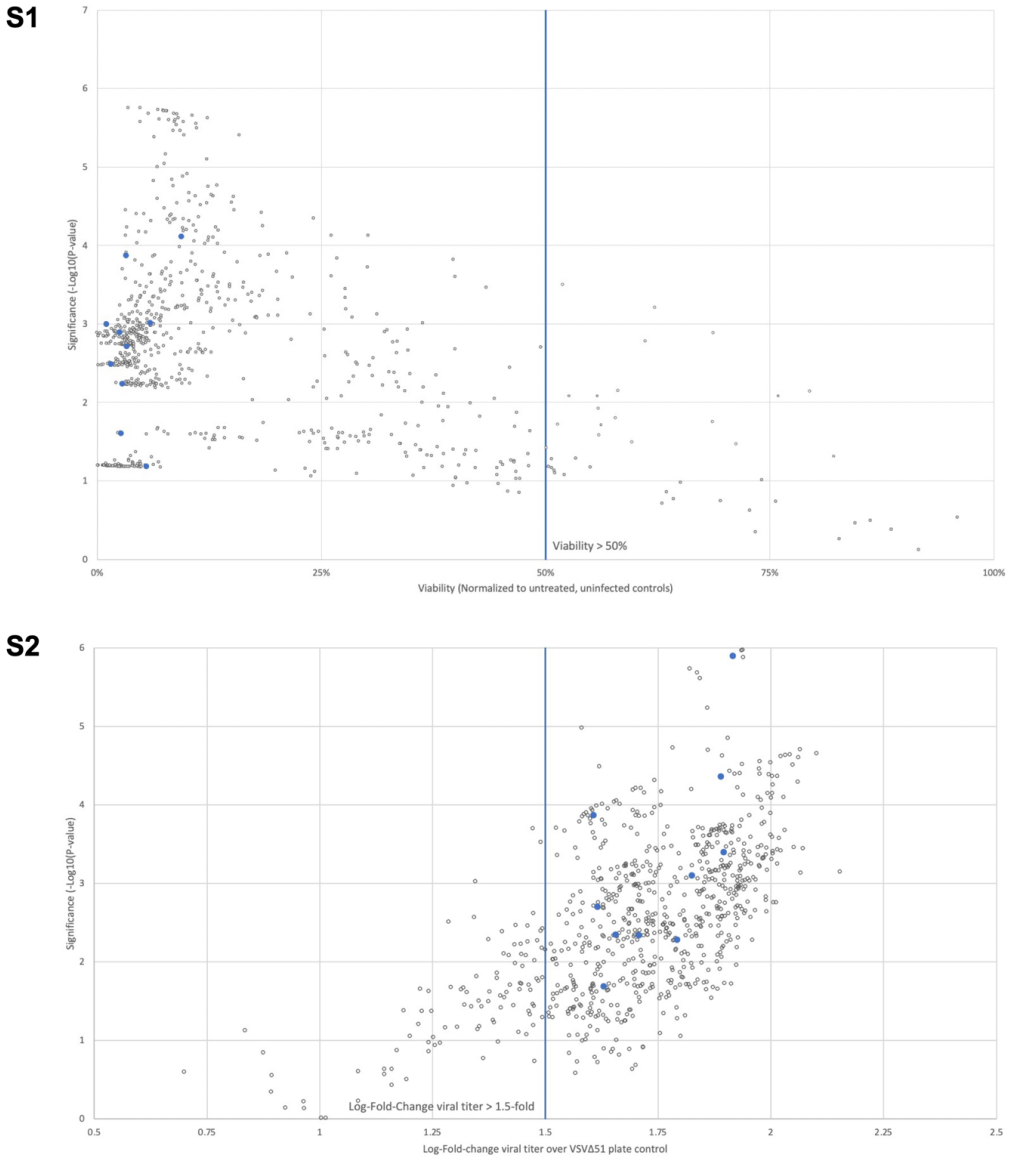

Figure S2.1: Scatter plot of reverse kinase screen viability. 786-0 cells were pre-treated with a drug library of kinase inhibitors (1μM) and vanadate (125μM) for four hours and subsequently infected with VSVΔ51-FLuc at a MOI of 0.1. Vanadate controls are shown in blue. 48 hours post infection (hpi), the metabolic activity (surrogate for viability) was measured

using resazurin (Alamar blue) assay. Values were blank-controlled then normalized against infected, untreated 786-0 (mock-infected) controls. An unpaired t-test assuming unequal variances was performed, the y-axis represents the calculated $-Log_{10}$(P-value) (n=2-3).

Figure S2.2: Scatter plot of reverse kinase screen vial titer. 48 hours post infection (hpi), the viral titer was determined using high-throughput virus assay. Values were normalized against infected, untreated 786-0 (mock-infected) controls. An unpaired t-test assuming unequal variances was performed, the y-axis represents the calculated $-Log_{10}$(P-value) (n=2-3).

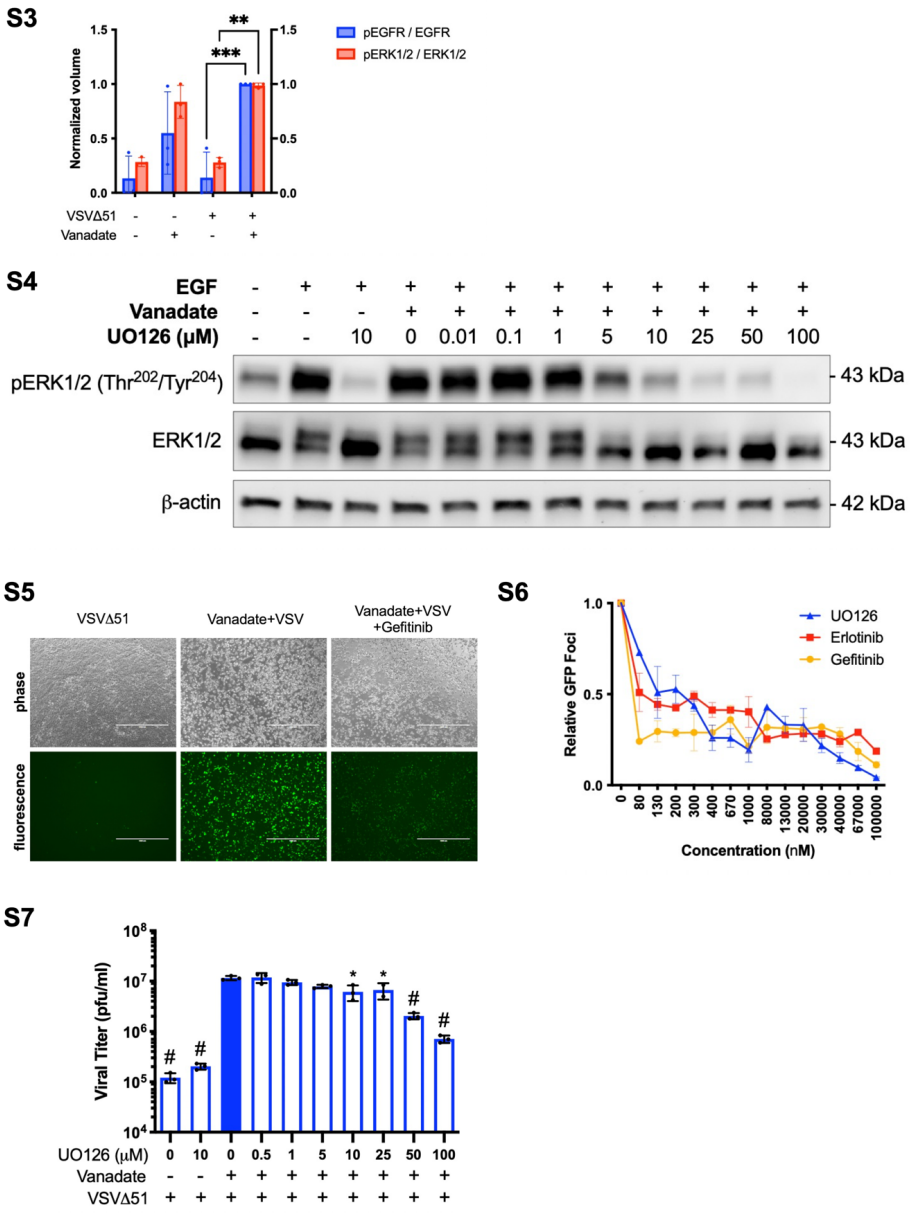

Figure S2.3: pEGFR:EGFR and pERK1/2:ERK1/2 volume densitometry ratios corresponding to Figure 1D (n=3, mean ± SD).

Figure S2.4: Human 786-0 renal carcinoma cells were treated pre-treated with or without vanadate (150 μM) and varying concentrations of UO126 (0 – 100μM) as indicated for four

hours. Cells were then treated with 10ng/mL EGF for 10 minutes and lysates were probed by western blot for phosphorylated ERK1/2, total ERK1/2 and β-actin.

Figure S2.5: Human 786-0 cells were pretreated ± vanadate (150μM) ± gefitinib (10μM) for 4 hours, then consequently infected with VSVΔ51-GFP (MOI 0.01). Phase and fluorescence images were taken 24 hours post infection (hpi); scale bar = 1000μm.

Figure S2.6: Count of GFP foci were obtained from Figure 2B and plotted relative to the vanadate + VSVΔ51 condition without kinase inhibitor (n=2, mean ± SEM).

Figure S2.7: Human 786-0 cells were pretreated ± vanadate (150μM) ± UO126 (0 – 100μM) for 4 hours, then consequently infected with VSVΔ51-GFP (MOI 0.01). Supernatants were collected 24hpi and titered by viral plaque assay (n=3, mean ± SD; *$P<0.05$, $^{\#}P<0.0001$; one-way ANOVA compared to the infected VSVΔ51 + vanadate only condition as indicated by the filled bar).

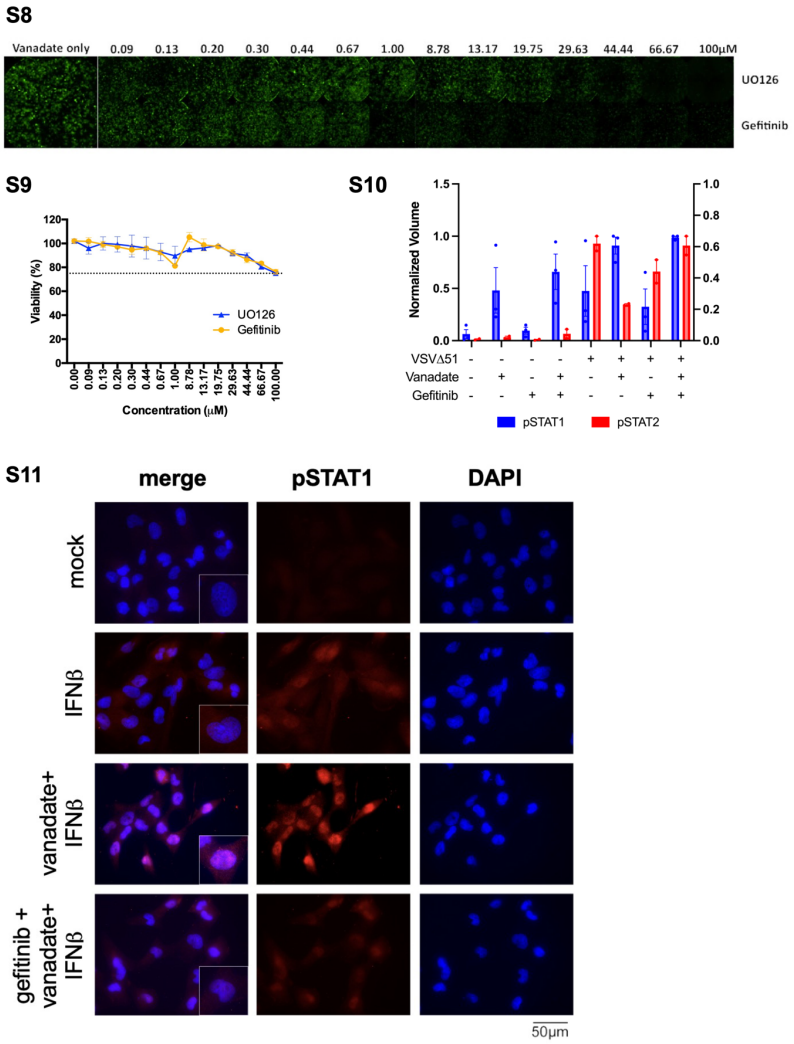

Figure S2.8: Human renal 786-0 cancer cells were simultaneously treated with varying concentrations of gefitinib or UO126 (0 - 100 μM) and vanadate (150 μM). Four hours later, cells were infected with measles virus expressing GFP (MOI 0.3). Representative fluorescent images were taken 24 hours post infection (hpi).

Figure S2.9: Cell viability was measured by Alamar blue assay and compared relative to the vanadate + VSVΔ51 condition without kinase inhibitor (n=2, mean ± SEM). Dotted line represents 75% viability.

Figure S2.10: Volume densitometry of pSTAT1 and pSTAT2 levels from Figure 3A (n=3, mean ± SD).

Figure S2.11: Representative immunofluorescence images corresponding to Figure 3D. Scale bar = 50µm.

S12

TF	*Pval*	*Eval*	∩	#TG	RC (%)
STAT1	< 1.0E-06	< 1.0E-06	8	25	0
NFKB1	4.00E-05	1.68E-03	7	63	0

S13

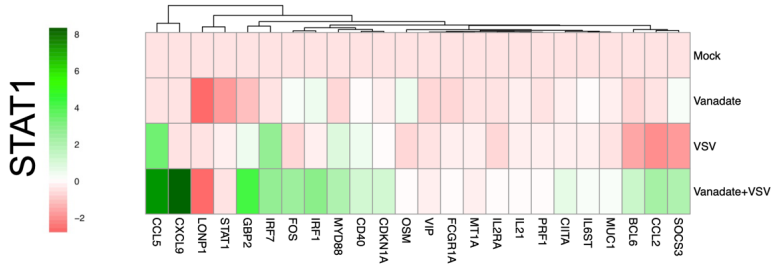

S14

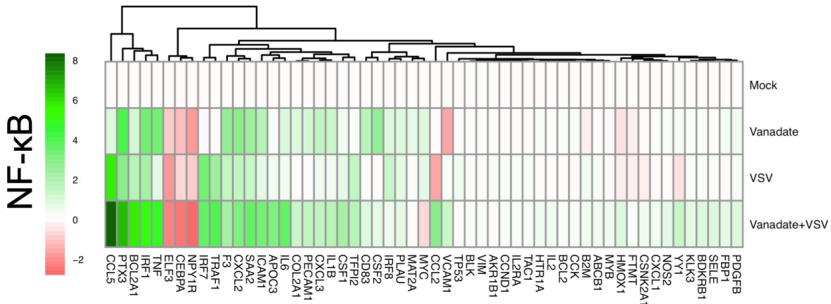

S15

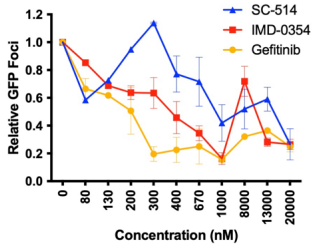

S16

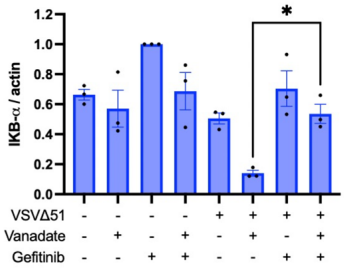

Figure S2.12: Table listing STAT1 and NF-κB transcription factors from the TFactS *in silico* analysis: *Pval* is P-value, *Eval* is E-value, ⋂ is the number of genes common between TF target genes and the query list, #TG is number of target genes for the corresponding TF and RC(%) is random control percentage which is a non-parametric control of false positives. Refer to published paper for more details on these parameters [29].

Figure S2.13: Heatmap of genes downstream to STAT1 transcription factor on 786-0 cells treated ± vanadate (150μM) and ±VSVΔ51 infection (MOI 0.01).

Figure S2.14: Heatmap of genes downstream to NF-κB transcription factor on 786-0 cells treated ± vanadate (150μM) and ±VSVΔ51 infection (MOI 0.01).

Figure S2.15: Count of GFP foci were obtained from Figure 4B and plotted relative to the vanadate + VSVΔ51 condition without kinase inhibitor (n=2, mean ± SEM).

Figure S2.16: Volume densitometry of IκB-α levels from Figure 4E (n=3, mean ± SD, *P<0.05 by one-way ANOVA).

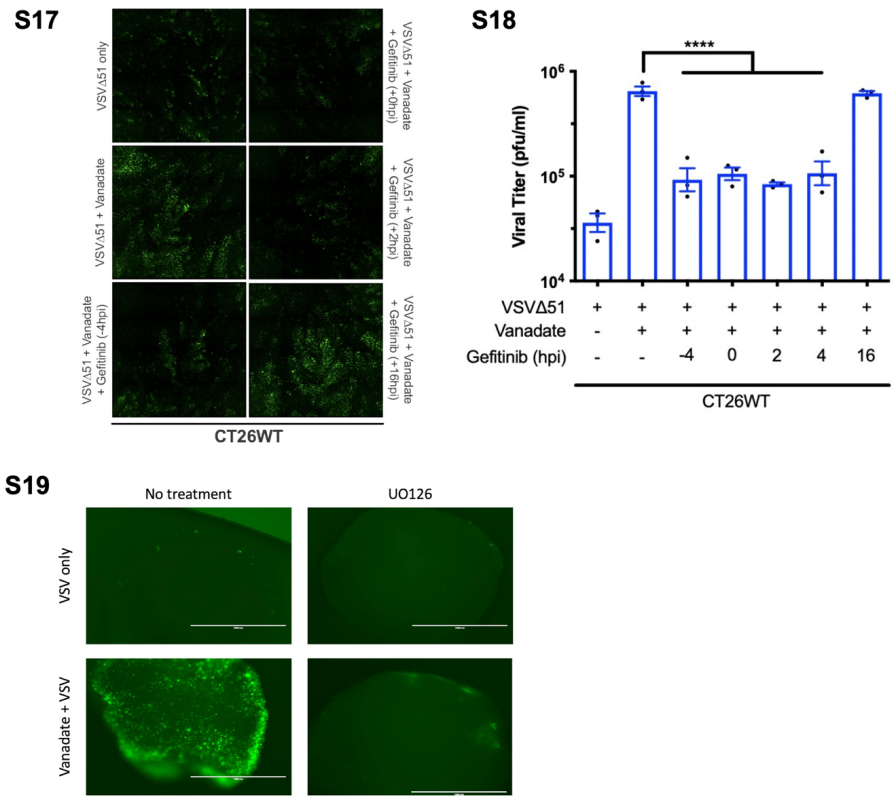

Figure S2.17: Mouse CT26WT colon carcinoma cells were pretreated ± vanadate (150µM) for 4 hours ± gefitinib (10µM) at -4, 0.5, 1, 2, 4 and 16 hours post infection (hpi), then consequently infected with VSVΔ51-GFP (MOI 0.01). Representative images are shown.

Figure S2.18: Supernatant from Figure S16 was collected 24hpi and titered by plaque assay (n=3, mean ± SD; ****P<0.0001 by one-way ANOVA).

Figure S2.19: *Ex vivo* mouse CT26WT tumors implanted subcutaneously in Balb/c mice were pretreated ± vanadate (150µM) ± UO126 (20µM) for 4 hours, then consequently infected with VSVΔ51-GFP (3e4 pfu/core). Representative fluorescence images were taken 24 hours post infection. Scale bar = 1000 µm.

Appendix C. Chapter 3 Supplemental Information

SUPPLEMENTARY TABLES

Table S3.1: Key Resources Table

REAGENT or RESOURCE	SOURCE	IDENTIFIER
Antibodies		
Acid Phosphatase 2 Polyclonal Antibody	Thermo Scientific	PA5-29961
hFAB™ Rhodamine Anti-Actin	Bio-Rad	12004163
Anti-rabbit HRP Secondary Antibody	New England Biolabs	7074
Bacterial and virus strains		
VSVΔ51-Green fluorescent protein (GFP)	Dr. Jean-Simon Diallo	
VSVΔ51-Firefly luciferase (FLuc)	Dr. Jean-Simon Diallo	
Chemicals, peptides, and recombinant proteins		
Critical commercial assays		
Deposited Data		
All uncropped Western blot images and raw data	Mendeley Data	doi:10.17632/zzpvtnmdw7.1
Experimental models: Cell lines		
786-0, human renal cell carcinoma	ATCC	RRID: CVCL_1051
A549, human lung carcinoma	ATCC	RRID:CVCL_0023
HT1080, human fibrosarcoma	ATCC	RRID:CVCL_L898
MCF7, human breast carcinoma	ATCC	RRID:CVCL_0031
Oligonucleotides		
Please see supplementary table S2 for oligonucleotides	Thermo Scientific	
Software and algorithms		
Prism 9.0	GraphPad	

Table S3.2: List of primers used in this study.

Model	**Gene**	**Forward primer (5' to 3')**	**Reverse primer (5' to 3')**
VSV	M	ATACTCAGATGTGGCAGCCG	GATCTGCCAATACCGCTGGA

Human	ACP2	TCCATTGGTCTTCTGTCACCCG	AGACCATCCACCTCCACTTCTC
	GAPDH	ACAGTCAGCCGCATCTTCTT	GTTAAAAGCAGCCCTGGTGA
	IFNβ	CATTACCTGAAGGCCAAGGA	CAGCATCTGCTGGTTGAAGA
	MX2	GAACGTGCAGCGAGCTTGTC	AAGGCTTGTGGGCCTTAGAC
	IFITM1	CCGTGAAGTCTAGGGACAGG	GGTAGACTGTCACAGAGCCG
siRNA	ACP2	CAGACUUUGACCGGACUCUUU	AGAGUCCGGUCAAAGUCUGUU
miRNA	miR-30 ACP2	AACAGACTTTGACCGGACTCTC	Generic poly-A tail primer (Agilent)

SUPPLEMENTARY FIGURES

S1

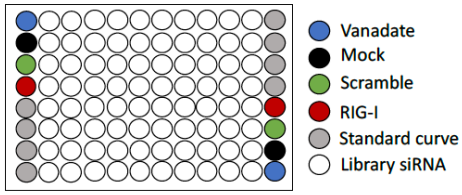

S2

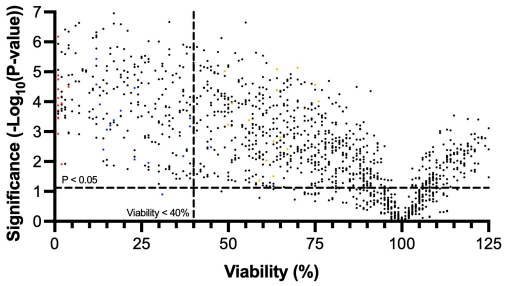

S3

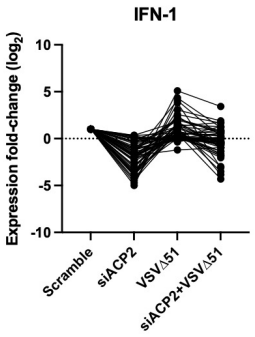

S4

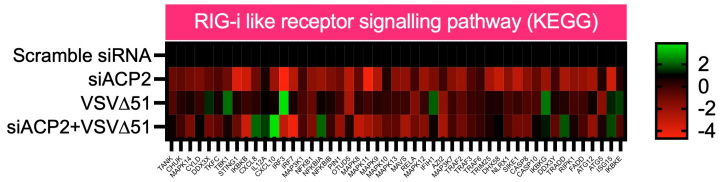

S5

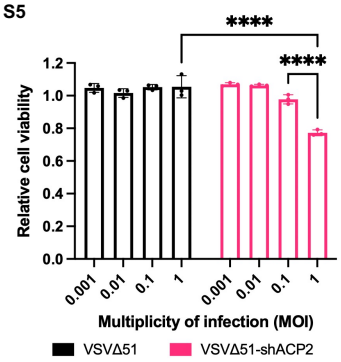

Fig S3.1. Plate map for the siPP high-throughput screen performed in Fig 1.

Fig S3.2. Volcano plot of viability decrease and significance from siPP screen.

Fig S3.3. Fold-change expression of genes related to the “type 1 interferon” gene ontology term were plotted from Fig 3.

Fig S3.4. A heatmap of the fold-change expression of gene related to the ”RIG-I like receptor signaling pathway” GO term was plotted from Fig 3.

Fig S3.5. 786-0 cells infected with VSVΔ51-NTC or VSVΔ51-shACP2 with indicated multiplicity of infection (MOI). Cell viability was measured using resazurin metabolic dye 48 hours post infection (hpi) (n=3, mean ± SD; ****P<0.0001 by two-way ANOVA).

Appendix D. Chapter 4 Supplemental Information

SUPPLEMENTAL TABLES

Supplemental Table S4.1: Resources Table

REAGENT or RESOURCE	SOURCE	IDENTIFIER
Antibodies		
NEDD8 (19E3), rabbit	Cell Signaling Technology	RRID:AB_659972
Caspase-3, rabbit	Cell Signaling Technology	RRID:AB_2070042
PARP, rabbit	Cell Signaling Technology	RRID:AB_2160739
Phosphorylated STAT1 (Tyr701), rabbit	Cell Signaling Technology	RRID:AB_10950970
STAT1, rabbit	Cell Signaling Technology	RRID:AB_2198300
Phosphorylated STAT2 (Tyr690), rabbit	Cell Signaling Technology	RRID:AB_2800123
STAT2, rabbit	Cell Signaling Technology	RRID:AB_2799824
IRF-9 (D2T8M), rabbit	Cell Signaling Technology	RRID:AB_2799885
Phosphorylated NF-κB/p65 (Ser536), rabbit	Cell Signaling Technology	RRID:AB_331284
NF-κB/p65, rabbit	Cell Signaling Technology	RRID:AB_10859369
IκB-α (Amino Terminal), mouse	Cell Signaling Technology	RRID:AB_390781
NAE1/APPBP1 (D9I4Z), rabbit	Cell Signaling Technology	RRID:AB 2798448
Lamin B1, rabbit	Cell Signaling Technology	RRID:AB_2650517
α-tubulin, mouse	Santa Cruz	RRID:AB_628408
VSV, rabbit	Gift from Dr. Earl Brown	
hFAB™ Rhodamine Anti-Actin	Bio-Rad	RRID:AB_2861334
Anti-rabbit HRP Secondary Antibody, goat	New England Biolabs	RRID:AB_2099233
Anti-mouse IgG, HRP-linked antibody, goat	Cell Signaling Technology	RRID:AB_330924
Anti-rabbit IgG (H+L) Alexa Fluor® 555, goat	Cell Signaling Technology	RRID:AB_10694110
Armenian Hamster Anti-CD3e Monoclonal Antibody, FITC Conjugated	BD Pharmingen	RRID:AB_394595
Rat Anti-Mouse CD4 Monoclonal Antibody, V450 Conjugated	BD Pharmingen	RRID:AB_1645271
Rat monoclonal Anti-CD8α Monoclonal Antibody	BD Pharmingen	RRID:AB_11152075
Armenian Hamster Anti-mouse CD69 BV605 Monoclonal Antibody	BD Pharmingen	RRID:AB_2738120
HSV-1 N212 - GFP	Dr. Karen Mossman	
Vaccinia virus, Wyeth strain - GFP	Dr. Andrea McCart	
Chemicals, peptides, and recombinant proteins		
Pevonedistat (MLN4924)	Cedarlane Labs	A11260
Human TNF-alpha	Cedarlane Labs	210-TA-020

Human IFN-beta	PBL Assay Science	11415-1
Human IFN-alpha	PBL Assay Science	11200-1
Poly I:C	Invivogen	tlrl-pic
Z-VAD-FMK	Promega	G7231
Human TNF-alpha neutralizing antibody	R&D Systems	MAB210-SP
Critical commercial assays		
Caspase-Glo® 8 Assay System	Promega	G8201
Lumit™ HMGB1 Human/Mouse Immunoassay	Promega	W6110
Human IFN Beta ELISA Kit	PBL Assay Science	41410
Deposited Data		
All uncropped Western blot images and raw data	Mendeley Data	doi:10.17632/2fnzs3jpg4.1
Experimental models: Cell lines		
786-0, human renal cell adenocarcinoma	ATCC	RRID: CVCL_1051
Vero, African green monkey renal epithelial	ATCC	RRID: CVCL_0059
76-9, human rhabdomyosarcoma	Dr. Robert Korneluk	
A549, human lung carcinoma	ATCC	RRID:CVCL_0023
MCF7, human breast adenocarcinoma	ATCC	RRID:CVCL_0031
HeLa, human cervical adenocarcinoma	ATCC	RRID:CVCL_0030
HT1080, human fibrosarcoma	Dr. John Bell	RRID:CVCL_L898
HT29, human colorectal adenocarcinoma	ATCC	RRID: CVCL 0320
THP-1, human acute monocytic leukemia	Dr. William Stanford	RRID:CVCL_IR08
JIMT1, human breast adenocarcinoma	ATCC	RRID: CVCL_2077
SKOV3, human ovarian adenocarcinoma	Dr. Barbara Vanderhyden	RRID: CVCL_0532
4T1, mouse breast carcinoma	ATCC	RRID:CVCL_0125
B16F10, mouse melanoma	ATCC	RRID:CVCL_0159
CT26WT, mouse colon carcinoma	ATCC	RRID:CVCL_7256
CT2A, mouse glioma	Dr. John Bell	RRID:CVCL_ZJ44
DBT, mouse astrocytoma	Dr. John Bell	RRID:CVCL_4W75
ID8, mouse ovarian	Dr. Barbara Vanderhyden	RRID:CVCL_IU14
L1210, mouse leukemia	Dr. William Stanford	RRID:CVCL_0382
PAN02, mouse pancreatic ductal adenocarcinoma	ATCC	RRID:CVCL_D627
S-180, mouse sarcoma	ATCC	RRID:CVCL_2874
D17, canine osteosarcoma	ATCC	RRID:CVCL_1916
Experimental models: Organisms/strains		
Female 6-week-old Balb/c mice	Charles River Laboratories	RRID:IMSR_APB:4790
Oligonucleotides		
Please see supplemental table S1 for oligonucleotides	Thermo Scientific	
Software and algorithms		
Prism 9	GraphPad	RRID:SCR_002798

ImageJ	ImageJ	RRID:SCR_003070

Supplemental Table S4.2: List of primers used in this study.

Model	Gene	Forward primer (5' to 3')	Reverse primer (5' to 3')
VSV	M	ATACTCAGATGTGGCAGCCG	GATCTGCCAATACCGCTGGA
	N	GATAGTACCGGAGGATTGACG	TCAAACCATCCGAGCCATTC
Human	STAT1	ATGGCAGTCTGGCGGCTGAATT	CCAAACCAGGCTGGCACAATTG
	STAT2	CAGGTCACAGAGTTGCTACAGC	CGGTGAACTTGCTGCCAGTCTT
	GAPDH	ACAGTCAGCCGCATCTTCTT	GTTAAAAGCAGCCCTGGTGA
	IFN-β	CATTACCTGAAGGCCAAGGA	CAGCATCTGCTGGTTGAAGA
	IL-1β	CCACAGACCTTCCAGGAGAATG	GTGCAGTTCAGTGATCGTACAGG
	TNF-α	GCTGCACTTTGGAGTGATCG	GAGGGTTTGCTACAACATGGG
	CCL5	GCAGTCGTCCACAGGTCAAG	TCTTCTCTGGGTTGGCACAC
	IL-6	ACCCCCAATAAATATAGGACTGGA	GAAGGCGCTTGTGGAGAAGG
	IFITM1	CCGTGAAGTCTAGGGACAGG	GGTAGACTGTCACAGAGCCG
	IRF7	GCAAGGTGTACTGGGAGCG	GATGGTATAGCGTGGGGAGC
	IRF9	TTCTTCAAGGCCTGGGCAAT	CCTGGTGGCAGCAACTGATA
	NEDD8	CGCTGACCGGAAAGGAGATT	CAGAGCCAACACCAGGTGAA
	UBA3	AATCTCCAGCCATCACAGCCAC	GTGACATCAGCAACCGCCAGTT

SUPPLEMENTAL FIGURES

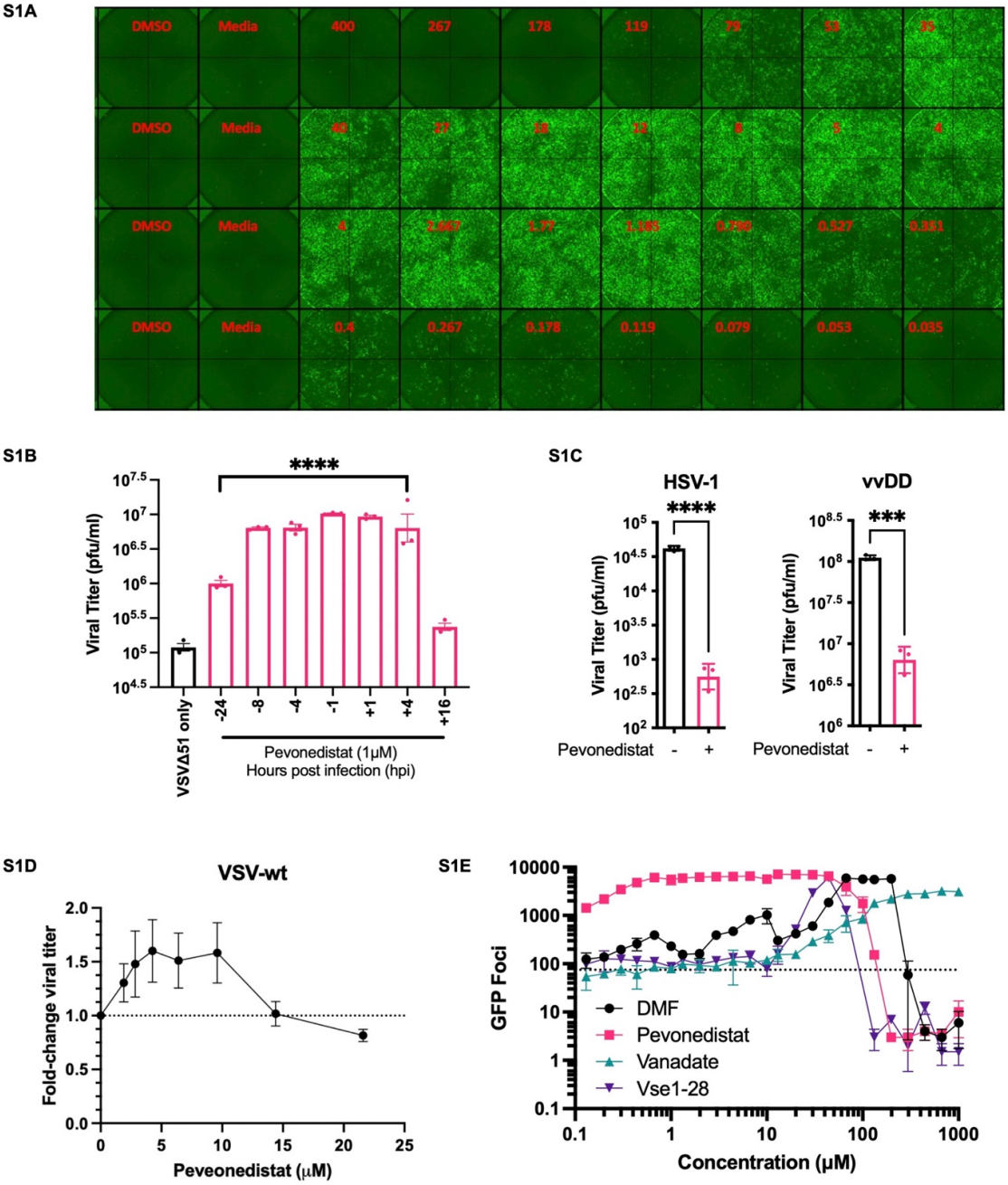

Fig. S4.1. Pevonedistat confers viral sensitization across multiple concentrations and timepoints. (A) Fluorescent images corresponding to Fig. 4.1D. (B) 786-0 renal carcinoma cells were treated with pevonedistat (1μM) at indicated timepoints prior to or after infection

with VSVΔ51 (MOI 0.01). Viral titers were measured 24 hours post infection (hpi) by plaque assay (n=3, ****P<0.0001 by two-way ANOVA compared to the VSVΔ51 only condition). (C) 786-0 cells were pre-treated with pevonedistat (1μM) for 4 hours, then infected with HSV-1 (MOI 0.01) or vaccinia, Wyeth strain (MOI 0.01). Viral titers were measured by plaque assay 24hpi (n=3, ***P<0.001, ****P<0.0001 by Student two-tailed t-test). (D) 786-0 cells were pre-treated with a variety of concentrations for 4 hours, then infected with wild type VSV-FLuc (MOI 0.01). Viral titer was expressed relative to untreated controls (n=3). (E) 786-0 cells were treated with a concentration range (130nM - 1mM) of multiple viral-enhancing compounds (dimethyl fumarate, pevonedistat, sodium orthovanadate, VSe1-28) for 4 hours, then infected with VSVΔ51-GFP (MOI 0.01). GFP foci were quantified 24hpi and plotted (n=2).

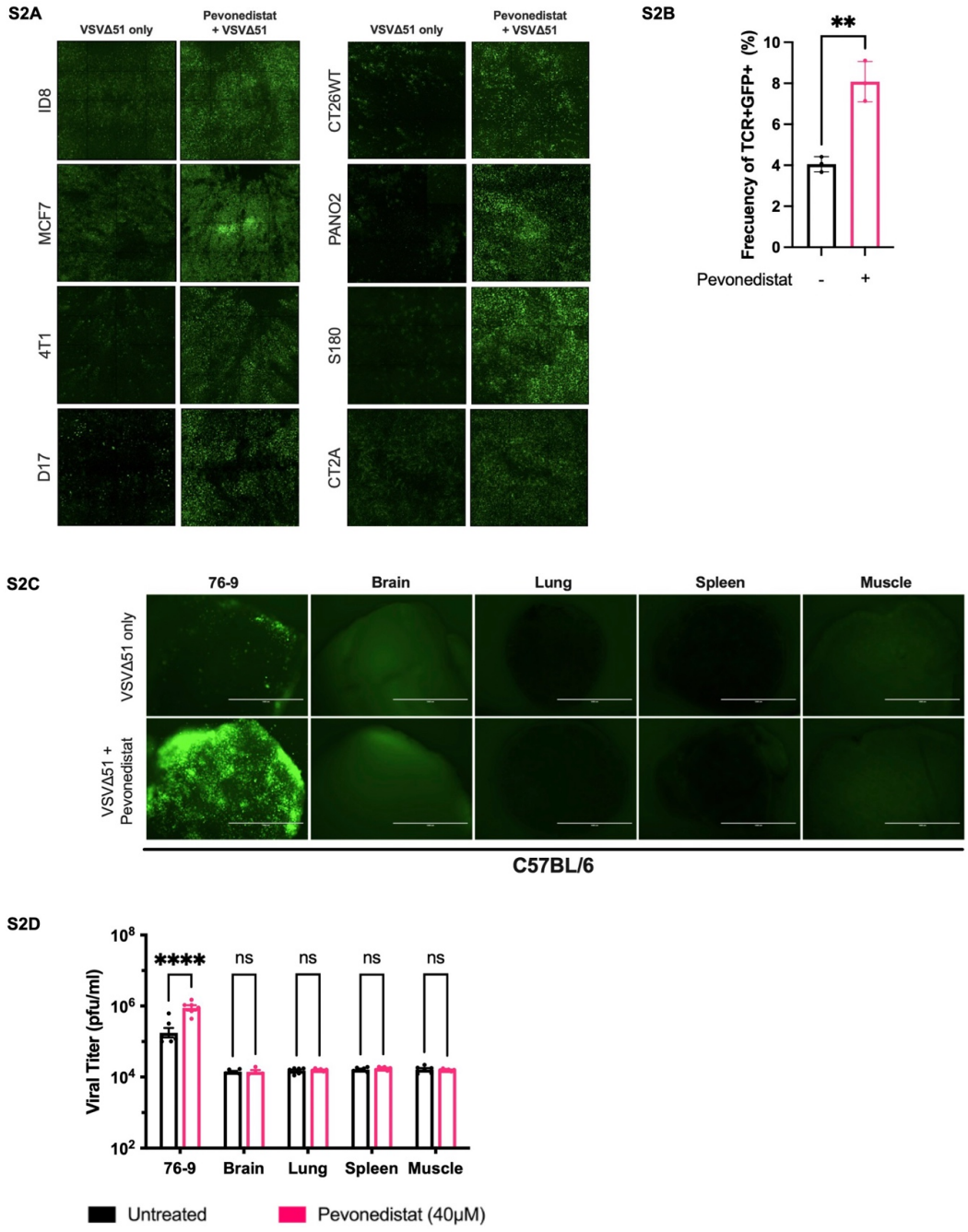

Fig. S4.2. Pevonedistat sensitizes different tumor models to VSVΔ51. (A) Indicated cell types were pre-treated with pevonedistat (1μM) for 4 hours, then infected with VSVΔ51-GFP (MOI

0.01). Fluorescent images were taken 24 hours post infection (hpi). (B) Isolated human T-cells were treated with pevonedistat (100nM) for 4 hours, then infected with VSVΔ51-GFP (MOI 0.01). 24 hours later, cells were assessed for positive GFP signal by flow cytometry and expressed as a percentage of the population (n=3, **P<0.01 by Student's two-tailed t-test). (C,D) Murine 76-9 rhabdosarcoma cells were implanted subcutaneously in C57BL/6 mice, then excised and cored upon reaching 1500mm^3. Normal brain, lung, spleen, and muscle tissues were also obtained and cored. Cores were treated *ex vivo* with pevonedistat (10μM) for 4 hours, then infected with VSVΔ51-GFP (3 x 10^4 pfu/core). (C) At 24hpi, representative fluorescent images were obtained (scale bar = 1000μm). (D) Supernatants were taken 48hpi and quantified for viral titer (n>6, mean ± SD; ns = no significance, ****P<0.0001 by two-tailed t-test).

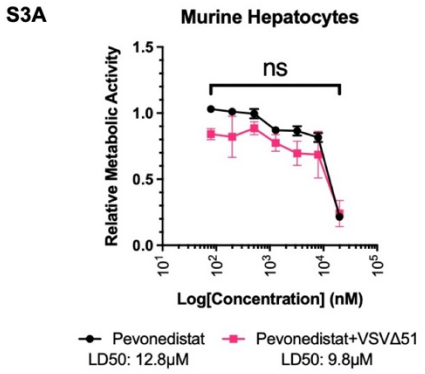

Fig. S4.3. Pevonedistat increases tumor cell death. (A) Isolated murine hepatocytes were treated a concentration range of pevonedistat for 4 hours, then infected with VSVΔ51 (MOI 0.01). Cell viability was measured by Alamar blue assay and expressed relative to untreated, uninfected controls (n=3, ns is not significant by two-way ANOVA).

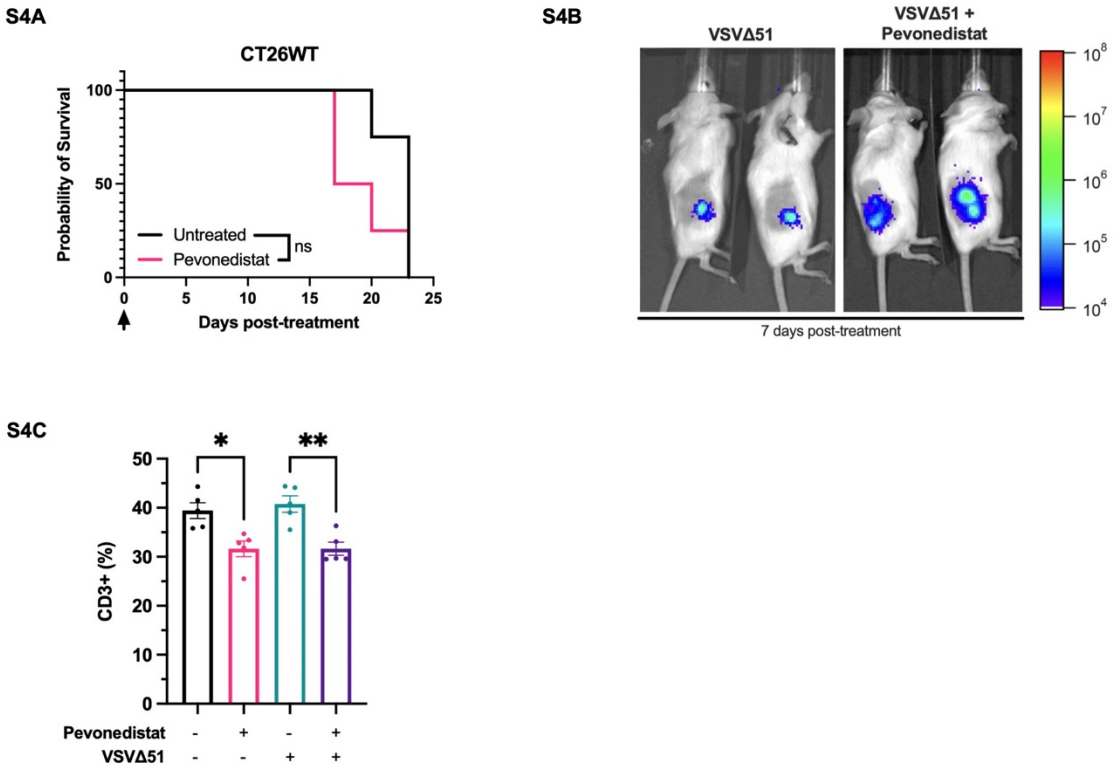

Fig. S4.4. Pevonedistat increases the *in vivo* therapeutic efficacy of VSVΔ51. (A) 3 x 10^5 CT26WT cells were implanted subcutaneously into BALB/c mice and allowed to progress to 100mm^3. Mice were then treated by intratumoral injection of pevonedistat (90mg/kg), then 1 x 10^8 VSVΔ51 4 hours later for one dose. Mice were culled at 1500 mm^3 and Kaplan-Meier survival curves were plotted (n=5, ns = no significance by log-rank test). (B) Representative luminescence images were taken 7 days after first treatment in Fig. 4A using a live in vivo imaging (IVIS) system. (C) Melanoma B16 tumors overexpressing OVA antigen (B16-OVA) were implanted into the right flank of C57BL/6 mice. When tumor volume reached 100mm^3, mice were injected intratumorally with three doses of pevonedistat (90mg/kg), then VSVΔ51 (1 x 10^8 pfu/tumor), spaced one day apart. Tumours were extracted 7 days after first treatment,

processed and analyzed by flow cytometry for CD3+ T-cell populations (n=3, *P<0.05, **P<0.01 by one-way ANOVA).

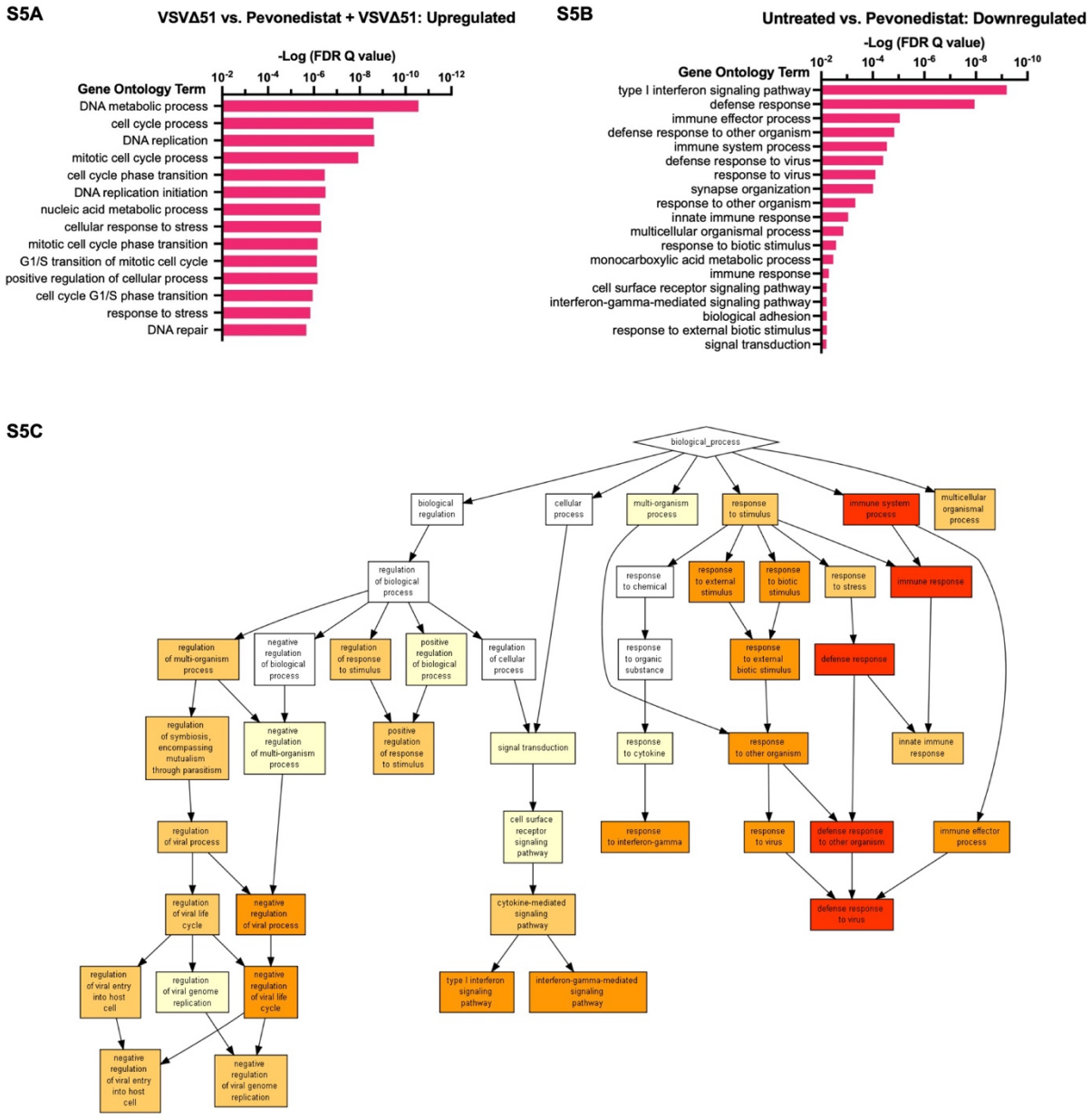

Fig. S4.5. Pevonedistat regulates multiple cellular processes. (A-C) RNA sequencing data processed as described in Fig. 5 was used. (A) Significantly upregulated (>2 log2-fold change)

gene expressions were processed by GOrilla to identify relevant gene ontology (GO) terms between the VSVΔ51 infected only condition and the combination with pevonedistat condition. (B) Significantly downregulated (>2 log2-fold change) gene expressions were processed by GOrilla to identify relevant gene ontology (GO) terms between the untreated, uninfected control and cells treated only with pevonedistat. (C) The gene ontology tree of Fig. 4.5B.

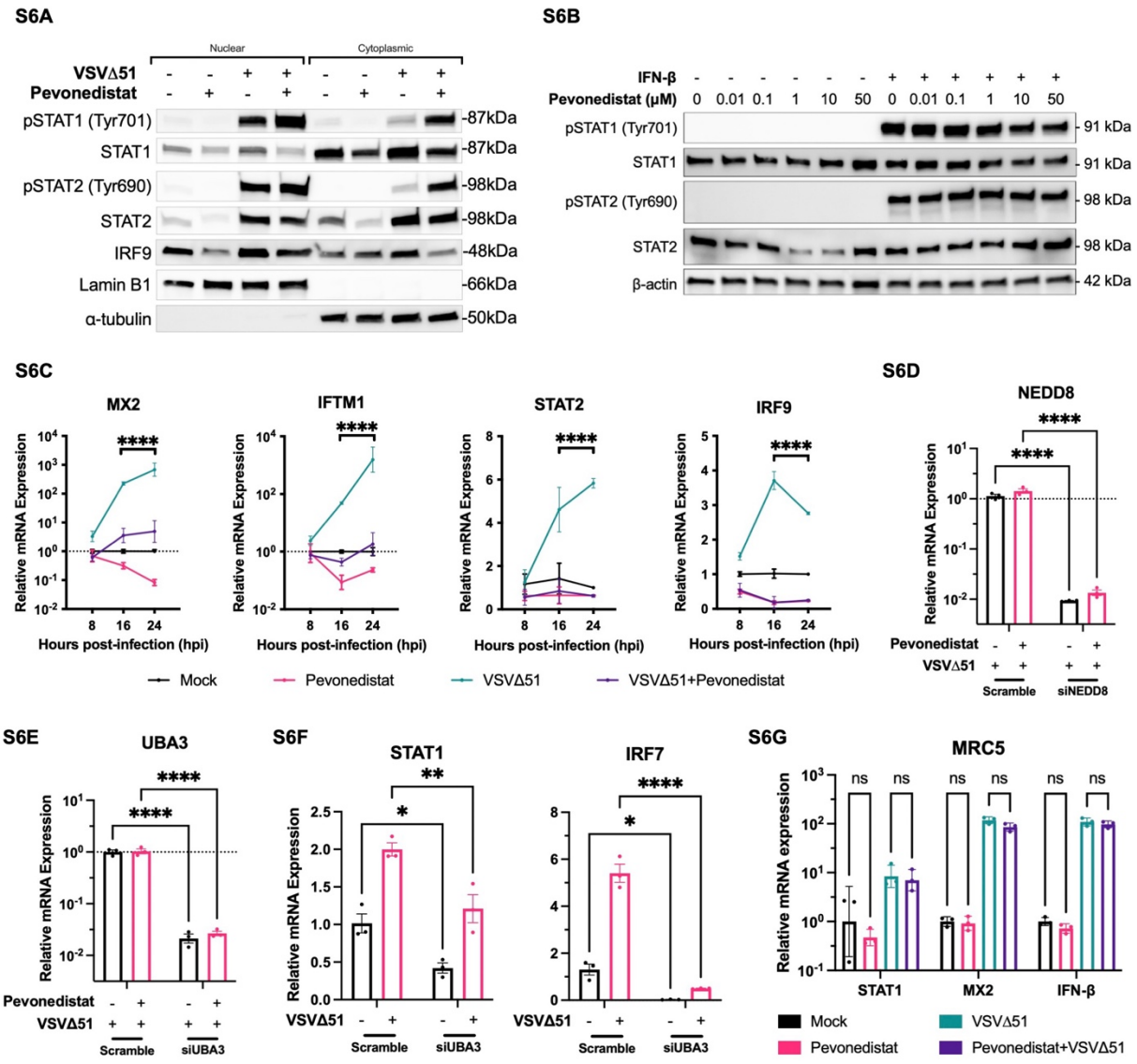

Fig. S4.6. Pevonedistat regulates STAT1 and downstream effectors. (A,C) Human 786-0 renal carcinoma cells were pre-treated with pevonedistat (1μM) for 4 hours, then infected with VSVΔ51 (MOI 0.01). (A) Following 24 hours post infection (hpi), cells were lysed, and nuclear/cytoplasmic fractions were isolated. Lysate fractions were then probed by western blot for the indicated proteins. (B) 786-0 cells were pre-treated with varying concentrations of pevonedistat (0.01 – 50μM), then treated with human IFN-β (1000 U/mL) for 2 hours. Cells

were then lysed and probed by western blot for phosphorylated and total STAT1 and STAT2. (C) At 8, 16 and 24hpi, cells were lysed and RNA was extracted. Indicated genes were quantified by qPCR (n=3, ****P<0.0001 by two-way ANOVA). (D,E) 786-0 cells were seeded and transfected with siRNA against NEDD8 or UBA3. Two days following transfection, cells were infected with VSVΔ51 (MOI 0.01) for 24 hours. RNA was extracted and probed for (D) NEDD8 or (E) UBA3 mRNA expression by qPCR respectively. (F) RNA was extracted and probed for STAT1 and IRF7 mRNA expression 24hpi by qPCR (n=3, *P<0.05, **P<0.01, ****P<0.0001 by two-way ANOVA). (G) Human lung fibroblast MRC5 cells were pre-treated with pevonedistat (1μM) for 4 hours, then infected with VSVΔ51 (MOI 0.01). Cells were lysed, RNA extracted and probed for *STAT1, MX2* and *IFN-β* transcripts by qPCR (n=3, mean ± SD; ns = no significance by two-way ANOVA).

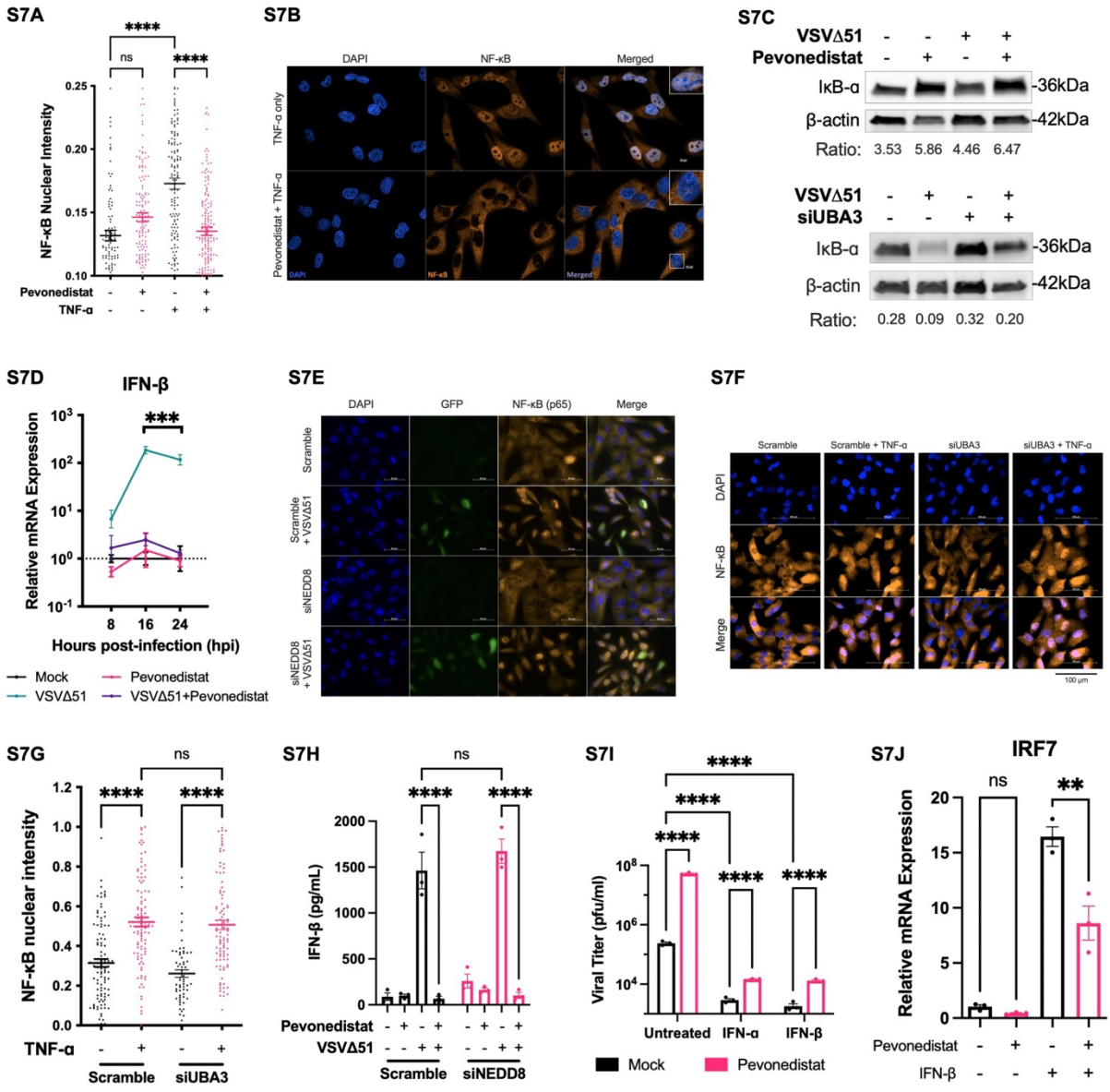

Fig. S4.7. Pevonedistat controls NF-κB to regulate IFN-1 cytokines. (A) 786-0 cells were seeded on glass coverslips, pre-treated for 4 hours with pevonedistat (10μM). After treatment, cells were then treated with human TNF-α (10ng/mL) for 30 minutes. Cells were fixed and immunostained for NF-κB and nuclei (DAPI). (B) Nuclear NF-κB intensity was quantified (n=3, mean ± SD; ****P<0.0001). (C) 786-0 cells were treated with pevonedistat (1μM) for 4 hours or transfected with siRNA against UBA3 (20nM) for 2 days. Cells were then infected

with VSVΔ51 for 24 hours, then lysed and probed for IκB-α by western blot. Densitometry was performed to quantify band intensity and normalized to the loading control. (D) 786-0 cells were treated with pevonedistat (1μM) for four hours, then infected with VSVΔ51. Cell lysates were obtained 8, 16 and 24 hpi and probed for IFN-β mRNA by qPCR (n=3, ***P<0.001 by two-way ANOVA). (E) Representative immunofluorescent images from Fig. 7F. (F,G) 786-0 cells were seeded on glass coverslips and transfected with siRNA against UBA3 for two days. (F) Cells were then treated with TNF-α (30ng/mL) for 30 minutes, then fixed and stained for NF-κB by immunocytochemistry. Representative immunofluorescent images are shown. (G) NF-κB nuclear intensity was quantified and plotted (n=3, ****P<0.0001 by two-way ANOVA). (H) 786-0 cells were seeded and transfected with siRNA against NEDD8 for two days. Cells were then treated with pevonedistat (1μM) for 4 hours, then infected with VSVΔ51 (MOI 0.01). Supernatant was collected 24hpi and quantified for IFN-β by ELISA (n=3, ****P<0.0001 by two-way ANOVA). (I,J) 786-0 cells were seeded and treated with pevonedistat (1μM) ± IFN-α (250 U/mL) ± IFN-β (1000 U/mL) and four hours later, cells were infected with VSVΔ51. (I) Viral titer was quantified by plaque assay 24hpi (n=3, ****P<0.0001 by two-way ANOVA). (J) Cells were lysed 24hpi and RNA was extracted. IRF7 mRNA expression was quantified by qPCR (n=3, **P<0.01 by two-way ANOVA).

Appendix E. Curriculum Vitae (CV)

Boaz Wong

Website: https://med.uottawa.ca/md-phd/people/wong-boaz

EDUCATION

September 2018 – present:

- **Doctor of Medicine (MD), Combined Program** – University of Ottawa, Ottawa, ON
- Anticipated graduation date: June 2024

September 2018 – present:

- **Doctor of Philosophy (PhD), Combined Program** – University of Ottawa, Ottawa, ON
- Graduate studies in Department of Biochemistry, Microbiology and Immunology
- Anticipated graduation date: June 2024

September 2014 – May 2018

- **Bachelor of Medical Sciences (BMSc), Honours** – University of Western Ontario, London, ON
- Honours Specialization in Physiology with Distinction, Schulich School of Medicine & Dentistry

RESEARCH EXPERIENCE

June 2019 – present

- **MD/PhD Candidate** – Ottawa Hospital Research Institute, Ottawa, ON
- Supervisor: Dr. Jean-Simon Diallo
- Cellular Antagonization of the Type 1 Interferon Response for the Potentiation of Oncolytic Virotherapy

September 2023 – present

- **Clinical Research Assistant** – Ottawa Hospital Research Institute, Ottawa, ON
- Supervisor: Dr. Marcio Gomes
- Pathological trends in the incidence of peritoneal mesothelioma over the last decade

October 2023 – present

- **Clinical Research Assistant** – Ottawa Hospital Research Institute, Ottawa, ON
- Supervisor: Dr. Jordan Sim
- The role of immunohistochemistry in the pathological identification of carcinoma of unknown primary (CUP)

January 2019 – present

- **Clinical Research Assistant** – Ottawa Hospital Research Institute, Ottawa, ON
- Supervisor: Dr. Paul Wheatley-Price
- Improving the diagnosis and treatment of carcinoma of unknown primary (CUP) using next-generation sequencing (NGS) tools

November 2018 – June 2020

- **Clinical Research Assistant** – The Ottawa Hospital, Ottawa, ON
- Supervisor: Dr. Carolyn Nessim
- Analysis of the impact of various surgical factors on the prognosis of liposarcoma (LPS) patients undergoing surgical resection

May 2018 – August 2018

- **Summer Research Student** – Mount Sinai Hospital, Toronto, ON
- Supervisor: Dr. Jeffrey Wrana
- Exploring cytoskeletal control of Hippo/TGFβ signalling crosstalk in intestinal regeneration and cancer organoid models.

September 2017 – April 2018

- **Honours Thesis Candidate**– Department of Physiology, University of Western Ontario, London, ON
- Supervisor: Dr. John Di Guglielmo
- Role of TGFβ type 3 receptor in non-small cell lung cancer metastasis

January 2015 – April 2018

- **Research Assistant** – Lawson Health Research Institute, London, ON
- Supervisor: Dr. Lisa Hoffman
- Identification of contributory biomarkers and treatment by ANG1 in Duchenne Muscular Dystrophy (DMD).

May 2016 – August 2017

- **Summer Research Student** – Matrix Dynamics Group, University of Toronto, Toronto, ON
- Supervisor: Dr. Boris Hinz
- Characterization of dynamic strain fields generated by actively contracting myofibroblasts for the attraction of macrophages in the extracellular matrix.

PUBLICATIONS AND COMMUNICATIONS

Life-Time Summary

- Articles in refereed journals	12
- Articles in non-refereed journals	0
- Manuscripts in submission	2
- Published abstracts	2

- Patents	1
- Presentations	24
- Other academic materials	2

Articles in refereed journals

1. Alwithenani A, Taha Z, Thomson M, Chen A, **Wong B**, Diallo JS. Unlocking the Potential of Dimethyl Fumarate: Enhancing Oncolytic HSV-1 Efficacy for Wider Cancer Applications. Accepted to *Front Immunol*, December 2023. **Co-author, IF: 7.3**
2. **Wong B,** Bergeron A, Maznyi G, Ng K, Jirovec A, Birdi HK, Serrano D, Spinelli M, Thomson M, Taha Z, Alwithenani A, Chen A, Lormier I, Vanderhyden B, Arulanandam R*, Diallo JS*. Pevonedistat, a First in-class NEDD8-activating Enzyme Inhibitor, sensitizes cancer cells to VSVΔ51 Oncolytic Virotherapy. *Mol Ther*, 2023 Sept 27; 31(11):3176-3192. **First author, IF: 12.4**
3. **Wong B*,** Birtch R*, Rezaei R, Jamieson T, Crupi M, Diallo JS, Ilkow CI. Optimal delivery of RNA interference by viral vectors for cancer therapy. *Mol Ther*, 2023 Sept 20; 31(11):3127-3145. **First author, review, IF: 12.4**
4. Bastin DJ, Montroy J, Kennedy MA, Martel AB, Shorr R, Ghiasi M, Boucher DM, **Wong B**, Gresham L, Diallo JS, Fergusson DA, Lalu MM, Kekre N, Auer RC. Safety and efficacy of autologous cell vaccines in solid tumors: a systematic review and meta-analysis of randomized control trials. *Sci Rep,* 2023 Feb 27; 13:3347. doi: 10.1038/s41598-023-29630-9. **Co-author, IF: 4.996.**
5. **Wong B,** Bergeron A, Alluqmani N, Maznyi G, Chen A, Arulanandam R, Diallo JS. Dependency of EGFR activation in Vanadium-based Sensitization to Oncolytic Virotherapy. *Mol Ther – Oncolytics*, 2022 Apr 19; 24:146-159. doi: 10.1016/j.omto.2022.04.004. **First author, IF: 7.2**
6. **Wong B,** Moore S, Wheatley-Price P. Complex Germline K757N Mutation in Non-Small-Cell Lung Cancer: A Case Report. *Case Rep Oncol*, 2022 Mar; 15:285-290. doi: 10.1159/000523734. **First author, IF: 1.143**
7. Bastin DJ, Khan ST, Montroy J, Kennedy MA, Forbes N, Martel AB, Baker L, Gresham L, Boucher DM, **Wong B**, Shorr R, Diallo JS, Fergusson DA, Lalu MM, Auer RC, Kekre N. Safety and efficacy of autologous whole cell vaccines in hematologic malignancies: A systematic review and meta-analysis. *Hematol Oncol*, 2021 Oct;39(4):448-464. doi: 10.1002/hon.2875. **Co-author, IF: 5.271**
8. Apte SS, Radonjic A, **Wong B,** Dingley B, Boulva K, Chatterjee A, Purgina B, Ramsay T, Nessim C. Preoperative imaging of gastric GISTs underestimates pathologic tumor size: A retrospective, single institution analysis. *J Surg Oncol,* 2021 Jul;124(1):49-58. doi: 10.1002/jso.26494. **Co-author, IF: 3.454**
9. **Wong B,** Vickers MM, Wheatley-Price P. The Diminishing Importance of Primary Site Identification in Cancer of Unknown Primary: A Canadian Single-Center Experience. *Front Oncol,* 2021 Mar 3;11:634563. doi: 10.3389/fonc.2021.634563. **First author, IF: 6.244**
10. **Wong B,** Apte SS, Tirotta F, Parente A, Mathieu J, Ford SJ, Desai A, Almond M, Nessim C. Perioperative blood transfusion is not an independent predictor for worse outcomes in retroperitoneal sarcoma surgery. *Eur J Surg Onc,* 2021 Jul;47(7):1763-1770. doi: 10.1016/j.ejso.2021.01.007. **First author, IF: 4.424**

11. Pakshir P, Alizadehgiashi M, **Wong B,** Coelho NM, Chen X, Gong Z, Shenoy V, McCulloch C, Hinz B. Dynamic Fibroblast Contraction Attracts Remote Macrophages in Fibrillar Collagen Matrix. *Nat Commun,* 2019 Apr 23;10(1):1850. doi: 10.1038/s41467-019-09709-6. **Co-author, IF: 12.121**
12. Gutpell K, Tasevski N, **Wong B**, Hrinivish WT, Su F, Hadway J, Desjardins L, Lee TY, Hoffman LM. ANG1 treatment reduces muscle pathology and prevents a decline in perfusion in DMD mice. *PLoS One,* 2017 Mar 23;12(3):e0174315. doi: 10.1371/journal.pone.0174315. **Co-author, IF: 2.766**

Manuscripts in submission

1. **Wong B**, Birtch R, Bergeron A, Ng K, Maznyi G, Spinelli M, Chen A, Arulanandam A, Ilkow CS, Diallo JS. High throughput screen identifies lysosomal acid phosphatase 2 to regulate IFN-1 responses to potentiate oncolytic VSVΔ51 activity. *Sci Rep*. **First author.**
2. Wong B, Liu J, Yeo S, Akurang D, Lo AQ, Xu W, Wang Y, Welch S, Wheatley-Price P. Evolution in the diagnosis and treatment of carcinoma of unknown primary (CUP): a multi-centre Canadian analysis. *Ann Oncol*. **First author.**

Published abstracts

1. Kassouf E, **Wong B,** Castonguay M. Abstract only: How I treat COVID-19 webinars: A rapid communication platform between patients and physicians. *Ann Oncol,* 31:S1018 (2020). doi: 10.1016/j.annonc.2020.08.1807, abstract #1743P
2. **Wong B,** Apte S, Tirotta F, Parente A, Mathieu J, Ford S, Desai A, Almond M, Nessim C. Poster Presentation: Is Perioperative Blood Transfusion a Predictor of Outcomes After Retroperitoneal Soft Tissue. Society of Surgical Oncology SSO 2020. *Ann Surg Oncol,* 27, 1–230 (2020). doi: 10.1245/s10434-020-08278-z, abstract #321

Patents

1. "Neddylation-activating enzyme inhibitors as enhances of viral-based therapies". Inventors: **Boaz Wong,** Anabel Bergeron, Rozanne Arulanandam, Jean-Simon Diallo. *United States Provisional Application No. 63/389,064*.

Presentations

1. Poster presentation: High-throughput screen identifies ACP2 to potentiate VSVd51 oncolytic virotherapy. International Oncolytic Virotherapy Conference (IOVC) 2023. Banff, Alberta, Canada. November 2023.
2. Poster presentation: Evolution of the diagnosis and management of CUP: a decade analysis. European Society of Medical Oncologists (ESMO) Congress 2023. Madrid, Spain. October 2023.
3. Oral presentation: Does margin status after biopsy matter in melanoma? – A cohort study of micro- and macroscopic margin status and their impact on residual disease and survival. Canadian Surgical Forum. Vancouver, British Columbia, Canada. October 2023.
4. Poster presentation: Pevonedistat, a First In-Class Neddylation activating enzyme inhibitor, sensitizes cancer cells to VSVΔ51 Oncolytic Virotherapy. International

Oncolytic Virotherapy Conference (IOVC) 2022. Karuizawa, Nagano, Japan. October 2022.

5. Poster presentation: Exploiting oxidative stress regulation of the antiviral IFN-1 response for potentiation of VSVΔ51 oncolytic virotherapy. University of Ottawa BMI Symposium 2022. Montebello, Quebec, Canada. May 2022.
6. Poster presentation: Dependency of EGFR activation in Vanadium-based Sensitization to Oncolytic Virotherapy. International Oncolytic Virotherapy Conference (IOVC) 2021, Sedona, AZ, USA. November 2021.
7. Poster presentation: Dependency of EGFR activation in Vanadium-based Sensitization to Oncolytic Virotherapy. BioCanRX Immunotherapy Summit 2021, virtual due to COVID-19. November 2021.
8. Poster presentation: Dependency of EGFR activation in Vanadium-based Sensitization to Oncolytic Virotherapy. OHRI Research Day 2021, virtual due to COVID-19. November 2021.
9. Poster presentation: How I Treat COVID-19 Webinars: a rapid communication platform between patients and physicians. 2020 Canadian Society for Clinical Investigators – Clinician Investigator Trainee Association of Canada (CSCI-CITAC) Joint AGM, virtual due to COVID-19. November 2020.
10. Poster presentation: Histology and Tumour Biology are More Important in Predicting Overall Survival than Margins of Resection. Connective Tissue Oncology Society (CTOS) Annual Meeting 2020, virtual due to COVID-19. November 2020.
11. Poster presentation: How I Treat COVID-19 Webinars: a rapid communication platform between patients and physicians. European Society of Medical Oncology (ESMO) Congress 2020, Madrid, Spain. September 2020.
12. Poster Presentation: Is Perioperative Blood Transfusion a Predictor of Outcomes After Retroperitoneal Soft Tissue Sarcoma Resection?. The Ottawa Hospital General Surgery Research Day 2020, Ottawa, ON, Canada. August 2020.
13. Poster presentation: Perioperative blood transfusion is not an independent predictor for worse outcomes in retroperitoneal sarcoma surgery. Canadian Society of Surgical Oncology Annual Meeting 2020, Toronto, ON, Canada. April 2020.
14. Poster presentation: Perioperative blood transfusion is not an independent predictor for worse outcomes in retroperitoneal sarcoma surgery. Society of Surgical Oncology SSO 2020 General Meeting, Chicago, IL, USA. March 2020.
15. Poster Presentation: Cytoskeletal control of Hippo/TGFb signalling crosstalk in intestinal regeneration and cancer. Mount Sinai Hospital Summer Studentship Research Day, Toronto, ON, Canada. August 2018.
16. Mini Oral: Myofibroblasts attract macrophages in fibrillar collagen. Canadian Connective Tissue Conference 2018, Toronto, ON, Canada. May 2018.
17. Poster Presentation: Tumour Growth Factor Beta Receptor III Suppresses MMP-1 & MT-1 in NSCLC. University of Western Ontario, Department of Physiology and Pharmacology Thesis Research Day, London, ON, Canada. April 2018.
18. Poster Presentation: Characterization of Mechanosensing of Macrophages in Fibrillar Collagen Matrix. University of Toronto Faculty of Dentistry Research Day 2018, Toronto, ON, Canada. February 2018.

19. Poster Presentation: The Dynamic Nature of Macrophage-to-Myofibroblast Attraction. Institute of Biomaterials and Biomedical engineering (IBBME) Undergraduate Summer Research Symposium, Toronto, ON, Canada. August 2017.
20. Poster Presentation: The Dynamic Nature of Macrophage-to-Myofibroblast Attraction. University of Toronto Undergraduate Engineering Research Day (UnERD) 2017, Toronto, ON, Canada. August 2017.
21. Poster Presentation: Characterization of Mechanosensing of Macrophages in Fibrillar Collagen Matrix. Faculty of Dentistry Undergraduate Student Research Program 2017, Toronto, ON, Canada. August 2017.
22. Poster Presentation: Fibroblast Contraction is an Attraction for Macrophages in Fibrillar Collagen Matrix. Gordon Research Conference: Tissue Repair & Regeneration, New London, New Hampshire, USA. June 2017.
23. Poster Presentation: The Dynamic Nature of Macrophage-to-Myofibroblast Attraction. University of Toronto Faculty of Dentistry Research Day 2017, Toronto, ON, Canada. February 2017.
24. Poster Presentation: Macrophage-to-Myofibroblast Attraction. Faculty of Dentistry Undergraduate Student Research Program 2016, Toronto, ON, Canada. August 2016.

Other academic materials

1. Published report: Faces of Lung Cancer Report 2020: The Valuable Lessons from the COVID-19 Global Pandemic. Lung Cancer Canada. November 2020. Link to article.
2. Dissertation: TGFβ Receptor III Suppresses MMP-1 and MT-1 Expression in Non-Small Cell Lung Cancer. Honours Bachelor Thesis, University of Western Ontario. Supervisor: Dr. John Di Guglielmo. April 2018.

RESEARCH GRANTS AND AWARDS

Research Funding

May 2021 – April 2024

- **Frederick Banting and Charles Best Canada Graduate Scholarships – Doctoral (CGS-D)** – Canadian Institutes of Health Research (CIHR)
- Engineering and characterization of a novel immunomodulatory oncolytic virus via modification of cellular phosphorylation homeostasis (PI: Diallo, JS)
- Funded: $105000 ($35000/3 years)

September 2020 – April 2023

- **Canadian Partnership for Research in Immunotherapy Manufacturing Excellence (CanPRIME)** – Mathematics of Information Technology and Complex Systems (MITACS)
- Development and characterization of a novel type I to type II interferon-potentiating oncolytic virus biotherapeutic (PI: Diallo, JS)
- Funded: $45000 ($15000/3 years)

September 2020 – April 2021

- **Ontario Graduate Scholarships (OGS)** – Government of Ontario, University of Ottawa
- Development and characterization of a novel type I to type II interferon-potentiating oncolytic virus biotherapeutic, (PI: Diallo, JS)

- Funded: $15000, ($5000/3 terms)

June 2019 – April 2023
- **Scholarship of Excellence - Doctorate** – Faculty of Medicine, University of Ottawa
- Award: $33000 ($3000/11 terms)

May 2017 – August 2017
- **Undergraduate: Summer Studentship Award – Institute Community Support** – Canadian Institutes of Health Research (CIHR)
- Attraction of Inflammatory Macrophages to Fibrotic Myofibroblasts is Dynamic (PI: Hinz, B)
- Funded: $5000, one term

May 2016 – August 2016
- **Undergraduate: Mobility, Musculoskeletal Health and Arthritis – Institute Community Support** – Canadian Institutes of Health Research (CIHR)
- The fatal attraction between Macrophages and Myofibroblasts (PI: Hinz, B)
- Funded: $5000, one term

Awards

1. Faculty of Dentistry Research Program 2017: Canadian Connective Tissue Conference (CCTC) Travel Award. Faculty of Dentistry, University of Toronto. Award: $400. August 2017.
2. Director's Choice Finalist, Institute of Biomedical Engineering and Biomaterial (IBBME) Summer Research Program 2017. Award. August 2017.
3. Laurene Paterson Scholarship. University of Western Ontario. Scholarship: $1600. November 2015.
4. UWO Second Year Science Faculty Scholarship. University of Western Ontario. Scholarship: $700. November 2015.
5. Scholarship of Excellence. University of Western Ontario. Award: $2000. September 2014.
6. Dean's Honour List. University of Western Ontario. 2014-2018.
7. Thornhill Secondary School Alumni Association Next Step Bursary. Thornhill Secondary School. Scholarship: $1000. April 2014.

WORK EXPERIENCE

May 2013 – August 2014:
- **Student Nurse** – Vaughan Pediatric Clinic, Vaughan, ON
- Assisted with patient administrative work, prepared patients for appointment including physical measurements and simple medical procedures, clean-up.

July 2012 – August 2014
- **Computer Instructor** – LogicFusion Inc., Markham, ON
- Instructed recreational courses in technology for children including programming, robotics, and animation.

June 2012 – August 2012
- **Summer Co-op student** – The Scarborough Hospital, Scarborough, ON
- Introduction to working in a health-care setting.

CREDENTIALS AND CERTIFICATIONS

April 2023

- ***AdMare* BioInnovations Scientist (BIS) Level 1** – adMare BioInnovations, Montreal, Quebec, Canada

January 2022

- **Drug Development Product Management** – Skaggs School of Pharmacy & Pharmaceutical Sciences, University of California, San Diego

March 2021

- **Market Research: Qualitative** – LinkedIn Learning

May 2019

- **Tri-Council Policy Statement: Ethical Conduct for Research Involving Humans Course on Research Ethics (TCPS 2: CORE)** – Panel on Research Ethics, Government of Canada

January 2019

- **Good Clinical Practice (GCP) Level 1 Basic –** Collaborative Institutional Training Initiative (CITI)
- Under requirements set by: Ottawa Hospital Research Institute / The Ottawa Hospital (N2)

COMMUNITY AND VOLUNTEER EXPERIENCE

September 2022 - present:

- **Judge** – IgNITE Competition
- Judge for entries for scientific competition organized for high school and university students across North America designed to help them develop and present novel research proposals and gain valuable research skills.

April 2020 - present:

- **Volunteer Director** – Lung Cancer Canada
- Support for lung cancer patients, caregivers, and researchers. Directed a committee of physicians and patients to generative informational materials in response to the COVID-19 pandemic.

April 2020 – September 2022:

- **Writer** – 2 Minute Medicine, Harvard Medical School
- Weekly contribution to a medical media publishing and news company designed to curate and summarize latest, high-impact medical research articles. Link to articles.

March 2020 – November 2020

- **English Webinar Coordinator** – How I Treat COVID-19 (HITC)
- Spearheaded an initiative alongside Dr. Elie Kassouf to generate a platform for rapid communication of information on COVID-19 between physicians and cancer patients.

September 2019 – April 2020

- **President** – Oncology Interest Group, University of Ottawa Medical School
- Lead a group of medical students interested in the field of oncology in events to further interest and clinical competency.

January 2019 – February 2020

- **Volunteer** – The Ottawa Mission Hospice
- Accompanied and served clients in end-of-life care.

May 2013 – August 2018

- **Head Coach** – Chinese Christian Softball Association
- Managed and coached a youth softball team to increase their interest in the sport and to promote a more active lifestyle.

September 2017 – May 2018:

- **VP Communications** – University Student Council Charity, University of Western Ontario
- Directed a team of photographers, videographers, and graphic designers to promote and document official charity events of university.

September 2016 – April 2018

- **Volunteer** – Ark Aid Street Mission, London
- Served weekly at a lunch-meal initiative in food preparation, distribution, and clean-up for the homeless population in London, Ontario.

September 2014 – April 2018

- **President** – Canadian Feed the Children Western
- Lead the student division at the University of Western Ontario of Canadian Feed the Children charity to orchestrate events to increase awareness and fundraising.

September 2015 – April 2017

- **Graphics Manager** – CAISA Fashion Show Western
- Involved in graphics design for promotional materials for Canada's largest student-run charity fashion show contributing $50,000 annually towards local biomedical research.

February 2013 – May 2014

- **Volunteer** – St. John's Rehab, Sunnybrook Hospital
- Delivery and clean-up of patient bedside meals, attending to patent needs throughout mealtimes. First exposure to healthcare environment.